ILMATIETEEN LAITOS
METEOROLOGISKA INSTITUTET
FINNISH METEOROLOGICAL INSTITUTE

169
CONTRIBUTIONS

CHARACTERISTICS OF WINTER CLIMATE IN FINLAND IN A WARMING WORLD

ANNA LUOMARANTA

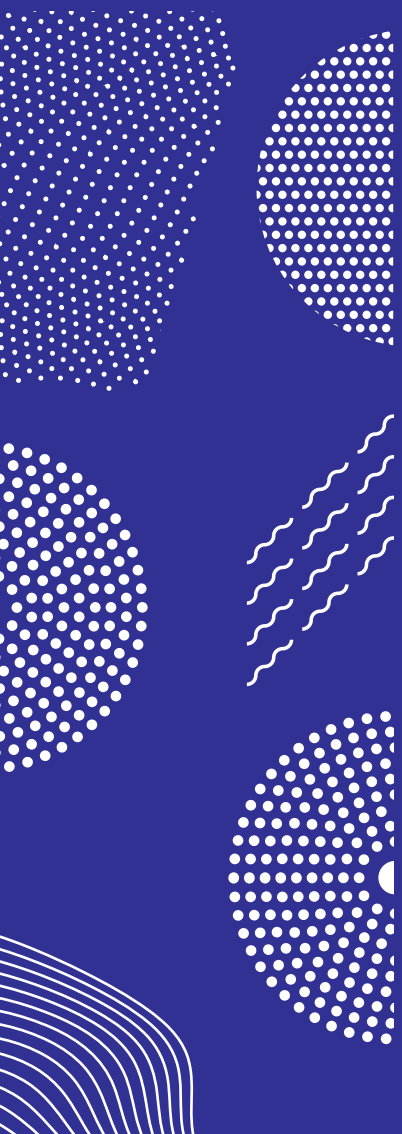

FINNISH METEOROLOGICAL INSTITUTE
CONTRIBUTIONS
No. 169

CHARACTERISTICS OF WINTER CLIMATE IN FINLAND IN A WARMING WORLD

Anna Luomaranta

Department of Physics
Faculty of Science
University of Helsinki
Helsinki, Finland

ACADEMIC DISSERTATION in meteorology

To be presented for public discussion with the permission of the Faculty of Science of the University of Helsinki, in Auditorium E204, Physicum Building, on the 21st of August, 2020 at 12 o'clock.

Finnish Meteorological Institute
Helsinki, 2020

Author: Anna Luomaranta
Weather and Climate Change Impact Research
Finnish Meteorological Institute

Supervisors: Docent Kirsti Jylhä
Weather and Climate Change Impact Research
Finnish Meteorological Institute, Finland

Professor Heikki Järvinen
Department of Physics
University of Helsinki, Finland

Reviewers: Professor Egidijus Rimkus
Department of Hydrology and Climatology
Vilnius University, Lithuania

Dr. Mats A. Granskog
Centre for Ice, Climate and Ecosystems
Norwegian Polar Institute, Norway

Custos: Professor Heikki Järvinen
Department of Physics
University of Helsinki, Finland

Opponent: Professor Jukka Käyhkö
Department of Geography and Geology
University of Turku

ISSN: 0782-6117
ISBN (paperback): 978-952-336-115-7
ISBN (pdf): 978-952-336-116-4
DOI: https://doi.org/10.35614/isbn.9789523361164

Edita Prima Oy
Helsinki 2020

ILMATIETEEN LAITOS
METEOROLOGISKA INSTITUTET
FINNISH METEOROLOGICAL INSTITUTE

Published by **Finnish Meteorological Institute**
(Erik Palménin aukio 1), P.O. Box 503
FIN-00101 Helsinki, Finland

Series title, number and report code of publication
Finnish Meteorological Institute Contributions 169
Date
June 2020

Author
Anna Luomaranta

ORCID iD
0000-0002-0891-7273

Title

Characteristics of winter climate in Finland in a warming world

Abstract

In northern countries, such as Finland, winter climate conditions affect the functionality of society in many ways. Due to the climate warming, the winter conditions are facing changes. Changes in snow and ice act as an indicator of the climate conditions in a region. The aim of this thesis is to examine what the winters are like in Finland in a changing climate.

The main results of this work are based on gridded observations, FMIClimGrid and E-OBS, and CMIP5 global climate model simulations. Using these, the observed snow, temperature and precipitation conditions in 1961-2014 were analyzed, and the future changes in Baltic Sea ice cover were projected for the ongoing century. In addition, two modeling studies were performed: The first assessed the performance of ECHAM5 atmospheric general circulation model in simulating snow melt timing in spring, and the second studied the ability of numerical convection-permitting weather prediction model HARMONIE to simulate a sea-effect snowfall case.

The results showed that, in Finland, the snow depth has decreased throughout the year and the snow season has shortened. Increasing liquid precipitation in winter was one of the main reasons for the changes. In spring, increasing air temperature has had an effect. The annual maximum sea ice extent and sea ice thickness in the Baltic Sea were projected to decrease during the ongoing century. However, the Baltic Sea is unlikely to become totally ice-free during typical winters in the coming decades.

When climate models are used to predict future climate conditions, it is essential that they describe the snow cover realistically, since it is an important element of the climate system. In the ECHAM5 climate model, Northern Eurasian snow melt timing was generally produced quite well when compared to satellite observations, but regional differences were also found. The reasons for the discrepancies turned out to be the simplifications in the calculations of the model's surface energy budget. The HARMONIE model also managed to simulate a known sea-effect snowfall case reasonably well. The simulation results improved when radar reflectivities were assimilated into the model.

As climate warming proceeds, the winter conditions will continue to change. The results of this thesis highlight the importance of continuous monitoring of climate conditions in the northern areas.

Publishing unit

Finnish Meteorological Institute, Weather and Climate Change Impact Research

Classification (UDC)
591.54, 504.7, 551.578, 551.467, 303.733.3, 519.233.5

Keywords
climate, climate change, snow cover, snowfall, trend, ice cover, climate model, regression model

ISSN and series title
0782-6117
Finnish Meteorological Institute Contributions

ISBN
ISBN (paperback): 978-952-336-115-7
ISBN (pdf): 978-952-336-116-4

DOI
https://doi.org/10.35614/isbn.9789523361164

Language
English

Pages
63

ILMATIETEEN LAITOS
METEOROLOGISKA INSTITUTET
FINNISH METEOROLOGICAL INSTITUTE

Julkaisija
Ilmatieteen laitos
(Erik Palménin aukio 1)
PL 503, 00101 Helsinki

Julkaisun sarja, numero ja raporttikoodi
Finnish Meteorological Institute
Contributions 169, FMI-CONT-169
Päiväys: Kesäkuu 2020

Tekijä
Anna Luomaranta

ORCID iD
0000-0002-0891-7273

Nimeke

Suomen talvi-ilmaston piirteitä lämpenevässä maailmassa

Tiivistelmä

Pohjoismaissa, joihin Suomikin kuuluu, talven ilmasto-olosuhteet vaikuttavat yhteiskunnan toimivuuteen monin tavoin. Ilmaston lämmetessä talviolosuhteet muuttuvat. Muutokset lumi- ja jääpeitteessä toimivat indikaattorina alueen ilmasto-oloista. Tämän väitöskirjan tavoitteena on tarkastella, millaisia Suomen talvet ovat muuttuvassa ilmastossa.

Väitöskirjan päätulokset perustuvat hilamuotoisiin havaintoaineistoihin, FMIClimGridiin ja E-OBS-aineistoon, sekä globaaleihin CMIP5-ilmastomallisimulaatioihin. Näistä aineistoista analysoitiin havaittuja lumi-, lämpötila- ja sadeolosuhteita jaksolla 1961-2014 sekä arvioitiin Itämeren jääpeitteen tulevia muutoksia vuoteen 2100 mennessä. Lisäksi työssä tehtiin kaksi mallinnustutkimusta: toisessa arvioitiin ECHAM5-ilmastomallin kykyä simuloida lumen sulannan ajankohtaa keväällä, ja toisessa tarkasteltiin säänennustusmalli HARMONIEN kykyä simuloida tunnettu rannikkolumisadetilanne.

Tulokset osoittivat, että lumensyvyys on Suomessa pienentynyt läpi vuoden ja lumikausi on lyhentynyt. Lisääntyneet talviaikaiset vesisateet olivat yksi pääsyy muutokseen. Keväällä myös lämpötilan nousu on vaikuttanut lumen vähenemiseen. Itämeren jääpeitteen vuotuisen maksimilaajuuden ja jäänpaksuuden arvioitiin pienentyvän kuluvalla vuosisadalla. On kuitenkin epätodennäköistä, että Itämeri muuttuisi kokonaan jäättömäksi tulevien vuosikymmenien tyypillisinä talvina.

Koska lumipeite on tärkeä osa ilmastojärjestelmää, on oleellista, että tulevaisuuden ilmasto-olosuhteita arvioivat ilmastomallit kuvaavat lumipeitteen realistisesti. ECHAM5-ilmastomalli kuvasi Pohjois-Euraasian lumensulannan ajankohdan yleisesti ottaen melko hyvin, mutta alueellisia eroja kuitenkin löytyi, kun tuloksia verrattiin satelliittihavaintoihin. Havaitut erot aiheutuivat yksinkertaistuksista ECHAM5-mallin maanpinnan säteilytaseen laskennassa. Myös HARMONIE-malli onnistui simuloimaan tunnetun rannikkolumisadetapauksen kohtuullisen hyvin. Simulaation tulokset paranivat, kun malliajoon lisättiin tutkahavainnot mukaan.

Kun ilmaston lämpeneminen etenee, talviolosuhteidenkin muutokset jatkuvat. Tämän väitöskirjan tulokset korostavat pohjoisten alueiden ilmasto-olosuhteiden jatkuvan seurannan tärkeyttä.

Julkaisijayksikkö

Sään ja ilmastonmuutoksen vaikutustutkimus

Luokitus (UDK)
591.54, 504.7, 551.578, 551.467, 303.733.3, 519.233.5

Asiasanat
ilmasto, ilmastonmuutos, lumipeite, lumisade, merijää, mallinnus, trendi, regressiomalli

ISSN ja avainnimeke
0782-6117 Finnish Meteorological Institute Contributions

ISBN
ISBN (paperback): 978-952-336-115-7
ISBN (pdf): 978-952-336-116-4

DOI
https://doi.org/10.35614/isbn.9789523361164

Kieli
englanti

Sivumäärä
63

ACKNOWLEDGEMENTS

Several people have helped in accomplishing this work. First, I would like to thank my supervisor Docent Kirsti Jylhä for all her support and guidance during this process which took a bit more time than I originally imagined. You have always had time for my questions and your advice has always shown a way forward. I would also like to thank Professor Heikki Järvinen for his support and for being my supervisor at the University of Helsinki. I wish to thank all my co-authors for their contributions, especially Dr. Juha Aalto, Dr. Sirpa Rasmus, Docent Petri Räisänen and M.Sc. Taru Olsson. I am also grateful to Professor Jukka Käyhkö for serving as opponent in my defence, and Professor Egidijus Rimkus and Dr. Mats A. Granskog for pre-examining this thesis.

This work was partially funded by the Academy of Finland projects SNOW-CLIM, ClimNext, MARISPLAN and PLUMES and by the State Nuclear Waste Management Fund project EXWE.

I acknowledge Finnish Meteorological Institute for providing me working facilities. I wish to thank my co-workers at Weather and Climate Change Impact Research unit, especially Hilppa Gregow, Antti Mäkelä, Natalia Korhonen and Sanna Luhtala for their help and support. I also thank all my co-workers in our unit for good working atmosphere and especially for refreshing morning coffee breaks during which it has been enjoyable to let thoughts and talks fly outside work-related issues.

Lastly, I wish to thank my friends and family, especially my parents, Leena and Lauri, for all their support and my dear husband Jaakko for his love and encouragement. You have always believed in me even in those moments when I have not. Finally, I wish to thank my three lovely daughters, Pinja, Helmi and Vilja, for teaching me patience which has been needed also with this work and for helping me in leaving work issues at work. You are my joy.

Anna Luomaranta

Espoo, June 2020

Table of Contents

LIST OF ORIGINAL PUBLICATIONS

I **Luomaranta, A.**, Aalto, J. and Jylhä, K. (2019) Snow cover trends in Finland over 1961–2014 based on gridded snow depth observations, *International Journal of Climatology*, 39, 3147– 3159. https://doi.org/10.1002/joc.6007.

II Rasmus, S., Turunen, M., **Luomaranta**, A., Kivinen, S., Jylhä, K. and Räihä, J. (2020) Climate change and reindeer management in Finland: co-analysis of practitioners knowledge and meteorological data for better adaptation, *Science of the Total Environment*, 710, 136229, https://doi.org/10.1016/j.scitotenv.2019.136229.

III **Luomaranta, A.**, Ruosteenoja, K., Jylhä, K., Gregow, H., Haapala, J. and Laaksonen, A. (2014) Multimodel estimates of the changes in the Baltic Sea ice cover during the present century, *Tellus A*, 66, 22617, http://dx.doi.org/10.3402/tellusa.v66.22617.

IV Räisänen, P., **Luomaranta, A.**, Järvinen, H., Takala, M., Jylhä, K., Bulygina, O. N., Riihelä, A., Laaksonen, A., Koskinen, J., and Pulliainen, J. (2014) Evaluation of North Eurasian snow-off dates in the ECHAM5.4 atmospheric general circulation model, *Geoscientific Model Development*, 7, 3037-3057, https://doi.org/10.5194/gmd-7-3037-2014.

V Olsson, T., Post, P., Rannat, K., Keernik, H., Perttula, T., **Luomaranta, A.**, Jylhä, K., Kivi, R. and Voormansik, T. (2018) Sea-effect snowfall case in the Baltic Sea region analysed by reanalysis, remote sensing data and convection-permitting mesoscale modelling, *Geophysica*, 53(1), 65-91.

Author's contribution

The author was solely responsible for the summary of this thesis. In **Paper I**, the author was responsible for most of the data analysis and did all the writing with the help of the co-authors, excluding the beginning of chapter 2 (before 2.1). In **Paper II**, the author participated in analyzing the winter-related variables from the meteorological data and writing of chapters 2.3, 3 and 4. In **Paper III**, the author was responsible for all the calculations and data analysis except for those concerning the selection and evaluation of climate model simulations. The author participated in most of the writing excluding chapters 2.1.2 and 2.1.3. In **Paper IV**, the author participated in planning and analyzing part of the ECHAM5 simulations and satellite observations. The author participated in the writing of chapters 1, 2.1, 5.1 and 6. In **Paper V**, the author participated in analyzing the HARMONIE simulations.

LIST OF ACRONYMS

AIREP	Aircraft weather report
ALB1	Simulation with prescribed surface albedo
ALB1_NDG	Simulation with prescribed surface albedo and nudging
ALB2	Simulation with modified surface albedo parameterization
ALB2_NDG	Simulation with modified surface albedo parameterization and nudging
AMDAR	Aircraft based meteorological observation system
BEG	The beginning time of the seasonal snow cover period
BUOY	Buoy observations
CLARA-SAL	Data set of observed surface albedos
CMIP5,6	Coupled Model Intercomparison projects, phase 5 and 6
DJF	December, January, February
ECHAM5	Atmospheric general circulation model
ECMWF	European Center for Medium Range Weather Forecasts
E-OBS	Gridded climate data set for Europe
FDD-model	Freezing Degree-Day model
FMIClimGrid	Finnish Meteorological Institute gridded climate data for Finland
GCM	General circulation model
h	fast ice thickness
HARMONIE	High-resolution weather prediction model
ID	Ice days, Number of days when the daily maximum temperature is equal or less than 0°C
IFS	Integrated Forecast System, an operating global forecasting system
LAI	Leaf area index
MAXSN	Annual maximum snow depth
MIB	Annual maximum ice extent in the Baltic Sea

NDJFM	November, December, January, February, March
NF	Study domain in northern Finland
PILOT	Wind profiler observations
PR	Precipitation
PR_s	Solid precipitation
Rain-d	Rain days, Number of days when the daily precipitation is at least 1mm and the daily minimum temperature is at least 0 °C
RCP	Representative Concentration Pathway, a scenario that describes a possible greenhouse gas concentration trajectory
RCP4.5	Scenario with mid-range development in greenhouse gases
RCP8.5	Scenario with very high greenhouse gas concentrations
REF	Reference simulation
REF_NDG	Reference simulation which uses nudging
S	The annual cumulative (°C x d) sum of daily mean temperatures below 0 degrees (freezing degree-day sum)
SAI	Stem area index
SF	Study domain in southwestern Finland
SHIP	Sea-based stations
SOD	Snow-off date
SWE	Snow water equivalent
SYNOP	Surface synoptic observations
T	Temperature
TEMP	Radiosonde weather observations
TMAX	Maximum temperature
UTC	Coordinated Universal Time
ΔT	Temperature change

1. INTRODUCTION

Finland is a country of four seasons. Thermal winter, meaning the period of the year when the daily mean temperature stays below 0°C, is the longest season in a large part of Finland. (https://en.ilmatieteenlaitos.fi/seasons-in-finland). Due to the length of the winter, society needs to be well-informed of the prevailing cold-season climate conditions to understand the possible risks and benefits they may cause. If the prevailing conditions change, society needs to adapt to the changes.

Finland is located between a very maritime and a continental climate and also in the pathway of moving low pressure systems from the west, which makes the climate conditions variable. In winter, low pressure areas from the west typically bring moist and warmer air with precipitation to Finland. On the other hand, temperature can drop to very low degrees, if Arctic air masses from the north and east prevail. Also the Baltic Sea affects the weather and climate conditions especially near the coast areas. Depending on temperature, the winter precipitation falls as snow, sleet or rain.

Snow and sea ice are an essential part of winter climate in Finland. Snow and ice cover affect society and its inhabitants in many ways. Snow cover serves multiple recreation possibilities in winter time (Hall, 2014; Neuvonen et al., 2015) and protects vegetation from cold. It is also a storage of fresh water. On the other hand, snow may cause problems for transportation and electricity distribution (e.g. Andersson, 2010; Juga et al., 2014), and sea ice affects the shipping in wintertime (Critch et al., 2013). Furthermore, the amount and extent of snow and ice cover and changes in them are a sensitive indicator of climatic conditions in the region. Assessments of the possible changes in the sea ice cover and snow conditions will help societies to adapt to changes.

Finland is surrounded by the Baltic Sea from the south (Gulf of Finland), southwest (Archipelago Sea) and west (Gulf of Bothnia). It is common that these sea areas partly or totally freeze during winter, and the ice cover is present on average five months from December to April (Raateoja and Setälä, 2016). The ice cover in the Baltic Sea will face

changes in response to global warming. A longer ice-free season of the Baltic Sea will again affect the climatic conditions of the surrounding regions. If a sea area remains ice-free in winter, it serves as a constant source of moisture and heat. If cold and dry air masses flow over the ice-free sea area, beneficial conditions for intensive convective snow bands to occur are generated. This sea-effect snowfall phenomenon is a typical part of Finland's winter climate. With certain wind directions, these snow showers may hit the coastline and cause problems to traffic, for example.

Objectives of this thesis

While global warming continues, it is the local effects that humans can perceive and that affect humans and society the most. This emphasizes the importance of local-scale climatological research. The main purpose of this thesis is to examine what the winters are like in Finland in the changing climate. This issue is addressed through the following questions:

- What changes have occurred in snow conditions and factors affecting them in Finland (**Papers I** and **II**)?
- What changes are expected to occur in sea ice conditions surrounding Finland (**Paper III**)?
- What factors affect climate model performance in simulating snow melt timing (**Paper IV**)?
- Based on a case study, how well can a sea-effect snowfall event be simulated over the Baltic Sea (**Paper V**)?

This thesis is organized as follows: In section 2, a review of snow- and ice-related climatological research is first given to put the results of this thesis in a broader context. In section 3, the approaches that were used in this thesis are introduced. Section 4 describes the observed conditions and changes in temperature, precipitation and snow cover in Finland and section 5 presents the future projections for Baltic Sea ice cover. In section 6, two examples of modeling studies benefiting climate research are presented. Finally, the results are summarized and discussed and the research questions are answered in section 7.

2. BACKGROUND

Warming due to the anthropogenic greenhouse effect is projected to be strongest in the northern areas of the Earth where also Finland is located. The observed and projected annual average temperature increase in the Arctic is assessed to be more than twice as strong as the global mean temperature increase (AMAP, 2019; Meredith et al., 2019). The warming in the north is largest in winter. Rising temperatures accelerate the melting of snow and ice, which has many direct and indirect impacts on the physical, chemical and biological systems in the Arctic area. The changes in the Arctic may also affect the conditions outside the region, for example through the changes in the atmospheric or ocean general circulation (AMAP, 2019; Meredith et al., 2019).

Snow and ice cover are the most important factors in the climate of the Northern Hemisphere and their presence in winter is typical at high latitudes. Snow and ice cover have a high albedo. Albedo is the fraction of solar radiation that is reflected from the surface. High albedo means that a large part of the incoming solar radiation is reflected back into space. This tends to cool the climate. When snow and ice decrease, surface albedo also decreases and a larger part of the incoming solar radiation is absorbed by the surface. This leads to warming which further reduces the ice and snow. Thus, this snow/ice-albedo feedback affects the energy budget of the Earth and highlights the significance of ice and snow cover in the climate system (Abram et al., 2019).

In several studies the recent past state and changes of the snow conditions have been reported at different spatial scales, ranging from the whole Northern Hemisphere (e.g. Brown and Mote, 2009; Choi et al., 2010; Park et al., 2012; Callaghan et al., 2012; Vaughan et al., 2013; Hernández-Henríquez et al., 2014; Mioduszewski et al., 2015; Derksen et al., 2016) or Eurasia (Bulygina et al., 2011; Ye and Cohen, 2013; Zhong et al. 2018) to individual countries or smaller districts within them (e.g. Kohler et al., 2006; Brown, 2010; Skaugen et al., 2012; Kerr et al., 2013; Stuefer et al., 2013; Najafi et al., 2016). The magnitude of the changes has not been spatially uniform in the Northern Hemisphere. For example, the changes in snow depth have differed between North America and Eurasia: an increase in snow depth in many regions over Eurasia was observed during the period 1966-2009, while in North America

decreasing snow depth trends occurred (Bulygina et al., 2011, Callaghan et al., 2012). On the other hand, updated trends in maximum snow depth over Russia in 1966-2014 show less evidence of significant increases compared to trends reported by Bulygina et al. (2011) (AMAP, 2017). Also Park et al. (2012) reported wide-spread negative snow depth trends in most of pan-Arctic after about 1990, clear positive trends occurring only in Western Siberia. Within Eurasia, the changes in snow conditions vary substantially depending on the latitude, elevation and the proximity to the sea. The largest decreases in snow water equivalent (SWE) and snow cover duration in recent decades have occurred in maritime regions in northern Scandinavia and the Pacific coast region of Russia (Callaghan et al., 2012).

Two main factors which affect snow conditions are temperature and precipitation (e.g. Räisänen, 2008; Brown and Mote, 2009; Mankin and Diffenbaugh, 2015; Mudryk et al., 2016). Temperature defines the form of precipitation, which affects the amount of snow on the ground. Besides altering the amount and form of precipitation, increasing temperatures also affect the snow cover by either increasing or decreasing the number of thaw days, the sign of the change depending on the prevailing baseline mean temperatures. In the late 20th century, the borderline between increasing and decreasing snow water equivalent (SWE) was found to have mainly corresponded to the -20°C isotherm of the cold season (NDJFM) mean temperature (Räisänen, 2008). The midlatitude snow margin zone was the most sensitive region for snow loss due to warming in 1981-2010 (Mudryk et al., 2016). Mankin and Diffenbaugh (2015) found that in 8 out of 9 of their study regions in the Northern Hemisphere near-future March snow accumulation trends responded negatively to temperature increases and all their study regions exhibited reductions in the fraction of precipitation falling as snow. However, internal variability can influence the magnitude of snow accumulation trends. Brown and Mote (2009) noted that, among various snow variables, snow cover duration has the strongest sensitivity to warming. They discovered that the largest decreases in Northern Hemisphere snow cover duration in 1966-2007 were located in a zone where the mean air temperature of the snow season varied from -5 to +5 degrees Celsius.

Climate model results project that drastic changes in snow conditions are expected to continue during the ongoing century (Bintanja and Andry, 2017). Mid-winter SWE and maximum SWE are projected to increase in the coldest regions of the Northern Hemisphere (Räisänen,

2008; Callaghan et al., 2012; AMAP, 2017), elsewhere SWE is expected to decrease. In spite of the projected increases in SWE in the coldest regions, snow season is expected to shorten at both ends in the whole Northern Hemisphere (Räisänen, 2008; Callaghan et al., 2012; AMAP, 2017). In Europe, the largest percentage reductions in the number of snow cover days and the average SWE are projected to occur in southern and western Europe (Jylhä et al., 2008). In Northern Fennoscandia, the annual number of snow cover days is projected to decrease most in the coastal regions and least in the mountainous areas (Lehtonen et al., 2013). In Northern Europe, the regional and interannual variability is projected to remain high: individual snow-rich winters can still occur in the future decades even where the long-term mean SWE is projected to decrease (Räisänen and Eklund, 2012). Snowfall is also projected to decrease across much of the Northern Hemisphere in the 21st century, the transition between negative and positive seasonal and annual trends occurring close to the corresponding average -10°C isotherms over the period 1986-2005 (Krasting et al., 2013). At the same time, rainfall is projected to increase throughout the year (Bintanja and Andry, 2017). In midwinter in the coldest regions, snowfall is still projected to increase (Räisänen and Eklund, 2012; Räisänen, 2015; Danco et al., 2016; Krasting et al., 2016) but the snowfall fraction is expected to decrease due to increasing rainfall (Bintanja and Andry, 2017). When using climate model data, it is important to realize that climate models have deficiencies and the model physics include simplifications and parametrizations. For example, many different processes affect the snow conditions in a climate model and improving a single process may either improve or deteriorate the agreement with observations.

Arctic sea ice extent has decreased since 1979 in each month (Meredith et al., 2019). The decrease has been largest in summer and smallest in winter. The loss of sea ice on a more regional scale is seen also in the Baltic Sea, which is a small inland sea bordering Finland in the south and west. Annual maximum ice extent in the Baltic Sea (MIB) has been monitored fairly accurately from 1880 onwards (Haapala et al., 2015). A large interannual variability is typical for the annual maximum ice extent. Still, a significant decreasing trend in MIB (-3400 km^2/decade or -2%/decade) has been observed for the past 100 years (1912-2011) (Haapala et al., 2015). In addition, a decreasing trend in the length of the ice season in the Finnish coastal zone has been observed (Ronkainen, 2013). In the Bothnian Bay (Kemi), the trend was -18 days/100 years and in the eastern Gulf of Finland (Loviisa) -41 days/100 years.

The decline of the Arctic sea ice is projected to continue through the ongoing century, but there is a large spread in the climate model results concerning the timing of when the Arctic may become ice-free in the summer (Meredith et al., 2019). Also the Baltic Sea ice will continue to face changes. Höglund et al. (2017) used a coupled ice-ocean model system with two global climate models and two scenarios to predict the future changes in the ice conditions of the Baltic Sea. According to their results, the annual maximum ice extent will decrease 46-57% under the RCP4.5 scenario, which describes a mid-range development in greenhouse gas concentrations, and 81-82% under a very high greenhouse gas scenario, RCP8.5, by the end of the century. Also the ice thickness and the length of the ice season were projected to decrease. The decrease in the ice extent and thickness can lead to increased ice mobility and thus more ridging events.

3. APPROACHES FOR STUDYING COLD CLIMATE FEATURES

The specific topics and materials used in this thesis are presented in Fig. 1. Several different data sets and approaches were used. Data sets consisted of observations and model-based data and they were used together or separately with different methods to gain information of observed winter climate conditions and future projections of sea ice. Observations and model-based data were both utilized also in two modeling studies concerning climate model performance in snow-melt timing and a sea-effect snowfall event. In this chapter, the different data sets are first introduced and then the methods are presented. Lastly, two numerical modeling experiments are described.

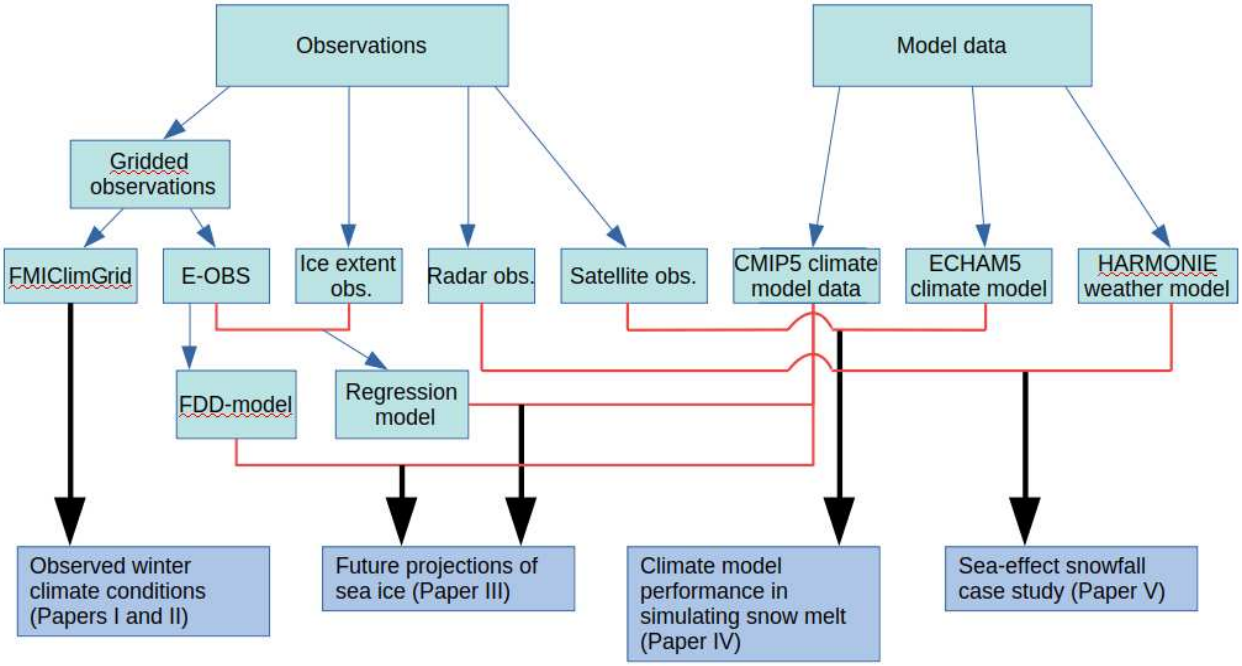

Figure 1. Flow diagram showing the main topics and materials of the thesis.

3.1 Data

3.1.1 Gridded datasets based on in situ -observations

Weather observations are made all around the world. Station observations tell us about the weather conditions only at a certain station and its direct vicinity. To get a more comprehensive picture of conditions and changes, gridded datasets are an advantageous approach for analysis.

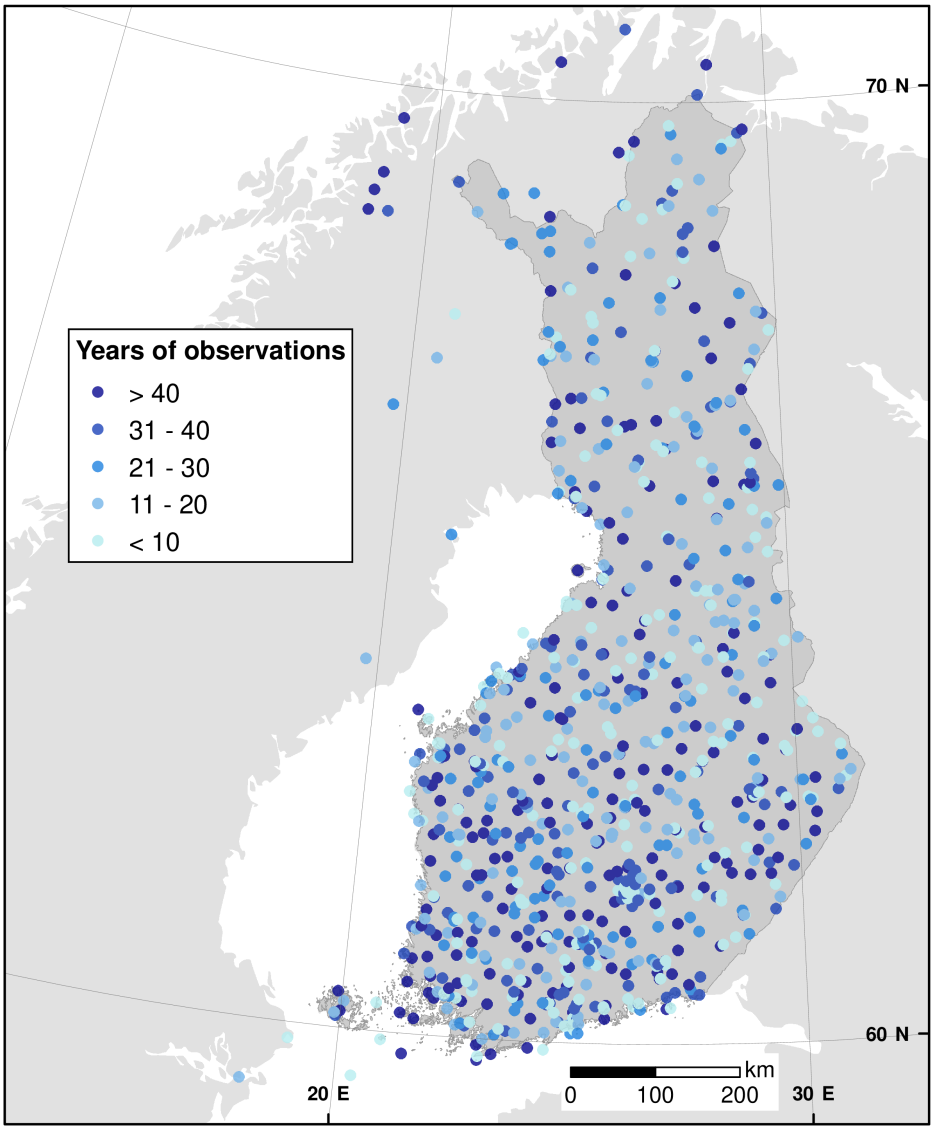

Figure 2. The station network that was used for producing gridded snow depth data. The points denote the stations in Finland and in neighboring countries. The colors indicate the total numbers of years with snow depth observations. (Reproduced from Fig. 1 of ***Paper I****.).*

The past conditions and changes in temperature, precipitation and snow cover were assessed using the daily gridded climate data for Finland (FMIClimGrid, version 1.0, Aalto et al. 2016). In this data set, meteorological station data is interpolated to a 10 km x 10 km grid, which covers whole Finland. The gridding of the station observations was produced with kriging interpolation (Matheron, 1963; Goovaerts, 2000). The background information for the

interpolation took into account the geographical locations of the stations, topography and the effects of water bodies. In Fig. 2, the station network used for producing gridded snow depth data is shown. In **Paper I**, precipitation, temperature and snow depth, and variables related to them, were examined. These were analyzed from FMIClimGrid data for the years 1961-2014 for the whole of Finland. In **Paper II**, we examined these variables for the shorter time range of 1981-2010 and a smaller study region which covered the reindeer management area in Finland.

In **Paper III**, we used E-OBS daily gridded dataset version 6.0 for the years 1951-1960 and version 7.0 for the years 1961-2012 (Haylock et al., 2008) together with observed values of annual maximum ice extent in the Baltic Sea (MIB) for the years 1951-2012. E-OBS gridded dataset is a dataset which covers Europe in a 0.1 or 0.25 degree grid. It includes temperature, precipitation and sea level pressure on land areas. In this work, we utilized data with a resolution of 0.25 degrees.

3.1.2 Climate model data

Future climate changes are assessed using climate models. **Paper III** used the air temperature data of simulations from 28 CMIP5 global climate models in projecting the future changes in the Baltic Sea ice cover. These simulations were under two greenhouse gas scenarios: RCP4.5 and RCP8.5 (Moss et al. 2010, van Vuuren et al. 2011). The former represents mid-range development in greenhouse gas concentrations and the latter represents very high greenhouse gas concentrations. The differences between the scenarios are small at the beginning of our study period, but increase over time.

Monthly mean temperature data for both scenarios were available for a total of 35 climate models. However, we excluded those models from the analysis that failed to meet three fundamental conditions. First, the simulated global mean temperature trend during the past 50 years was not allowed to exceed the observation-based estimate by more than 0.4°C. Second, the projected global mean temperature increase under the various RCP scenarios was not allowed to behave inconsistently, meaning that for an individual model the ratio of temperature responses to e.g., RCP8.5 and RCP4.5 scenarios was not permitted to notably differ from the multimodel median of that ratio. Third, the simulated baseline-period

climatological mean temperature and/or precipitation in Europe was not allowed to deviate markedly from the observations. Fulfilling these conditions led to the exclusion of seven models from the analysis.

The climate model data were smoothed by applying a 30 yr running mean and interpolated onto the same 0.25° grid as in E-OBS gridded dataset.

3.1.3 Other observations

Besides the gridded data, which was introduced in section 3.1.1, several other observation-based data sets were utilized in this work as reference material.

Observations of the annual maximum ice extent of the Baltic Sea (MIB) were used in **Paper III**. MIB is the most widely used parameter to indicate climate variability in the Baltic Sea region. Its recordings date back to 1720 (Seinä and Palosuo, 1996), but the most reliable observations begin in the late 19th century (Vihma and Haapala, 2009). We used MIB observations from the years 1952-2012. Furthermore, observations of the annual maximum ice thickness available for Kemi (63.73°N, 24.55°E) and Loviisa (60.42°N, 26.27°E) in 1971-2000 (Jevrejeva et al., 2002) were also used in **Paper III**.

2 m air temperature observations from Climate Research Unit (CRU) land surface air temperature data, v. 3 (CRUTEM3; Brohan et al. 2006) was employed in **Paper IV** as well as monthly mean surface albedo from the CLARA-SAL data set (Riihelä et al., 2013). Also satellite observations of snow melt timing over Northern Eurasia (Takala et al. 2009) were utilized in **Paper IV**.

Weather radar observations from Finland was used in **Paper V** as reference material for a sea-effect snowfall modeling study with weather prediction model HARMONIE (see Chapter 3.3.2).

3.2 Methods

3.2.1 Analyzing temporal averages and trends from the FMIClimGrid data

The following averages and trends of snow-related quantities were analyzed from FMIClimGrid data for the period 1961-2014 in **Paper I**:

- Monthly mean snow depth calculated from daily values.
- Annual maximum snow depth.
- The beginning time of the seasonal snow cover period (BEG): the first day after the autumn's last snow-free day when the snow depth reaches at least 1 cm.
- Snow-off date (SOD): the first snow-free day in spring after the winter's maximum snow depth. The maximum snow depth was assumed to occur after January 1st.

For two shorter time periods (1961-1987 and 1988-2014) and two smaller study domains, we also examined temperature- and precipitation-related quantities and the role of these in controlling snow depth (**Paper I**). These study domains represent two contrasting snow climate regimes within Finland: a southwestern maritime region (SF) and a northern region with Arctic conditions (NF). These quantities included:

- Monthly mean temperature (T): temperature affects the form of precipitation and melting of snow.
- Monthly mean amount of precipitation (PR): precipitation may increase or decrease the snow amount depending on its form.
- Monthly mean maximum temperature (TMAX).
- Monthly mean amount of solid precipitation (PR_s): precipitation falling on a day when daily maximum temperature is equal to or less than 0°C.

The significance of the change in these quantities over the two time periods was assessed for each month and winter period (DJF) using two-sided Mann-Whitney-tests.

For the shorter time period of 1981-2010 we analyzed averages, trends and standard deviations of following quantities in autumn, winter and spring for the reindeer management area in Finland (**Paper II**):

- Ice days (ID): Number of days when the daily maximum temperature is equal to or less than 0°C.
- Rain days (Rain-d): Number of days when the daily precipitation is at least 1 mm and the daily minimum temperature is at least 0°C.
- Annual maximum snow depth (MAXSN).
- The beginning time of the seasonal snow cover period (BEG).
- Snow-off date (SOD).

3.2.2 Regression model for predicting sea ice extent

E-OBS data and observations of the maximum ice extent in the Baltic Sea (Fig. 1) were combined to form a simple non-linear regression model, following Tinz (1996) and Jylhä et al. (2008). This model was then used with CMIP5 data to predict the future sea ice conditions. The regression equation was given by:

$$MIB = A e^{-BT} \quad (1)$$

where MIB is the annual maximum ice extent (km^2) and T is the November-March mean temperature (°C) averaged over the coastal grid points around the Baltic Sea. Based on the data (Fig. 3), the following values were derived for the coefficients: A= (90.2 ± 4.2) x 10^3 km^2 and B = (0.253 ± 0.015) $°C^{-1}$.

The regression model was used with E-OBS and CMIP5 climate model data to project the future changes in the annual maximum ice extent in the Baltic Sea. For assessing the future temperature, a simple delta-change method was used. We first calculated the change in November-March mean temperature, ΔT, at coastal grid points between the baseline period 1971-2000 and each of the seven future decades in the period 2021-2090 using CMIP5 air temperature. ΔT for each decade was calculated as a 30 yr mean, centered on that decade. For example, mean T in 2011-2040 represents the decade 2021-2030. These temperature increases for each future decade were added to the observed E-OBS mean temperature values in 1961-2010 (50 values) to create an artificial temperature distribution for each future decade. Next, these samples of T were used in Eq. 1 to obtain the frequency distribution of MIB for each of the future decades. The uncertainty in the results was assessed by performing the calculations

for each climate model and for both RCP scenarios. Also the 28-model average temperature was used in calculations to get a best estimate for the long-term trends. The model uncertainty assessment focused on the decade 2041-2050.

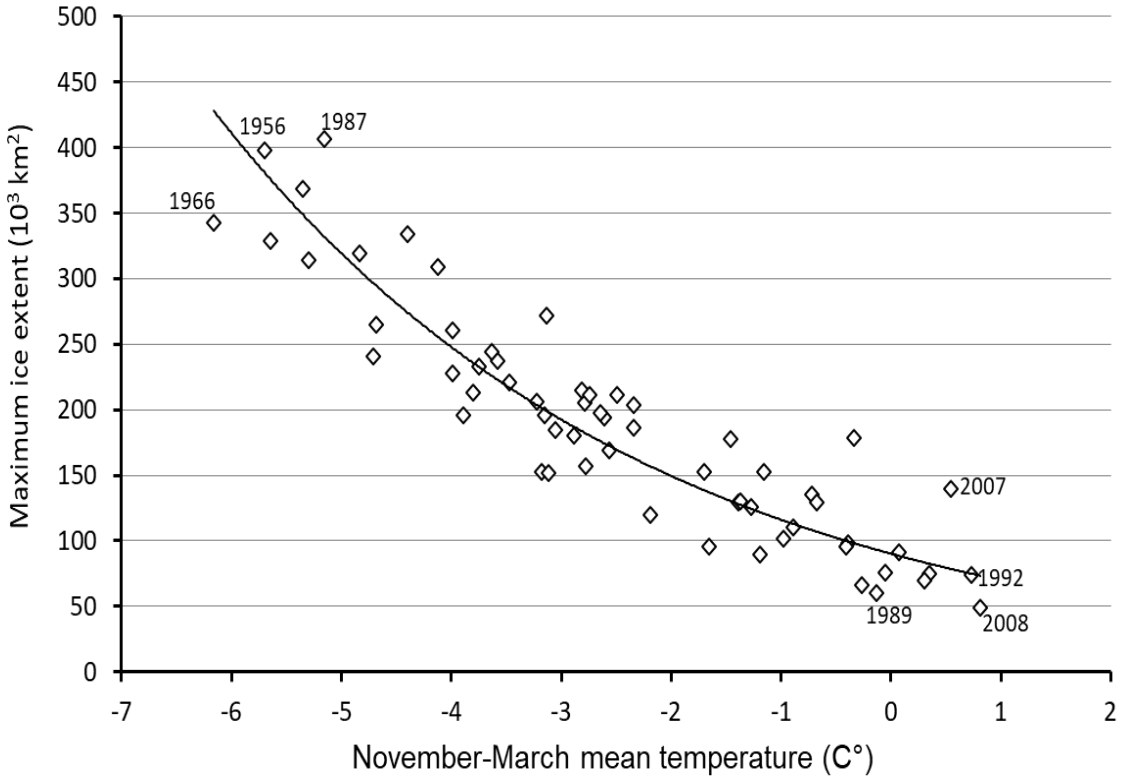

Figure 3. The regression model for the ice extent in the Baltic Sea. The model was fitted to the observed annual maximum sea ice extent and the November-March mean temperature in coastal grid points in 1951-2012. (Reproduced from Fig. 4 of ***Paper III****.)*

3.2.3 FDD-model for sea ice thickness

The 30 yr mean of the annual maximum fast ice thickness, h, was calculated using an analytical solution for the thermodynamic ice growth equation that is based on the sum of freezing-degree days (Stefan, 1891; Zubov, 1945; Leppäranta, 1993), so-called FDD-model (**Paper III**):

$$h = \sqrt{a^2 S + d^2} - d \quad (2)$$

where S = the annual cumulative (°C x d) sum of daily mean temperatures below 0 degrees (freezing degree-day sum), a = 3 cm(°C x d)$^{-1/2}$, d = 10 cm.

The sum of the freezing-degree days for future decades, that was needed in Eq. 2, was calculated from air temperature output data from the CMIP5 simulations. The changes in 30 yr monthly mean temperatures in coastal grid points, ΔT, for each decade in 2021-2090, were added to the observed 30 yr monthly mean temperatures in 1971-2010 derived from E-OBS. The sum of the freezing-degree days was obtained from monthly mean temperatures of each decade as follows: the negative monthly mean temperatures were multiplied by the number of days in the month. Then the sum of the contributions of all months with negative mean temperature was used in Eq. 2. These calculations were performed separately for temperatures of each CMIP5 model and for the 28-model mean.

Equation (2) does not take into account the snow layer lying on top of the ice cover. Ice thicknesses are thus systematically overestimated by up to 40 cm. The ice thickness calculated using (2) can be considered as the upper limit for the ice growth in a typical winter (Leppäranta, 1993). As the E-OBS gridded temperatures cover only land areas, the ice thickness could only be assessed in the coastal areas.

3.3 Numerical model experiments

3.3.1 ECHAM5 simulations

As the snow cover has both global and local climatic impacts, it is essential that climate models that are used to project future climate, produce the observed distribution of snow cover realistically. **Paper IV** examined the ability of ECHAM5.4 atmospheric general circulation model (GCM) to simulate the Northern Eurasian snow melt timing in 1979-2006 as an example of climate models. The model was used in resolution T63 which corresponds to a grid spacing of 1.875 degrees (Roeckner et al., 2003, 2006).

In ECHAM5's snow scheme, snow water equivalent (SWE) is a prognostic variable, but changes in snow density or grain size are not taken into account in the snow-related model

physics. In the model, SWE intercepted by the canopy (Roesch et al. 2001) and SWE on the ground (Roeckner et al. 2003) are calculated separately. The grid-mean surface albedo, which is closely related to the snow cover, is parameterized and it depends on the specified background albedo, the fractional forest area of the grid cell, the snow cover on the canopy, the snow cover on the ground and a specified snow albedo. The albedo of snow on land depends on the surface temperature and the albedo of snow-covered forests depends on the leaf-area index (LAI). A complete description of the parameterization is found in Roeckner et al. (2003).

First, a reference experiment (REF) was run using the default version of ECHAM5.4 in an ordinary climate simulation mode. The experiment was conducted for years 1978-2006 and all but the first year were used for analysis of the results. The snow-off date was evaluated in the experiment results based on daily mean SWE values. The snow-off date was defined to be the first day with zero SWE after a winter's maximum SWE. This definition is the same as was used for SOD in **Paper I** and **II**, except that in these **Papers** SOD was calculated using snow depth instead of SWE. The results from the REF experiment were compared to satellite observations of SOD and differences between these were found. In order to explain the discrepancies, we performed five more ECHAM5 experiments, where the model's surface albedo and/or atmospheric circulation was modified.

All six experiments used observed sea surface temperatures and sea ice (AMIP Project Office, 1996) as boundary condition and the concentrations of well-mixed greenhouse gases were held constant following AMIP II guidelines (AMIP Project Office, 1996). As surface albedo strongly influences the energy available for melting snow in spring, in two of the experiments, ALB1 and ALB2, the reduction of the biases in ECHAM5's surface albedo was attempted by modifying the model's surface albedo field. In experiment ALB1, the model's albedo field over continents was replaced by prescribed surface albedos based on observations (CLARA-SAL, Riihelä et al., 2013). In ALB2, two modifications were implemented in ECHAM5's surface albedo parameterization. First, the minimum snow albedo value was increased from 0.3 to 0.6. Second, a stem area index (SAI=2) was added to the equation which is used for calculating the albedo of snow-covered forests, as it was noted

by Roesch and Roeckner (2006) that the shadowing of the ground below the canopy by stems and branches was neglected in ECHAM5.

The remaining three experiments (REF_NDG, ALB1_NDG, ALB2_NDG) were primarily similar to the other three experiments (REF, ALB1 and ALB2), except that so-called nudging was used in all of them. In these nudging experiments four model fields were nudged towards ERA-Interim reanalysis data (Dee et al., 2011): vorticity, divergence, atmospheric temperature and logarithm of surface pressure. The nudging acts to minimize the errors in simulated atmospheric circulation, which is one possible cause for differences between simulated and observed snow-off dates.

3.3.2 HARMONIE simulations

Winter climate in Finland includes many small-scale weather events. One such is the so-called sea-effect snowfall phenomenon which is a common occurrence in sea areas around Finland in winter. **Paper V** examines the use of a high-resolution numerical weather prediction model, HARMONIE, together with other datasets for investigating the basic characteristics of a sea-effect snowfall case.

HARMONIE is a numerical convection-permitting mesoscale model (Bénard et al., 2010, Brousseau et al., 2011). In this kind of high-resolution models, the small-scale convective phenomena can be resolved and convection parameterization schemes are no longer needed. This is advantageous, as parameterization of convection is a large source of error and uncertainty in lower-resolution models (Prein et al., 2015, Weusthoff et al., 2010).

In our model setup, model version 40h1.1 was used and the model resolution was 2.5 km. The simulation domain covered Finland, Scandinavia and the Baltic countries. The boundary conditions were obtained from the Integrated Forecast System (IFS), which is an operational global forecasting system at ECMWF. The boundary conditions were updated every hour. Data assimilation is used in HARMONIE meaning that a running model simulation is corrected at regular time intervals with observations. The basic set of observations consisted of surface synoptic observations (SYNOP), sea-based stations (SHIP), aircraft reports

(AMDAR, AIREP), buoy observations (BUOY), radiosondes (TEMP) and wind profiler (PILOT) observations.

We ran two experiments with the HARMONIE model to simulate the selected sea-effect snowfall case. In the reference simulation, the above-mentioned basic set of observations was assimilated to the model. In the second simulation also radar reflectivities were utilised. The purpose was to examine if the assimilation of the radar reflectivities improves the simulation results. Both of the simulations consisted of several forecast cycles. We also qualitatively evaluated which cycle gave the best results compared to radar observations. The results from HARMONIE simulations were also compared to some other observational data in **Paper V**, but the focus in this thesis is on the HARMONIE model and its results.

4. OBSERVED WINTER CLIMATE CONDITIONS IN FINLAND

4.1 Temperature and precipitation

Temperature and precipitation are the main variables affecting snow conditions and other winter climate characteristics in Finland. In **Paper I**, changes in these were examined at monthly scale in two smaller domains (boxes in Fig. 6) between periods 1961-1987 and 1988-2014. These domains represented two contrasting snow climate regimes within Finland: SF in the southwestern maritime region and NF in the northern region with Arctic conditions. In **Paper I**, we also studied the changes in solid precipitation. The amount of solid precipitation was assessed so that the total precipitation falling on a day when the maximum temperature was less than or equal to zero degrees Celsius was classified as solid precipitation. Our findings indicated that in SF, both the monthly mean and monthly maximum temperatures (T and TMAX) increased in January-April and total precipitation increased in January and February (Fig. 4). In SF, the amount of solid precipitation did not change but the fraction of solid precipitation decreased in January and February meaning that the increase in total precipitation was due to increases in mixed and liquid precipitation.

In NF, T and TMAX increased in some winter and spring months, but because of the colder baseline climate they stayed below zero also during the latter period (Fig. 5). Solid precipitation was found to increase when the three months' sum over the winter months, December-February (DJF), was examined. Also total precipitation and mixed and liquid precipitation were found to increase when they were calculated over the DJF period. The changes in the annual amount of solid precipitation divided Finland into two parts (Fig. 6.). In northern and eastern Finland, solid precipitation increased in 1961-2014 whereas in southern and western Finland it decreased.

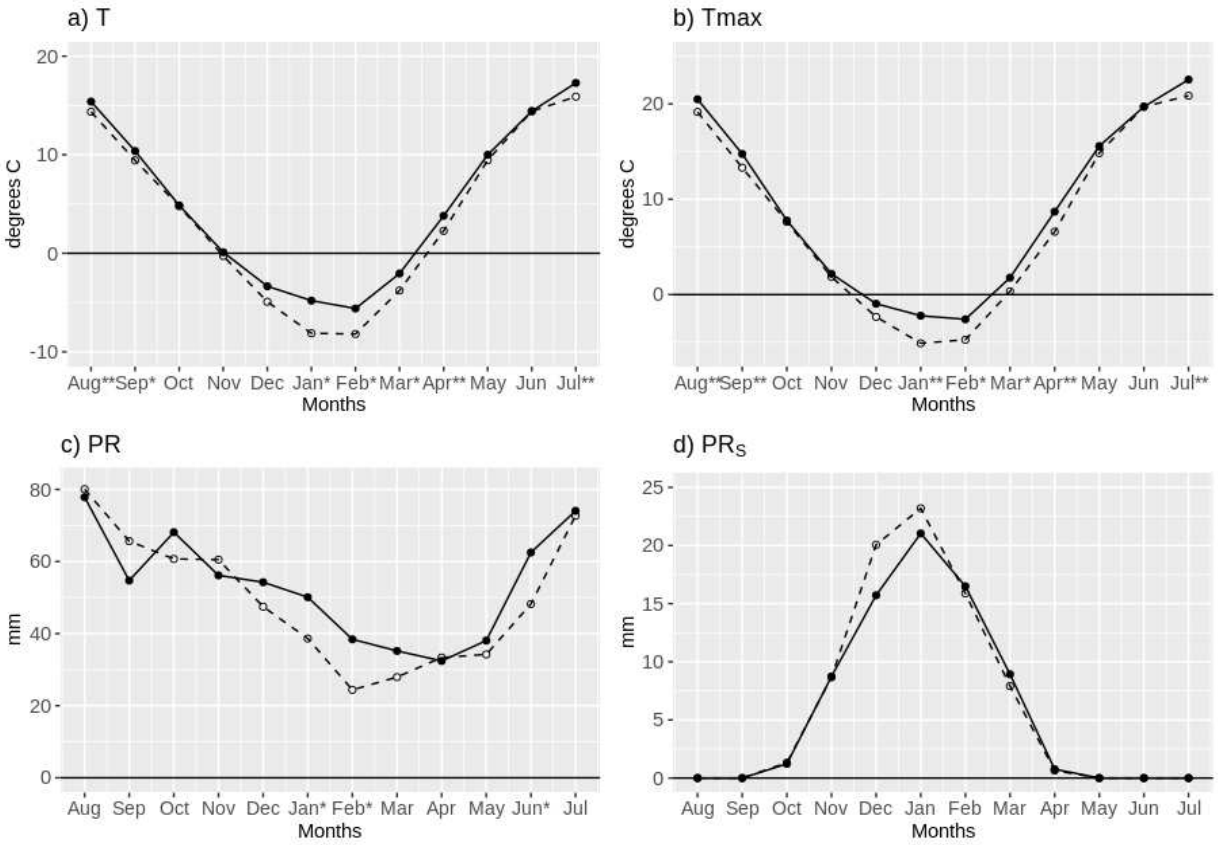

*Figure 4. Twenty-seven-year mean seasonal cycles of monthly mean temperature (a,T), monthly maximum temperature (b, TMAX), monthly mean amount of precipitation (c, PR) and monthly mean solid precipitation (d, PR_s) in southern Finland (SF). The dashed line indicates the 1961-1987 period and the solid line indicates the 1988-2014 period. The months when the change between the two periods is statistically significant at the 5% level and 1% level according to two-sided Mann-Whitney tests are denoted by * and **, respectively. (Reproduced from Fig. 4 of* ***Paper I****.)*

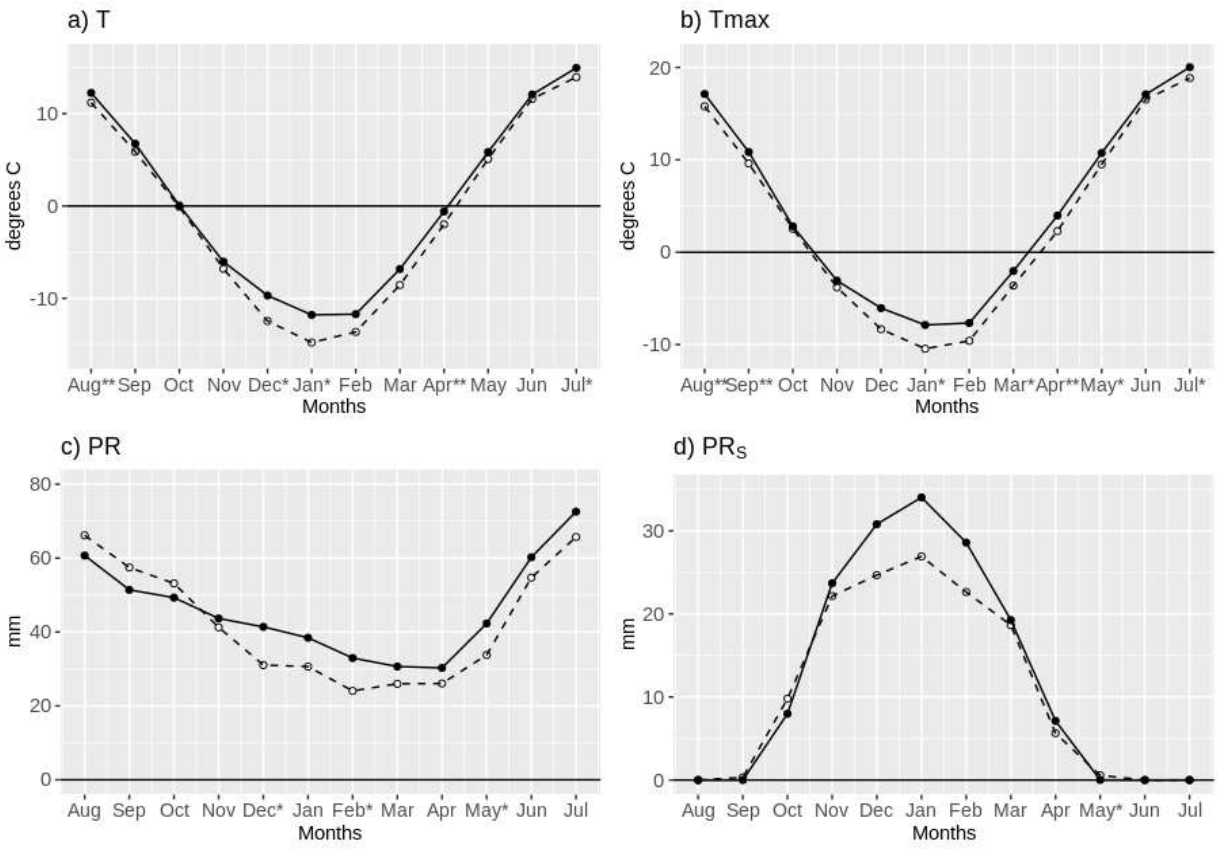

*Figure 5. As in Fig. 4 but for northern Finland (NF). (Reproduced from Fig. 5 of **Paper I**.)*

In **Paper II**, changes in rain days and ice days were examined in autumn, winter and spring in 1981-2010. A rain day was defined to be a day when the minimum temperature was above or equal to zero and daily precipitation amount was at least 1 mm. An ice day was defined to be a day when the maximum temperature was 0 degrees at the highest. Slight local statistically significant increases in the number of rain days in winter in the southern part of the reindeer management area were found in 1981-2010. There was no clear trend in the number of ice days in autumn or winter. In spring, the number of ice days was declining in the northwestern areas of the reindeer management area (Fig. 7.), locally 3-5 days/decade. The standard deviation of ID in these regions was 0.5-3 days. In spring, the rain days were found to slightly increase, especially in the southern parts of the reindeer management area. This trend was 2-3 days/decade and the corresponding standard deviation was 3-5 days in these areas.

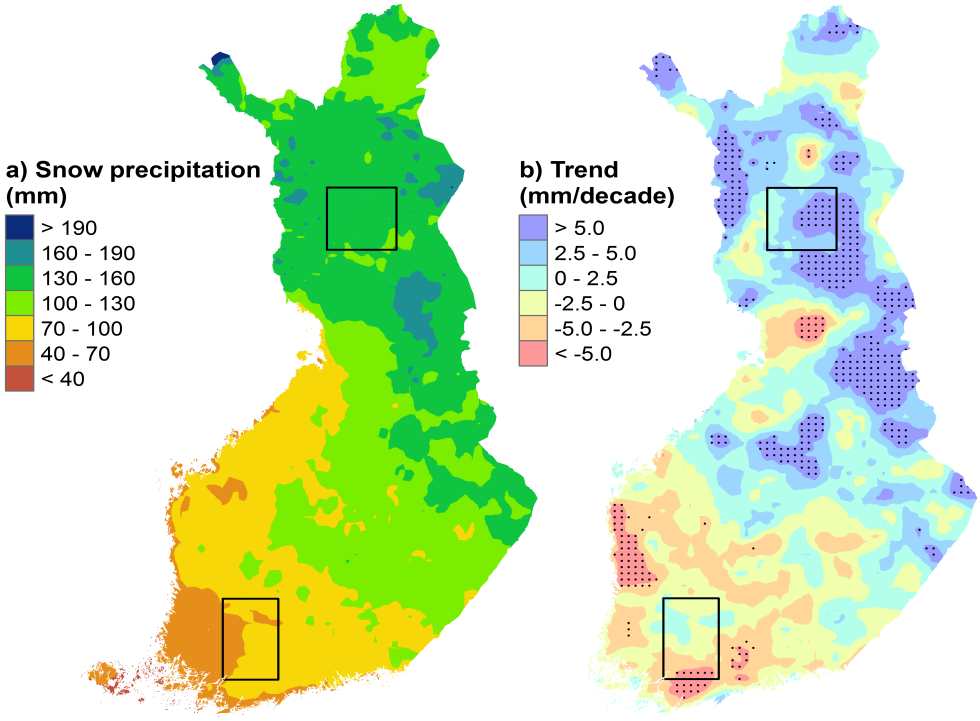

Figure 6. a) The mean annual snowfall in 1961-2014, b) The linear trend in annual snowfall in 1961-2014. Black dots mark the regions with a statistically significant trend at the 5% level. The boxes denote the domains of SF and NF. (Reproduced from Fig. 6 of ***Paper I****.)*

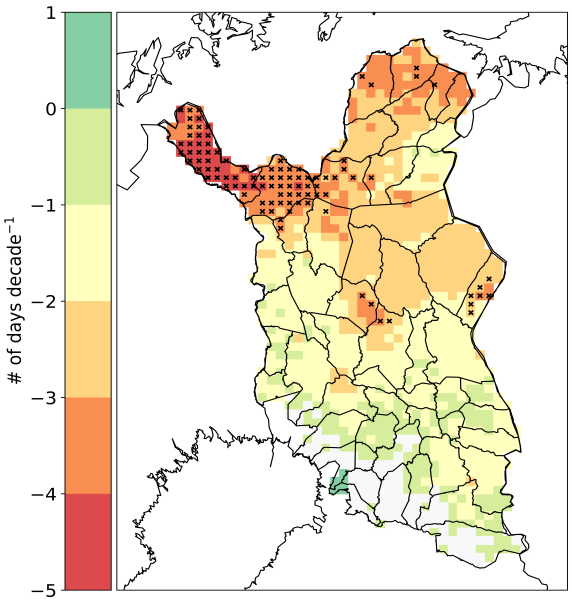

Figure 7. The linear trend in ice days (ID) in spring in 1981-2010 in the reindeer management area in Finland. The regions with statistically significant trend at the 5% level are marked with x. (Reproduced from Fig. 11 of ***Paper II****.)*

4.2 Snow depth and snow cover season

In **Paper I**, the changes in snow cover in Finland were analyzed for the years 1961-2014 from the FMIClimGrid data. In a typical winter in Finland in 1961-2014, snow depth gradually increased towards March. The snow depth values were the highest in northern Lapland and the lowest in southwestern Finland. The long-term trends in monthly mean snow depth were generally negative during the study period. The strongest absolute decrease, locally up to 4-6 cm/decade, occurred in February and in March in southern and western Finland and in April in central Finland. Annual maximum snow depth (MAXSN) decreased most in southwestern Finland – in places more than 4 cm/decade (Fig. 8). The trend in MAXSN was compared to the trend in the annual solid precipitation (Fig. 6). The spatial pattern correlation between these showed that in almost half of Finland's area MAXSN decreased despite increasing solid precipitation. In **Paper II**, MAXSN was analyzed for the shorter period of 1981-2010 and only for the reindeer management area. In this area and period, MAXSN showed a statistically significant decreasing trend of 5-10 cm/decade in the northern part of the reindeer management area and the standard deviation was 10-20 cm in the same region.

In 1961-2014, the seasonal snow cover period typically began in northern Finland before the end of October and in southwestern Finland at the end of December (Fig. 8). The seasonal snow cover period ended in southwestern Finland as early as the end of March, whereas in northern Finland, at the end of May. These beginning and end dates of the seasonal snow cover period (BEG and SOD) changed almost everywhere in Finland – BEG to later dates and SOD to earlier dates. The strongest change in BEG occurred in the central and southeastern parts of Finland, locally more than 4 days/decade, and the strongest change in SOD was found in the western coastal areas, locally more than -4 days/decade. The length of the seasonal snow cover period shortened practically everywhere in Finland. In **Paper II**, BEG and SOD were analyzed for the shorter period of 1981-2010 and only for the reindeer management area. During this period, there was a tendency towards later BEG, but this trend was significant only in the most northern regions. SOD had a significant decreasing trend only in the southern part of the reindeer management area, locally 3-5 days/decade.

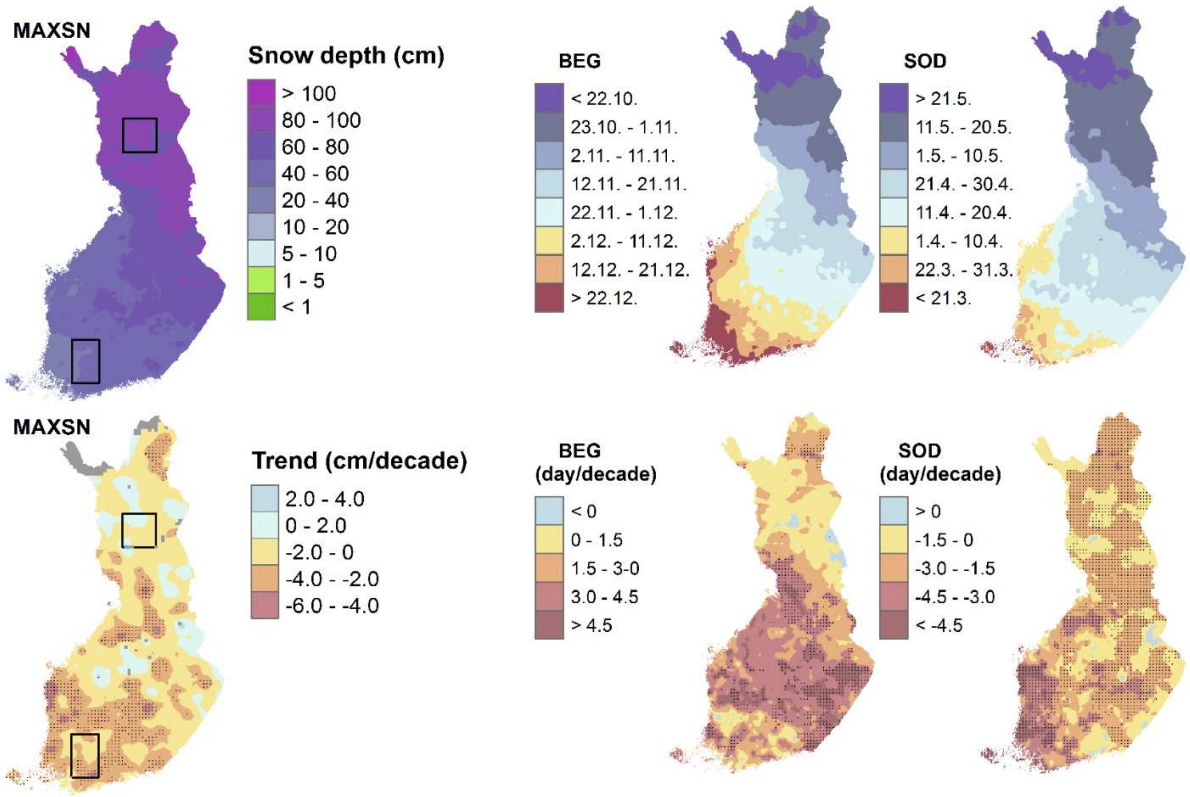

Figure 8. Upper row: The mean annual maximum snow depth (MAXSN), the average beginning (BEG) and end date (SOD) of seasonal snow cover period in 1961-2014. Lower row: The linear trends of MAXSN, BEG and SOD in 1961-2014. The small black dots denote the regions where the trend is statistically significant at the 5% level. (Reproduced from Figs. 2 and 3 of ***Paper I****.)*

5. PROJECTED CHANGES IN THE SEA ICE IN THE BALTIC SEA

5.1 Annual maximum ice extent in the Baltic Sea

Maximum ice extent (MIB) is the most widely used parameter to indicate climate variability in the Baltic sea region. Traditionally ice winters in the Baltic Sea have been sorted into ice severity classes on the basis of the observations of the annual maximum ice extent. According to the present standards (Vainio, 2011), winters with an ice extent smaller than $115x10^3$ km^2 are classified as mild, those from 115 to $230x10^3$ km^2 as average and those from 230 to $345x10^3$ km^2 as severe. If the ice extent exceeds $345x10^3$ km^2, it is classified as extremely severe.

In **Paper III**, we projected future changes in the Baltic Sea ice cover with a regression model using air temperature. The changes in annual maximum fast ice thickness (MIB), based on the ensemble mean of 28 models, were calculated for three percentiles: the median, and 5^{th} and 95^{th} percentiles. During the period 2021-2090, the linear trends for all percentiles under both scenarios, RCP4.5 and RCP8.5, were decreasing (Fig. 9). The 95^{th} percentile, which represented an uncommonly wide ice cover, was projected to diminish faster than the median or the 5^{th} percentile under both scenarios. If RCP8.5 is realized, according to our results the average ice winters would be very exceptional from the 2060s onward. Under RCP4.5, the 95^{th} percentile falls to the category of average ice winters still in the 2080s. Under both scenarios, the probability for unprecedentedly mild ice winters will increase during the study period.

Intermodel scatter around the median, 5^{th} and 95^{th} percentile was examined for the decade 2041-2050 to get an insight into the uncertainty caused by different climate models. For RCP8.5, there was a strong consensus among the model projections that the median MIB belongs to the class of mild ice winters in 2041-2050. Under RCP4.5 most of the models agreed with that. The scatter was widest for the 95^{th} percentile under both scenarios: for most of the model projections, the high percentile belonged to the class of average ice winters. According to RCP8.5, severe ice winters will not occur anymore in the 2040s. The scatter was smallest around the 5^{th} percentile: all model projections belong to the class of mild ice winters.

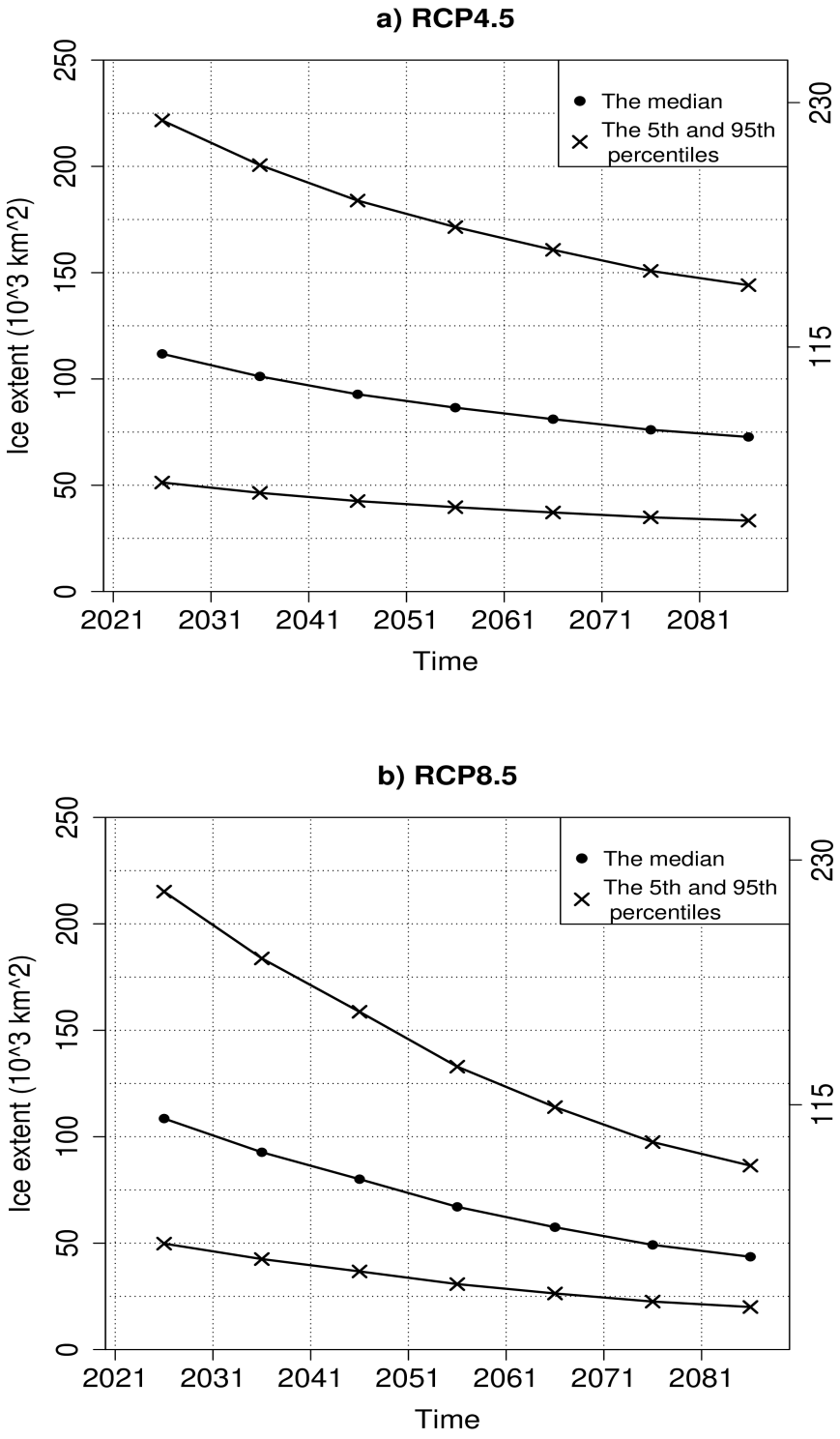

Figure 9. Temporal evolution of the 28-model mean annual maximum ice extent in the coming decades according to a) RCP4.5 and b) RCP8.5. The vertical axis on the right shows the upper limits for mild and average ice winters. (Reproduced from Fig. 5 of ***Paper III****.)*

5.2 Annual maximum fast ice thickness

Annual maximum fast ice thickness based on Eq. 2 was examined for two future decades, 2041-2050 and 2081-2090 as a response to the 28-model mean temperature projections. The ice thickness for the baseline period 1971-2000 was assessed using observed temperatures in Eq. 2. In the baseline period, most of the coastal areas become ice-covered in a typical contemporary winter (Fig. 10a). Still, there was a substantial variability in the ice thickness: in the Bay of Bothnia it was locally more than 90 cm, whereas in the southwestern parts of the Baltic Sea only 0-10 cm. The mean maximum ice thickness was projected to decrease in the coming decades according to both scenarios, but the decrease was faster under RCP8.5 scenario. Under RCP4.5, the ice thickness was projected to be about 60-80 cm in the Bay of Bothnia in 2041-2050 (Fig. 10b) and under RCP8.5 about 50-70 cm (Fig. 10c). In 2081-2090, the ice thickness in the Bay of Bothnia may locally still exceed 60 cm; elsewhere in the Gulf of Bothnia and in the Gulf of Finland, it is 10-40 cm, according to RCP4.5 (Fig. 10d). According to RCP8.5, most of the Baltic Sea will become ice-free in 2081-2090 (Fig. 10e). In the northernmost Bay of Bothnia ice thickness is still mainly 20-40 cm even if RCP8.5 is realized. Our results indicate that the Baltic Sea is unlikely to become totally ice-free in a typical winter during this century.

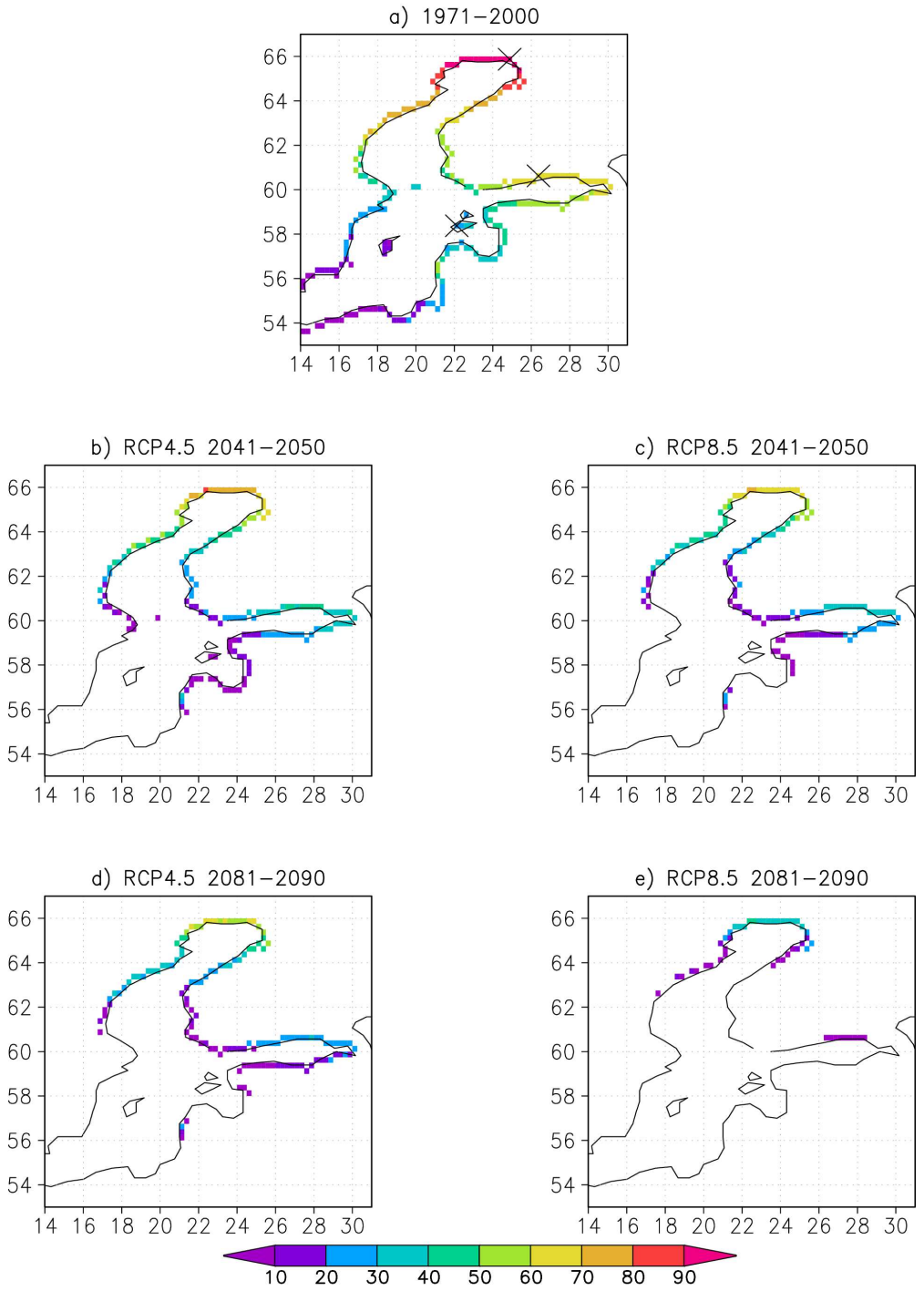

Fig. 10. The annual maximum fast ice thickness (cm) in the coastal regions of the Baltic Sea in a typical past and two future decade winters. The values are based on a) observed temperatures in 1971-2000 and b-e) the 28-model mean temperature projections under RCP4.5 and RCP8.5. (Reproduced from Fig. 8 of ***Paper III****.)*

The temporal evolution of ice thickness was examined separately at three locations, which are marked in Fig. 10a with crosses (Kemi, Loviisa and Vilsandi from north to south). The linear trends for Kemi and Loviisa, derived from the 28-model mean temperature responses, were about -3 cm/decade according to the RCP4.5 scenario and more than double under the RCP8.5. Relative to the period 1971-2000, the decline in 2041-2050 would be about 25-30% in Kemi and 40-50% in Loviisa (Table 1). At the most southern location, Vilsandi, there was little or no sea ice in a typical winter of the last three decades of the century, which made the trend notably weaker there than in Kemi or Loviisa. The disappearance of the ice cover in Vilsandi from the 2060s onwards does not, however, mean that sea ice cannot occur there at all in the late 21st century.

Table 1. The projected percentage reductions in the mean maximum ice thickness. The best estimates for the changes from the period 1971-2000 to future decades are based on the 28-model mean temperature projections. The 90% confidence intervals (given in parentheses) are derived from the inter-model differences in the temperature responses.

	Observation	RCP4.5		RCP8.5	
	1971-2000 (cm)	2041-2050 (%)	2081-2090 (%)	2041-2050 (%)	2081-2090 (%)
Kemi	75	25 (16-44)	37 (19-59)	32 (18-50)	63 (40-99)
Loviisa	38	40 (25-63)	57 (32-81)	50 (34-67)	83 (64-100)
Vilsandi		88 (46-100)	97 (81-100)	97 (80-100)	100

6. EXAMPLES OF NUMERICAL MODELING STUDIES IN CLIMATE RESEARCH

6.1 Performance of ECHAM5 in simulating snow melt timing

The snow-off date in ECHAM5 was analyzed first from the reference experiment (REF). Results of the experiment were compared to satellite observations (Fig. 11a) in all of Northern Eurasia. The comparison showed that the REF experiment (Fig. 11b) reproduced well the general pattern of snow-off dates that was seen in the satellite observations: the earliest snowmelt occurred in the Baltic Sea region (around julian day 80) and the latest in the Taymyr Peninsula (between days 150-160). However, in most of northern Eurasia, snow melted earlier in the model results than in the satellite observations, the difference being typically 5-20 days (Fig. 11c). On the other hand, in eastern Siberia and in some far eastern parts of Russia snow melted locally over 10 days later in REF experiment than in the satellite observations.

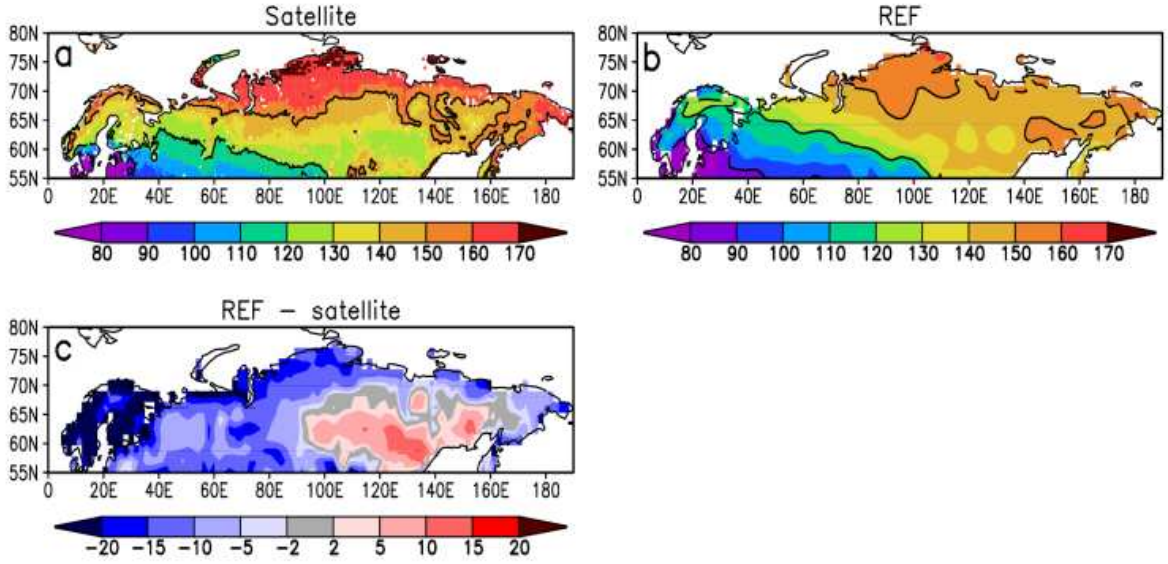

Figure 11. Mean snow-off date (SOD) in years 1979-2006 based on a) satellite retrievals and b) ECHAM5 REF experiment. Unit: Julian day. Snow-off dates of 90, 120 and 150 are indicated with black lines. c) The difference between b) and a). (Reproduced from Fig. 3 of ***Paper IV****.)*

To examine the possible reasons for the differences in snow-off dates we compared the temperature and surface albedo from REF simulation to observations. This comparison showed that in eastern Siberia, there were too high albedo values and too low temperatures and also too large accumulations of snow, whereas in the Taymyr region in spring, albedo values were underestimated and temperature overestimated and snow melted too early. The earlier than observed snow melt in western Russia and Scandinavia was due to too early start of snow melt. This occurs in spite of a slightly negative temperature bias in spring.

The sensitivity experiments, both nudging and different treatment of surface albedo, managed to reduce some of the model biases in snow-off date. Nudging made snow melt occur earlier in most northern Eurasia, with the largest effects (over 15 days) in southeastern Siberia and locally in Fennoscandia. In this region, the reason for earlier snow-off were higher temperatures and in eastern Siberia also slightly reduced snowfall. In northern parts of Northern Eurasia (e.g. Taymyr) and also in central Russia, snow-off was delayed. The changes in albedo parameterizations also made snow melt occur earlier in southeastern Siberia, and later in Taymyr and in a large area in central Russia and in Russian Far East. When nudging and albedo parameterizations were combined, the earlier snow melt in southeastern Siberia and later in Taymyr became even more pronounced. However, the early bias in snow melt in western parts of Northern Eurasia was not reduced considerably in any of the experiments. As this too early snow melt was accompanied by a negative bias in spring temperature, it implied that simulated temperature stays too low in the snow melt season. The main reason for this finding proved to be the simplifications in the calculations of surface energy budget: the surface energy budget was not computed separately for the snow-free and snow-covered parts of the grid cell. This means that the grid-mean surface temperature was not allowed to rise above 0°C, even if the snow-covered fraction was well below 1.

6.2 Sea-effect snowfall case on Finland’s west coast

On January 8, 2016, a record-breaking snowfall hit the west coast of Finland, in the municipality of Merikarvia, and accumulated 73 cm snowdrift in less than a day. On that day, all favorable conditions for cold-season convection (Jeworrek et al., 2017) were fulfilled. Due

to the warm autumn, the Baltic Sea was still open, which enabled a long fetch over relatively warm water at the same time as cold arctic air masses reached the region.

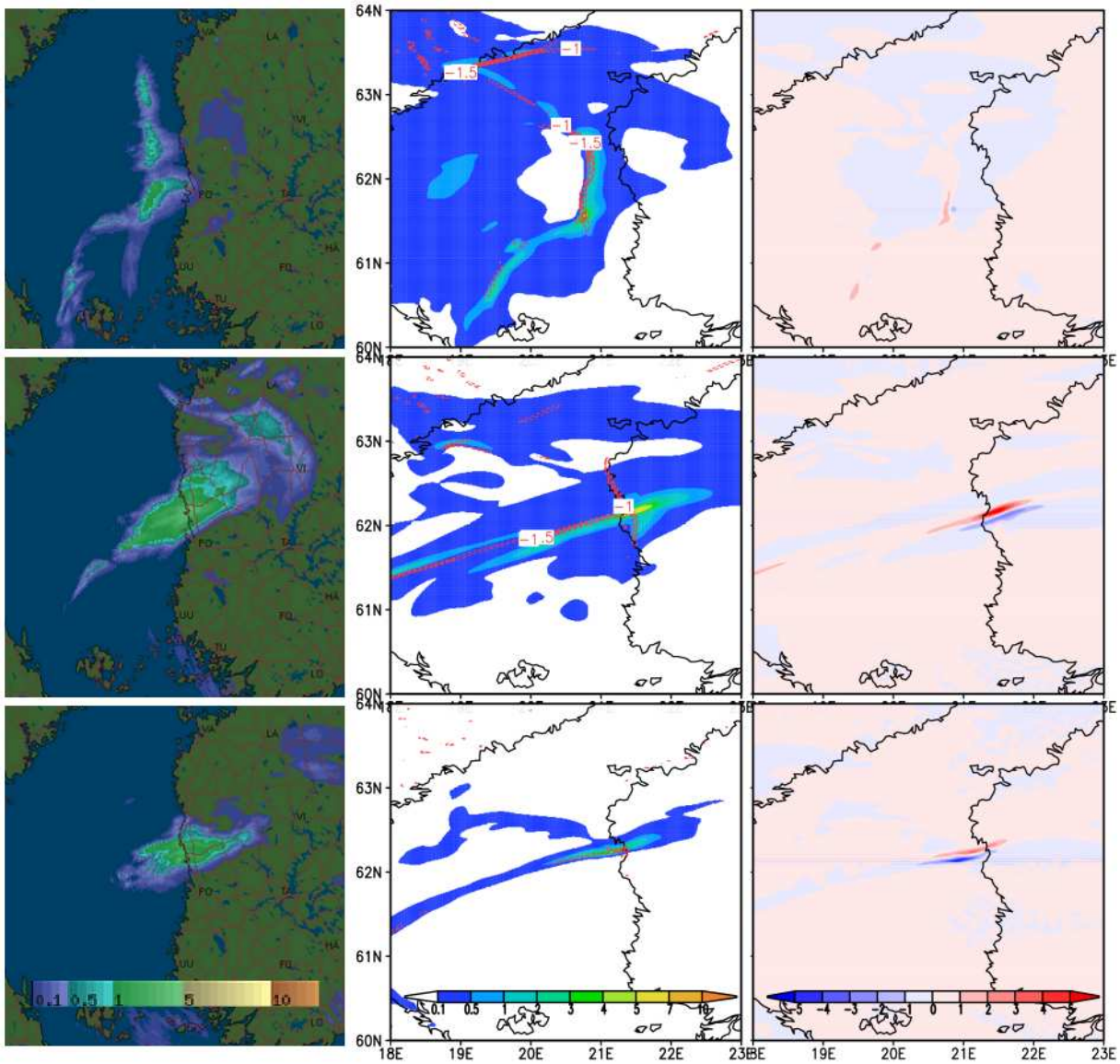

Figure 12. One-hour cumulative precipitation (mm/h) in the radar images (left panel) and forecast cycle 2016010803 at 05 (top), 13 (middle), and 21 (bottom) UTC on Jan 8 2016 simulated with HARMONIE with assimilated radar reflectivities (middle panel). Red contours show the simulated convergence zones. The difference between HARMONIE with and without assimilated radar reflectivities is shown in the right panel (mm/h). (Reproduced from Fig. 6 of ***Paper V****.)*

In **Paper V**, results from HARMONIE simulations of the snowfall case were compared to radar observations at 05, 13 and 21 UTC on January 8 (Fig. 12). At 05 UTC, the snowfall band was directed from south to north and was still located in the sea area offshore Merikarvia. At 13 UTC, the snowfall had intensified and was partly located over land areas and at 21 UTC, the snowfall area had become smaller and slightly weaker (Fig. 12, left column). When simulation results from the cycle that was initiated at 03 UTC on January 8 were qualitatively compared to radar observations, it showed that both HARMONIE simulations managed to capture the snowfall event. The assimilation of radar reflectivities (Fig. 12, middle column) spread the total area of simulated precipitation, produced a clearer hook to the coastline and the area of maximum precipitation grew slightly stronger. Radar assimilation especially intensified the precipitation more to the north when compared to simulation without radar assimilation. In Fig. 12, convergence zones are also shown. In these zones, near-surface winds converged, which further enhanced convective snowfall. When the results from other forecast cycles were compared with radar observations, it was found that the location of the snow band differed from the radar observations the most in the forecast cycles that were initiated 23-41 hours before the time of analysis. Also the simulated precipitation area was smaller than in later forecast cycles.

7. SUMMARY AND DISCUSSION

Knowing the prevailing climate conditions is relevant for society. As the global warming proceeds, it is crucial to understand that the global change affects the local conditions as well. Also for adaptation, the knowledge of the local scale conditions is needed. In this thesis, the main objective was to examine what the winters are like in Finland in the changing climate. In this section the research questions presented in section 1 are being answered.

- What kind of changes have occurred in snow conditions and factors affecting them in Finland?

This question was addressed in **Papers I** and **II**. The results from **Paper I** showed that snow depth has decreased and snow season shortened in large areas in Finland in 1961-2014. During this period, increasing precipitation and the changes in its composition had a significant role in observed changes in snow cover. In southern Finland, winters are becoming more rainfall-dominated. In northern Finland, the winter baseline temperature is still low enough that the increasing temperature has largely stayed below freezing. Thus, no clear change in snow cover occurred, even though increases in both solid and liquid precipitation were observed. In **Paper II**, the changes in the reindeer management area in northern Finland were analyzed for the years 1981-2010. The results were generally in agreement with the results of **Paper I**, but the strength of the trends were partly differing due to the shorter study period. This is an important fact to bear in mind when analysing trends: The selection of the time period always affects the results. Our findings of the changes in snow conditions are in line with those reported by Hannula (2012), Jylhä et al. (2014), Lehtonen (2015), Aalto et al. (2016), Lépy and Pasanen (2017) and Merkouriadi et al. (2017). The findings are also in line with the projections of the future snow conditions in northern Europe (Räisänen and Eklund, 2012; Räisänen, 2015).

- What kind of changes are expected to occur in sea ice conditions surrounding Finland?

In **Paper III**, the future changes in the Baltic Sea ice cover were assessed for 2020-2090 based on CMIP5 climate model simulations. The annual maximum ice extent in the Baltic Sea was found to decrease markedly under both RCP scenarios. According to RCP8.5, in practice only mild ice winters occur from the 2060s onwards. If the RCP4.5 is realized, the decline of the ice extent is slower and average ice winters may still occur even in the 2080s. Also the mean maximum sea ice thickness in coastal areas was found to decrease in the coming decades. According to RCP8.5, in the 2080s sea ice would occur only in the Bay of Bothnia with a maximum thickness of 30-40 cm. Based on RCP4.5, the coastal areas of the Gulf of Finland and the Gulf of Bothnia will still be ice-covered. Maximum ice thicknesses in the Bay of Bothnia would locally exceed 60 cm. Uncertainties in the results are largely due to the statistical calculation methods and the large spread among the individual models. On the other hand, the use of statistical methods enabled us to examine data from several climate models. The simple delta-change method that we used in constructing the future coastal temperatures assumed that the shape and width of the temperature distributions remained unchanged. In near-term temperature projections, this method is found to be a reasonable approach (Räisänen and Räty, 2013; Kämäräinen, 2013). For projections for the end of the century, a method including changes in the interannual variability would probably be beneficial. Despite the scatter in the rate of the future changes, the direction of the long-term trends is clear: sea-ice will significantly decrease, although the Baltic Sea is unlikely to become totally ice-free during this century.

The decreases in the ice-cover will have consequences on the ecosystems in the Baltic Sea. For example, the breeding habitats of the Baltic ringed seal will decline (Meier et al., 2004) or the timing of the spring bloom of phytoplankton will change (Eilola et al., 2013). On the other hand, shipping in the area will benefit from the longer ice-free period. As ice-free conditions become more common in wintertime, it may increase the number of sea-effect snowfall cases. This phenomenon is dependent also on other factors, which is why more research is needed of the favorable sea-effect snowfall circumstances in the future.

- What are the factors affecting climate model performance in simulating snow melt timing?

When climate model data is used, it is essential to understand that models have deficiencies. An example of these deficiencies was seen in our results in **Paper IV**, when the ability of ECHAM5 to describe the snow melt timing was evaluated. In general, ECHAM5 produced the observed geographical pattern of snow melt date quite well. Still, in some regions snow clearly melted too early and in some other regions too late. The biases that were found, were partly alleviated when nudging and surface albedo modification were used to correct the biases in simulated atmospheric circulation. Still, there were regional differences even after the albedo modifications and nudging. An important factor causing biases especially in the western parts of Northern Eurasia turned out to be too low a temperature in the snowmelt season, which resulted from simplifications in the model's surface energy budget.

It is worth noting that our results for performance concern only one model. Climate models with a more advanced snow and/or surface radiation scheme may perform differently. Thus, it would be beneficial to repeat these kinds of analyses with more advanced models. Overall, the results showed that many different processes affect the snow conditions in a climate model and improving a single process may either improve or deteriorate the agreement with observations. When climate models are used to predict future climate, it is thus important to use several models instead of just one and still regard the results with certain reservation. Continuous development of climate models is crucial for obtaining more reliable and accurate climate projections.

- How well can a sea-effect snowfall case be simulated over the Baltic Sea?

Paper V analyzed a sea-effect snowfall event which occurred on the west coast of Finland in 2016 causing a record-breaking snow depth increase of 73 cm in less than a day. High-resolution convection-permitting weather prediction model, HARMONIE, was used in the analysis with and without the assimilation of radar reflectivities. Both simulations managed to simulate the event quite well but assimilation of radar reflectivities improved the simulation results by spreading the most intense precipitation area and intensifying the precipitation

more to the north. It was also found that the forecast cycles which were initiated closer to the event corresponded best with the radar observations in both simulations. However, these results were based on a qualitative assessment of a single sea-effect snowfall case. More cases need to be identified and analyzed to get a broader outlook of this phenomenon and to enable more accurate model predictions. This kind of small-scale heavy snowfall events may cause serious troubles for infrastructure near the coastline. Reliable prediction of such events is thus important for society as ice-free conditions become more common in wintertime.

Final remarks

Based on our results, some points arose that would be interesting to include in possible future studies.

- CMIP6 models are the newest generation of global climate models that are used to predict future climate conditions. How well are the snow conditions described in these models?
- When ice cover in the Baltic Sea decreases, it may affect the occurrence of sea-effect snowfall events. Further research is needed of the future conditions of these events.
- The gridded datasets, such as FMIClimGrid, will be available in higher resolution in the future. It would be interesting to examine more localized climate changes using, for example, 1 km resolution.
- There are many variables related to winter climate conditions that were excluded from this work. These include for example changes in the intensities of solid precipitation events and spatial changes in snow water equivalent.

It is obvious that winter climate conditions in Finland are changing and so far the changes have occurred more clearly in southern than in northern Finland. The need for high quality observations and data sets will most probably increase in the future when climate warming proceeds. Also improved climate and weather prediction models are necessary to produce more realistic climate projections which can help in considering possible impacts of the changes. The impacts of the changes can be very complicated and both beneficial and harmful even within the same region. For example, less snow in winter may decrease road maintenance costs but at the same time reduce wintertime outdoor recreation possibilities. For

ecosystems, the strongest and most rapid impacts of climate change are expected in environments characterized by snow, ice and permafrost (Ministry of Agriculture and Forestry, 2014). When selecting the adaptation measures, it is thus important to assess all the relevant impacts in order to benefit from the positive effects and to reduce the adverse impacts. As the global warming continues, the importance of monitoring the climate conditions in the northern areas will amplify, which is shown in the findings presented in this thesis.

SUMMARIES OF THE ORIGINAL PUBLICATIONS

I **Luomaranta, A.**, Aalto, J. and Jylhä, K. (2019) Snow cover trends in Finland over 1961–2014 based on gridded snow depth observations, *International Journal of Climatology,* 39, 3147– 3159. https://doi.org/10.1002/joc.6007.

Paper I analyses the changes in monthly mean and annual maximum snow depth and several other snow-related indices in Finland during 1961-2014 using gridded observations of snow depth, temperature and precipitation. We found that snow depth has decreased and snow season has shortened in large areas in Finland. In Southern Finland the decrease in snow depth was driven by increasing mixed and liquid precipitation and, especially in spring, rising temperature. In Northern Finland, the decrease in snow depth was most evident in spring. In winter months, the solid precipitation was found to increase, but the increasing mixed and liquid precipitation and rising temperature likely counteracted the effect of increasing solid precipitation and thus we found no change in snow depth in winter months. The annual maximum snow depth was found to decrease in over 85% of Finland's area.

II Rasmus, S., Turunen, M., **Luomaranta, A.**, Kivinen, S., Jylhä, K. and Räihä, J. (2019) Climate change and reindeer management in Finland: co-analysis of practitioners knowledge and meteorological data for better adaptation, *Science of the Total Environment*, 710, 136229, https://doi.org/10.1016/j.scitotenv.2019.136229.

In **Paper II**, the interannual variability and changes in selected temperature-, precipitation- and snow-related indices in 1981-2010 in Northern Finland's reindeer management area were analyzed using gridded observation data. The results from the analysis were examined together with knowledge from reindeer herders, which was gathered via a survey questionnaire. The found climatic changes in the gridded data were generally consistent with earlier studies. The practitioner experiential knowledge was mainly in line with the results from meteorological observations.

III **Luomaranta, A.**, Ruosteenoja, K., Jylhä, K., Gregow, H., Haapala, J. and Laaksonen, A. (2014) Multimodel estimates of the changes in the Baltic Sea ice cover during the present century *Tellus A*, 66, 22617, http://dx.doi.org/10.3402/tellusa.v66.22617.

Paper III examines the changes in the annual maximum ice extent and the maximum coastal fast ice thickness in the Baltic Sea during the ongoing century. A non-linear regression model was fitted to coastal temperatures and annual maximum ice extent data for the years 1952-2012 and this regression model was then used together with CMIP5 climate model data to predict the maximum ice extents in the coming decades. According to both RCP scenarios studied, the annual maximum ice extent was found to decrease markedly. Under the RCP8.5 scenario, virtually only mild ice winters occur from the 2060s onwards. Under RCP4.5, the decline of the ice extent is slower: average ice winters may still occur even in the 2080s. For assessing the coastal fast ice thickness an analytical solution based on the sum of freezing-degree days was used. According to RCP8.5, in a conventional winter of the 2080s, sea ice would only occur in the Bay of Bothnia, with a maximum ice thickness of 30-40 cm, and in the north-eastern parts of the Gulf of Finland, with an ice thickness of 0-10 cm. According to RCP4.5, the coastal areas of the Gulf of Bothnia and the Gulf of Finland will still be ice-covered in the 2080s.

IV Räisänen, P., **Luomaranta, A.**, Järvinen, H., Takala, M., Jylhä, K., Bulygina, O. N., Riihelä, A., Laaksonen, A., Koskinen, J. and Pulliainen, J. (2014) Evaluation of North Eurasian snow-off dates in the ECHAM5.4 atmospheric general circulation model, *Geoscientific Model Development*, 7, 3037-3057, https://doi.org/10.5194/gmd-7-3037-2014.

Paper IV evaluates the timing of spring-time snow-off in Northern Eurasia in the ECHAM5 atmospheric GCM using satellite observations as reference data. In southeastern Siberia and in far eastern parts of Russia, snow was found to melt too late

in the ECHAM5 simulations whereas in the western parts and Taymyr region snow melt occurred too early. Several sensitivity experiments with ECHAM5 were conducted where found biases were corrected through nudging and/or modifying the treatment of surface albedo. The results from sensitivity experiments led to the conclusion that the treatment of surface energy budget in the model was one of the main reasons for the differences between observed and modeled snow-off.

V Olsson, T., Post, P., Rannat, K., Keernik, H., Perttula, T., **Luomaranta, A.**, Jylhä, K., Kivi, R. and Voormansik, T. (2018) Sea-effect snowfall case in the Baltic Sea region analysed by reanalysis, remote sensing data and convection-permitting mesoscale modelling, *Geophysica*, 53(1), 65-91.

Paper V analyses a strong small-scale sea-effect snowfall case in Merikarvia, Finland, which led to a new national record-breaking snowdrift of 73 cm. The event was investigated using ERA5 reanalysis data, the Global Navigation Satellite System (GNSS) and the numerical weather prediction model HARMONIE with and without assimilation of observed radar reflectivities. HARMONIE simulated the intensity of the snowfall situation well but the spatial spread of the snowfall remained too narrow. Assimilation of radar reflectivities improved the simulation results by increasing the moisture content of the boundary layer and by spreading the most intense precipitation area. The results showed that the combination of these three methods can help in obtaining the best possible insight into local severe weather events.

REFERENCES

Aalto, J., Pirinen, P. and Jylhä, K. (2016) New gridded daily climatology of Finland: Permutation based uncertainty estimates and temporal trends in climate, Journal of Geophysical Research: Atmospheres 121(8), 3807-3823.

Abram, N., Gattuso, J.-P., Prakash, A., Cheng, L., Chidichimo, M. P., Crate, S., Enomoto, H., Garschagen, M., Gruber, N., Harper, S., Holland, E., Kudela, R. M., Rice, J., Steffen, K. and von Schuckmann, K. (2019): Framing and Context of the Report. In: IPCC Special Report on the Ocean and Cryosphere in a Changing Climate [H.-O. Pörtner, D.C. Roberts, V. Masson-Delmotte, P. Zhai, M. Tignor, E. Poloczanska, K. Mintenbeck, A. Alegría, M. Nicolai, A. Okem, J. Petzold, B. Rama, N.M. Weyer (eds.)]. In press.

AMAP (2019) AMAP Climate Change Update 2019: An Update to Key Findings of Snow, Water, Ice and Permafrost in the Arctic (SWIPA) 2017. Arctic Monitoring and Assessment Programme (AMAP), Oslo, Norway. 12 pp.

AMAP (2017) Snow, Water, Ice and Permafrost in the Arctic (SWIPA) (2017). Oslo, Norway: Arctic Monitoring and Assessment Programme (AMAP) xiv+ 267 pp.

AMIP Project Office (1996) AMIP II Guidelines, AMIP Newsletter, 8, available at: https://pcmdi.llnl.gov/mips/amip/NEWS/amipnl8.html (last access: 14 January 2020).

Andersson, A. (2010) Winter road conditions and traffic accidents in Sweden and UK: present and future climate scenarios. Dissertation A131, University of Gothenburg, Sweden, 113 p.

Bénard, P., Vivoda, J., Masek, J., Smolíková, P., Yessad, K., Smith, C., Brozková, R. and Geleyn, J.F. (2010) Dynamical kernel of the Aladin-NH spectral limited-area model: Revised formulation and sensitivity experiments. Quarterly Journal of the Royal Meteorological Society, 136, 155–169.

Bintanja, R. and Andry, O. (2017) Towards rain-dominated Arctic. Nature Climate Change, 7, 263–267. https://doi.org/10.1038/NCLIMATE3240.

Brohan, P., Kennedy, J. J., Harris, I., Tett, S. F. B., and Jones, P. D. (2006) Uncertainty estimates in regional and global observed temperature changes: a new data set from 1850, Journal of Geophysical Research, 111, D12106, doi:10.1029/2005JD006548.

Brousseau, P., Berre, L., Bouttier, F. and Desroziers, G. (2011) Background-error covariances for a convective-scale data-assimilation system: AROME–France 3D-Var. Quarterly Journal of the Royal Meteorological Society, 137, 409–422. doi:10.1002/qj.750.

Brown, R.D. (2010) Analysis of snow cover variability and change in Quebec, 1948–2005. Hydrological Processes, 24, 1929–1954. https://doi.org/10. 1002/hyp.7565.

Brown, R.D. and Mote, P.W. (2009) The response of Northern Hemisphere snow cover to a changing climate. Journal of Climate, 22, 2124–2145. https://doi.org/10.1175/2008JCLI2665.1.

Bulygina, O.N., Groisman, P.Y., Razuvaev, V.N. and Korshunova, N.N. (2011) Changes in snow cover characteristics over Northern Eurasia since 1966. Environmental Research Letters, 6, 045026. https://doi.org/10.1088/1748-9326/6/4/045204.

Callaghan, T.V., Johansson, M., Brown, R.D., Groisman, P.Y., Labba, N., Radionov, V., Barry, R.G., Bulygina, O.N., Essery, R.L.H., Frolov, D.M., Golubev, V.N., Grenfell, T.C., Petrushina, M.N., Razuvaev, V.N., Robinson, D.A., Romanov, P., Shindell, D., Shmakin, A.B., Sokratov, S.A., Warren, S. and Yang, D. (2012) The changing face of Arctic snow cover: a synthesis of observed and projected changes. Ambio, 40, 17–31. https://doi.org/10.1007/s13280-011-0212-y.

Choi, G., Robinson, D.A. and Kang, S. (2010) Changing Northern Hemisphere snow seasons. Journal of Climate, 23, 5305–5310. https://doi.org/10. 1175/2010JCLI3644.1.

Critch, S., Goerlandt, F., Montewka, J. and Kujala, P. (2013) Towards a risk model for the Northern Baltic maritime winter navigation system, International Workshop on Next Generation Nautical Traffic Models (2013, November), pp. 21-30

Danco, J.F., DeAngelis, A.M., Raney, B.K. and Broccoli, A.J. (2016) Effects of a warming climate on daily snowfall events in the Northern Hemisphere. Journal of Climate, 29, 6295–6318. https://doi.org/10.1175/JCLI-D-15-0687.1.

Dee, D. P., Uppala, S. M., Simmons, A. J., Berrisford, P., Poli, P., Kobayashi, S., Andrae, U., Balmaseda, M. A., Balsamo, G., Bauer, P., Bechtold, P., Beljaars, A. C., van de Berg, L., Bidlot, J., Bormann, N., Delsol, C., Dragani, R., Fuentes, M., Geer, A. J., Haimberger, L., Healy, S. B., Hersbach, H. , Hólm, E. V., Isaksen, L., Kållberg, P., Köhler, M., Matricardi, M., McNally, A. P., Monge Sanz, B. M., Morcrette, J., Park, B., Peubey, C., de Rosnay, P., Tavolato, C., Thépaut, J. and Vitart, F. (2011) The ERA-Interim reanalysis: configuration and performance of the data assimilation system. Quarterly Journal of the Royal Meteorological Society, 137, 553-597. doi:10.1002/qj.828.

Derksen, C., Brown, R.D., Mudryk, L. and Luojus, K. (2016) Terrestrial Snow Cover [in Arctic Report Card 2016], http://www.arctic.noaa.gov/ReportCard.

Goovaerts, P. (2000) Geostatistical approaches for incorporating elevation into the spatial interpolation of rainfall, Journal of hydrology, 228, 113-129.

Haapala J.J., Ronkainen I., Schmelzer N., Sztobryn M. (2015) Recent Change — Sea Ice. In: The BACC II Author Team (eds.) Second Assessment of Climate Change for the Baltic Sea Basin. Regional Climate Studies. Springer, Cham

Hannula, H.-R. (2012) Napapiirin eteläpuolisen Suomen lumipeite maaliskuussa 1919-1020 [Snow cover in Finland south from the Arctic Circle in March 1919-2010]. M.Sc. Thesis, Department of Geography and Geology, University of Turku (only in Finnish).

Hernández-Henríquez, M. A., Déry, S. J. and Derksen, C. (2014) Polar amplification and elevation-dependence in trends of Northern Hemisphere snow cover extent, 1971–2014. Environmental Research Letters, 10, 044010. https://doi.org/10.1088/1748-9326/10/4/044010.

Hall, C. M. (2014) Will Climate Change Kill Santa Claus? Climate Change and High-Latitude Christmas Place Branding, Scandinavian Journal of Hospitality and Tourism, 14(1), 23-40, doi: 10.1080/15022250.2014.886101.

Haylock, M., Hofstra, N., Klein Tank, A., Klok, E., Jones, P. and New, M. (2008). A European daily high resolution gridded data set of surface temperature and precipitation for 1950–2006, Journal of Geophysical Research: Atmospheres (1984–2012), 113(D20).

Höglund, A., Pemberton, P., Hordoir, R. and Schimanke, S. (2017) Ice conditions for maritime traffic in the Baltic Sea in future climate. Boreal Environment Research, 22, 245-265.

Jevrejeva, S., Drabkin, V. V., Kostjukov, J., Lebedev, A. A., Leppäranta, M., Mironov, Ye. U., Schmelzer, N. and Sztobryn, M. (2002) Ice Time Series of the Baltic Sea. Report Series in Geophysics, No 44. University of Helsinki, Helsinki.

Jeworrek, J., Wu, L., Dieterich, C. and Rutgersson, A. (2017) Characteristics of convective snowbands along the Swedish east coast. Earth System Dynamics, 8, 163–175. doi:10.5194/esd-8-163-2017.

Juga, I., Hippi, M., Karsisto V. and Nurmi, P. (2014) Weather factors triggering the massive car crashes on 3 February 2012 in the Helsinki metropolitan area. In: *Proceedings of the 17th SIRWEC Conference, 30 January–1 February 2014, La Massana, Andorra*.

Jylhä, K., Fronzek, S., Tuomenvirta, H., Carter, T. R. and Ruosteenoja, K. (2008) Changes in frost, snow and Baltic sea ice by the end of the twenty-first century based on climate model projections for Europe. Climatic Change, 86, 441–462. https://doi.org/10.1007/s10584-007-9310-z.

Jylhä, K., Laapas, M., Ruosteenoja, K., Arvola, L., Drebs, A., Kersalo, J., Saku, S., Gregow, H., Hannula, H.-R. & Pirinen, P. (2014) Climate variability and trends in the Valkea-Kotinen region, southern Finland: comparisons between the past, current and projected climates. Boreal Environment Research, 19, 4–30.

Kerr, T., Clark, M., Hendrikx, J. and Anderson, B. (2013) Snow distribution in a steep mid-latitude alpine catchment. Advances in Water Resources, 55, 17–24. https://doi.org/10.1016/j.advwatres.2012.12.2010.

Kohler, J., Brandt, O., Johansson, M. and Callaghan, T. (2006) A long-term Arctic snow depth record from Abisko, northern Sweden, 1913–2004. Polar Research, 25, 91–113. https://doi.org/10.1111/j.1751-8369.2006.tb00026.x.

Krasting, J.P., Broccoli, A.J., Dixon, K. and Lanzante, J. (2013) Future changes in northern hemisphere snowfall. Journal of Climate, 26, 7813–7828. https://doi.org/10.1175/JCLI-D-12-00832.1.

Kämäräinen, M. (2013) Projections of future daily temperatures in Finland. Master’s thesis. University of Helsinki, Finland, 53 p.

Lehtonen, I. (2015) Four consecutive snow-rich winters in southern Finland: 2009/2010-2012/2013. Weather, 70, 3-8.

Lehtonen, I., Venäläinen, A., Ikonen, A., Puttonen N. and Gregow, H. (2013) Some features of winter climate in Northern Fennoscandia, Ilmatieteen laitos, Raportteja, Finnish Meteorological Institute, Report number: 2013:3, 32 pp.

Leppäranta, M. (1993) A review of analytical models of Sea-Ice growth. Atmosphere-Ocean. 31, 123-138.

Lépy, É and Pasanen, L. (2017) Observed regional climate variability during the last 50 years in Reindeer Herding cooperatives of Finnish Fell Lapland, Climate, 5, 81, https://doi.org/10.3390/cli5040081

Mankin, J.S. and Diffenbaugh, N.S. (2015) Influence of temperature and precipitation variability on near-term snow trends. Climate Dynamics, 45, 1099–1116. https://doi.org/10.1007/s00382-014-2357-4.

Matheron, G. (1963) Principles of geostatistics, Economic geology, 58, 1246-1266.

Meredith, M., Sommerkorn, M., Cassotta, S., Derksen, C., Ekaykin, A., Hollowed, A., Kofinas, G., Mackintosh, A., Melbourne-Thomas, J., Muelbert, M. M. C., Ottersen, G., Pritchard, H. and Schuur, E.A.G. (2019) Polar Regions. In: IPCC Special Report on the Ocean and Cryosphere in a Changing Climate [H.-O. Pörtner, D.C. Roberts, V. Masson-Delmotte, P. Zhai, M. Tignor, E. Poloczanska, K. Mintenbeck, A. Alegría, M. Nicolai, A. Okem, J. Petzold, B. Rama, N.M. Weyer (eds.)]. In press.

Merkouriadi, I., Leppäranta, M. and Järvinen, O. (2017) Interannual variability and trends in winter weather and snow conditions in Finnish Lapland. Estonian Journal of Earth Sciences, 66, 47-57. https://doi.org/10.3176/earth.2017.03

Ministry of Agriculture and Forestry. (2014) Finland’s National Climate Change Adaptation Plan 2022. Government Resolution 20 November 2014. Ministry of Agriculture and Forestry, Helsinki. Publications of Ministry of Agriculture and Forestry 5b/2014. 40 p. http://mmm.fi/en/national-climate-change-adaptation-plan

Mioduszewski, J.R., Rennermalm, A.K., Robinson, D.A. and Wang, L. (2015) Controls on spatial and temporal variability in Northern Hemisphere terrestrial snow melt timing, 1979–2012. Journal of Climate, 28, 2136–2153. https://doi.org/10.1175/JCLI-D-14-00558.1.

Moss, R. H., Edmonds, J. A., Hibbard, K. A., Manning, M. R., Rose, S. K., van Vuuren, D. P., Carter, T. R., Emori, S., Kainuma, M., Kram, T., Meehl, G. A., Mitchell, J. F. B., Nakicenovic,

N., Riahi, K., Smith, S. J., Stouffer, R. J., Thomson, A. M., Weyant, J. P. and Wilbanks, J. (2010) The next generation of scenarios for climate change research and assessment. Nature. 463, 747-756.

Mudryk, L. R., Kushner, P. J., Derksen, C. and Thackeray, C. (2016) Snow cover response to temperature in observational and climate model ensembles. Geophysical Research Letters, 44, 919-926. https://doi.org/10.1002/2016GL071789.

Najafi, M. R., Zwiers, R. and Gillett, N. (2016) Attribution of the observed spring snowpack decline in British Columbia to anthropogenic climate change. Journal of Climate, 40, 4113–4130. https://doi.org/10.1175/JCLI-D-16-0189.s1.

Neuvonen, M., Sievänen, T., Fronzek, S., Lahtinen, I., Veijalainen, N. and Carter, T. R. (2015) Vulnerability of cross-country skiing to climate change in Finland – an interactive mapping tool. Journal of Outdoor Recreation and Tourism, 11, 64-79. https://doi.org/10.1016/j.jort.2015.06.010.

Park, H., Yabuki, H. and Ohata, T. (2012) Analysis of satellite and model data-sets for variability and trends in Arctic snow extent and depth, 1948–2006. Polar Science, 6, 23–37. https://doi.org/10.1016/j.polar.2011.11.002.

Prein, A. F., Langhans, W., Fosser, G., Ferrone, A., Ban, N., Goergen, K., Keller, M., Tölle, M., Gutjahr, O., Feser, F., Brisson, E., Kollet, S., Schmidli, J., van Lipzig, N. P. M. and Leung, R. (2015) A review on regional convection permitting climate modeling: Demonstrations, prospects, and challenges. Reviews of Geophysics, 53, 323–361. doi:10.1002/2014RG000475.

Raateoja, M. and Setälä, O (2016) The Gulf of Finland assessment, Reports of The Finnish Environment Institute, 2016:27.

Riihelä, A., Manninen, T., Laine, V., Andersson, K., and Kaspar, F. (2013) CLARA-SAL: a global 28 yr timeseries of Earth's black-sky surface albedo, Atmos. Chem. Phys., 13, 3743–3762, doi:10.5194/acp-13-3743-2013.

Roeckner, E., Bäuml, G., Bonaventura, L., Brokopf, R., Esch, M., Giorgetta, M., Hagemann, S., Kirchner, I., Kornblueh, L., Manzini, E., Rhodin, A., Schlese, U., Schulzweida, U., and Tompkins, A. (2003) The atmospheric general circulation model ECHAM5, Part I, Model description, Max Planck Institute for Meteorology Rep. 349, 127 pp., available at: www.mpimet.mpg.de/fileadmin/publikationen/Reports/max_scirep_349.pdf (last access: 13 December 2019).

Roeckner, E., Brokopf, R., Esch, M., Giorgetta, M., Hagemann, S., Kornblueh, L., Manzini, E., Schlese, U., and Schulzweida, U. (2006) Sensitivity of simulated climate to horizontal and vertical resolution in the ECHAM5 atmosphere model, Journal of Climate, 19, 3771–3791.

Roesch, A. and Roeckner, E. (2006) Assessment of snow cover and surface albedo in the ECHAM5 general circulation model, Journal of Climate, 19, 3828-3843.

Roesch, A., Wild, M., Gilgen, H., and Ohmura, A. (2001) A new snow cover fraction parametrization for the ECHAM4 GCM, Climate Dynamics, 17, 933–946.

Ronkainen, I. (2013) Long-term changes in Baltic Sea ice conditions. Master's Thesis, University of Helsinki, Finland, http://urn.fi/URN:NBN:fi-fe2017112251979.

Räisänen, J. (2008) Warmer climate: less or more snow? Climate Dynamics, 30(2), 307–331. https://doi.org/10.1007/s00382-007-0289-y.

Räisänen, J. (2015) Twenty-first century changes in snowfall climate in Northern Europe in ENSEMBLES regional climate models, Climate Dynamics, 46, 339-353, https://doi.org/10.1007/s00382-015-2587-0.

Räisänen, J. and Eklund, J. (2012) 21st century changes in snow climate in Northern Europe: a high-resolution view from ENSEMBLES regional climate models. Climate Dynamics, 38, 2575-2591, https://doi.org/10.1007/s00382-011-1076-3.

Räisänen, J. and Räty, O. (2013) Projections of daily mean temperature variability in the future: cross-validation tests with ENSEMBLES regional climate simulations. Climate Dynamics, 41, 1553-1568.

Seinä, A. and Palosuo, E. (1996) The classification of the maximum annual extent of ice cover in the Baltic Sea 1720-1995. Meri. (Report Series of the Finnish Institute of Marine Research, Helsinki) 27, 79-91.

Skaugen, T., Stranden, H.B. and Saloranta, T. (2012) Trends in snow water equivalent in Norway (1931–2009). Hydrology Research, 43, 489–499. https://doi.org/10.2166/nh.2012.109.

Stefan, J. (1891) Über die Theorie der Eisbildung, insonderes über die Eisbildung im Polarmeere [On the theory of ice formation, in particular in polar seas]. Annalen der Physik und Chemie, neue Folge, 42, 269-286.

Stuefer, S., Kane, D.L. and Liston, G.E. (2013) In situ snow water equivalent observations in the US Arctic. Hydrology Research, 44, 21–34. https://doi.org/10.2166/nh.2012.177.

Takala, M., Pulliainen, J., Metsämäki, S., and Koskinen, J. (2009) Detection of snow melt using spaceborne microwave radiometer data in Eurasia from 1979 to 2007, IEEE Transactions on Geoscience and Remote Sensing, 47, 2996–3007.

Tinz, B. (1996) On the relation between annual maximum extent of ice cover in the Baltic Sea level pressure as well as air temperature field. Geophysica. 32, 319-341.

Vainio, J. (2011) Jäätalvien ankaruuden uusi luokittelu. Ilmastokatsaus [Revised severity classification of the maximum annual extent of ice cover in the Baltic Sea] 2011, 2. Finnish

Meteorological Institute. ISSN: 1239-0291. [In Finnish only.]. Online at: https://ilmatieteenlaitos.fi/c/document_library/get_file?uuid=3475052f-c3c7-4016-9e68-a35a70563c05&groupId=30106. (last access: 14 January 2020)

Vaughan, D. G., Comiso, J. C., Allison, I., Carrasco, J., Kaser, G., Kwok, R., Mote, P., Murray, T., Paul, F., Ren, J., Rignot, E., Solomina, O., Steffen, K.and Zhang, T. (2013) Observations: cryosphere. In: Stocker, T. F., Qin, D., Plattner, G.-K., Tignor, M., Allen, S.K., Boschung, J., Nauels, A., Xia, Y., Bex, V. and Midgley, P.M. (Eds.) Climate Change 2013: The Physical Science Basis. Contribution of Working Group I to the Fifth Assessment Report of the Intergovernmental Panel on Climate Change. Cambridge, United Kingdom and New York, NY: Cambridge University Press.

van Vuuren, D. P., Edmonds, J. A., Kainuma, M., Riahi, K.,Thomson, A. M., Hibbard, K., Hurtt, G. C., Kram, T., Krey, V., Lamarque, J.-F., Masui, T., Meinshausen, M., Nakicenovic, N., Smith, S. J. and Rose, S. K. (2011) The representative concentration pathways: an overview. Climatic Change, 109, 5-31.

Vihma, T. and Haapala, J. (2009) Geophysics of sea ice in the Baltic Sea – a review. Progress in Oceanography, 80, 129-148.

Weusthoff, T., Ament, F., Arpagaus, M. and Rotach, M.W. (2010) Assessing the Benefits of Convection-Permitting Models by Neighborhood Verification: Examples from MAP D-PHASE. Monthly Weather Review, 138, 3418–3433. doi:10.1175/2010MWR3380.1.

Ye, H. and Cohen, J. (2013) A shorter snowfall season associated with higher air temperatures over northern Eurasia. Environmental Research Letters, 8, 014052. https://doi.org/10.1088/1748-9326/8/1/014052.

Zhong, X., Zhang, T., Kang, S., Wang, K., Zheng, L., Hu, Y. and Wang, H. (2018) Spatiotemporal variability of snow depth across the Eurasian continent from 1966 to 2012. The Cryosphere, 12, 227–245. https://doi.org/10.5194/tc-12-227-2018.

Zubov, N. N. (1945) L’dy Arktiki [Arctic Ice]. Izdatel’stvo Glavsermorputi, Moscow. [English translation 1963] US Naval Oceanographic Office and American Meteorological Society, San Diego.

I

Received: 21 June 2018 | Revised: 11 January 2019 | Accepted: 15 January 2019

DOI: 10.1002/joc.6007

International Journal of Climatology RMetS

RESEARCH ARTICLE

Snow cover trends in Finland over 1961–2014 based on gridded snow depth observations

Anna Luomaranta[1] | Juha Aalto[2] | Kirsti Jylhä[1]

[1]Weather and Climate Change Impact Research, Finnish Meteorological Institute, Helsinki, Finland

[2]Department of Geosciences and Geography, University of Helsinki, Helsinki, Finland

Correspondence
Anna Luomaranta, Weather and Climate Change Impact Research, Finnish Meteorological Institute, P.O. Box 503, FI-00101 Helsinki, Finland
Email: anna.luomaranta@fmi.fi

Funding information
Academy of Finland, Research Council for Natural Sciences and Engineering, Grant/Award Number: 278067; State Nuclear Waste Management Fund in Finland

Snow conditions in high-latitude regions are changing in response to climate warming, and these changes are likely to accelerate as the warming proceeds. Here, we analyse daily gridded snow depth, temperature and precipitation data from Finland over the period 1961–2014 to discover the ongoing changes in monthly average snow depths (SN) and several snow-related indices. Our results indicate that regional differences of changes in snow conditions can be relatively large, even within such a small district as Finland. Moreover, the interannual variation of the various snow indices was found to be larger in southern Finland than in northern Finland. The largest decrease in snow depth occurred in the southern, western and central parts of Finland in late winter and early spring. This decrease was driven by increasing mixed and liquid precipitation and, especially in spring, increasing temperature. In northern Finland, the decreasing trend of snow depth was most evident in spring, but no change occurred during winter months, although the amount of solid precipitation was found to increase in December–February. In the same months, temperature and the amount of mixed and liquid precipitation increased, likely counteracting the effects of the increasing solid precipitation on snow depth. The annual maximum snow depth that typically occurs in March was found to decrease in over 85% of Finland's area, most strongly in western coastal areas. In almost half of Finland's area, this decrease occurred despite increasing solid precipitation. Our findings highlight the complexity of the responses of snow conditions to climatic variability in northern Europe.

KEYWORDS
climate, precipitation, snow depth, snowfall, temperature, trend

1 | INTRODUCTION

Northern European countries such as Finland are highly sensitive to variability and changes in snowfall and snow cover. Intense snowfall may cause severe problems for traffic and electricity supply (Andreescu and Frost, 1998; Andersson, 2010; Juga *et al.,* 2014; Vajda *et al.,* 2014; Lehtonen, 2015), and maintaining sufficient snow removal equipment requires financial resources (Keskinen, 2012; Lehtonen, 2015). Snow cover conditions and the changes in them also impact reindeer herding (Hansen *et al.,* 2011, 2014; Rasmus *et al.,* 2014, 2016; Turunen *et al.,* 2016) and boreal agriculture and vegetation, especially in spring (Bjerke *et al.,* 2014; Peltonen-Sainio *et al.,* 2016). On the other hand, the presence of snow in the winter season is essential for recreation and wintertime tourism (Tervo-Kankare *et al.,* 2013; Hall, 2014; Neuvonen *et al.,* 2015).

Several studies have reported the recent past state and changes in the snow conditions at different spatial scales ranging from the entire Northern Hemisphere (e.g., Brown and Mote, 2009; Choi *et al.,* 2010; Takala *et al.,* 2011; Park *et al.*, 2012; Callaghan *et al.,* 2012; Vaughan *et al.,* 2013;

Mioduszewski *et al.,* 2015; Hernández-Henríquez *et al.,* 2014; Derksen *et al.,* 2016) or Eurasia (Bulygina *et al.,* 2011; Ye and Cohen, 2013; Zhong *et al.,* 2018) to individual countries or smaller districts within them (e.g., Kohler *et al.,* 2006; Brown, 2010; Skaugen *et al.,* 2012; Kerr *et al.,* 2013; Stuefer *et al.,* 2013; Najafi *et al.,* 2016). Within the Arctic, the largest decreases in snow water equivalent (SWE) and snow cover duration in recent decades have occurred in maritime regions, including northern Scandinavia (Callaghan *et al.,* 2012). Drastic changes in snow conditions are expected to continue during the ongoing century (Bintanja and Andry, 2017). In Europe, the largest percentage reductions in the number of snow cover days and the average SWE are projected to occur in southern and western Europe (Jylhä *et al.,* 2008). In northern Europe, the amount of snow is also generally projected to decrease, but the regional and interannual variability is expected to remain high; individual snow-rich winters can still occur in future decades, even where long-term mean SWE is projected to decrease (Räisänen and Eklund, 2012). In northern Fennoscandia, the annual number of snow cover days is projected to decrease most in the coastal regions and least in the mountainous areas (Lehtonen *et al.,* 2013).

The main factors affecting snow conditions are temperature and precipitation (e.g., Räisänen, 2008; Brown and Mote, 2009; Mankin and Diffenbaugh, 2015; Mudryk *et al.,* 2016). Changes in both or one of them lead to changes in snow cover, especially in those regions and times of the year experiencing temperatures close to 0°C (Brown and Mote, 2009; Mudryk *et al.,* 2016). Rising temperature influences the form of precipitation, increasing rainfall at the cost of snowfall, and enhances air moisture content. The latter can be expected to further increase precipitation regardless of the changes in extratropical cyclone frequency (Yettella and Kay, 2017). In nearly all of northern Europe, the winter total snowfall is projected to decrease, even though in the coldest regions, snowfall is still expected to increase in the middle of winter (Räisänen and Eklund, 2012; Räisänen, 2015; Danco *et al*., 2016; Krasting *et al*., 2013). In addition to temperature and precipitation, atmospheric humidity was recently noted as a third important variable affecting the changes in snowpack (Harpold and Brooks, 2018).

In Finland, previous studies of trends in snow depth (SN) have tended to be regional in scope, so there is no clear picture of snow cover changes at the national scale. During the period 1919–2010 the strongest, statistically significant decrease in SN on March 15 in gridded observations was located in southwestern Finland (Hannula, 2012); elsewhere, in southern, western and central parts, the decreasing trend was not statistically significant. In the same study, a negative correlation between SN in March and seasonal mean temperature was found, the correlation being stronger in southern Finland and weaker in northern Finland. For a shorter period of three to five decades, Aalto *et al*. (2016) reported statistically significant decreases in the gridded annual mean SN in most areas of Finland, whereas Rasmus *et al*. (2014), Lepy and Pasanen (2017) and Merkouriadi *et al*. (2017) found no consistent trends in the annual maximum SN among weather stations in Finnish Lapland. Statistically significant decreases in the annual maximum SN (Lehtonen, 2015) and the average December–February SN (Jylhä *et al.,* 2014) were found at some stations in southern Finland during the last five to six decades.

The main goals of the present paper are to first characterize the spatio-temporal changes in snow cover in Finland over 1961–2014 and to then examine the roles of temperature- and precipitation-related variables in the observed changes. We base our analyses on a gridded daily dataset of snow depth, temperature and precipitation recently developed at the Finnish Meteorological Institute (Aalto *et al.,* 2016). Finally, we discuss our findings with respect to changes in snow conditions in northern Eurasia.

2 | DATA AND METHODS

The present analyses are built on the newly developed daily gridded climate data for Finland ("*FMIClimGrid*", version 1.0) spanning 1961–2014 at a spatial resolution of 10 × 10 km. The dataset (e.g., quality control, station network and statistical interpolation) is fully documented in Aalto *et al*. (2016), so only a brief description (focusing on daily snow depth) is provided here.

The observation data used for gridding have been extracted from both national (Finnish Meteorological Institute, FMI) and international source (European Climate Assessment & Dataset (ECA&D) databases (Klok and Klein Tank, 2009)). Meteorological station data from the neighbouring countries (i.e., Sweden, Norway, Russia and Estonia) were used to reduce the uncertainty near the border regions of Finland. The snow observation network is relatively evenly distributed across the study area (Figure 1). On average, the number of stations per day available for interpolation was 351 over the period 1961–2014. The station density dropped towards the 21st century due to the automation of the measurement stations. In Finland, the transition from manual to automated measurements has been gradually progressing from the end of the 1990s until now, and at the moment, approximately 50% of the snow measuring stations are automated. The interpolation errors remained relatively stable throughout the years (the mean root mean square error [RMSE] over 1961–2014 was 5.3 cm, excluding months from June to August).

For the gridding procedure, kriging interpolation was used (Matheron, 1963; Goovaerts, 1999), which has been widely applied in climatological studies (e.g., Haylock *et al.,* 2008; Hofstra *et al.,* 2008). The kriging method is based on spatial correlations of the observed variable and external background information (Goovaerts, 2000). The

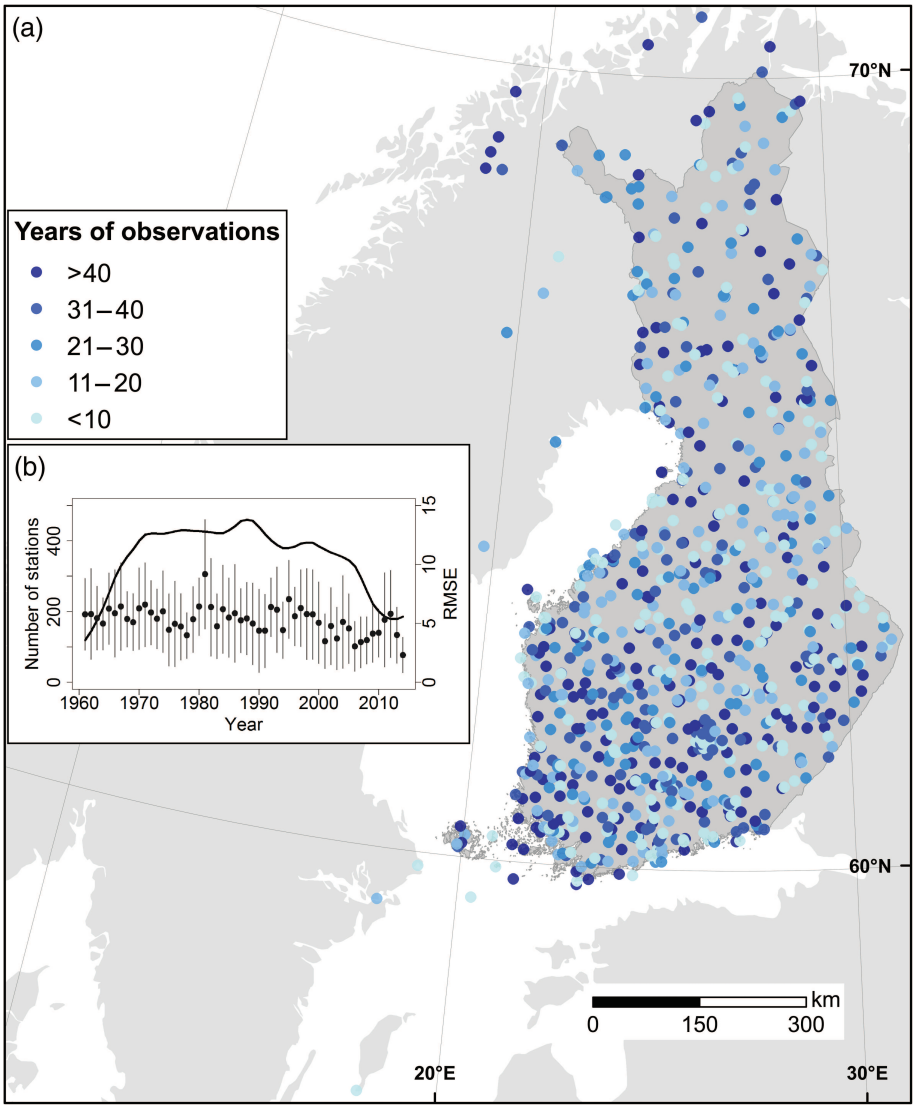

FIGURE 1 Spatio-temporal characteristics of the station network used for producing the gridded snow depth data in Aalto *et al.* (2016). (a) The points depict the stations in Finland and in the neighbouring countries ($n = 842$), with the colours indicating the total number of years with snow depth observations and (b) the curve shows the general temporal patterns of daily station data availability (smoothed using a local polynomial regression). The black points show the annually averaged interpolation error in terms of root mean squared error (RMSE), with the vertical lines indicating *SD* (months from June to August were excluded)

interpolation routine used by Aalto *et al.* (2016) accounts for the effects of geographical location (i.e., stations' latitudinal and longitudinal positions), topography and water bodies (sea and lake effects), thus adding local scale realism to the gridded data. For precipitation and snow depth, a stepwise gridding procedure was deployed, where interpolated amounts were combined with interpolated probability of occurrence of precipitation and snow (Barancourt *et al.,* 1992; following Haylock *et al.,* 2008). Using such an approach aids in accurately delineating areas with no precipitation or snow.

The accuracy and uncertainties of the dataset used in the present work concern spatiotemporal inconsistencies in station network, the incomplete sample of background data used as external predictors, inhomogeneity in the observation data and the sensitivities of the interpolation model parameters (Aalto *et al.,* 2016). Moreover, Aalto *et al.* (2016) deployed an uncertainty analysis based on a repeated resampling approach, where multiple daily gridded outputs were produced using slightly different station networks. Grid points categorized as uncertain (*SD* larger than the 90th percentile of all *SD* values) were excluded from the subsequent analyses (Figure 2e–h).

2.1 | Analysing temporal averages and trends

We defined long-term averages and trends of several snow related indices.

- Monthly mean snow depth (SN) calculated from the daily values.
- Annual maximum snow depth (MAXSN).

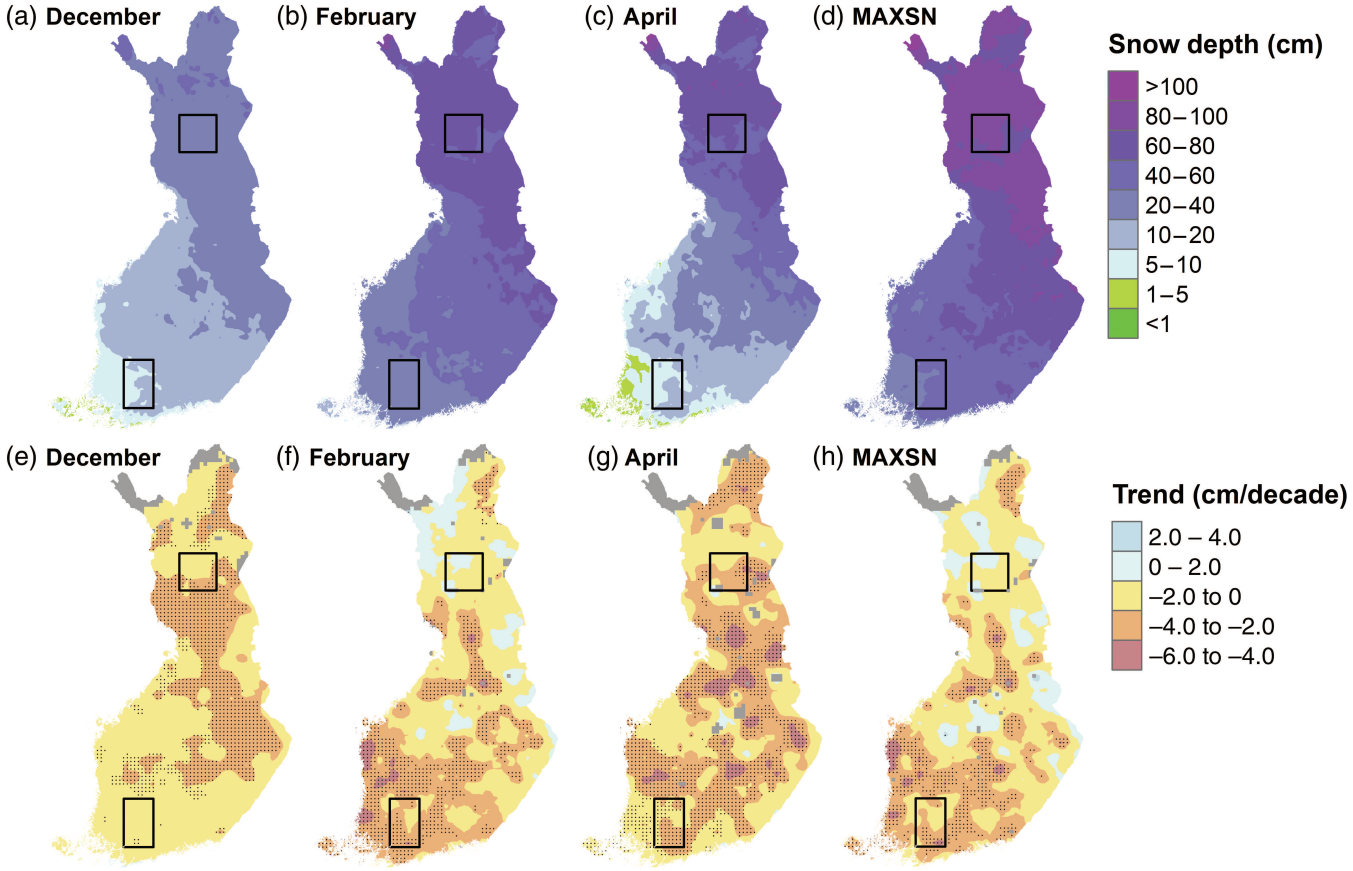

FIGURE 2 Monthly mean snow depth (SN, a–c, upper row) and the linear trend of SN (e–g, lower row) in December, February and April in 1961–2014. The last panels in the first and second rows show the winter mean maximum snow depth in 1961–2014 (d, MAXSN) and the linear trend of the maximum snow depth (h). Black dots mark the areas where the trend is statistically significant at the 5% level. The areas with the largest uncertainties in the gridded snow data are marked in grey in the panels of linear trend. The two boxes in the panels denote the SF (southern Finland) and NF (northern Finland) districts

- The beginning time of the seasonal snow cover period (BEG): the first day after the autumn's last snow-free day when the snow depth reaches at least 1 cm.
- Snow-off date (SOD): the first snow-free day in spring after the winter's maximum snow depth. The maximum snow depth is assumed to occur after January 1. If several equal maximum values are found, the date of the first maximum value is chosen to be the starting point to search for the SOD.
- The length of the seasonal snow cover period (LSS): the number of days between the previous two variables.
- The date of the winter's maximum snow depth (MAXD): the date when the snow depth reaches its maximum value. MAXD is assumed to occur between January 1 and June 30. If equal maximum values are observed several times, the date of the first observed maximum snow depth is chosen to represent the date of the winter's maximum snow depth.
- The number of snow days (N1): the number of days during the winter when snow depth is at least 1 cm.
- The number of days during the winter when the snow depth is equal or greater than 15 cm (N15).
- The number of days during the winter when the snow depth is equal or greater than 25 cm (N25).

Note that when calculating N1, N15 and N25, we also took into account snowy days outside the seasonal snow cover period, that is, before BEG and after SOD. To estimate the spatial variation in temporal trends of the snow related indices, a pixel-wise least squares linear regression model was fitted to the yearly values ($n = 54$). The significance of the trends was assessed using two-tailed t tests.

In addition to whole country, the statistics of the snow-related indices, including maximum, minimum and mean values, *SD* and slope of the linear trend, were examined in two smaller study domains (Figures 2 and 6) of approximately 110 × 110 km (or approximately 120 grid points), one being located in the south (SF) and the other in the north (NF). These domains represent two contrasting snow climate regimes within Finland: a southwestern maritime region and a northern region with Arctic conditions. We also examined the role of temperature and precipitation related quantities in controlling SN in these two snow climate regimes in Finland. Therefore, the relations between spatially averaged

long-term trends of SN and the following quantities were investigated for the study domains of SF and NF.

- Monthly mean temperature (T): temperature affects the form of precipitation and melting of snow cover.
- Monthly mean amount of precipitation (PR): precipitation may increase or decrease the snow amount depending on its form.
- Monthly mean maximum temperature (TMAX).
- Monthly number of ice days (ID): monthly number of days having the daily maximum temperature equal or less than 0°C. These are the potential days for solid precipitation to occur.
- Monthly mean amount of solid precipitation (PR_S): precipitation falling during ice days of each month. An increase in solid precipitation tends to increase snow depth.
- Monthly fraction of solid precipitation (FR_{PRS}).
- Monthly mean amount of mixed and liquid precipitation (PR_{ML}): the difference between monthly amount of precipitation (PR) and monthly amount of solid precipitation (PR_S). An increase in PR_{ML} tends to decrease snow depth.

These quantities were analysed over two shorter periods (1961–1987 and 1988–2014) and the significance of the change between the periods was assessed for each month and winter period (DJF) using two-sided Mann–Whitney-tests.

It is worth noting that our method of identifying solid precipitation ignores the fact that some snow may also fall during frost days (i.e., on days having daily minimum temperatures equal to or less than 0°C). Precipitation during frost days may thus include snowfall, rainfall and a mixture of both, that is, sleet. In Finland, no gridded datasets exist separately for snowfall and rainfall. Although precipitation during ice days provides only an approximation for snowfall, we considered the method sufficient for the needs of the present work. Moreover, the amount of precipitation caused by snowfall is a difficult quantity to measure, and the equipment for measuring precipitation has developed over time (Kuusisto, 1984; Taskinen and Söderholm, 2016). The changes in precipitation gauges create uncertainty to snowfall trends, which is why we examined the linear trends of annual and DJF PR_S also for two shorter time periods of 1961–1980 and 1983–2014 (not shown). These trends were in general in line with the results presented in this paper.

3 | RESULTS

3.1 | Spatial variations in long-term means and trends of snow depth

In an average winter of the period 1961–2014, a large part of Finland had already received its first snow during November. In December (Figure 2a), the snow cover was thinnest in southwestern Finland and thickest in northern Finland. During the remaining winter months, the spatial patterns of snow depth resembled that in December: lowest in the southwest and highest in the north (Figure 2b). In April (Figure 2c), snow was generally melting, but the variation in snow depth within Finland was large. Expectedly, the long-term mean annual maximum snow depth was lowest in southwestern Finland and highest in northern Finland (Figure 2d).

The long-term trends in SN over the period 1961–2014 were generally negative (Figure 2e–g). The strongest absolute decrease, locally up to 4–6 cm/decade, occurred in February (Figure 2f) and in March in southern and western Finland and in April (Figure 2g) in central Finland. In December, the snow depth decreased in eastern and northern parts of the country. In May, the decreasing trend of 2–4 cm/decade was statistically significant in many areas in northern Finland; elsewhere, snow had melted already. MAXSN changed most in southwestern parts of Finland—in places more than −4 cm/decade (Figure 2h) or −7%/decade in relative terms.

3.2 | Characteristics of the snow season and their changes in time

The climatological beginning time of the seasonal snow cover period (BEG) and snow-off date (SOD) in 1961–2014 are shown in Figure 3a,b. Over that time, BEG shifted to later dates and SOD to earlier dates almost everywhere in Finland (Figure 3e,f). The areas of the strongest and statistically significant positive trend in BEG were mainly located in central and southeastern parts of Finland. The strongest negative trend in SOD was found in western coastal areas, where SOD advanced locally more than 4 days/decade. Snow depth reached its maximum value mainly in March (Figure 3c). No clear statistically significant change occurred in MAXD during the study period (Figure 3g).

The seasonal snow cover period (LSS) lasted on average less than 85 days in the southwestern coastal area and the Archipelago (not shown). In northern Finland, LSS varied from 175 to 225 days. During the period 1961–2014, LSS shortened practically everywhere in Finland. The shortening was strongest in western parts of Finland, where the negative trend was locally 8–14 days/decade, and weakest in Lapland, where the negative trend varied from 0 to 5 days/decade. The trend was significant at the 5% level in western and central parts and locally also in Lapland.

The climatological mean N1 was on average 85–130 days in southwestern Finland. In Lapland, N1 was mainly over 190 days, and in northern Lapland, N1 was locally over 225 days. Similar to LSS, N1 decreased everywhere in Finland during the study period. The trend was strongest in western and central Finland, where it was mainly −5 to −8 days/decade and locally −8 to

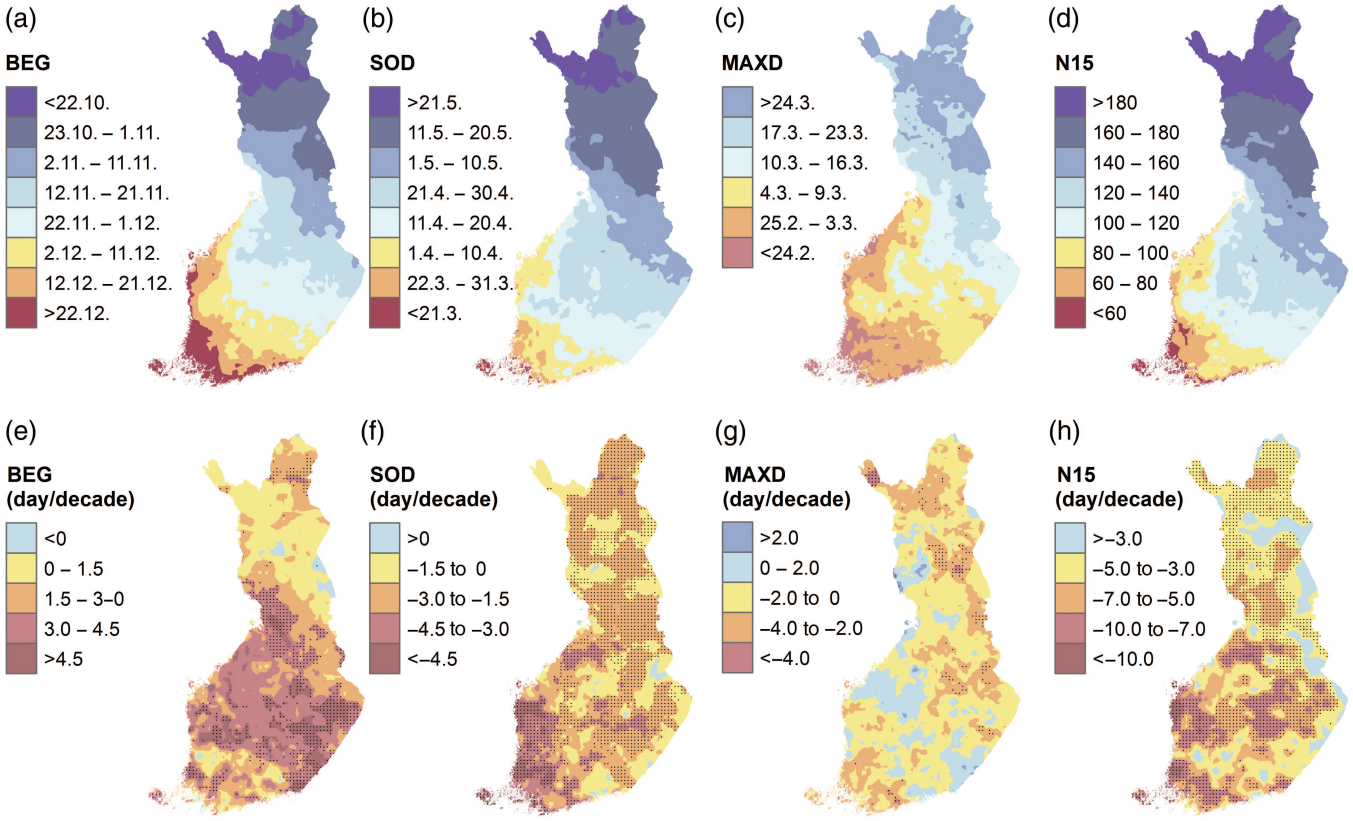

FIGURE 3 The beginning of the permanent snow season (a, BEG), snow-off date (b, SOD), the date of the winter's maximum snow depth (c, MAXD) and the number of the days when the snow depth is at least 15 cm (d, N15) in 1961–2014 (upper row) and their corresponding linear trends (e–h, lower row). Black dots mark the areas where the trend is statistically significant at the 5% level

−14 days/decade. While N15 (Figure 3d) and N25 were clearly smaller than N1, their negative trends were considerably stronger. The climatological means varied from less than 80 days for N15 and approximately 7 days for N25 on the southwestern coastline to over 180 days (N15) and 160 days (N25) in northern Lapland. The decrease in N15 was strongest in central, western and southwestern parts of Finland—in relative terms, −8 to −11%/decade (not shown).

3.3 | Interannual variation and trends in the northern and southern study domains

The summary statistics for MAXSN, MAXD, SOD, BEG, LSS, N1, N15 and N25 for 1961–2014 are provided in Table 1 for the two domains of southern Finland (SF) and northern Finland (NF) (see the domains in Figures 2 and 6), and the time series and linear trends for BEG, SOD, MAXD and N15 are shown in Supporting Information Figure S1. The values of MAXSN, MAXD, LSS, N1, N15 and N25 were consistently smaller in SF than in NF. Correspondingly, the earliest and latest MAXD and SOD occurred earlier in SF than in NF, and the earliest and latest BEG occurred later in SF than in NF. The *SD*s of all the indices were larger in SF than in NF, indicating that the interannual variation was larger in SF than in NF.

While the trends generally indicated less snow, not all were statistically significant (Table 1). The linear trend of SOD was statistically significant both in SF and NF. In terms of absolute values, it was stronger than the linear trend of BEG in both districts, meaning that the change in the snow season was stronger in spring than in autumn. Similar to SOD, the decreasing trends of N1 and N25 were statistically significant over both domains (Table 1). In SF, LSS had a stronger negative trend than N1, which implies that the snow season in SF has become more fragmental—snow falls and then melts away several times during winter.

3.4 | Potential drivers of observed changes in snow conditions

We observed significant changes in potential drivers of the snow conditions over the two study domains of SF and NF between the 1961–1987 and 1988–2014 time periods. In SF, both the monthly mean and monthly maximum temperatures increased in January–April (Figure 4a,b). For TMAX, the change between the periods was critical in March—the near-zero TMAX in 1961–1987 rose clearly above zero in 1988–2014. Total precipitation increased in January and February, and the fraction of solid precipitation decreased in the same months (Figure 4c–e). These changes in PR and FR_{PRS} were due to increased mixed and liquid precipitation (Figure 4f), as the amount of solid precipitation did not change (Figure 4d). Additionally, ID decreased in January and February. The decrease in SN between the two periods

TABLE 1 The mean, minimum and maximum values, together with the *SD*s and the slopes of the linear trends of selected snow related indices in 1961–2014 in two study domains in Finland (Figure 1a), one of which is in the south (SF), and the other of which is in the north (NF)

	Mean		Minimum/earliest value		Maximum/latest value		*SD*		Slope (per decade)	
Variable (units)	**SF**	**NF**	**SF**	**NF**	**SF**	**NF**	**SF**	**NF**	**SF**	**NF**
MAXSN (cm)	43.9	82.7	15.3 (2014)	58.4 (1990)	78.4 (1966)	121.5 (2000)	15.2	14.5	−2.1	−0.3
MAXD (date)	February 26	March 23	January 5, 1989	February 11, 2003	April 2, 1996	April 24, 1992	18.4	15.7	−1.7	−1.6
SOD (date)	April 7	May 14	February 19, 1975	April 27, 1990	May 3, 1966	May 27, 1968	16.5	7.1	−3.3 *	−1.6 **
BEG (date)	December 15	October 28	November 9, 2002	October 6, 1968	January 30, 2008	November 21, 2011	21.8	11.9	2.3	0.8
LSS (days)	112.0	197.0	22 (1974–1975)	159 (1989–1990)	165 (1965–1966)	231 (1968–1969)	31.6	14.8	−5.7 *	−2.4
N1 (days)	137.4	206.8	78 (2013–2014)	181 (1989–1990)	178 (1980–1981)	243 (1968–1979)	22.0	12.6	−4.8 *	−2.9 **
N15 (days)	85.6	169.1	3 (2013–2014)	121 (1989–1990)	152 (1980–1981)	228 (1968–1969)	32.9	19.6	−5.6	−3.8 *
N25 (days)	56.1	149.3	0 (2013–2014)	96 (1989–1990)	144 (1965–1966)	214 (1968–1969)	34.9	22.7	−6.5 *	−4.1*

The year when the maxima/minima occurred is given in brackets. MAXSN: annual maximum snow depth; MAXD: the date of the winter's maximum snow depth; SOD: snow-off date; BEG: the beginning of the permanent snow season; LSS: the length of the permanent snow season; N1, N15, N25: number of days during the winter when the snow depth is at least 1, 15 or 25 cm, respectively.
*Statistically significant trends at the 5% level according to two-sided *t* tests.
**Statistically significant trends at the 1% level according to two-sided *t* tests.

was evident in SF in February–April (Figure 4g). Based on the changes seen in temperature and precipitation related variables, we state that in February, SN decreased most likely due to increasing PR_{ML} and rising temperature. In March and April, the main reason is probably increasing temperature. The strong effect of increasing liquid and mixed precipitation on snow depth is also seen in Supporting Information Figure S2. The decrease in snow depth began approximately at the same time PR_{ML} began to increase in November–December. Supporting Information Figure S3 shows the strong relationships between regionally averaged annual MAXSN and November–March mean temperature, PR_S and PR_{ML} in SF.

In NF, the changes were not as clear as in SF. Monthly mean T increased in December, January and April, and TMAX increased in January, March, April and May (Figure 5a,b). Despite the increases, T and TMAX stayed below 0°C also during the latter period in mid-winter because of the colder baseline climate. In precipitation (Figure 5c–f), there seems to be no clear pattern of changes in the individual months, except for February, and thus the changes in 3 months sum over the winter months (December, January and February, referred to as DJF hereafter) were also analysed. The increases in DJF PR, DJF PR_S and DJF PR_{ML} were all statistically significant (Table 2), but in monthly mean SN (Figure 5g) or in DJF mean SN (Table 2), there occurred no change due to the counteracting effects of increasing DJF PR_S and DJF PR_{ML}. The counteracting behaviour of the PR_S and PR_{ML} change is more clearly shown in Supporting Information Figure S2. A slight decrease in November–December snow depth originated in October due to decreased solid precipitation. An increase in December–February solid precipitation acted to compensate this decrease, but at the same time, increasing liquid and mixed precipitation counteracted it. Supporting Information Figure S4 shows that in NF, the role of November–March precipitation is stronger than the role of November–March temperature for the annual MAXSN. In NF, DJF ID decreased (Table 2). The inverse changes in DJF PR_S and DJF ID in NF may imply that snowfall events have become more intense, causing more snowfall in less time.

The changes in the annual amount of solid precipitation divide Finland into two parts (Figure 6). The decrease was the strongest and locally also statistically significant in western and southwestern coast areas (in relative terms, −3 to −6%/decade [not shown]) or locally more. In eastern and northern Finland, the annual PR_S increased in many areas, the strongest increase being mainly 3–6%/decade in relative terms. When the spatial pattern correlation between annual PR_S and MAXSN trends (Figures 6b and 2h) was examined, we found that in almost half of Finland's area, MAXSN decreased despite increasing PR_S (Figure 7), whereas in 40% of the area, both MAXSN and PR_S decreased (Pearson's correlation = 0.60, $p < 0.001$). This result indicates that even in the areas where PR_S increases, it cannot fully counteract the effects of increasing mixed and liquid precipitation and temperature in reducing snow depth.

4 | DISCUSSION

In the present work, we analysed gridded snow depth and several snow related indices characterizing snow season in Finland. During the study period of 1961–2014, snow depth decreased in each winter month nearly everywhere in Finland, most strongly so in western and southern parts of the country in February and March. These findings mostly follow expectations. At these southern locations, the more maritime climate and milder winters make snow cover more sensitive to increasing temperature when compared to more northern locations, as noted by Callaghan *et al.* (2012). Southern Finland is estimated to belong to the zone where climate warming influences on maximum SWE are first expected to appear (fig. 3.21 in Brown *et al.,* 2017). Our findings of the changes in snow conditions are also in line

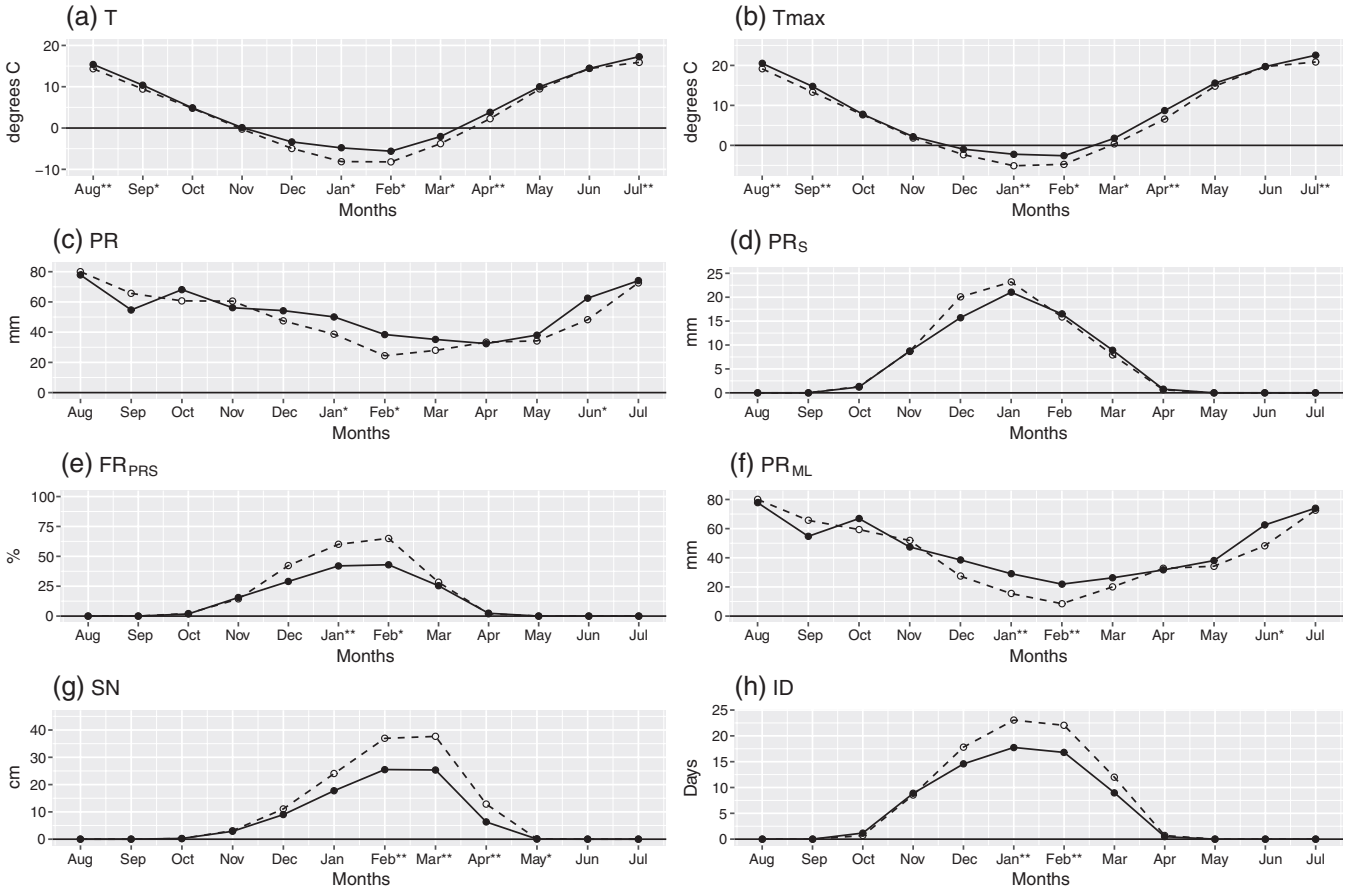

FIGURE 4 Twenty-seven-year mean seasonal cycles of monthly mean temperature (a, T), monthly mean maximum temperature (b, TMAX), monthly mean amount of precipitation (c, PR), monthly mean solid precipitation (d, PR_S), monthly fraction of solid precipitation (e, FR_{PRS}), monthly mean mixed and liquid precipitation (f, PR_{ML}), monthly mean snow depth (g, SN) and monthly number of ice days (h, ID) in southern Finland (SF). The dashed line indicates the 1961–1987 period, and the solid line indicates the 1988–2014 period. The months when the change between the two periods is statistically significant at the 5% level and 1% level according to two-sided Mann–Whitney tests are denoted by * and **, respectively

with those reported by Hannula (2012), Jylhä *et al*. (2014), Lehtonen (2015), Aalto *et al*. (2016), Lepy and Pasanen (2017) and Merkouriadi *et al*. (2017).

Long term increases in snow depth in February and in annual maximum snow depth over northern Eurasia were reported by Bulygina *et al*. (2011) and Callaghan *et al*. (2012). Updated trends for Russia in 1966–2014 show less evidence of increases in maximum snow depth and more evidence of decreases (Brown *et al.,* 2017). We did not find any statistically significant increase in February SN or MAXSN in Finland but decreases occurred in southern and western parts of the country. Our results correspond in general with the results of Park *et al*. (2012), who found a long-term decrease in January–March snow depth in 1948–2006 in large areas of northern Eurasia (see fig. 5b in Park *et al*. (2012)). Additionally, Zhong *et al*. (2018) detected a decreasing trend in annual mean snow depth over the western areas of European Russia and some other areas, even though the trend for the entire Eurasia was increasing. Callaghan *et al*. (2012) linked their finding to a long-term increase in cold season precipitation (north of 60°N), without distinguishing the form of the precipitation. An increase in winter precipitation was seen also in our results for the two study domains (Table 2). In the south, the increase in precipitation was due to mixed and liquid precipitation, whereas solid precipitation amounts remained practically invariant. These changes in the form of winter precipitation along with the increase in winter and spring temperatures explain the decrease in SN in the south. In the north, we found increases in DJF and annual amounts of solid precipitation, but these increases did not cause a long-term increase in SN or MAXSN. This increase in solid precipitation is in line with Zhong *et al*. (2018), who found an increasing trend in annual snowfall across the former USSR. The area indicating recent past increases in the annual snowfall sum (Figure 6b) roughly corresponds to an area of projected increases in heavy snow loads in forests (Lehtonen *et al.,* 2016). This suggests that even though an increase in snowfall does not increase the monthly amount of snow on the ground, it may still affect snow loads in forests.

Various studies have reported the strongest decrease in Northern Hemisphere snow cover duration and snow cover extent occurring in spring and little or no change in autumn (Brown and Mote, 2009; Brown and Robinson, 2011; Callaghan *et al.,* 2012; Kunkel *et al.,* 2016). Our findings regarding the changes in SOD and BEG in Finland support that

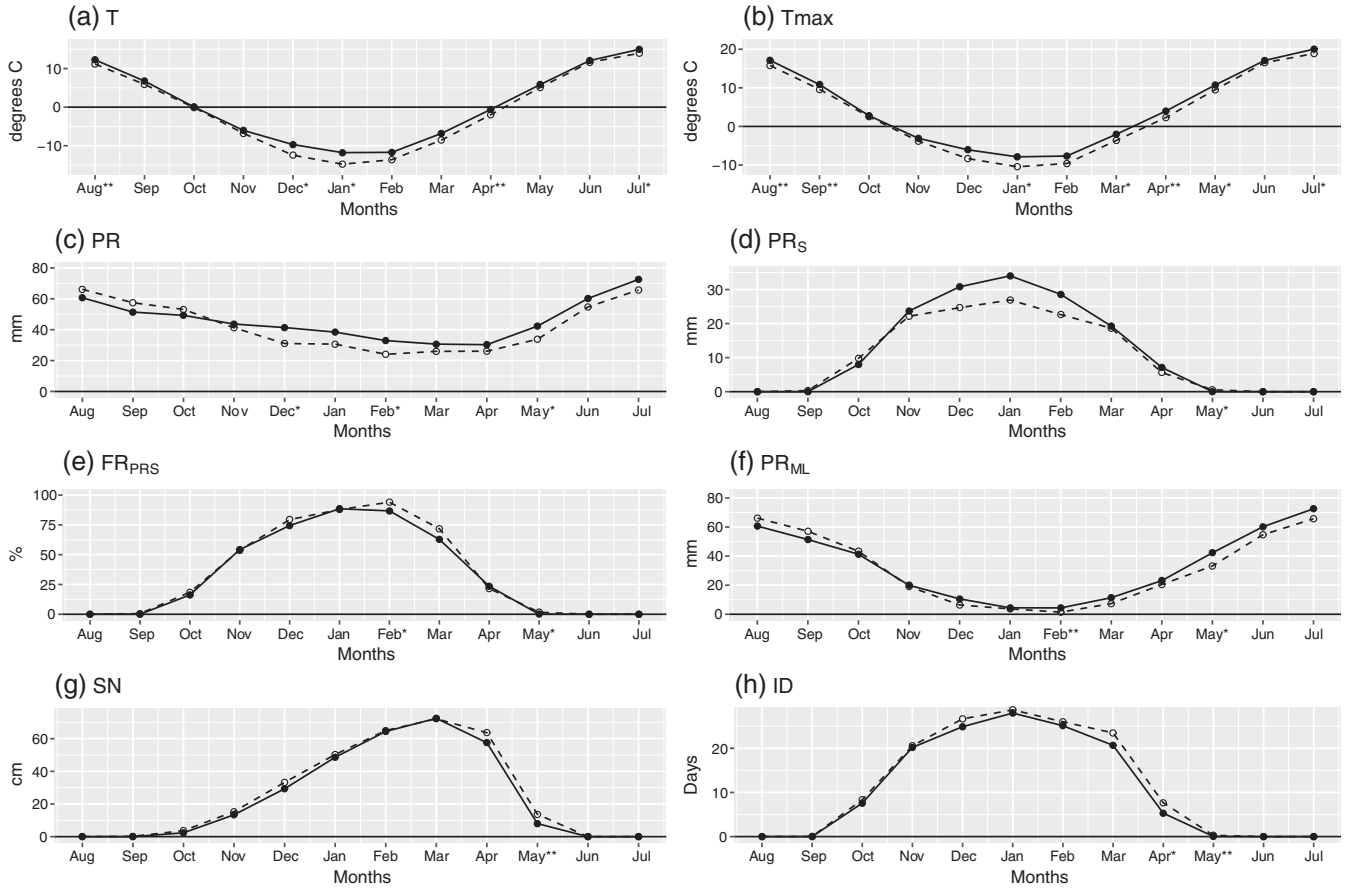

FIGURE 5 Twenty-seven-year mean seasonal cycles of monthly mean temperature (a, T), monthly mean maximum temperature (b, TMAX), monthly mean amount of precipitation (c, PR), monthly mean solid precipitation (d, PR_S), monthly fraction of solid precipitation (e, FR_{PRS}), monthly mean mixed and liquid precipitation (f, PR_{ML}), monthly mean snow depth (g, SN) and monthly number of ice days (h, ID) in northern Finland (NF). The dashed line indicates the 1961–1987 period, and the solid line indicates the 1988–2014 period. The months when the change between the two periods is statistically significant at the 5% level and 1% level according to two-sided Mann–Whitney tests are denoted by * and **, respectively

TABLE 2 The DJF mean values for T, Tmax and FR_{PRS}, and DJF sum for PR, PR_S, PR_{ML} and ID in two study domains in Finland (Figure 2a), one in the south (SF) and the other in the north (NF), for two periods, 1961–1987 and 1988–2014

	SF			NF		
Variable (units)	**1961–1987**	**1988–2014**	***p***	**1961–1987**	**1988–2014**	***p***
T (C) (mean)	−7.1	−4.6	0.0012**	−13.6	−11.1	0.0012**
Tmax (C)	−4.1	−1.9	0.00087**	−9.5	−7.2	0.0019**
PR (mm)	110.5	142.8	0.0011**	85.8	112.8	0.00015**
PR_S (mm)	59.1	53.2	0.23	74.2	93.4	0.0031**
FR_{PRS} (%)	56.8	39.5	0.0020**	87.1	83.1	0.084
PR_{ML} (mm)	51.4	89.5	0.00050**	11.5	19.4	0.015**
ID (days)	62.9	49.1	0.00081**	81.4	78.0	0.039*

Note. *Statistically significant change at the 5% level.
**Statistically significant change at the 1% level.
The *P*-values for the change between the two periods according to two-sided Mann–Whitney tests are also shown. T: mean temperature; Tmax: mean maximum temperature; PR: total precipitation; PR_S: solid precipitation; FR_{PRS}: fraction of solid precipitation; PR_{ML}: mixed and liquid precipitation; ID: ice day sum.

result. Still, regional differences can be relatively large, even within such a small district as Finland. For example, in western and northern parts of Finland, the last date of the seasonal snow cover period generally changed more than its onset date, but the reverse occurred in eastern and central parts of Finland. A strong retreat in snow cover in spring is generally associated with the positive snow-albedo feedback (Dery and Brown, 2007; AMAP, 2017)—the loss of snow in spring accelerates the warming because the surface becomes darker, which reduces the albedo. On the other hand, the earlier snowmelt has been linked to increases in carbon uptake during spring, which in part counteracts the positive feedback of the earlier snowmelt (Pulliainen *et al.,* 2017).

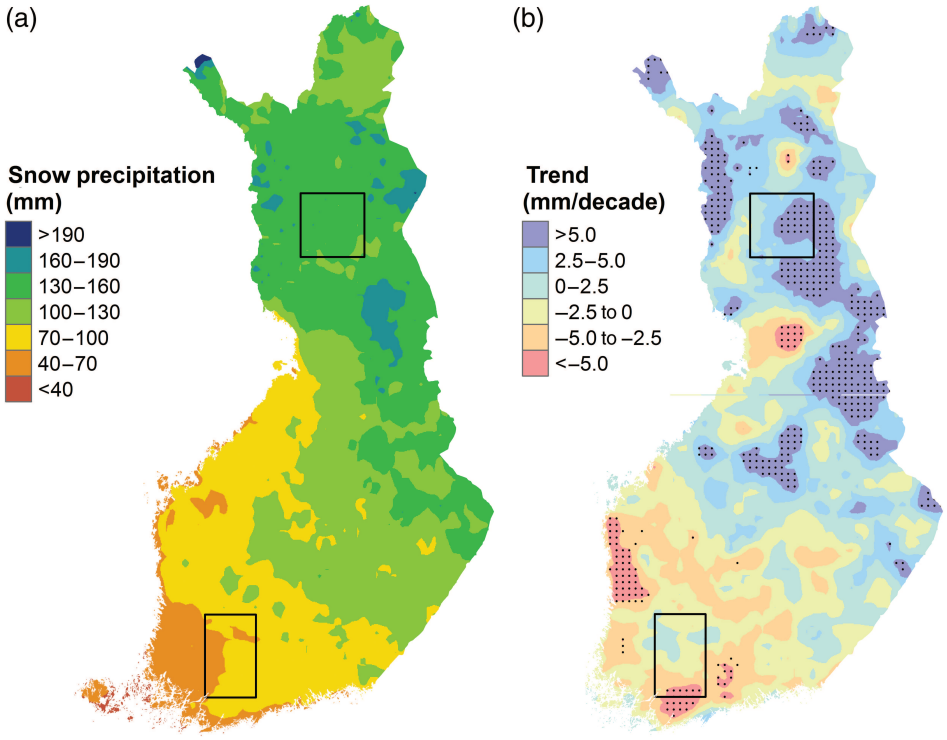

FIGURE 6 (a) Annual amount of solid precipitation (PR_S) in 1961–2014 and (b) its linear trend. The black dots in b mark the areas where the linear trend is significant at the 5% level. The two boxes in the panels denote the SF (southern Finland) and NF (northern Finland) districts

Our results regarding changes in precipitation form in southern Finland agree with the future projections (Bintanja and Andry, 2017), according to which the rainfall is expected to strongly increase and snowfall to moderately decrease throughout the entire Arctic by the end of the 21st century. We also found indications that snowfall events may have become more intense in northern Finland as the solid precipitation increased, but ice days, which are the potential days for snowfall to occur, decreased. Räisänen (2015) found similar results in future projections for the end of the present century; the frequency of days with at least 1 mm of snowfall was projected to decrease in the whole of Finland, most strongly in southwestern Finland, but the intensity of snowfall on those days was simulated to slightly increase everywhere.

Snow density and SWE are connected to snow depth. In an approximately 50-year long time series of snow bulk density at five snow survey locations of the Finnish Environment Institute (SYKE), only weak trends could be detected, but if present, they most often showed either slight decreases in early winter or slight increases in spring density (Rasmus, 2013). Some datasets of SWE do exist, such as the SYKE snow survey data (Reuna, 1994) and the GlobSnow SWE product (Luojus *et al.*, 2013), but they typically cover a shorter time range or are of coarser temporal or spatial resolution than the *FMIClimGrid* dataset utilized in this paper. An option is also to apply a snowpack model to simulate SWE, as undertaken by Irannezhad *et al.* (2016) for three stations in Finland. They found that during a recent century-long period, the simulated annual peak SWE decreased and shifted in time to earlier dates and the continuous snow cover duration shortened at three weather stations located in southern, central and northern parts of the country. Contrary to our results, however, they attributed the changes in snow cover to decreasing snowfall and unchanged wintertime rainfall at all three stations they considered.

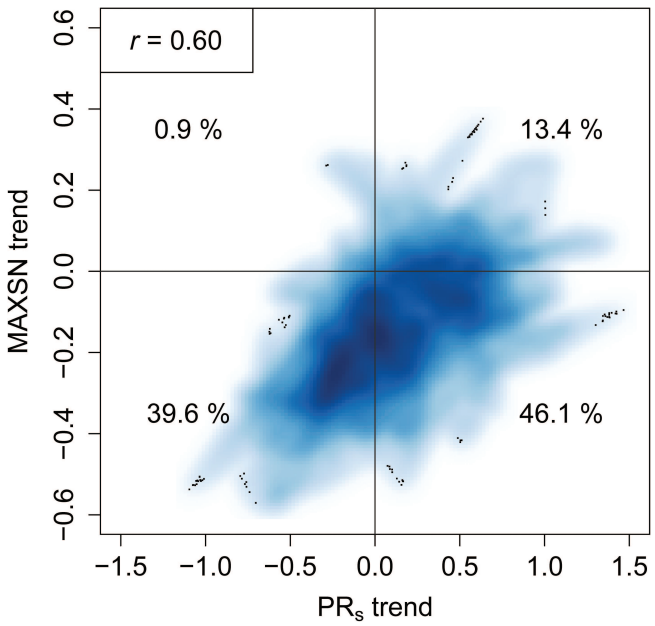

FIGURE 7 Density scatterplot showing the spatial pattern correlation between the linear trends of annual PR_S (mm/decade) and MAXSN (cm/decade). For calculating local densities, 128 bins for both directions were used (default in R function smoothScatter). The percentages depict the proportion of data falling inside each quadrat. The correlation is expressed as Pearson's correlation coefficient (r)

5 | CONCLUSIONS

Snow depth decreased and snow season shortened in large areas in Finland. Increasing precipitation and the changes in its form played a significant role in the changes that were observed. In southern Finland, increasing mixed and liquid precipitation and rising temperature drove the changes. Our results clearly show that in southern Finland, winters are becoming more rainfall-dominated. In northern Finland, the changes and the factors driving them were not as straightforward, as both solid and liquid precipitation were found to increase, and thus the decrease in snow depth was smaller than in southern Finland or non-existent. The change in annual snowfall amount divided Finland roughly to two parts. In northern areas, the winter baseline temperature is still low enough that the increasing temperature largely stays below 0°C, and the increasing precipitation mostly falls as snow.

Despite decreasing monthly snow depth and shortening of the snow season, short-term strong snowfall events may still occur. An example of those was seen on the west coast of Finland in January 2016, when a new national daily snowfall record of 71 cm was measured due to a lake-effect phenomenon (Olsson *et al.,* 2017). Additionally, blizzards may still occur, although their probability of occurrence is projected to decrease in a major part of northern Europe during the ongoing century (Groenemeijer *et al.,* 2016).

Our findings of decreased snow depth, increased mixed and liquid precipitation and, in northern Finland, increased solid precipitation, are in line with the contemporary projections of the future snow conditions for northern Europe (Räisänen and Eklund, 2012; Räisänen, 2015). The general agreement between our results for the past and projected future changes supports the reliability of climate model predictions. However, the exact rate of the future changes is highly dependent on the evolution of the GHG concentrations and natural climatic variability. Using a long-term gridded dataset of snow depth and multiple indices, we can show substantial past changes in local scale snow conditions. These kinds of findings are highly relevant for planning efficient climate change adaptation strategies for multiple sectors.

ACKNOWLEDGEMENTS

This work has been funded by the Academy of Finland through the PLUMES project (Pathways Linking Uncertainties in Model Projections of Climate and its Effects; decision number 278067) and, in its final phase, by the State Nuclear Waste Management Fund in Finland through the Finnish Nuclear Power Plant Safety Research Programme 2015–2018. We thank our colleagues Dr. Ilari Lehtonen and Dr. Heikki Tuomenvirta for their helpful comments regarding precipitation measurements in Finland. We also thank the two anonymous reviewers whose comments helped us to improve this paper.

ORCID

Anna Luomaranta https://orcid.org/0000-0002-0891-7273
Juha Aalto https://orcid.org/0000-0001-6819-4911
Kirsti Jylhä https://orcid.org/0000-0003-0853-4747

REFERENCES

Aalto, J., Pirinen, P. and Jylhä, K. (2016) New gridded daily climatology of Finland: permutation-based uncertainty estimates and temporal trends in climate. *Journal of Geophysical Research – Atmospheres*, 121, 3807–3823. https://doi.org/10.1002/2015JD024651.

AMAP. (2017) *Snow, Water, Ice and Permafrost in the Arctic (SWIPA) (2017).* Oslo, Norway: Arctic Monitoring and Assessment Programme (AMAP) xiv + 267 pp.

Andersson, A. (2010) *Winter road conditions and traffic accidents in Sweden and UK: present and future climate scenarios.* Dissertation A131, University of Gothenburg, Sweden, 113 pp.

Andreescu, M.P. and Frost, D.B. (1998) Weather and traffic accidents in Montreal, Canada. *Climate Research*, 9, 225–230.

Barancourt, C., Creutin, J. and Rivoirard, J. (1992) A method for delineating and estimating rainfall fields. *Water Resources Research*, 28, 1133–1144. https://doi.org/10.1029/91WR02896.

Bintanja, R. and Andry, O. (2017) Towards rain-dominated Arctic. *Nature Climate Change*, 7, 263–267. https://doi.org/10.1038/NCLIMATE3240.

Bjerke, J.W., Karlsen, S.R., Hogda, K.A., Malnes, E., Jepsen, J.U., Lovibond, S., Vikhamer-Schuler, D. and Tømmervik, H. (2014) Record-low primary productivity and high plant damage in the Nordic Arctic Region in 2012 caused by multiple weather events and pest outbreaks. *Environmental Research Letters*, 9, 084006. https://doi.org/10.1088/1748-9326/9/8/084006.

Brown, R.D. (2010) Analysis of snow cover variability and change in Quebec, 1948–2005. *Hydrological Processes*, 24, 1929–1954. https://doi.org/10.1002/hyp.7565.

Brown, R.D. and Mote, P.W. (2009) The response of Northern Hemisphere snow cover to a changing climate. *Journal of Climate*, 22, 2124–2145. https://doi.org/10.1175/2008JCLI2665.1.

Brown, R.D. and Robinson, D.A. (2011) Northern Hemisphere spring snow cover variability and change over 1922–2010 including an assessment of uncertainty. *The Cryosphere*, 5, 219–229. https://doi.org/10.5194/tc-5-219-2011.

Brown, R.D., Schuler, D.V., Bulygina, O., Derksen, C., Luojus, K., Mudryk, L., Wang, L. and Yang, D. (2017) Arctic terrestrial snow cover. In: *Snow, Water, Ice and Permafrost in the Arctic (SWIPA) 2017*. Oslo, Norway: Arctic Monitoring and Assessment Programme (AMAP), pp. 25–64.

Bulygina, O.N., Groisman, P.Y., Razuvaev, V.N. and Korshunova, N.N. (2011) Changes in snow cover characteristics over Northern Eurasia since 1966. *Environmental Research Letters*, 6, 045026. https://doi.org/10.1088/1748-9326/6/4/045204.

Callaghan, T.V., Johansson, M., Brown, R.D., Groisman, P.Y., Labba, N., Radionov, V., Barry, R.G., Bulygina, O.N., Essery, R.L.H., Frolov, D.M., Golubev, V.N., Grenfell, T.C., Petrushina, M.N., Razuvaev, V.N., Robinson, D.A., Romanov, P., Shindell, D., Shmakin, A.B., Sokratov, S.A., Warren, S. and Yang, D. (2012) The changing face of Arctic snow cover: a synthesis of observed and projected changes. *Ambio*, 40, 17–31. https://doi.org/10.1007/s13280-011-0212-y.

Choi, G., Robinson, D.A. and Kang, S. (2010) Changing Northern Hemisphere snow seasons. *Journal of Climate*, 23, 5305–5310. https://doi.org/10.1175/2010JCLI3644.1.

Danco, J.F., DeAngelis, A.M., Raney, B.K. and Broccoli, A.J. (2016) Effects of a warming climate on daily snowfall events in the Northern Hemisphere. *Journal of Climate*, 29, 6295–6318. https://doi.org/10.1175/JCLI-D-15-0687.1.

Derksen, C., Brown, R.D., Mudryk, L. and Luojus, K. (2016) Terrestrial Snow Cover [in Arctic Report Card 2016], http://www.arctic.noaa.gov/Report-Card.

Déry, S.J. and Brown, R.D. (2007) Recent Northern Hemisphere snow cover extent trends and implications for the snow-albedo feedback. *Geophysical Research Letters*, 34, L22504. https://doi.org/10.1029/2007GL031474.

Goovaerts, P. (1999) Geostatistics in soil science: state-of-the-art and perspectives. *Geoderma*, 89, 1–45. https://doi.org/10.1016/S0016-7061(98)00078-0.

Goovaerts, P. (2000) Geostatistical approaches for incorporating elevation into the spatial interpolation of rainfall. *Journal of Hydrology*, 228, 113–129. https://doi.org/10.1016/S0022-1694(00)00144-X.

Groenemeijer, P., Vajda, A., Lehtonen, I., Kämäräinen, M., Venäläinen, A., Gregow, H., Becker, N., Nissen, K., Ulbrich, U., Paprotny, D., Morales Napoles, O. and Púčik, T. (2016) Present and future probability of meteorological and hydrological hazards in Europe. Rain project, D2.5 (Hydro-) meteorological hazard probability in Europe. 165 pp. https://www.researchgate.net/publication/308034040_Present_and_future_probability_of_meteorological_and_hydrological_hazards_in_Europe

Hall, C.M. (2014) Will climate change kill Santa Claus? Climate change and high-latitude Christmas place branding. *Scandinavian Journal of Hospitality and Tourism*, 14, 23–40. https://doi.org/10.1080/15022250.2014.886101.

Hannula, H.-R. (2012). *Napapiirin eteläpuolisen Suomen lumipeite maaliskuussa 1919–2010* [*Snow cover in Finland south from the Arctic Circle in March 1919–2010*]. M.Sc. Thesis, Department of Geography and Geology, University of Turku (Only in Finnish).

Hansen, B.B., Aanes, R., Kohler, I.H.J. and Saether, B.E. (2011) Climate, icing, and wild arctic reindeer: past relationships and future prospects. *Ecology*, 92, 1917–1923. https://doi.org/10.1890/11-0095.1.

Hansen, B.B., Isaksen, K., Benestad, R.E., Kohler, J., Pedersen, Å.Ø., Loe, L.E., Coulson, S.J., Larsen, J.O. and Varpe, Ø. (2014) Warmer and wetter winters: characteristics and implications of an extreme weather event in the High Arctic. *Environmental Research Letters*, 9, 114021. https://doi.org/10.1088/1748-9326/9/11/114021.

Harpold, A.A. and Brooks, P.D. (2018) Humidity determines snowpack ablation under a warming climate. *Proceedings of the National Academy of Sciences of the United States of America*, 115(6), 1215–1220. https://doi.org/10.1073/pnas.1716789115.

Haylock, M., Hofstra, N., Klein Tank, A., Klok, E., Jones, P. and New, M. (2008) A European daily high-resolution gridded data set of surface temperature and precipitation for 1950–2006. *Journal of Geophysical Research*, 113, D20119. https://doi.org/10.1029/2008JD010201.

Hernández-Henríquez, M.A., Déry, S.J. and Derksen, C. (2014) Polar amplification and elevation-dependence in trends of Northern Hemisphere snow cover extent, 1971–2014. *Environmental Research Letters*, 10, 044010. https://doi.org/10.1088/1748-9326/10/4/044010.

Hofstra, N., Haylock, M., New, M., Jones, P. and Frei, C. (2008) Comparison of six methods for the interpolation of daily, European climate data. *Journal of Geophysical Research*, 113, D21110. https://doi.org/10.1029/2008JD010100.

Irannezhad, M., Ronkanen, A.-K. and Kløve, B. (2016) Wintertime climate factors controlling snow resource decline in Finland. *International Journal of Climatology*, 36, 110–131. https://doi.org/10.1002/joc.4332.

Juga, I., Hippi, M., Karsisto V. and Nurmi, P. (2014) Weather factors triggering the massive car crashes on 3 February 2012 in the Helsinki metropolitan area. In: *Proceedings of the 17th SIRWEC Conference, 30 January–1 February 2014*, *La Massana, Andorra.*

Jylhä, K., Fronzek, S., Tuomenvirta, H., Carter, T.R. and Ruosteenoja, K. (2008) Changes in frost, snow and Baltic sea ice by the end of the twenty-first century based on climate model projections for Europe. *Climatic Change*, 86, 441–462. https://doi.org/10.1007/s10584-007-9310-z.

Jylhä, K., Laapas, M., Ruosteenoja, K., Arvola, L., Drebs, A., Kersalo, J., Saku, S., Gregow, H., Hannula, H.-R. and Pirinen, P. (2014) Climate variability and trends in the Valkea-Kotinen region, southern Finland: comparisons between the past, current and projected climates. *Boreal Environment Research*, 19(Supplement A), 4–30.

Kerr, T., Clark, M., Hendrikx, J. and Anderson, B. (2013) Snow distribution in a steep mid-latitude alpine catchment. *Advances in Water Resources*, 55, 17–24. https://doi.org/10.1016/j.advwatres.2012.12.2010.

Keskinen, A. (2012) *Lumilogistiikan tehostaminen kaupungeissa* [*Enhanced snow removal logistics in suburban areas*]. Master's Thesis, Aalto University (Only in Finnish).

Klok, E. and Klein Tank, A. (2009) Updated and extended European dataset of daily climate observations. *International Journal of Climatology*, 29, 1182–1191. https://doi.org/10.1002/joc.1779.

Kohler, J., Brandt, O., Johansson, M. and Callaghan, T. (2006) A long-term Arctic snow depth record from Abisko, northern Sweden, 1913–2004. *Polar Research*, 25, 91–113. https://doi.org/10.1111/j.1751-8369.2006.tb00026.x.

Krasting, J.P., Broccoli, A.J., Dixon, K. and Lanzante, J. (2013) Future changes in northern hemisphere snowfall. *Journal of Climate*, 26, 7813–7828. https://doi.org/10.1175/JCLI-D-12-00832.1.

Kunkel, K.E., Robinson, D.A., Champion, S., Xungang, Y., Estilow, T. and Frankson, R.M. (2016) Trends and extremes in Northern Hemisphere snow characteristics. *Current Climate Change Reports*, 2, 65–73. https://doi.org/10.1007/s40641-016-0036-8.

Kuusisto, E. (1984) *Snow accumulation and snowmelt in Finland.* Publ. of the Water Research Institute 55, National Board of Waters, Finland, 149 pp. Available at https://helda.helsinki.fi/bitstream/handle/10138/31432/Vesientutkimuslaitoksen?sequence=1.

Lehtonen, I. (2015) Four consecutive snow-rich winters in southern Finland: 2009/2010–2012/2013. *Weather*, 70, 3–8.

Lehtonen, I., Kämäräinen, M., Gregow, H., Venäläinen, A. and Peltola, H. (2016) Heavy snow loads in Finnish forests respond regionally asymmetrically to projected climate change. *Natural Hazards and Earth System Sciences*, 16, 2259–2271. https://doi.org/10.5194/nhess-16-2259-2016.

Lehtonen, I., Venäläinen, A., Ikonen, J., Puttonen, N. and Gregow, H. (2013) *Some features of winter climate in northern Fennoscandia, Ilmatieteen laitos, Raportteja.* Finnish Meteorological Institute. Report number: 2013:3, 32 pp.

Lépy, É. and Pasanen, L. (2017) Observed regional climate variability during the last 50 years in Reindeer Herding Cooperatives of Finnish Fell Lapland. *Climate*, 5, 81. https://doi.org/10.3390/cli5040081.

Luojus, K., Pulliainen, J., Takala, M., Kangwa, M., Smolander, T., Wiesmann, A., Derksen, C., Metsämäki, S., Salminen, M., Solberg, R., Nagler, T., Bippus, G. Wunderle, S. and Hüsler, F. (2013) GlobSnow-2 Product User Guide Version 1.0., 24 p. Available at: http://www.globsnow.info/se/GlobSnow2_SE_SWE_Product_User_Guide_v1_r1.pdf

Mankin, J.S. and Diffenbaugh, N.S. (2015) Influence of temperature and precipitation variability on near-term snow trends. *Climate Dynamics*, 45, 1099–1116. https://doi.org/10.1007/s00382-014-2357-4.

Matheron, G. (1963) Principles of geostatistics. *Economic Geology*, 58, 1246–1266.

Merkouriadi, I., Leppäranta, M. and Järvinen, O. (2017) Interannual variability and trends in winter weather and snow conditions in Finnish Lapland. *Estonian Journal of Earth Sciences*, 66(1), 47–57. https://doi.org/10.3176/earth.2017.03.

Mioduszewski, J.R., Rennermalm, A.K., Robinson, D.A. and Wang, L. (2015) Controls on spatial and temporal variability in Northern Hemisphere terrestrial snow melt timing, 1979–2012. *Journal of Climate*, 28, 2136–2153. https://doi.org/10.1175/JCLI-D-14-00558.1.

Mudryk, L.R., Kushner, P.J., Derksen, C. and Thackeray, C. (2016) Snow cover response to temperature in observational and climate model ensembles. *Geophysical Research Letters*, 44, 919–926. https://doi.org/10.1002/2016GL071789.

Najafi, M.R., Zwiers, R. and Gillett, N. (2016) Attribution of the observed spring snowpack decline in British Columbia to anthropogenic climate change. *Journal of Climate*, 40, 4113–4130. https://doi.org/10.1175/JCLI-D-16-0189.s1.

Neuvonen, M., Sievänen, T., Fronzek, S., Lahtinen, I., Veijalainen, N. and Carter, T.R. (2015) Vulnerability of cross-country skiing to climate change in Finland— an interactive mapping tool. *Journal of Outdoor Recreation and Tourism*, 11, 64–79. https://doi.org/10.1016/j.jort.2015.06.010.

Olsson, T., Perttula, T., Jylhä, K. and Luomaranta, A. (2017) Intense sea-effect snowfall case on the western coast of Finland. *Advances in Science and Research*, 14, 231–239. https://doi.org/10.5194/asr-14-231-2017.

Park, H., Yabuki, H. and Ohata, T. (2012) Analysis of satellite and model datasets for variability and trends in Arctic snow extent and depth, 1948–2006. *Polar Science*, 6, 23–37. https://doi.org/10.1016/j.polar.2011.11.002.

Peltonen-Sainio, P., Pirinen, P., Laapas, M., Mäkelä, H.M., Ojanen, H. and Venäläinen, A. (2016) Spatial and temporal variation in weather events critical for boreal agriculture: III Frost and winter time fluctuation. *Agricultural and Food Science*, 25, 71–80.

Pulliainen, J., Aurela, M., Laurila, T., Aalto, T., Takala, M., Salminen, M., Kulmala, M., Barr, A., Heimann, M., Lindroth, A., Laaksonen, A., Derksen, C., Mäkelä, A., Markkanen, T., Lemmetyinen, J., Susiluoto, J., Dengel, S., Mammarella, I., Tuovinen, J.P. and Vesala, T. (2017) Early

snowmelt significantly enhances boreal springtime carbon uptake. *Proceedings of the National Academy of Sciences of the United States of America*, 114, 11081–11086. https://doi.org/10.1073/pnas.1707889114.

Räisänen, J. (2008) Warmer climate: less or more snow? *Climate Dynamics*, 30 (2), 307–331. https://doi.org/10.1007/s00382-007-0289-y.

Räisänen, J. (2015) Twenty-first century changes in snowfall climate in Northern Europe in ENSEMBLES regional climate models. *Climate Dynamics*, 46, 339–353. https://doi.org/10.1007/s00382-015-2587-0.

Räisänen, J. and Eklund, J. (2012) 21st Century changes in snow climate in Northern Europe: a high-resolution view from ENSEMBLES regional climate models. *Climate Dynamics*, 38, 2575–2591. https://doi.org/10.1007/s00382-011-1076-3.

Rasmus, S. (2013) Spatial and temporal variability of snow bulk density and seasonal snow densification behavior in Finland. *Geophysica*, 49, 53–74.

Rasmus, S., Kivinen, S., Bavay, M. and Heiskanen, J. (2016) Local and regional variability in snow conditions in northern Finland: a reindeer herding perspective. *Ambio*, 45, 398–414. https://doi.org/10.1007/s13280-015-0762-5.

Rasmus, S., Kumpula, J. and Jylhä, K. (2014) Suomen poronhoitoalueen muuttuvat talviset sää- ja lumiolosuhteet. [The changing winter weather and snow conditions in Finnish reindeer husbandry area]. *Terra*, 126, 4.

Rasmus, S., Kumpula, J. and Siitari, J. (2014) Can a snow structure model estimate snow characteristics relevant to reindeer husbandry? *Rangifer*, 34, 37–56.

Reuna, M. (1994) An operational grid method for estimation of the areal water equivalent of snow. *Geophysica*, 30, 107–121.

Skaugen, T., Stranden, H.B. and Saloranta, T. (2012) Trends in snow water equivalent in Norway (1931–2009). *Hydrology Research*, 43, 489–499. https://doi.org/10.2166/nh.2012.109.

Stuefer, S., Kane, D.L. and Liston, G.E. (2013) In situ snow water equivalent observations in the US Arctic. *Hydrology Research*, 44, 21–34. https://doi.org/10.2166/nh.2012.177.

Takala, M., Luojus, K., Pulliainen, J., Derksen, C., Lemmetyinen, J., Kärnä, J.-P., Koskinen, J. and Bojkov, B. (2011) Estimating northern hemisphere snow water equivalent for climate research through assimilation of space-borne radiometer data and ground-based measurements. *Remote Sensing of Environment*, 115, 3517–3529. https://doi.org/10.1016/j.rse.2011.08.014.

Taskinen, A. and Söderholm, K. (2016) Operational correction of daily precipitation measurements in Finland. *Boreal Environment Research*, 21, 1–24.

Tervo-Kankare, K., Hall, C.M. and Saarinen, J. (2013) Christmas Tourists' perceptions to climate change in Rovaniemi, Finland. *Tourism Geographies*, 15, 292–317. https://doi.org/10.1080/14616688.2012.726265.

Turunen, M.T., Rasmus, S., Bavay, M., Ruosteenoja, K. and Heiskanen, J. (2016) Coping with difficult weather and snow conditions: reindeer herders' views on climate change impacts and coping strategies. *Climate Risk Management*, 11, 15–36. https://doi.org/10.1016/j.crm.2016.01.002.

Vajda, A., Tuomenvirta, H., Juga, I., Nurmi, P., Jokinen, P. and And Rauhala, J. (2014) Severe weather affecting European transport systems: the identification, classification and frequencies of events. *Natural Hazards*, 72(1), 169–188. https://doi.org/10.1007/s11069-013-0895-4.

Vaughan, D.G., Comiso, J.C., Allison, I., Carrasco, J., Kaser, G., Kwok, R., Mote, P., Murray, T., Paul, F., Ren, J., Rignot, E., Solomina, O., Steffen, K. and Zhang, T. (2013) Observations: cryosphere. In: Stocker, T.F., Qin, D., Plattner, G.-K., Tignor, M., Allen, S.K., Boschung, J., Nauels, A., Xia, Y., Bex, V. and Midgley, P.M. (Eds.) *Climate Change 2013: The Physical Science Basis. Contribution of Working Group I to the Fifth Assessment Report of the Intergovernmental Panel on Climate Change*. Cambridge, United Kingdom and New York, NY: Cambridge University Press.

Ye, H. and Cohen, J. (2013) A shorter snowfall season associated with higher air temperatures over northern Eurasia. *Environmental Research Letters*, 8, 014052. https://doi.org/10.1088/1748-9326/8/1/014052.

Yettella, V. and Kay, J.E. (2017) How will precipitation change in extratropical cyclones as the planet warms? Insights from a large initial condition climate model ensemble. *Climate Dynamics*, 49, 1765–1781. https://doi.org/10.1007/s00382-016-3410-2.

Zhong, X., Zhang, T., Kang, S., Wang, K., Zheng, L., Hu, Y. and Wang, H. (2018) Spatiotemporal variability of snow depth across the Eurasian continent from 1966 to 2012. *The Cryosphere*, 12, 227–245. https://doi.org/10.5194/tc-12-227-2018.

SUPPORTING INFORMATION

Additional supporting information may be found online in the Supporting Information section at the end of the article.

How to cite this article: Luomaranta A, Aalto J, Jylhä K. Snow cover trends in Finland over 1961–2014 based on gridded snow depth observations. *Int J Climatol*. 2019;1–13. https://doi.org/10.1002/joc.6007

APPENDIX

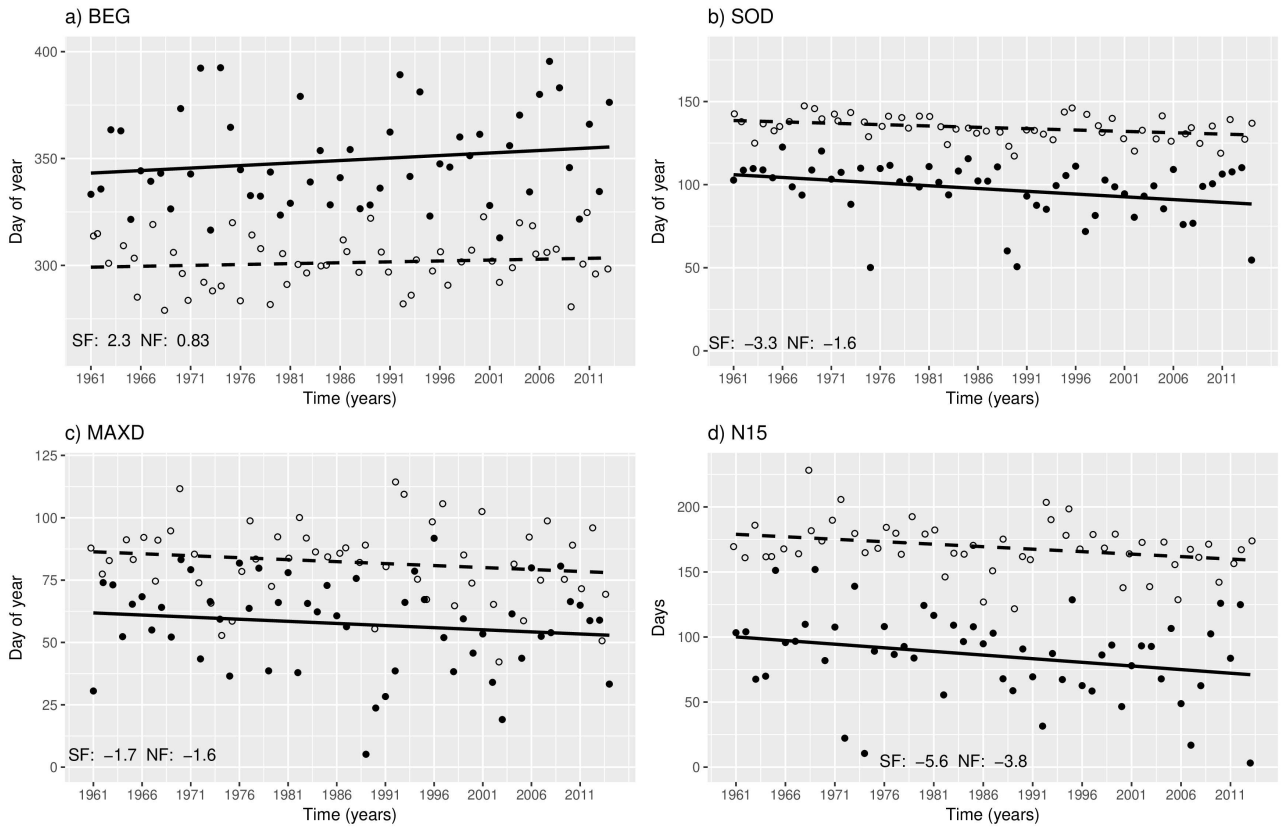

Fig. A1. The regionally averaged time series for a) BEG, b) SOD, c) MAXD and d) N15 and their linear trends in the SF (black dots) and NF (open circles) study domains. The slopes for the trends are given in each graph.

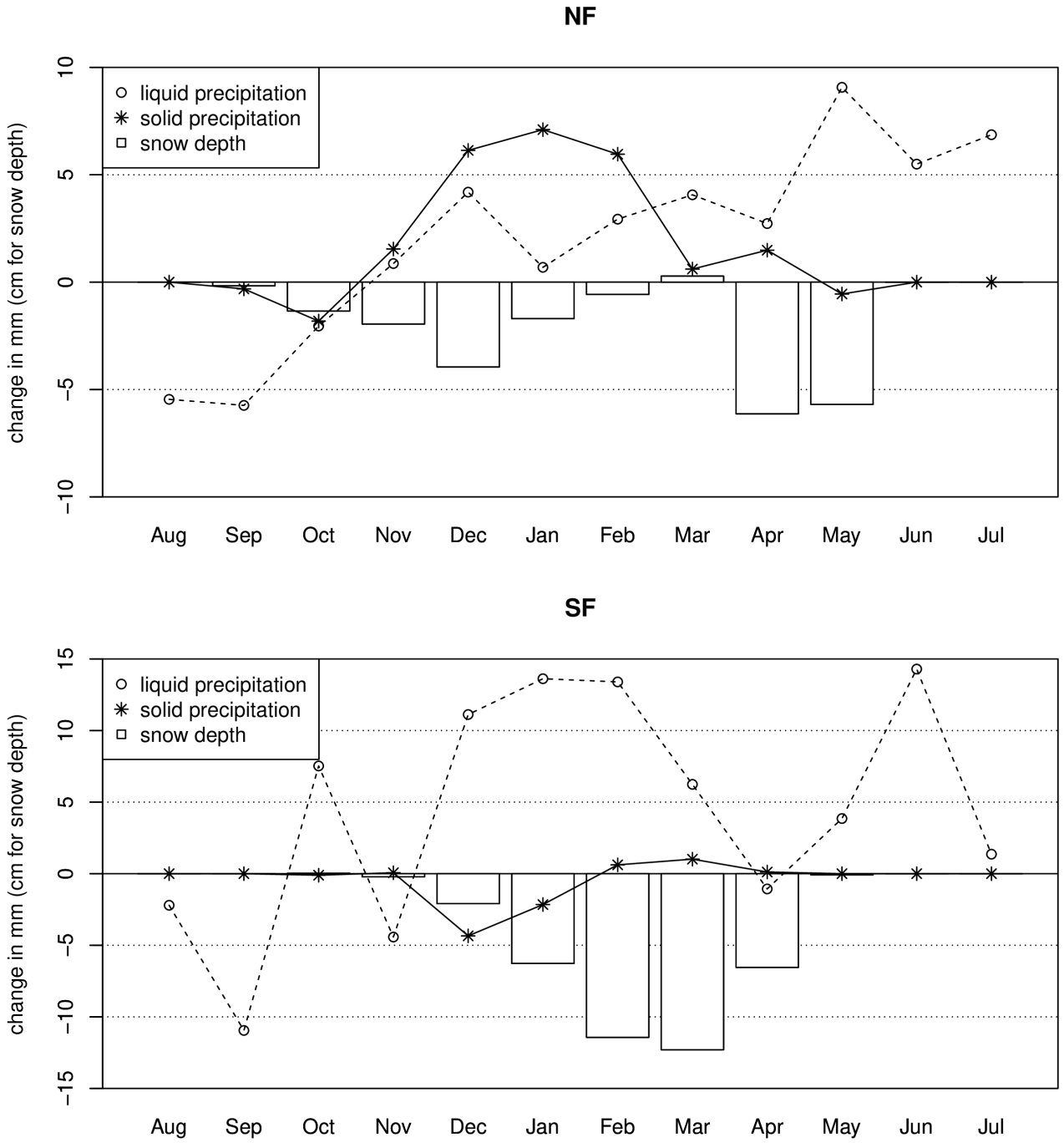

Fig. A2. The absolute change in monthly mean snow depth (cm), monthly amount of solid precipitation (mm) and monthly amount of liquid and mixed precipitation (mm) between the two study periods 1961-1987 and 1988-2014 in NF (upper panel) and SF (lower panel). Note the different units for precipitation and snow depth.

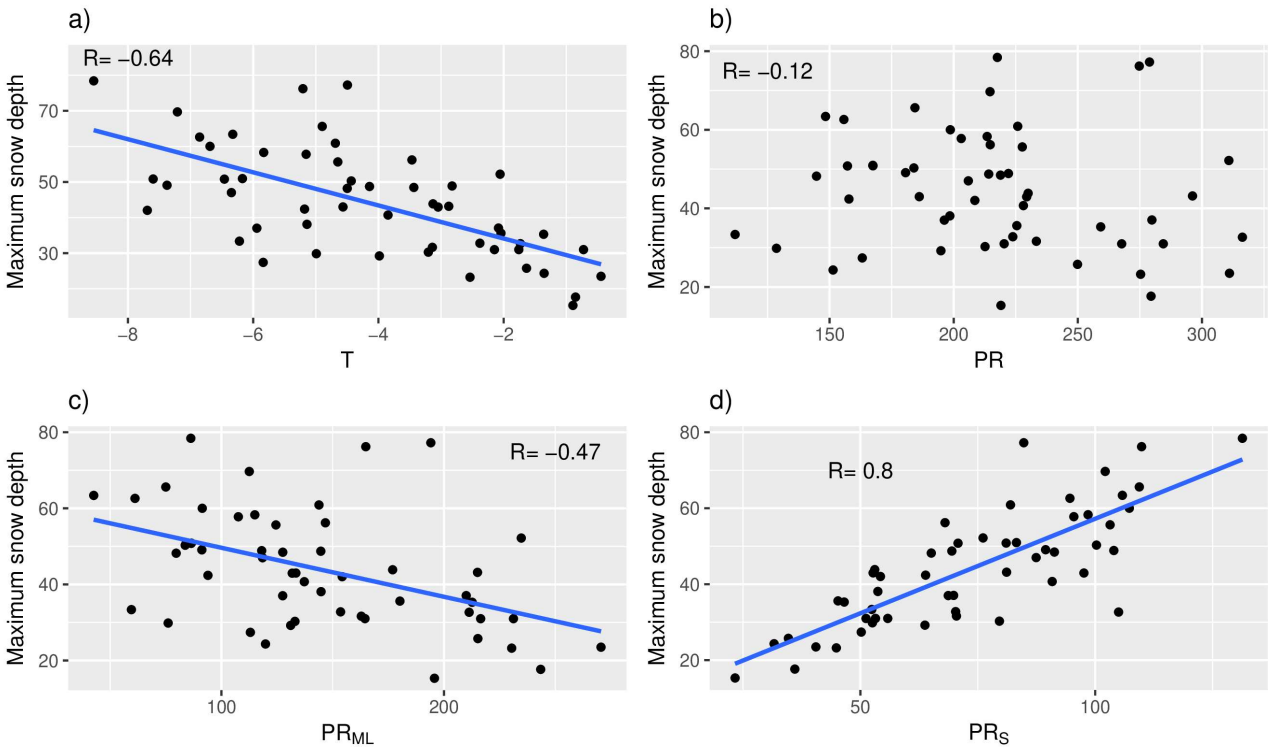

Figure A3. Scatterplots showing the relationships between regionally averaged annual maximum snow depth and a) November-March mean temperature (T), b) November-March total precipitation (PR), c) November-March mixed and liquid precipitation (PR_{ML}), and d) November-March solid precipitation (PR_S) for each year of the 1961-2014 study period in domain SF. Pearson's correlation coefficient (R) is given in each graph. The linear trend is fitted if the correlation is significant at the 5% level.

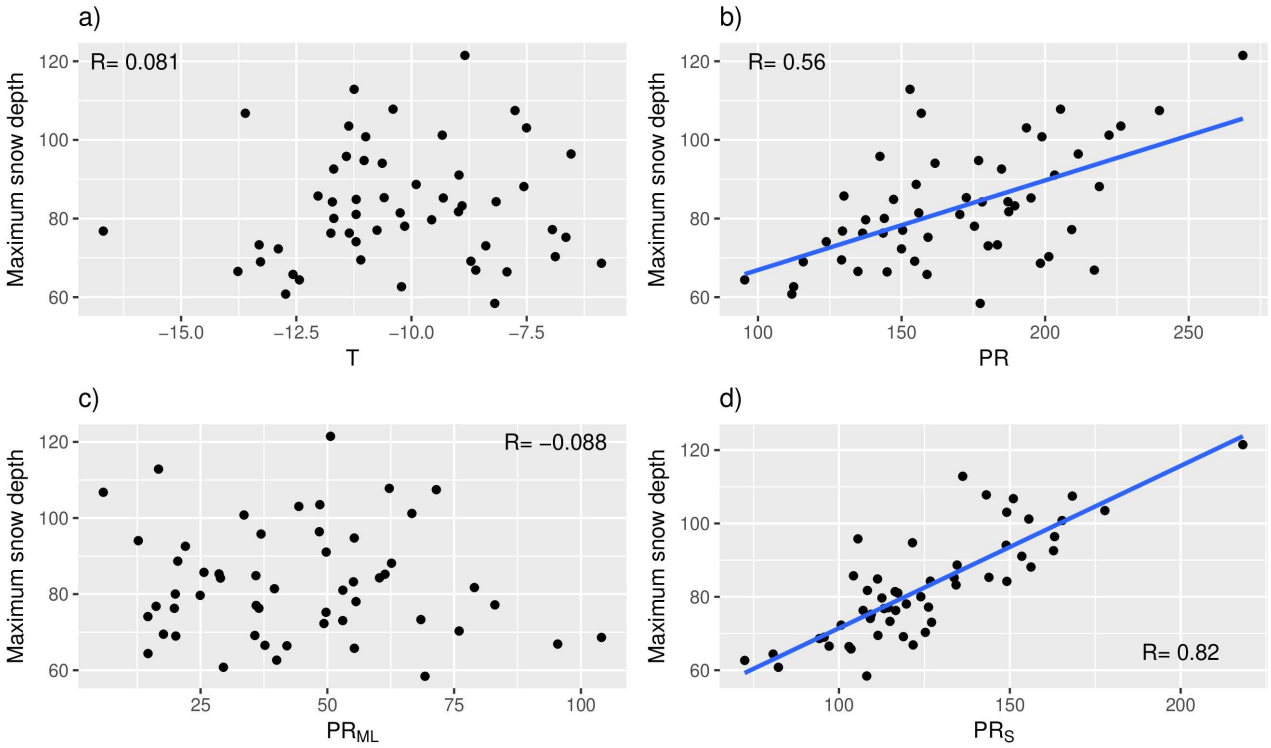

Figure A4. Scatterplots showing the relationships between regionally averaged annual maximum snow depth and a) November-March mean temperature, b) November-March total precipitation, c) November-March mixed and liquid precipitation, and d) November-March solid precipitation for each year of the 1961-2014 study period in domain NF. Pearson's correlation coefficient (R) is given in each graph. The linear trend is fitted if the correlation is significant at the 5% level.

II

Science of the Total Environment 710 (2020) 136229

Contents lists available at ScienceDirect

Science of the Total Environment

journal homepage: www.elsevier.com/locate/scitotenv

Climate change and reindeer management in Finland: Co-analysis of practitioner knowledge and meteorological data for better adaptation

Sirpa Rasmus [a,b,*], Minna Turunen [a], Anna Luomaranta [c], Sonja Kivinen [d], Kirsti Jylhä [c], Jani Räihä [c]

[a] Arctic Centre, University of Lapland, P.O. Box 122, FI-96101 Rovaniemi, Finland
[b] Department of Biological and Environmental Science, University of Jyväskylä, P.O. Box 35, FI-40014 University of Jyväskylä, Finland
[c] Finnish Meteorological Institute, P. O. Box 503, FI-00101 Helsinki, Finland
[d] Department of Geographical and Historical Studies, University of Eastern Finland, P. O. Box 111, FI-80101 Joensuu, Finland

HIGHLIGHTS

- Systematically collected reindeer herder knowledge was combined to weather data.
- Practitioner knowledge was mainly in line with the long-term meteorological data.
- Changing seasonal climate affects reindeer condition and herding practices.
- Adaptation requires development of work practices and the governance of herding.
- Our approach can ease the dialogue between the practitioners and policy makers.

GRAPHICAL ABSTRACT

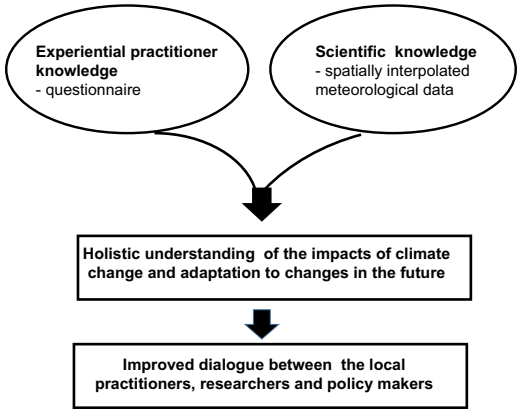

ARTICLE INFO

Article history:
Received 9 August 2019
Received in revised form 18 December 2019
Accepted 18 December 2019
Available online 27 December 2019

Editor: SCOTT SHERIDAN

Keywords:
Adaptation
Climate change
Northern Fennoscandia
Practitioner knowledge
Reindeer management
Seasonal weather

ABSTRACT

We studied interannual variability and changes over time in selected climate indices in the reindeer management area (RMA) in northern Finland. We present together the knowledge possessed by reindeer herders with information from meteorological measurements over three decades. The practitioner knowledge was gathered via a survey questionnaire addressing herder observations of long-term changes (approximately during the past 30 years) in climatic conditions and their impacts on herding during the four seasons. A set of temperature-, precipitation- and snow-related indices relevant for herding within the RMA was derived from spatially interpolated daily meteorological data (1981–2010). Climatic changes detected based on the measurement data were mainly consistent with earlier studies, and practitioner knowledge was generally in line with the meteorological data. The herders had experienced the largest number of changes during the winter, and the smallest number of changes during the summer. The herders reported various impacts of changing seasonal weather on reindeer condition and behavior, and on herding practices. Adaptation to the changing conditions requires adoption of various coping strategies by the herders in their everyday work, continuous development of professional techniques and practices, as well as support received from the governance of reindeer management. We conclude that holistic understanding of the impacts of climate change and adaptation to changes in the future requires simultaneous analyses of data from different sources, more research co-defined with local practitioners, and co-

* Corresponding author at: Arctic Centre, University of Lapland, P.O. Box 122, FI-96101 Rovaniemi, Finland.
E-mail address: sirpa.rasmus@ulapland.fi (S. Rasmus).

https://doi.org/10.1016/j.scitotenv.2019.136229

planned governance solutions. The approach presented in this work can ease the dialogue between the local practitioners, researchers and policy makers.

1. Introduction

Knowledge sets gained outside the scientific communities such as *indigenous knowledge (IK)*, *traditional ecological knowledge (TEK)* or *practitioner knowledge* are often defined as contextual, local knowledge, typically passed on from one generation to the next, and often attributed to a particular ethnic group inhabiting a given area. This knowledge has been used as a basis for local level decision-making within a given livelihood and community (Agrawal, 1995; Ingold and Kurttila, 2000; Menzies and Butler, 2006; Berkes, 2008; Buchanan et al., 2016). Its use for scientific purposes has been criticized for lack of systematic approach to data collection, uncertainties and potential bias within the dataset, missing common terminology, and for being incommensurate with the spatial and temporal scales of observational data (Couzin, 2007; Monastersky, 2009; Alexander et al., 2011; Huntington, 2011). Nevertheless, during the 21st century, the value of local knowledge is being increasingly acknowledged, particularly in the sparsely populated areas where observational data may be scarce or seasonally biased and the time-series length insufficient (Couzin, 2007; Alexander et al., 2011; Huntington, 2011; IPCC, 2019).

Arctic and subarctic regions have shown significant warming trends during the recent decades (AMAP, 2017; Kivinen et al., 2017; IPCC, 2018; Marshall et al., 2018). Experiences of northern communities of changing climate have been collected in different parts of the circumpolar area (e.g. ACIA, 2004). Reindeer herders in northern Fennoscandia and Russia have extensive knowledge on weather. Weather conditions can strongly affect reindeer pastures, reindeer condition, reproduction, and mortality, and increase the workload and costs of reindeer husbandry (Heggberget et al., 2002; Kumpula and Colpaert, 2003; Helle and Kojola, 2008; Kumpula, 2012; Turunen et al., 2016). Herders thus need to continually monitor the grazing conditions during different seasons (e.g. Helle, 1984; Ryd, 2001; Eira et al., 2013).

Climate change, manifesting itself as long-term warming and changes in precipitation and snow conditions, is expected to have both positive and negative impacts on herding (Moen, 2008; Turunen et al., 2016). For example, on one hand, warmer early winters with varying temperatures and events like rain-on-snow (ROS) or thaw-freeze may lead to more frequent icing of snow and basal ice, which can hinder reindeer access to ground lichens (Rasmus et al., 2016, 2018; Eira et al., 2018). Warm autumns may also result in the growth of mycotoxin-producing microfungi (molds) below the snow in reindeer pastures (Kumpula et al., 2000; Rasmus et al., 2018). On the other hand, warmer winter weather can help reindeer keep fit, and early snowmelt and increased availability of fresh forage in spring are favorable for lactating reindeer and the new-born calves (Kumpula and Colpaert, 2003; Mårell et al., 2006; Helle and Kojola, 2008; Turunen et al., 2009; Tveraa et al., 2013). Warmer summers with increased precipitation may lead to more severe insect harassment and more frequent parasite epidemics (Soppela et al., 1986; Soppela, 2009; Laaksonen et al., 2007, 2010; Härkönen et al., 2010). Further, cold summers with heavy rains are considered harmful to young calves (Helle and Aspi, 1984; Helle and Kojola, 1994; Hagemoen and Reimers, 2002; Weladji et al., 2003; Turunen et al., 2016).

Both indigenous Saami and non-Saami Finns practice reindeer husbandry in Finland, unlike in Sweden and Norway where it is mainly an exclusive right of the Saami (Helle and Jaakkola, 2008; Soppela and Turunen, 2017). We consider the knowledge of herders as *practitioner knowledge* (Ingold, 2000). Practitioner knowledge widens the scope of IK or TEK to acknowledge the non-ethnic nature of knowledge gained in certain livelihoods by spending time on the land, developing skills, and evolving knowledge through practice and experience. Practitioner knowledge on reindeer and the environment possessed by the herders is acquired since childhood and passed on from one generation to the next (Forbes, 2006; Forbes and Stammler, 2009; Vuojala-Magga et al., 2011). Reindeer herders traditionally have various coping strategies to deal with adverse weather and pasture conditions. These strategies are based on context-situated learning where new knowledge about new situations and new practices adopted is accumulated and exchanged within the herding community (Turunen and Vuojala-Magga, 2014). Today, in the rapidly changing Arctic environments, unprecedented challenges related to adverse weather conditions may emerge, and no coping strategies operate for them exist thus far (Peltonen-Sainio et al., 2017; Eira et al., 2018).

In previous studies, collection of reindeer herder knowledge has been rather localized in space and time (Helander, 2004; Vuojala-Magga et al., 2011; Turunen et al., 2016; Jaakkola et al., 2018), systematic collection of herder knowledge for research purposes has been rare, and relating such local knowledge with scientific observations even rarer. We anticipate that relating practitioner knowledge of herders and meteorological measurements gives more in-depth understanding of the environmental changes in northern regions, also of aspects like experiences, impacts and coping. In this article, we examine the changes in climate conditions in the reindeer management area (RMA) in northern Finland during the past 30 years using knowledge of reindeer herders together with information originating from meteorological measurements. Rather than compare, nor validate either of the knowledge sets in detail, we aim at presenting the knowledge sets together to bring out the most important outcomes of both. We also review which coping strategies the herders use in their daily herding work and what kinds of governance level adaptation strategies exist. The objectives of this paper are to:

1) Study reindeer herder observations of changes in seasonal weather characteristics and their consequent impact on herding in forest and fell regions during the past 30 years.
2) Examine the inter-annual variability and changes over time of various climate indices relevant for herding, using high-resolution daily meteorological data covering approximately the same period;
3) Give an overview of the strategies to cope with difficult weather conditions, both from the viewpoint of everyday herding work and regarding policies that govern the reindeer management in Finland;
4) Discuss how these different knowledge sets can be used together, to create new understanding of the effects of climate change on the nature-based livelihoods, such as reindeer management, and to support decision-making on adaptation to climate change.

2. Materials and methods

2.1. Reindeer management area

In the Finnish reindeer management area (RMA) covering 36% of the country (Fig. 1, Supplementary text S1, Fig. S1 and Table S1), the semi-domesticated reindeer (*Rangifer tarandus tarandus*) has, in principle, a free grazing right. The RMA is divided into 54 herding districts, the organization and activities of which are guided by the Reindeer Husbandry Act (848/1990). The 21 northernmost districts

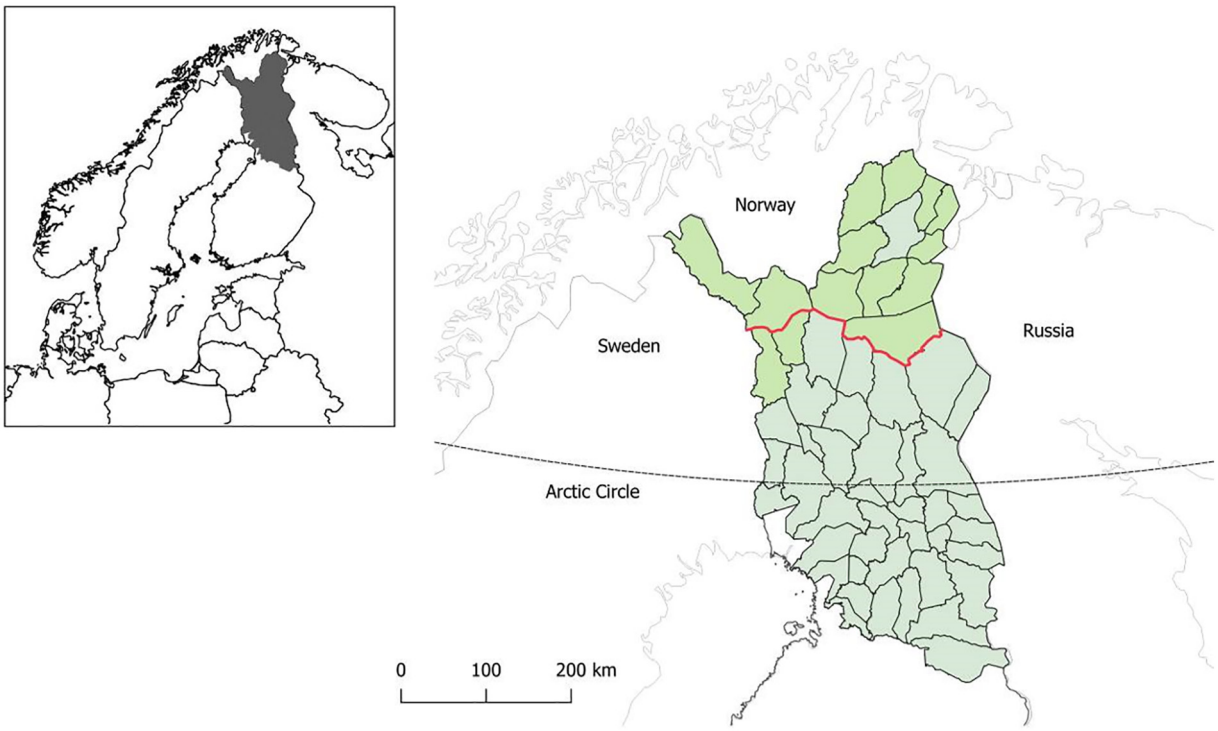

Fig. 1. The reindeer management area (RMA) of Finland. The thin black lines show borders of herding districts. Green and gray shading indicate fell and forest reindeer husbandry regions, respectively. The border between the regions generally follows the southern border of the Saami Homeland area in Finland (red line). (For interpretation of the references to colour in this figure legend, the reader is referred to the web version of this article.)

belong to an area specially intended for reindeer husbandry,[1] and 13 of these are located within the Saami Homeland area. The maximum allowed number of reindeer over one-year-old (the winter stock) is currently 203,700 within the whole RMA. About 100,000 calves are born in the spring, and 80,000 calves and 20,000 over one-year-old reindeer are slaughtered in the autumn (RHA, 2018).

We have divided the RMA into two major study areas, which differ from their environmental conditions, reindeer herding practices and culture: 1) forest reindeer husbandry region and 2) fell reindeer husbandry region (Fig. 1, Table 1). Forest reindeer husbandry region is situated within the boreal forest zone and fell reindeer husbandry region within the mountain birch woodland zone. The border between the forest and fell reindeer husbandry regions generally follows the southern border of the Saami Homeland area as well as southern timberline of spruce (Franke et al., 2015). In the Saami Homeland, reindeer herds are generally larger and herding is more commonly the main source of livelihood, whereas in southern districts, herding is traditionally more often combined with other livelihoods, particularly forestry and tourism (Soppela and Turunen, 2017; Jaakkola et al., 2018).

2.2. Survey on the practitioner knowledge possessed by reindeer herders

Practitioner knowledge of reindeer herders was gathered via a survey which was planned in collaboration with Metsähallitus, Reindeer Herders' Association, Finnish Environment Institute (SYKE), the University of Lapland and the University of Jyväskylä (see also Markkula et al., 2019). The survey was part of the assessment of threatened habitat types in Finland in 2018 (Pääkkölä et al., 2018). It was conducted in the form of a questionnaire using the Webropol survey tool. The survey was open from 13 October 2016 to 28 February 2017 (Supplementary text S2). The survey was distributed systematically to all herding districts through the information services of the Reindeer Herders' Association using its Internet page, Facebook page, electronic mailing list and the professional journal *Poromies* which, in theory, reaches every reindeer owner in Finland.

The questionnaire comprised of 26 arguments that addressed changes in climate on a seasonal basis and their impacts on herding during the past 30 years (approximately from the 1980s to the 2010s). Young herders who participated in the survey were instructed to consider the changes they had experienced during their whole life. The arguments were formulated using existing knowledge on projected climate change in northern Finland (e.g. Ruosteenoja et al., 2015, 2016) and knowledge of the impacts of weather conditions on reindeer well-being and herding (e.g. Vuojala-Magga et al., 2011; Turunen et al., 2016; Supplementary text S1). The arguments were formulated to express the changes generally associated with warming climate. Because of this, some framing effect cannot be ruled out.

The respondents were asked to express their level of agreement/disagreement with the arguments on a five-point scale, coded as follows: 1) I have observed a change in this feature into the direction of the argument 2) I have observed some change in this feature into the direction of the argument 3) I have not observed any change in this feature 4) I have observed some change in this feature, but into the opposite direction 5) I have observed a change in this feature, but into the opposite direction. Respondents also had the possibility to describe the observed changes and their impacts on herding in more detail in a free-form text field in the questionnaire.

For this study we define a person as a herder if he/she owns reindeer, practices herding either full-time or part-time, and earns at least part of the income through practicing herding - and most importantly, defines himself/herself as a herder. It is estimated that there are approximately 2000 active reindeer herders in Finland (RHA, 2018). A total of 90

[1] When referring to reindeer as a livelihood, we use the term "reindeer husbandry". "Herding" refers to day-to-day practices (and it also appears in the term "reindeer herding district"), whereas husbandry considers reindeer as a resource and is related e.g. to the profits, breeding, and social mechanisms. "Reindeer management" is related to all of the practices pertaining to the keeping of reindeer, including governance (Forbes, 2006).

Table 1
Main characteristics of fell and forest reindeer husbandry regions.

	Fell reindeer husbandry region	Forest reindeer husbandry region
Vegetation zone[a]	Mountain birch woodland, treeless heaths, boreal forest (Scots pine)	Boreal forests (Scots pine, Norway spruce)
Total area (km^2)[b]	37,221	85,600
Climate		
Mean annual temperature (°C)[c]	−1.3	0.3
Mean annual precipitation (mm)[c]	486	581
Mean maximum snow depth (cm)[c]	86	85
Reindeer management		
Number of reindeer[b]	82,745	115,576
Number of reindeer owners[b]	1383	3047
Reindeer/owner[b]	70.4	37.4
Supplementary winter feeding[d]:		
-in enclosures (% of reindeer)	8.5	76.5
-in the field or to support herding (%)	65.2	17.4
-no supplementary winter feeding (%)	26.4	6.1
Pasture rotation in use (% of districts)[d]	100	21

[a] Oksanen and Virtanen (1995) and Virtanen et al. (2016).
[b] During a herding year 2016–2017; approximately one third of reindeer owners are women, and 10–15% are under-aged (RHA, 2018), reindeer owners belonging to these groups are less involved in the daily practices of herding.
[c] During 1981–2010 (Pirinen et al., 2012).
[d] During 2004–2015 (RHA, 2018).

reindeer herders from 42 herding districts responded to the survey. This gives us a response rate of 4.5%.

Responses were received from nine out of 14 districts of the fell reindeer husbandry region (henceforth fell districts), and from 33 out of 40 districts of the forest reindeer husbandry region (henceforth forest districts). About 44% of respondents had herding as their full-time job and 56% as a part-time job. The average age of respondents was 51 years. Based on the age distribution of respondents, we estimate that at least 80% of the respondents have at least 30 years of experience on practicing the livelihood. Respondents gave altogether 160 in-depth descriptions of the seasonal weather changes (41 for summer, 39 for autumn, 36 for winter and 44 for spring) and 194 descriptions of consequent effects on herding (46 for summer, 47 for autumn, 50 for winter and 51 for spring).

The reindeer herder responses were analyzed separately for the fell and forest districts in Fig. 1. We classified the replies as agreements (values 1–2; change observed into the direction of the argument), neutrals (3; no change observed) and disagreements (values 4–5; change observed into opposite direction). The key findings of the study are presented in the form of maps, while more detailed results are shown as column charts in the Supplementary material (Figs. S2–S9).

Adaptation actions performed in response to climate changes were not explicitly addressed by the survey, but, in their free-form comments, many respondents explained the coping strategies they had adopted in their everyday herding work (altogether 62 references). The free-form comments are presented in full in the Supplementary material (Tables S2–S9) and some excerpts of this material are presented in this article to illustrate the effects of the ongoing climate change on the nature-based livelihoods from a more holistic perspective.

2.3. Climate indices

Alongside analyses of the herder observations and perceptions, a suite of seasonal and annual climate indices were calculated on the basis of information from meteorological measurements during the period 1981–2010. A total of 14 temperature-, precipitation- and snow-related indices relevant for reindeer herding were considered (Table 2). Three of the indices (ID, R1d, RR10) belong to the core set of extreme indices recommended by the Expert Team on Climate Change Detection and Indices (ETCCDI; e.g. Sillmann et al., 2013). The snow-related indices were selected from a set of indices examined by Luomaranta et al. (2019). The indices for prolonged warm and wet periods (Warm1w and Wet2w) were originally defined by Peltonen-Sainio et al. (2016a) and used in studies on weather risks in agriculture (Peltonen-Sainio et al., 2016b, 2016c).

For calculating the indices, seasons were defined as JJA (summer), SON (autumn), DJF (winter) and MAM (spring). The number of rainfall days (Rain-d) was set equal to the number of wet days having daily minimum temperature equal to or above zero. When the number of rain-on-snow days (ROS-d) was calculated, a condition of at least 1 cm snow depth was added to this definition. In northern Finland, the day is generally regarded as hot if the daily mean temperature is higher than 20 °C, and cold if it is lower than −25 °C. The number of hot days (Hot-d) and cold days (Cold-d) were defined accordingly (Table 2).

The climate indices were derived from FMIClimGrid, a daily gridded climate dataset covering Finland with a spatial resolution of 10 km × 10 km (Aalto et al., 2016). The dataset consists of daily values of seven climate variables, of which five were used in the present study: minimum, maximum and mean temperature, precipitation and snow depth (Table 2). FMIClimGrid is based on weather observations at meteorological stations in Finland and the neighboring countries (i.e., Sweden, Norway, Russia and Estonia). A kriging interpolation method was used for the gridding procedure (Matheron, 1963; Goovaerts, 1999). The effects of the geographical location of the weather stations, topography and water bodies (sea and lake effects) were taken into account in the interpolation routine used by Aalto et al. (2016). The uncertainties in the dataset were related to spatiotemporal inconsistencies in the station network, the incomplete sample of background data used as external predictors, inhomogeneity in the observation data, and the sensitivity of the interpolation model parameters. The dataset is fully documented in Aalto et al. (2016).

The climate indices are presented in this paper as 1) time series showing annual values calculated separately for the fell and forest districts, 2) maps showing the mean values (in Supplementary material), and 3) maps showing the temporal trend values for selected indices at 10 km resolution within the RMA. The trends in indices were calculated using the non-parametric Sen's slope method. The statistical significance of the trends was calculated using the Mann-Kendall trend test. These methods are generally considered as robust and reliable, except that in the case of rare events, the trend may appear significant even though it is, in practice, nonexistent. We also calculated the standard deviations of yearly values of annual and seasonal climate indices and compared these to time-mean average changes per decade in the regions of RMA where the trends were statistically significant. The purpose of this comparison was to support our interpretations regarding the questionnaire survey results (for a human observer it may be difficult to separate the possible change in a variable from interannual variation, when the standard deviation is of the same magnitude or larger than the decadal trend). Some of the indices corresponded directly to the arguments presented in the questionnaire survey, whereas other indices were rather discrete or stand-alone ones. Some of the arguments

Table 2
Climate indices calculated from the FMIClimGrid dataset for daily mean temperature (Tmean), daily maximum temperature (Tmax), daily minimum temperature (Tmin), daily precipitation sum (Prec) and snow depth (SN). The indices have been calculated for a 3-month season, unless marked with an asterisk (annual values used).

Index	Description	Unit	Season
Temperature			
Hot-d	Days with Tmean >20 °C	Nr of days	ANN
DD	Degree day sum for Tmean >5 °C	°C days	ANN
Cold-d	Days with Tmean < −25 °C	Nr of days*	ANN
ID	Days when Tmax ≤0 °C	Nr of days	SON, DJF, MAM
Zero	Zero-crossing days: Tmin <0 °C and Tmax >0 °C	Nr of days	SON, DJF, MAM
Warm1w	Periods of seven consecutive days with Tmean ≥ Tsea[a] +3 °C, and in at least six of them Tmean ≥ Tave[b] + 3 °C	Nr of periods	JJA, SON, DJF, MAM
Precipitation			
Rain-d	Days when Prec ≥1 mm and Tmin ≥0 °C	Nr of days	JJA, SON, DJF, MAM
R1d	Largest daily precipitation	mm/day	JJA
RR10	Days with Prec ≥10 mm	Nr of days	JJA
Wet2w	Periods with Prec2w[c] ≥ Pmon[d] and at least seven days with Prec ≥0.5 mm and at maximum two consecutive days with Prec <0.5 mm	Nr of periods	JJA
ROS-d	Days when Prec ≥1 mm, Tmin ≥0 °C and SN ≥ 1 cm	Nr of days	SON, DJF, MAM
Snow			
BEG	Snow cover formation date	Date*	ANN
SOD	Snow cover melt day, first snow free day after the winter maximum snow depth	Date*	ANN
MaxSN	Annual maximum snow depth	cm*	ANN

[a] Tsea = climatological mean temperature of a season.
[b] Tave = mean temperature of a 30-day period (moving average).
[c] Prec2w = precipitation sum during a 2-week period.
[d] Pmon = climatological monthly mean precipitation sum.

of the survey were difficult to translate into climate indices (e.g. more frequent mold/ice layer formation).

3. Results

Mean climatic conditions vary considerably within the RMA (Figs. S10–S13). Climate indices show also remarkable interannual variability, both in fell and forest districts (Figs. S14–S17). In this section, we present the changes in the seasonal weather as experienced by the herders, and as manifested through the climate indices calculated for the RMA for the period from 1981 to 2010. We start from the summer season, following the seasonal cycle in reindeer life and herding (Table S1 and Fig. S1). Also, the reindeer herder observations of the effects of these changes on herding practice are described. See Table 3 for the summary of the survey results and Supplementary material (Figs. S2–S9; Tables S2–S9) for further details not shown here.

3.1. Summer – warmer or wetter?

3.1.1. Herder experiences and meteorological observations of summer climate

In the questionnaire survey, nearly 80% of the herders reported that summer precipitation has increased, and over 70% reported that heavy rains have become more common. Instead, the herders had not generally observed any particular changes in the summer temperatures, although some divergent views on warming and more frequent heat periods were expressed (Table 3, Table S2). Present-day summers were perceived as warmer than before in some districts in the southern and northwestern parts of the RMA (Fig. 2a). The majority of the herders reported having observed greater variability in summer weather. They noted that variation in the summer temperature and precipitation is large not only interannually but also within the season. The views of the herders of the fell and forest districts concerning the changes in summer weather were mostly similar to each other.

Statistically significant increasing temporal trends in the annual number of hot days (Hot-d) were detected rather widely in the southern part of the RMA (Fig. 2b). In these regions, the increase was 1–1.5 days per decade and, on the other hand, the standard deviation of yearly values was 2–6 days. In only four districts located within these regions, a majority of respondents reported about warming summers (Fig. 2a). The annual degree day sum (DD) has significantly increased all around the RMA (Fig. 3b), most strongly in the southern and central RMA where the trend was 80–100 days per decade, the standard deviation being 110–130 days or locally more. This is not only related to warmer summers, but also to the lengthening of the growing season.

All precipitation indices had remarkable interannual and spatial variability (shaded areas in the Fig. S14). The number of rain days (Rain-d) increased significantly (by 4–6 days per decade) in some rather localized areas only (Fig. 4). In these areas the standard deviation of Rain-d was 3–5 days. Indices related to the heavy precipitation events also showed increasing trends in some northern locations: 3–6 mm per decade for the largest daily precipitation (R1d; Fig. 5a) and approximately 1 day per decade for the number of heavy precipitation days (RR10; Fig. 5b). The corresponding standard deviations for R1d and RR10 were mainly 5–10 mm and 3–4 days, respectively. For R1d, decreasing trends occurred in the southern areas, locally −2 to −4 mm per decade, standard deviation being 5–10 mm and locally up to 15 mm.

3.1.2. Effects of the changes in the summer climate on herding

According to the free-form comments of the herders of the fell districts (Table S6 in Supplementary material), a cold and rainy summer is worse for herding than a dry and warm one. Delayed and poor development of vegetation can have negative impacts on milk production of dams and growth of calves. A rainier but warmer and longer growing season may increase the growth of vegetation and availability of high-quality forage, e.g. mushrooms, for reindeer. On the other hand, rainy summers, wet ground and flooding rivers can make gathering and moving reindeer to the round-up sites with terrestrial vehicles more difficult. Interestingly, lack of insect harassment, which is dependent on temperature and precipitation, can hamper reindeer moving to the round-up sites. Only 11% of the respondents had not observed any impacts of changes in the summer weather on herding so far.

The herders of the forest districts reported that collecting and moving reindeer to the calf-marking round-up sites has become more difficult, because due to, e.g. short heat periods and lack of insect harassment, reindeer do not gather into herds as early as they

Table 3
A summary of the survey results. Agreements, i.e., changes observed into the direction of the argument (median values 1–2) are bolded. Percentages of responses with values 1–2 (change observed into the direction of the argument), 3 (no change observed) and 4–5 (change observed into opposite direction) are also given. NA means missing answers; no answers were missing from the fell districts. The category including the majority of the responses is shaded.

	Fell districts; n=18				**Forest districts; n=72**				
	Median	1-2 (%)	3 (%)	4-5 (%)	Median	1-2 (%)	3 (%)	4-5 (%)	NA (%)
SUMMER									
Increased precipitation	**1**	78	22	0	**2**	78	21	0	1
More frequent heavy rainfalls	**1**	72	28	0	**2**	74	25	0	1
More variable weather	**2**	72	28	0	**2**	83	17	0	0
More frequent sleet or hail precipitation	3	28	61	11	3	25	68	6	1
Warmer summers	3	39	33	28	3	21	61	17	1
More rare cold periods	3	22	56	22	3	22	58	17	3
More frequent heat periods	3	22	56	22	3	17	57	25	1
More frequent droughts	3	28	61	11	3	17	57	26	0
AUTUMN									
Delayed frost season	**1.5**	78	22	0	**2**	83	17	0	0
Delayed soil frost	**2**	78	22	0	**2**	72	15	0	3
Delayed snow cover formation	**1**	72	22	6	**2**	82	14	4	0
Less soil frost	**2**	67	33	0	**2**	76	22	0	1
More frequent mold formation on the pastures	3	44	56	0	**2**	68	29	0	3
Increased precipitation	3	39	50	11	**2**	58	39	1	1
WINTER									
Warmer winters	**1.5**	94	6	0	**2**	89	8	1	1
Decreased number of frost days	**2**	94	0	6	**2**	89	11	0	0
More variable weather	**2**	67	33	0	**2**	90	10	0	0
More snow-loads on trees	**1**	72	28	0	**2**	74	25	0	1
More frequent rainfalls	**2**	67	33	0	**2**	79	18	1	1
Increased windiness	**2**	56	44	0	**2**	78	22	0	0
More frequent formation of icy layers in the snow cover	2.5	50	50	0	**2**	85	14	1	0
More frequent formation of basal ice in the snow cover	2.5	50	44	6	**2**	75	25	0	0
Deeper snow	3	44	44	11	3	29	56	15	0
SPRING									
Earlier start of the growing season	**2**	72	28	0	**2**	78	19	1	1
Earlier snow melt and earlier snow-free patches	**2**	72	17	11	**2**	75	24	1	0
Earlier discontinuation of the frost season	**2**	67	11	22	**2**	83	15	0	1

did before. Many herders also pointed out that lack of long dry periods in the summer has led to difficulties in producing hay for supplementary winter feed for reindeer, and that hay is of worse quality than earlier. Some herders had observed that reindeer in the forest districts are in any case doing better due to lack of long heat periods and weaker insect harassment: "*Cool summer has helped reindeer keep fit… The heat periods have been relatively short.*" Some of the herders held the view that the changing summer weather is insignificant for reindeer herding.

3.2. Longer and warmer autumn?

3.2.1. Herder experiences and meteorological observations of autumn climate

The herder views on delayed frost season in autumn and its consequent impacts on snow and ice phenomena are rather unanimous (Table 3, Table S3). Herders of the fell and forest districts had experienced a delayed onset of the frost period (subzero temperatures), later formation of the ground frost as well as ground frost being

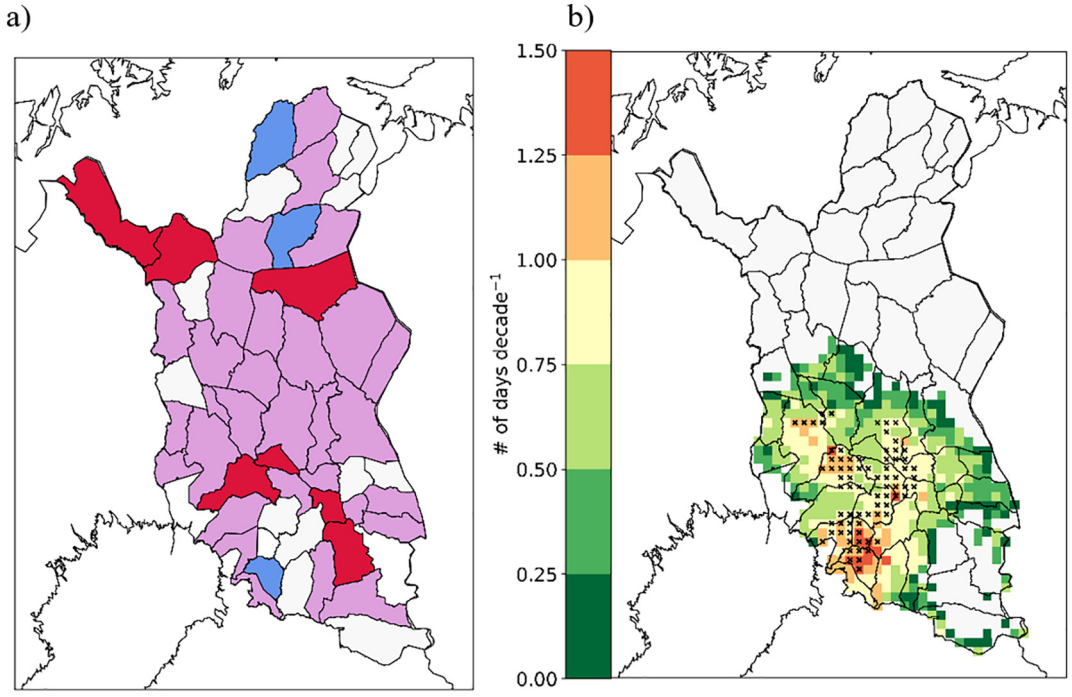

Fig. 2. a) Median values of answers by district to the argument "Summers are warmer than before" in the survey targeted to reindeer herders. Violet = no change observed (median 2.5–3.5); red = change/some change observed into the direction of the argument (median < 2.5); blue = change observed into the opposite direction (median > 3.5); white = missing data. b) The change in the annual number of hot days (Hot-d) per decade within the RMA in 1981–2010. Locations with significant trends (at 5% significance level) are marked with black check marks. The trend is zero in the white area. (For interpretation of the references to colour in this figure legend, the reader is referred to the web version of this article.)

shallower than before, and later formation of the snow cover. Experiences of autumn precipitation changes differed regionally. About 58% of the herders of the forest districts and only 39% of herders of the fell districts had observed increased precipitation in autumn. As many as 68% of the herders of the forest districts had observed increased formation of mold in the vegetation compared to 44% of the herders of the fell districts.

Meteorological data for 1981–2010 showed a tendency towards later snow cover formation dates, but the trends in BEG were significant only in some northern parts of the RMA (Fig. 6), locally 4–7 days per decade. In the same areas the standard deviation was 5–15 days. The number of ice days (ID) declined in the whole RMA, but the trend was not significant during the study period. Further, the number of zero-crossing days (Zero) and the number of rain-on-snow days (ROS-d), the indices considered among the main drivers of formation of icy foraging conditions, did not change significantly during the study period. It is nevertheless clear that there was large annual variability in the values of these indices (Fig. S15), and their number alone could not describe the occurrence of conditions favoring ice formation on the ground and the severity of icing on reindeer pastures.

3.2.2. Effects of the changes in the autumn climate on herding

According to the free-form comments of the herders of the fell districts (Table S7 in Supplementary material), reindeer, particularly calves, benefit from late formation of the snow cover through higher availability of forage. Herders of the fell districts also reported that variable and warm autumn weather may delay the timing and impair the intensity of the rut. Round-ups may be delayed even until January, and reindeer need to be collected and moved to the round-up sites by terrestrial vehicles instead of snowmobiles due to lack of snow or thin snow cover. Some herders of the fell districts pointed out that the need for supplementary winter feeding has increased due to an increased risk of poor digging conditions (risk of icing of the snow cover).

The herders of the forest districts reported that, due to warm autumn weather, reindeer stay longer in summer pastures. Foraging conditions in autumn have deteriorated because the frosts arrive later than before, soil does not freeze before the snow comes, mold may be formed on the vegetation and if it rains there is a risk of basal ice formation on the soil. Because of poor foraging conditions, reindeer may start roaming and the herds are dispersed, which may make the gathering of the herds difficult and delay the round-ups. Also, the rut can be weaker and delayed. Use of terrestrial vehicles (ATVs) has increased due to lack of frost periods and snow, and their period of usage has been extended. Lack of or a weak ice cover on the waterbodies and mires may increase the risk of reindeer drowning when they are moved to the round-up sites. Herders also reported that supplementary feeding needs to be started earlier in some regions than before. Reindeer tend to move to familiar feeding places and enclosures much earlier than 20–30 years ago. Furthermore, in particular the herders from the southernmost districts noted that warmer autumns have increased the occurrence of new parasites, such as the deer ked, (*Lipoptena cervi*), which worsens the condition of the reindeer. One herder pointed out that warm and moist autumn weather makes the reindeer more susceptible to diseases.

3.3. Warmer and wetter winters?

3.3.1. Herder experiences and meteorological observations of winter climate

The respondents were rather unanimous in their views of most of the arguments about the changes in winter climate presented in the survey (Table 3; Table S4). The herders from both the fell and the forest districts reported that winters have become warmer and the number of subzero days has decreased. The majority of the herders also reported that rainfalls during the winter have become more frequent. The argument about increased snow depth yielded somewhat divergent responses (Table 3). Many of the herders had not observed

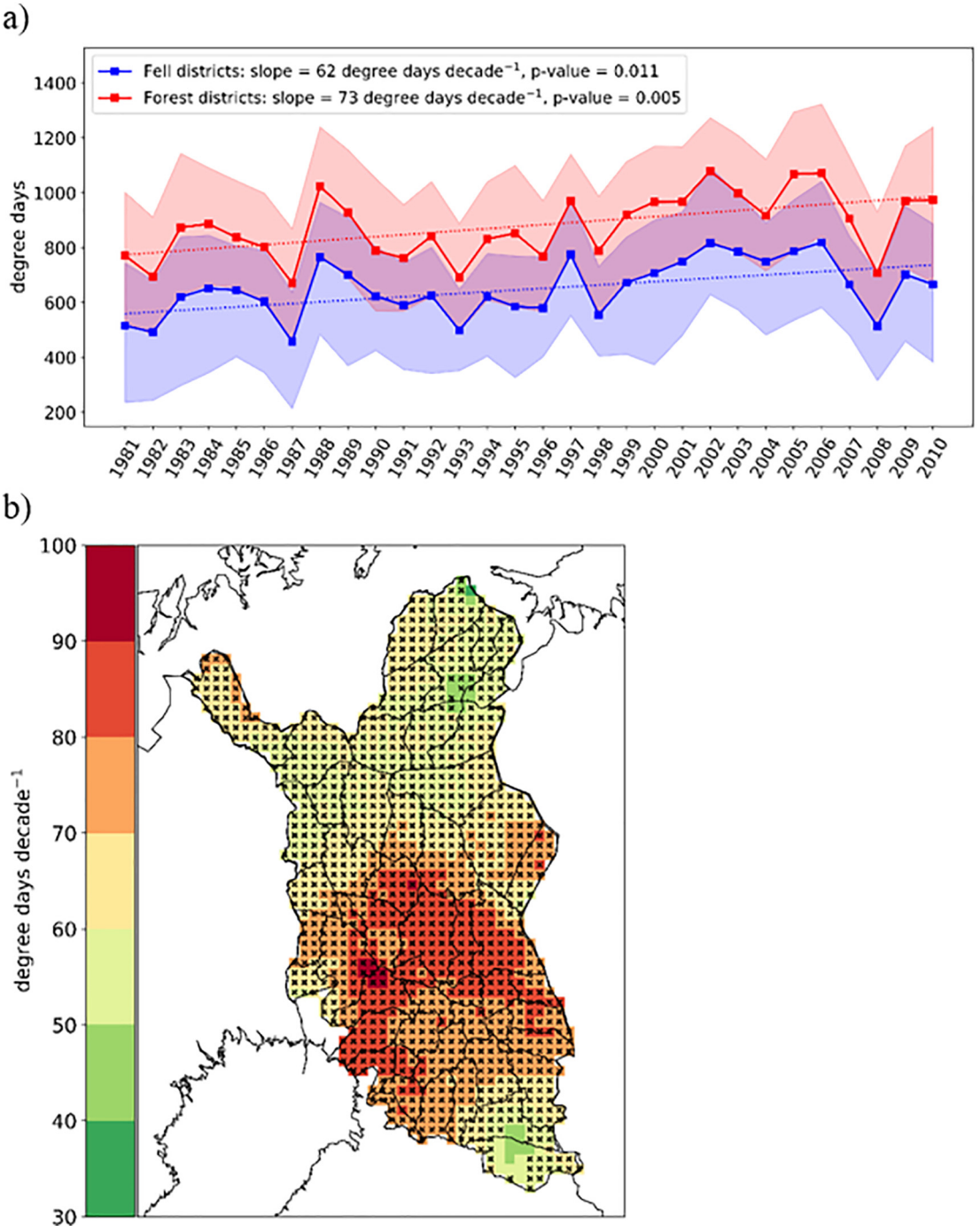

Fig. 3. a) The annual degree day sum (DD) as a function of time in fell and forest districts during 1981–2010, indicating significant increasing trends. The dots depict spatial averages and the shaded areas show the ranges (the highest and lowest annual values) across the grid boxes of the regions. b) The change in DD within the RMA in 1981–2010. Locations with significant trends (at 5% significance level) are marked with black check marks.

changes in snow depth during the study period. However, deeper snow covers had been recently experienced in the northern part of the RMA in particular (Fig. 10a). The herders also pointed out that accumulation of snow and hard rime loads on tree branches ("*tykky*") has increased. The herders from the forest districts in particular reported that winters have become windier. They had also observed that winter weather has become more variable and that the formation of icy layers within the snow cover and basal ice has become more common (Table 3).

According to the indices calculated from the meteorological data, winter warming was evident in the whole of the RMA. The number of warm weeks (Warm1w) has increased (Fig. 7) in large areas, most strongly in the southern and central parts of the RMA (about 1 week per decade). The standard deviation in these areas was 1.5–2.5 weeks. The number of cold days (Cold-d) has decreased in parts of the RMA 2–4 days per decade (Fig. 8), standard deviation in these parts being mainly 6–10 days. There were also local increases in the number of rain days (Rain-d); most notably in the southern part of the area (Fig. 9) where the trend was 1–2 days per decade and standard deviation was 1–2 days. Annual maximum snow depth (MaxSN) had a decreasing trend of 5–10 cm per decade, or locally more, in the northern part of the RMA (Fig. 10b). The

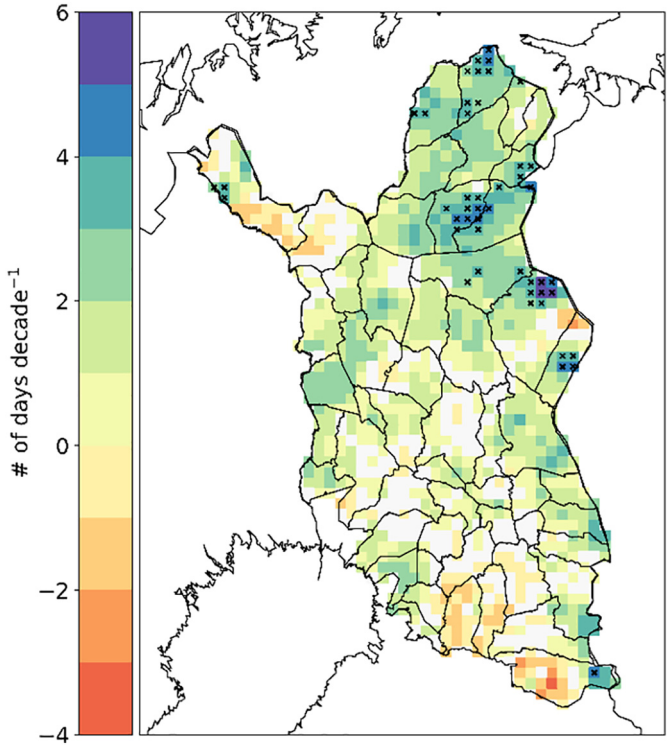

Fig. 4. The change in the number of rain days (Rain-d) in the summer season within the RMA in 1981–2010. Locations with significant trends (at 5% significance level) are marked with black check marks. The trend is zero in the white area.

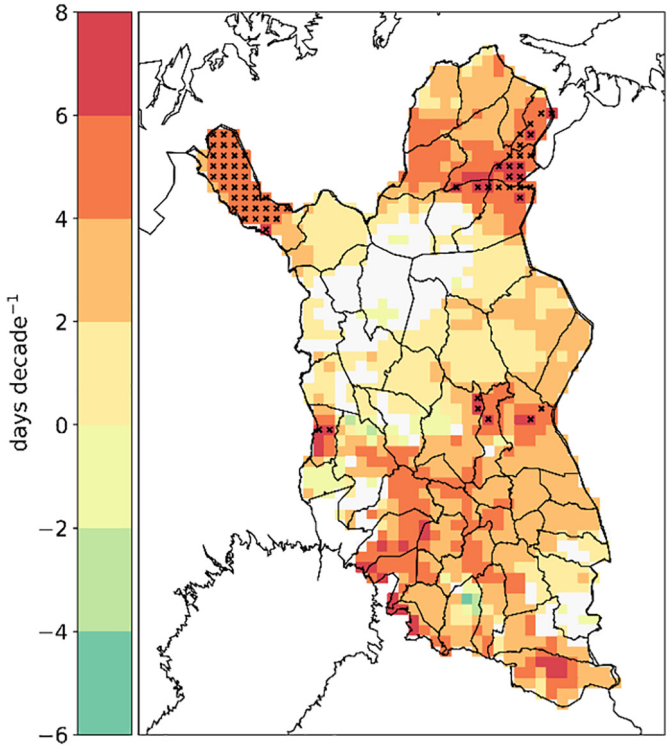

Fig. 6. The change in the snow cover formation date (BEG) within the RMA in 1981–2010. Locations with significant trends (at 5% significance level) are marked with black check marks. The trend is zero in the white area.

standard deviation of MaxSN in these regions was 10–20 cm. The region where the herders reported deeper snow covers (Fig. 10a) partly coincides the area with weak increases detected in the MaxSN. The trend was, however, not statistically significant during the study period.

3.3.2. Effects of the changes in the winter climate on herding

There was a great local variation in the responses among the herders of the fell districts on how changing winter conditions affect herding (Table S8 in Supplementary material). Some herders reported that reindeer foraging conditions have been deteriorated

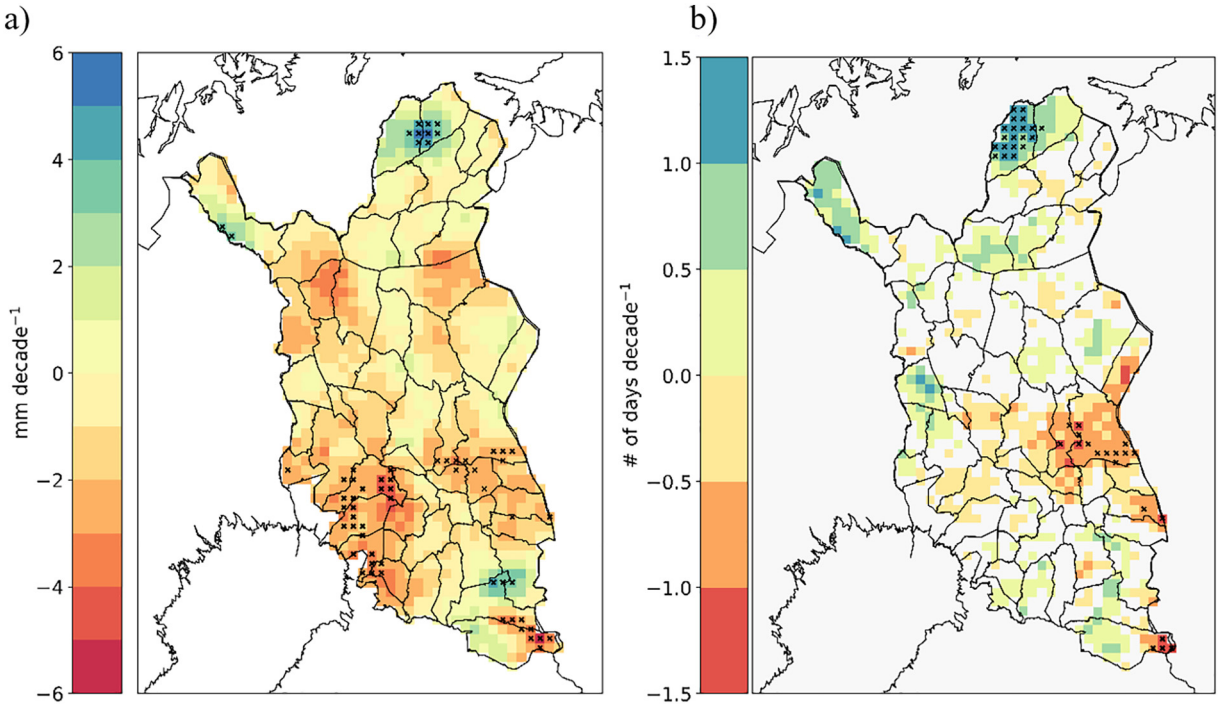

Fig. 5. a) The change in the largest daily precipitation (R1d) and b) the number of heavy precipitation days (RR10) in the summer season within the RMA in 1981–2010. Locations with significant trends (at 5% significance level) are marked with black check marks. The trend is zero in the white area.

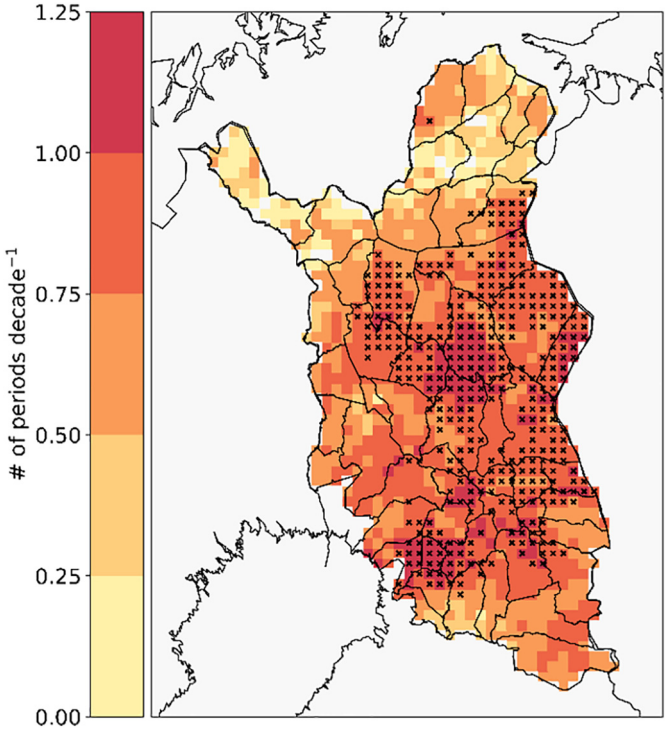

Fig. 7. The change in the number of warm weeks (Warm1w) in the winter season within the RMA in 1981–2010. Locations with significant trends (at 5% significance level) are marked with black check marks. The trend is zero in the white area.

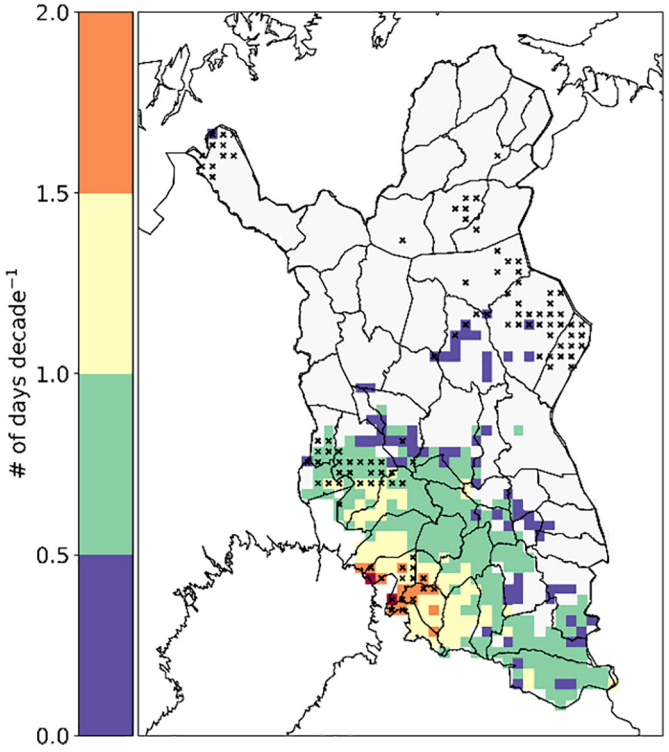

Fig. 9. The change in the number of rain days (Rain-d) in the winter season within the RMA in 1981–2010. Locations with significant trends (at 5% significance level) are marked with black check marks. The trend is zero in the white area.

due to deep snow and ice formation, whereas others had experienced an improvement in winter conditions through less snow. Also, in forest districts, both positive and negative impacts of changes in winter conditions were experienced. Thinner snow cover, milder weather and shorter periods of very low temperatures are favorable for reindeer, because reindeer stay more fit due to higher availability of forage and lower energy expenditure. Some herders reported that foraging conditions have been deteriorated due to hard snow and icy layers formed on the soil and snow cover resulting in declined availability of ground lichens for reindeer. Hard snow and rime accumulated on the branches of trees have also decreased the availability of arboreal lichens. As a consequence, reindeer herds can be dispersed and the animals move more than usual, which can present challenges to reindeer round-ups, leading to delays in them. Changing winter conditions have increased the need for taking reindeer into enclosures. Feeding reindeer in the enclosures have largely replaced feeding in the field, and supplementary feeding has to be started earlier than before. In some districts, the conditions were more favorable for the use of snowmobile over extended time periods.

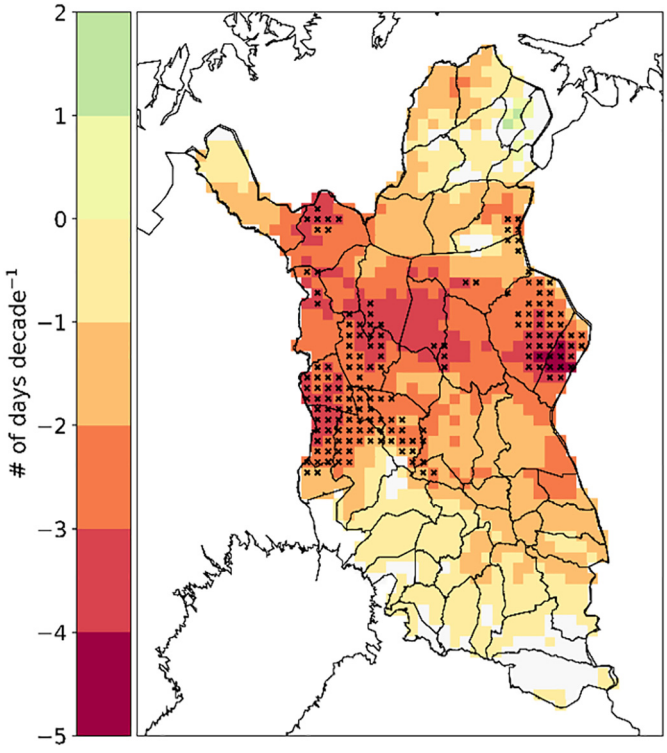

Fig. 8. The change in the number of cold days (Cold-d) within the RMA in 1981–2010. Locations with significant trends (at 5% significance level) are marked with black check marks. The trend is zero in the white area.

3.4. Earlier and warmer springs?

3.4.1. Herder experiences and meteorological observations of spring climate

Most of the herders of both fell and forest districts reported that the frost period ends earlier in the spring, and some had experienced that the spring heat waves occur earlier than before (Table 3, Table S5). The growing season was found to start earlier and the development of birch leaves was more advanced when compared to the earlier decades. There was some divergence in the views of the herders from the fell districts (Table 3). Some experienced that the duration of the frost period during the spring has become longer, whereas most of the herders had experienced earlier discontinuation of the frost period. Most of the herders had experienced ice- and snowmelt occurring earlier, but some stated that snowmelt now occurs later than before. Some herders pointed out that the season of hard night frosts (affecting the snow hardness during the spring) is shorter than before, being over already before March. Some herders also noted that, due to evaporation of snow, spring flooding is not as strong as before.

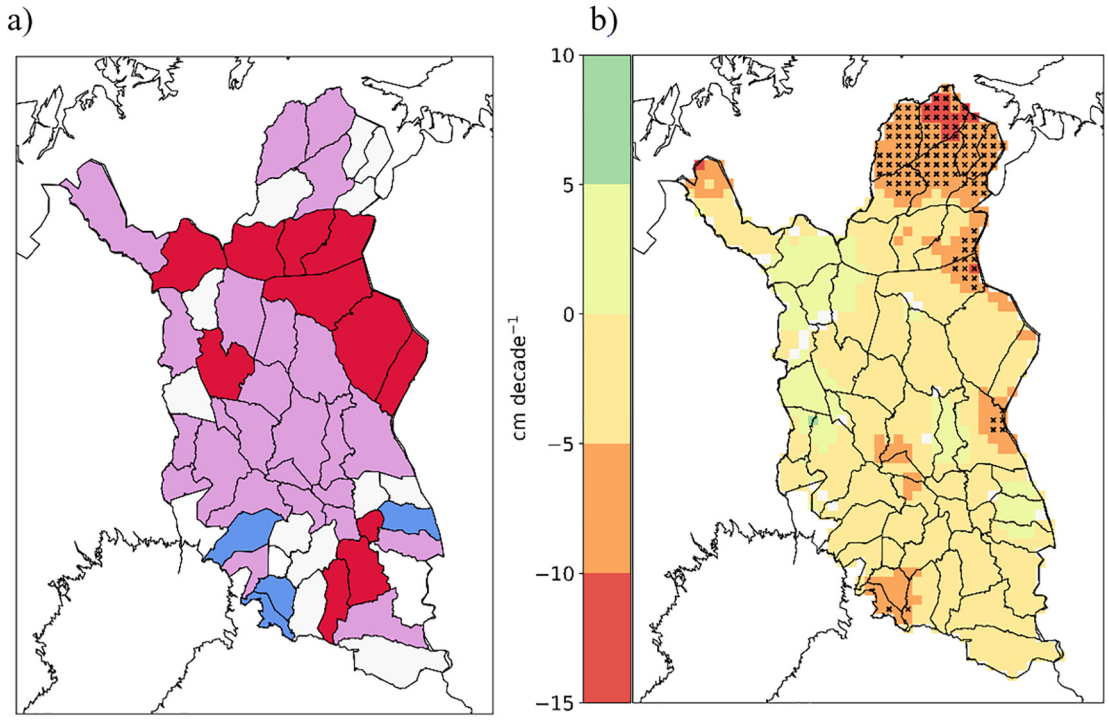

Fig. 10. a) Median values of answers by district to the argument "Snow cover is deeper than before" in the survey targeted to reindeer herders. Violet = no change observed (median 2.5–3.5); red = change/some change observed into the direction of the argument (median < 2.5); blue = change observed into the opposite direction (median > 3.5); white = missing data. b) The change in the annual maximum snow depth (MaxSN) within the RMA in 1981–2010. Locations with significant trends (at 5% significance level) are marked with black check marks. The trend is zero in the white area. (For interpretation of the references to colour in this figure legend, the reader is referred to the web version of this article.)

A decrease in the number of ice days (ID) in spring was found particularly in the northern part of the study area (Fig. 11), where it was locally 3–5 days per decade. The standard deviation of ID in these regions is 0.5–3 days. A trend towards an earlier snowmelt date (SOD), locally 3–5 days per decade, was statistically significant only in the southern part of the RMA (Fig. 12). The standard deviation of SOD

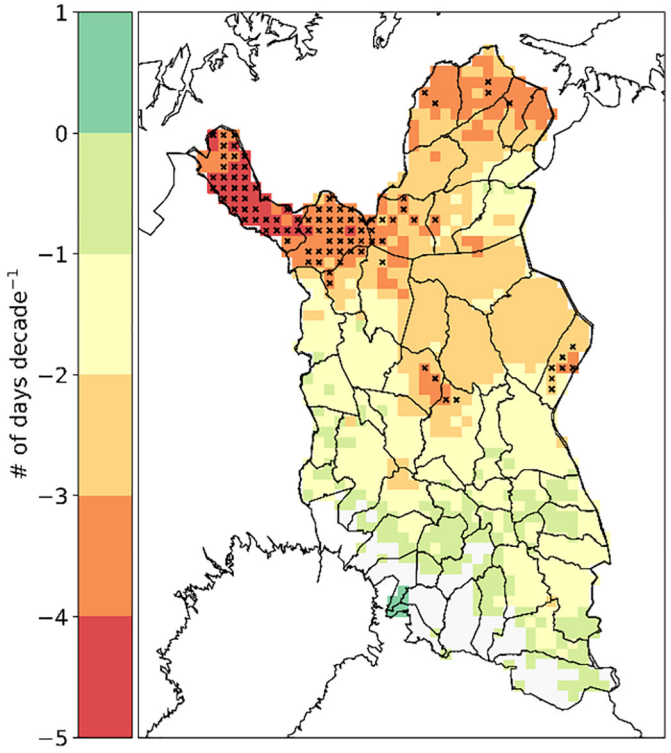

Fig. 11. The change in the number of ice days (ID) in the spring season within the RMA in 1981–2010. Locations with significant trends (at 5% significance level) are marked with black check marks. The trend is zero in the white area.

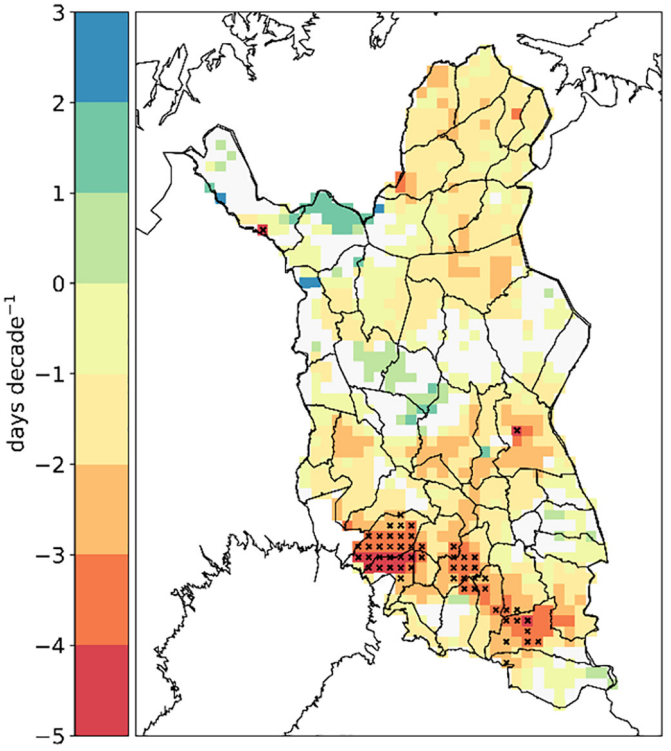

Fig. 12. The change in snowmelt date (SOD) within the RMA in 1981–2010. Locations with significant trends (at 5% significance level) are marked with black check marks. The trend is zero in the white area.

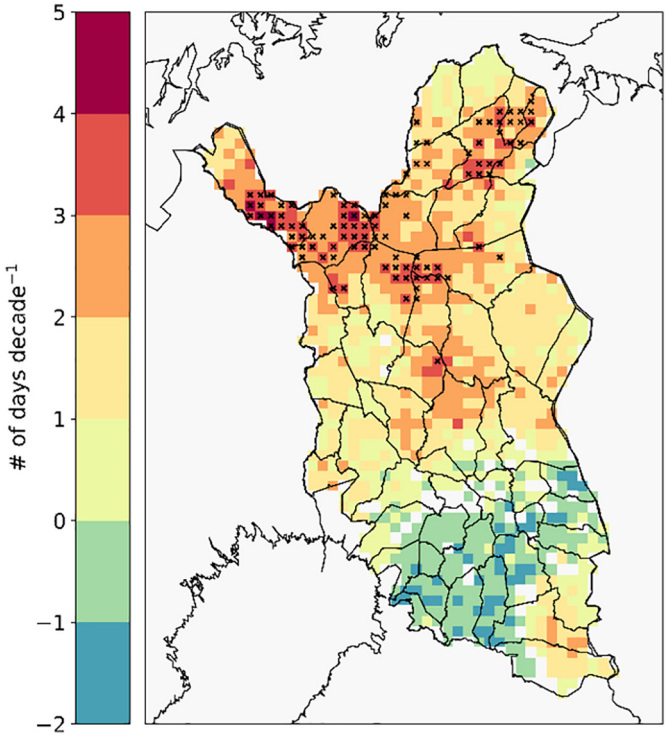

Fig. 13. The change in the number of zero-crossing days (Zero) in the spring season within the RMA in 1981–2010. Locations with significant trends (at 5% significance level) are marked with black check marks. The trend is zero in the white area.

was 9–12 days in these areas. The number of zero-crossing days (Zero) related to the night frosts showed an increasing trend of 3–5 days per decade in the northern parts of the region (Fig. 13) (standard deviation 6–8 days). Slight, local increases in the number of rain days (Rain-d) were found within the RMA, most clearly in its southern parts where the trend was 2–3 days per decade (map not shown). Standard deviation of Rain-d was 3–5 days in these areas. Precipitation in spring was not explicitly addressed in our questionnaire.

3.4.2. Effects of the changes in the spring climate on herding

According to the free-form comments of the herders of the fell districts (Table S9 in Supplementary material), earlier arrival of spring has had a positive impact on reindeer herding. Snow-free patches on the fells were available for reindeer grazing earlier than before. Due to advanced development of vegetation and the consequent higher availability of fresh forage plants for milk-producing dams and their calves, the calves will be fit by the time the calf marking period starts in the summer. Spring can also be a difficult time for herding on the fells: Start of the growing season is uncertain, it can snow heavily at calving time, and riverine flooding can be strong, which exposes the calves to accidents.

In the forest districts, as well, most of the herders reported that earlier spring can have positive impacts on herding. Due to earlier snowmelt, the risk of reindeer calving taking place in snowy conditions is nowadays smaller, and due to advanced emergence of spring vegetation, reindeer can feed on natural forage earlier than before. Early spring lowers the expenses of supplementary feeding. The winter feeding period is shorter because reindeer can be released from enclosures to the summer pastures much earlier than before. Some herders report that the interannual variation of spring conditions is great and that the arrival of spring has not advanced. A few herders reported that the earlier arrival of spring has not had any impact on reindeer herding. Some others list negative impacts related to early springs, such as strong flooding and increased predatory threat.

3.5. Coping strategies of herders

Gathering and moving reindeer to the calf marking round-up sites has become more difficult in the summer, because reindeer do not necessarily gather into herds due to e.g. short warm periods and lack of insect harassment (Table S6). Therefore, many herders have given up the summer calf-marking period and, instead, mark calves only during the autumn-winter round-ups or already in the spring in the case of enclosure calving. Rescheduling the calf marking was also reported as a way to cope with long heat periods and severe insect harassment during summer (see also Turunen et al., 2016). In the autumn, weather-related factors, such as mold or ice on pastures may cause herds to be dispersed over a wide area, which delays round-ups (Table S7). Due to lack of snow or thin or non-uniform snow cover, reindeer are collected and moved to the round-up sites increasingly by terrestrial vehicles, particularly ATVs, or helicopters instead of snowmobiles.

In winter, supplementary feeding plays an important role in adaptation of reindeer to the changing weather conditions (Table S8). The need for supplementary winter feeding of reindeer has increased, and in some regions, it needs to be started earlier than before. Many herders held the view that although supplementary winter feeding increases expenses, taking reindeer into enclosures is nowadays the only way to gain regular income from herding (see also Turunen et al., 2013; Turunen and Vuojala-Magga, 2014; Turunen et al., 2016). The majority of the herders of the forest districts reported that changing winter conditions have increased the need for taking reindeer into enclosures, and that feeding reindeer in the enclosures has largely replaced feeding of reindeer in the field. The herders of fell districts reported several strategies for coping with deteriorated foraging conditions. These included moving herds to lower elevations of fells with less snow or to wind-exposed habitats where snow cover is thinner; adjusting the time the herds (of a village or a siida) are kept together; moving the herds from one pasture to another with the aid of hay earlier in the spring; starting supplementary winter feeding; and monitoring ice formation in the snow cover more carefully. Some herders reported (Table S9) that supplementary feeding can be discontinued earlier in the spring because of early snowmelt, which reduces the expenses for feeding. Reindeer can also be released from enclosures to the summer pastures much earlier than before.

4. Discussion

Our findings of the trends in climate indices were mainly consistent with earlier studies in northern Fennoscandia. According to earlier studies, summers in northernmost Finland have become warmer in many locations, but the trends in the amount of summer precipitation are not clear (Virtanen et al., 2010; Lépy and Pasanen, 2017; Maliniemi et al., 2018). Warmer autumns have been reported in several earlier studies (Vuojala-Magga et al., 2011; Turunen et al., 2016; Kivinen et al., 2017; Lépy and Pasanen, 2017; Jaakkola et al., 2018) as well as shorter snow season with later formation of the snow cover (Rasmus et al., 2014; Luomaranta et al., 2019). Only local increases in autumn precipitation have been reported (Kivinen et al., 2017; Lépy and Pasanen, 2017). Our observations of increased winter temperatures are in accordance with earlier studies (Vikhamar-Schuler et al., 2010; Vuojala-Magga et al., 2011; Kivinen et al., 2012; Rasmus et al., 2014; Kivinen and Rasmus, 2015; Lépy and Pasanen, 2017). Winter precipitation has increased within the study region (Rasmus et al., 2014; Lépy and Pasanen, 2017). Increasing amount of mixed and liquid precipitation has also been reported (Luomaranta et al., 2019) together with more frequent and more intense rainy periods (Vikhamar-Schuler et al., 2016). Previous studies have not found any significant changes in thickness of the winter snow cover in the region (Rasmus et al., 2014; Lépy and Pasanen, 2017; Luomaranta et al., 2019). Increasing spring temperatures have been observed in previous studies (e.g. Kivinen et al., 2017; Lépy and Pasanen, 2017), as well as earlier

snowmelt (Vikhamar-Schuler et al., 2010; Rasmus et al., 2014; Lépy and Pasanen, 2017) and thinner spring snow covers (Luomaranta et al., 2019).

Reindeer herder observations of changes in seasonal weather characteristics, gathered via a survey questionnaire, were generally in line with the meteorological data. The observations of herders from the forest and the fell districts were mainly consistent with each other. Some regional differences were seen in the observations concerning the warming of summers, and changes in the autumn precipitation and snow depth. Local variation was seen in the responses among the herders when the arrival of spring was in question. The herders had experienced the largest number of changes during the winter, and the smallest number of changes during the summer. Furthermore, herders had experienced more variable weather, which has also been reported in earlier studies based on local knowledge (e.g. ACIA, 2004; Helander, 2004; Vuojala-Magga et al., 2011). Weather variability is a complex concept. Conclusions drawn in the scientific studies depend on the temporal scales and measures of variability used (Fischer and Knutti, 2014). If the variance of daily temperatures is considered as a measure of variability (or spread), it is evident that there is a general decreasing trend in variability in northern mid- and high latitudes, as cold days have warmed more than warm days (Screen, 2014; Lorenz et al., 2019). Furthermore, in the mid-latitudes the warming may cause weather patterns to move more slowly, increasing weather persistence (Overland et al., 2015). The replies in our survey may be interpreted as a common perception of a decrease, rather than an increase, in weather persistence from one day to the next, meaning rapid, intermittent change in the daily weather. To the knowledge of the authors, weather persistence of sub-arctic Scandinavia has not been explicitly studied, but there are several recent studies on high latitude cyclone activity. Changes in cyclone activity in the vicinity of our study area could lead to changes in weather persistence. Studies concentrating on Arctic cyclone activity during past decades observe no clear trends, or regional decreases or increases (Koyama et al., 2017; Wei et al., 2017; Zahn et al., 2018). According to Koyama et al. (2017), more intense cyclones have been experienced due to the increases in precipitable water in the atmosphere. Zhang et al. (2004) and Sepp and Jaagus (2011) also report on increase in the number and intensity of cyclones entering the Arctic from the mid-latitudes.

There were some interesting discrepancies between herder observations and the meteorological data. For example, warming of summers was seen more in the analysis of climate indices, than in the answers of the survey respondents. The herders had generally experienced an increase in summer precipitation and reported that heavy precipitation has become more frequent, while meteorological data showed only local increases in the indices related to the heavy precipitation events. The human memory is believed to emphasize recent and rare conditions. Our survey opened in autumn 2016, just after the summer during which record-breaking precipitation sums had been observed in several locations around the northern Finland (FMI, 2017). Both summer of 2016 and also 2015 had been relatively cool and rainy; autumns, winters and springs of these recent years had, on the other hand, been warmer than average. The use of climate data from the period of 1981–2010 (current three-decade normal period in use, not extending to the most immediate past) has most probably contributed to these discrepancies. Furthermore, for a human observer it may be difficult to separate the possible change from interannual variation (Figs. S14–S17). Standard deviations of climate indices were generally of the same magnitude or larger than the changes per decade. The detected decadal change was stronger than the standard deviation only for the number of rain days (Rain-d) in the summer, locally, and the number of ice days (ID) in the spring. For example, the decrease in the ID per decade in northwestern fell region was 3–5 days, standard deviation being 0.5–3 days. In this case, most of the herders from the fell districts had experienced discontinuation of the frost period in spring. Large interannual variability, together with a relatively short study period, may also mask trends possibly present in a longer time series.

Experienced impacts on herding and adaptation needs were rather consistent between the forest and fell districts, but more numerous and varied in the forest districts compared to the fell region. Local variation was seen in the herder views concerning the impacts of changing winter climate on herding. Reindeer management adapts to changing climatic conditions through adoption of various coping strategies in the everyday work of herders. Professional techniques and practices are also continuously developed, e.g. regulating the reindeer numbers and herd structure, or utilizing pasture rotation systems. The coping capacity of herding is dependent on the geographical space available for adaptation actions and facilitated by variations in topography, vegetation and herding practices (Tyler et al., 2007; Moen, 2008; Riseth et al., 2016; Turunen et al., 2016, 2019; Peltonen-Sainio et al., 2017). Large, diverse and peaceful pastures give herders more choice regarding the coping strategies available during various weather conditions. The fell and forest districts differ in terms of herding practices and pastureland types (Table 1) as well as are involved with different kinds of disturbance factors. Seasonal coping strategies of herders (Tables S6–S9) mirror these differences.

It is crucial that the coping strategies adopted in everyday herding work are supported by local, regional and national governance of reindeer management. When preparing adaptation strategies, governance level of reindeer management needs to understand the local impacts of seasonal changes, and to acknowledge that the coping strategies already in use are based on local practitioner knowledge – experiences and perceptions on what is normal and what can be expected. In Finland, national adaptation to climate change is guided by The National Climate Change Adaptation Plan 2022 (MAF, 2014). A separate adaptation plan does not exist for reindeer husbandry, although need for this has been acknowledged (MAF, 2005, 2014). Reindeer management in Finland has recognized the need for adaptation measures, impacts of climate change are known qualitatively, and some adaptation measures have been identified and are being planned (MAF, 2009, 2013; Peltonen-Sainio et al., 2017). Measures mentioned to mitigate the adverse effects of climate change are maintaining the uniformity and diversity of the pasture areas, improving reindeer health, limiting the expansion of invasive alien species, environment protection, considering reindeer management in the legislation regulating land-use planning, developing the financial instruments, and relevant research. Accordingly, adaptation to climate change requires consolidation of different land use needs and participatory planning approaches (Oinonen et al., 2014; RHA, 2014), consideration of sustainable development and socio-economic and cultural aspects in planning processes, and research and education on climate risks (Forbes, 2006; Hukkinen et al., 2006; Finland's Strategy for the Arctic Region, 2013; Soppela and Turunen, 2017). Furthermore, legislation has recently recognized the need of reindeer herding to cope with difficult weather events. Act on compensation of damages caused to reindeer herding (987/2011 and 655/2016) aims at supporting herders to cope with extensive and unexpected damages resulting from natural events like exceptional weather conditions. To our knowledge, at the time of writing this article, there have been no cases in which this legislation has been applied in practice. In the time of rapid change, it may be challenging to define what constitutes “normal”, “rare”, “exceptional” and “unexpected” weather conditions and set the corresponding compensation amounts.

Both meteorological observations and practitioner knowledge are needed for understanding of the effects of climate change on reindeer management, and to support decision-making on adaptation to climate change. To clarify the useful features of the knowledge sets, also critical evaluation is needed. Meteorological data are objective, systematical, and have full spatial coverage on the study area. However, fine-scale variability seen in the northern nature may cause errors and uncertainties into the interpolation of the climate data, even when a grid with high spatial scale is used. Also aspects like experiences, impacts

on, and coping of local communities are missing. Herder experiences on seasonal weather are very much local in nature. On one hand this knowledge is unsystematic, spatially inconsistent and potentially biased (Couzin, 2007; Monastersky, 2009; Alexander et al., 2011; Huntington, 2011). There may, e.g. be seasonal bias causing the critical seasons to get disproportionate attention. On the other hand, herder observations provide valuable information on local conditions, the occurrence of extreme and harmful weather events and their consequences on the livelihood (see e.g. Rasmus et al., 2018).

Climate indices provide a quantitative ground which serves as an easy starting point for discussions on climate change and the adaptation actions it calls for. We aimed at using indices with a temporal scale that is comparable to human experience and easy to relate to the daily work of herding. High spatial resolution of the meteorological data and its full spatial coverage on the study area also enable bringing changing seasonal weather to the scale of the herder experiences as they move around and work in the landscape. Time series data and spatial visualizations of observed changes enable discussions on topics such as the regional differences in extreme events and the reasons for adopting different coping strategies. It should be noted that some of the indices could be easily connected with practitioner knowledge, whereas some of the arguments used in the questionnaire were difficult to translate into indices which could be derived from the data set used (more frequent mold/ice layer formation). The data set itself had some inherent limitations as e.g. humidity and wind data were not available.

5. Conclusions

Parallel examination of meteorological observations and practitioner knowledge can provide new insights into the temporal and spatial variability of the warming of the northern latitudes. In our work, relating the different knowledge sets enabled us not only to study the ongoing climate change in general, but also to examine its specific impacts on the northern environment with a particular focus on the nature-based livelihoods. We conclude that using different knowledge sets together will support decision making related to climate change adaptation. This view is shared also by IPCC (2019), who recently called for learning to relate different knowledge sets, as through this process new and relevant understanding for improved decisions and solutions can be created.

It is expected that, in the future, research problems will be increasingly co-defined and governance solutions co-planned with local practitioners. In these processes, new tools to present data and discuss the implications of observed changes are needed. Important features of these new tools are defining quantities, indices and observations relevant for all involved in the process, consideration of temporal and spatial scales when presenting the data, and genuine data fusion, where both local practitioner knowledge and scientific knowledge are treated with appreciation, acknowledging the strengths and weaknesses of both forms of knowledge. The approach presented in this work can facilitate the dialogue between the local practitioners, researchers and policy makers. Our study focused on reindeer husbandry, but the approach is applicable to other nature-based livelihoods (e.g. hunting, gathering, fishing and small-scale farming and forestry) facing adaptation needs caused by changing climate.

Declaration of competing interest

The authors declare that they have no known competing financial interests or personal relationships that could have appeared to influence the work reported in this paper.

Acknowledgements

We would like to thank Elisa Pääkkö (Metsähallitus), Marja Anttonen (Reindeer Herders' Association) and Katariina Mäkelä (Finnish Environment Institute SYKE) for their collaboration with the planning of the questionnaire. The personnel of the Reindeer Herders' Association distributed the questionnaire, which we warmly acknowledge. We are grateful to Timo Vihma at the Finnish Meteorological Institute for valuable discussions and to Arto Vitikka at the Arctic Centre of the University of Lapland for technical help. Thanks are also due to Sari Kokkola for checking the language of the manuscript. Sirpa Rasmus was funded through the project "Changing operational environment of Finnish reindeer herding" by the Finnish Cultural Foundation and Nordforsk Nordic Centre of Excellence ReiGN (project number 76915). Sonja Kivinen was funded by the Academy of Finland Strategic Research Council project IBC-CARBON (project number 312559).

Appendix A. Supplementary data

Supplementary data to this article can be found online at https://doi.org/10.1016/j.scitotenv.2019.136229.

References

Aalto, J., Pirinen, P., Jylhä, K., 2016. New gridded daily climatology of Finland: permutation-based uncertainty estimates and temporal trends in climate. Journal of Geophysical Research: Atmosphere 121, 3807–3823. https://doi.org/10.1002/2015JD024651.
ACIA, 2004. Arctic Climate Impact Assessment. Cambridge University Press, Cambridge, United Kingdom and New York, NY, USA.
Agrawal, A., 1995. Dismantling the divide between indigenous and scientific knowledge. Dev. Chang. 26 (3), 413–439.
Alexander, C., Bynum, N., Johnson, E., King, U., Mustonen, T., Neofotis, P., Oettlé, N., et al., 2011. Linking indigenous and scientific knowledge of climate change. BioScience 61 (6), 477–484.
AMAP, 2017. Adaptation Actions for a Changing Arctic: Perspectives From the Barents Area. Oslo: Arctic Monitoring and Assessment Programme (AMAP).
Berkes, F., 2008. Sacred Ecology. Routledge, New York.
Buchanan, A., Reed, M., Lidestav, G., 2016. What's counted as a reindeer herder? Gender and the adaptive capacity of Sami reindeer herding communities in Sweden. Ambio 45 (Suppl. 3), 352–362. https://doi.org/10.1007/s13280-016-0834-1.
Couzin, J., 2007. Opening doors to native knowledge. Science 315, 1518. https://doi.org/10.1126/science.315.5818.1518.
Eira, I.M.G., Jaedicke, C., Magga, O.H., Maynard, N.G., Vikhamar-Schuler, D., Mathiesen, S.D., 2013. Traditional Sami snow terminology and physical snow classification – two ways of knowing. Cold Reg. Sci. Technol. 85, 117–130. https://doi.org/10.1016/j. coldregions.2012.09.004.
Eira, I.M.G., Oskal, A., Hanssen-Bauer, I., Mathiesen, S.D., 2018. Snow cover and the loss of traditional indigenous knowledge. Nat. Clim. Chang. 8, 928–931. https://doi.org/10.1038/s41558-018-0319-2.
Finland"s Strategy for the Arctic Region, 2013. Government Resolution on 23 August 2013. 16. Prime Minister's Office Publications, p. 2013.
Fischer, E., Knutti, R., 2014. Impacts: heated debate on cold weather. Nat. Clim. Chang. 4, 537–538. https://doi.org/10.1038/nclimate2286.
FMI (Finnish Meteorological Institute), 2017. Vuoden 2016 sää. https://ilmatieteenlaitos.fi/vuosi-2016, Accessed date: 4 May 2019 (in Finnish).
Forbes, B.C., 2006. The challenges of modernity for reindeer management in northernmost Europe. In: Forbes, B.C., Bölter, M., Müller-Wille, L., Hukkinen, J., Müller, F., Gunslay, N., Konstantinov, Y. (Eds.), Reindeer Management in Northernmost Europe: Linking Practical and Scientific Knowledge in Social-ecological System. Ecological Studies vol. 184. Springer-Verlag, Berlin, pp. 11–25.
Forbes, B.C., Stammler, F., 2009. Arctic climate change discourse: the contrasting politics of research agendas in the West and Russia. Polar Res. 28, 28–42.
Franke, A.K., Aatsinki, P., Hallikainen, V., Huhta, E., Hyppönen, M., Juntunen, V., Mikkola, K., et al., 2015. Quantifying changes of the coniferous forest line in Finnish Lapland during 1983–2009. Silva Fennica 49 (4), 1408. https://doi.org/10.14214/sf.1408.
Goovaerts, P., 1999. Geostatistics in soil science: state-of-the-art and perspectives. Geoderma 89, 1–45. https://doi.org/10.1016/S0016-7061(98)00078-0.
Hagemoen, R.I.M., Reimers, E., 2002. Reindeer summer activity pattern in relation to weather and insect harassment. J. Anim. Ecol. 71 (5), 883–892.
Härkönen, L., Härkönen, S., Kaitala, A., Kaunisto, S., Kortet, R., Laaksonen, S., Ylönen, H., 2010. Predicting range expansion of an ectoparasite – the effect of spring and summer temperatures on deer ked *Lipoptena cervi* (*Diptera: Hippoboscidae*) performance along a latitudinal gradient. Ecography 33, 906–912.
Heggberget, T.M., Gaare, E., Ball, J.P., 2002. Reindeer (*Rangifer tarandus*) and climate change: importance of winter forage. Rangifer 22 (1), 13–31.
Helander, E., 2004. Global change – climate observations among the Sami. In: Mustonen, T., Helander, E. (Eds.), Snowscapes, Dreamscapes: SnowChange Book on Community Voices of Change. Tampere Polytechnic publications, ser. C. Tampere: Tampereen ammattikorkeakoulu.
Helle, T., 1984. Foraging behaviour of semi-domesticated reindeer (*Rangifer tarandus tarandus*) in relation to snow in Finnish Lapland. Reports from the Kevo Subarctic Research Station 19, 35–47.

Helle, T., Aspi, J., 1984. Do sandy patches help reindeer against insects? Reports From the Kevo Subarctic Research Station. 19, pp. 57–62

Helle, T.P., Jaakkola, L.M., 2008. Transitions in herd management of semi-domesticated reindeer in northern Finland. Annales Zoologi Fennici 45 (2), 81–101. https://doi.org/10.5735/086.045.0201.

Helle, T., Kojola, I., 1994. Body mass variation in semidomesticated reindeer. Can. J. Zool. 72 (4), 681–688.

Helle, T., Kojola, I., 2008. Demographics in an alpine reindeer herd: effects of density and winter weather. *Ecography* 31, 221–230.

Hukkinen, J., Müller-Wille, L., Aikio, P., Heikkinen, H., Jääskö, O., Laakso, A., Magga, H., et al., 2006. Development of participatory institutions for reindeer management in Finland: a diagnosis of deliberation, knowledge integration and sustainability. Ecological Studies 184, 47–71.

Huntington, H., 2011. The local perspective. Nature 478, 182–183.

Ingold, T., 2000. The Perception of the Environment: Essays in Livelihood, Dwelling and Skill. Routledge, London.

Ingold, T., Kurttila, T., 2000. Perceiving the environment in Finnish Lapland. Body and Society 6, 183–196.

IPCC (International Panel on Climate Change), 2018. Summary for policymakers. In: Masson-Delmotte, V., Zhai, P., Pörtner, H.-O., Roberts, D., Skea, J., Shukla, P.R., Pirani, A., et al. (Eds.), Global Warming of 1.5°C. An IPCC Special Report on the Impacts of Global Warming of 1.5°C Above Pre-industrial Levels and Related Global Greenhouse Gas Emission Pathways, in the Context of Strengthening the Global Response to the Threat of Climate Change, Sustainable Development, and Efforts to Eradicate Poverty. World Meteorological Organization (WMO), Geneva, Switzerland.

IPCC (International Panel on Climate Change), 2019. Chapter 1: framing and context of the report. IPCC Special Report on Ocean and Cryosphere in a Changing Climate (SROCC). World Meteorological Organization (WMO), Geneva, Switzerland.

Jaakkola, J.J.K., Juntunen, S., Näkkäläjärvi, K., 2018. The holistic effects of climate change on the culture, well-being, and health of the Saami, the only indigenous people in the European Union. Current Environmental Health Reports https://doi.org/10.1007/s40572-018-0211-2.

Kivinen, S., Rasmus, S., 2015. Observed cold season changes in a Fennoscandian fell area over the past three decades. Ambio 44 (3), 214–225. https://doi.org/10.1007/s13280-014-0541-8.

Kivinen, S., Kaarlejärvi, E., Jylhä, K., Räisänen, J., 2012. Spatiotemporal distribution of threatened high-latitude snowbed and snow patch habitats in warming climate. Environ. Res. Lett. 7, 034024. https://doi.org/10.1088/1748-9326/7/3/034024.

Kivinen, S., Rasmus, S., Jylhä, K., Laapas, M., 2017. Long-term climate trends and extreme events in Northern Fennoscandia (1914–2013). Climate 5 (1), 16. https://doi.org/10.3390/cli5010016.

Koyama, T., Stroeve, J., Cassano, J., Crawford, A., 2017. Sea ice loss and Arctic cyclone activity from 1979 to 2014. J. Clim. 30. https://doi.org/10.1175/JCLI-D-16-0542.1. JCLI-D-16-0542.1.

Kumpula, J., 2012. Ilmastonmuutos ja poronhoito. In: Ruuhela, R. (Ed.), Miten väistämättömään ilmastonmuutokseen voidaan sopeutua? Yhteenveto suomalaisesta sopeutumistutkimuksesta eri toimialoilla. 6. Maa- ja metsätalousministeriön julkaisuja, p. 2011 (In Finnish).

Kumpula, J., Colpaert, A., 2003. Effects of weather and snow conditions on reproduction and survival of semi-domesticated reindeer (*R.t.tarandus*). Polar Res. 22 (2), 225–233.

Kumpula, J., Parikka, P., Nieminen, M., 2000. Occurence of certain microfungi on reindeer pastures in northern Finland during winter 1996–97. Rangifer 20 (1), 3–8.

Laaksonen, S., Kuusela, J., Nikander, S., Nylund, M., Oksanen, A., 2007. Outbreak of parasitic peritonitis in reindeer in Finland. Veterinary Records 16, 835–841.

Laaksonen, S., Pusenius, J., Kumpula, J., Venäläinen, A., Kortet, R., Oksanen, A., Hoberg, E., 2010. Climate change promotes the emergence of serious disease outbreaks of filarioid nematodes. Eco-Health 7 (1), 7–13.

Lépy, E., Pasanen, L., 2017. Observed regional climate variability during the last 50 years in reindeer herding cooperatives of Finnish fell Lapland. Climate 5 (4), 81. https://doi.org/10.3390/cli5040081.

Lorenz, R., Stalhandske, Z., Fischer, E.M., 2019. Detection of a climate change signal in extreme heat, heat stress, and cold in Europe from observations. Geophys. Res. Lett. 46, 8363–8374. https://doi.org/10.1029/2019GL082062.

Luomaranta, A., Aalto, J., Jylhä, K., 2019. Snow cover trends in Finland over 1961–2014 based on gridded snow depth observations. Int. J. Climatol. https://doi.org/10.1002/joc.6007.

MAF (Ministry of Agriculture and Forestry), 2005. Ilmastonmuutoksen kansallinen sopeutumisstrategia. *Maa-ja metsätalousministeriön julkaisuja* 1/2005 (in Finnish).

MAF (Ministry of Agriculture and Forestry), 2009. Ilmastonmuutoksen kansallisen sopeutumisstrategian toimeenpanon arviointi 2009. *Maa- ja metsätalousministeriön julkaisuja* 4/2009 (in Finnish).

MAF (Ministry of Agriculture and Forestry), 2013. Ilmastonmuutoksen kansallisen sopeutumisstrategian arviointi 2013. 5. Maa- ja metsätalousministeriön työryhmämuistio, p. 2013 (in Finnish).

MAF (Ministry of Agriculture and Forestry), 2014. Kansallinen ilmastonmuutokseen sopeutumissuunnitelma 2022. *Maa-ja metsätalousministeriön julkaisuja* 5/2014 (in Finnish).

Maliniemi, T., Kapfer, J., Saccone, P., Skog, A., Virtanen, R., 2018. Long-term vegetation changes of treeless heath communities in northern Fennoscandia: links to climate change trends and reindeer grazing. J. Veg. Sci. 29, 469–479.

Mårell, A., Hofgaard, A., Danell, K., 2006. Nutrient dynamics of reindeer forage species along snowmelt gradients at different ecological scales. Basic and Applied Ecology 7, 13–30.

Markkula, I., Turunen, M., Rasmus, S., 2019. A review of climate change impacts on the ecosystem services in the Saami homeland in Finland. Sci. Total Environ. 692, 1070–1085. https://doi.org/10.1016/j.scitotenv.2019.07.272.

Marshall, G.J., Kivinen, S., Jylhä, K., Vignols, R.M., Rees, W.G., 2018. The accuracy of climate variability and trends across Arctic Fennoscandia in four reanalyses. Int. J. Climatol. 38, 3878–3895. https://doi.org/10.1002/joc.5541.

Matheron, G., 1963. Principles of geostatistics. Econ. Geol. 58, 1246–1266.

Menzies, C.R., Butler, C., 2006. Introduction: understanding ecological knowledge. In: Menzies, C.R. (Ed.), Traditional Ecological Knowledge and Natural Resource Management. University of Nebraska Press, Lincoln.

Moen, J., 2008. Climate change: effects on the ecological basis for reindeer husbandry in Sweden. Ambio 37 (4), 304–311.

Monastersky, R., 2009. The social pole? Nature 457, 1077–1078.

Oinonen, K., Kumpula, J., Shemeikka, P., Väänänen, M., Kontio, P., Siitari, J., Siitari, S., et al., 2014. Tools for taking reindeer herding into account in land use planning – POROT project. NJ. Report 10, 8.

Oksanen, L., Virtanen, R., 1995. Topographic, altitudinal and regional patterns in continental and suboceanic heath vegetation of northern Fennoscandia. Acta Bot. Fenn. 153, 1–80.

Overland, J., Francis, J., Hall, R., Hanna, E., Kim, S.-J., Vihma, T., 2015. The melting Arctic and Midlatitude weather patterns: are they connected? J. Clim. 28. https://doi.org/10.1175/JCLI-D-14-00822.1.

Pääkkölä, E., Mäkelä, K., Saikkonen, A., Tynys, S., et al., 2018. Tunturit. In: Kontula, T., Raunio, A. (Eds.), Suomen luontotyyppien uhanalaisuus 2018. Luontotyyppien punainen kirja. Osa 1 – tulokset ja arvioinnin perusteet (Threatened Habitat Types in Finland 2018. Red Book of Habitats. Part 1 – Results and Basis of the Assessment). Ympäristökeskus ja Ympäristöministeriö, Helsinki, Finland, pp. 255–313 (Suomen ympäristö 5/2018 Osa 1).

Peltonen-Sainio, P., Venäläinen, A., Mäkelä, H.M., Pirinen, P., Laapas, M., Jauhiainen, L., Kaseva, J., et al., 2016a. Harmfulness of weather events and the adaptive capacity of farmers at high latitudes of Europe. Clim. Res. 67, 221–240. https://doi.org/10.3354/cr01378.

Peltonen-Sainio, P., Pirinen, P., Mäkelä, H., Hyvärinen, O., Huusela-Veistola, E., Ojanen, H., Venäläinen, A., 2016b. Spatial and temporal variation in weather events critical for boreal agriculture: I elevated temperatures. Agric. Food Sci. 25 (1), 44–56. https://doi.org/10.23986/afsci.51465.

Peltonen-Sainio, P., Pirinen, P., Mäkelä, H., Ojanen, H., Venäläinen, A., 2016c. Spatial and temporal variation in weather events critical for boreal agriculture: II precipitation. Agric. Food Sci. 25 (1), 57–70. https://doi.org/10.23986/afsci.51466.

Peltonen-Sainio, P., Sorvali, J., Müller, M., Huitu, O., Neuvonen, S., Nummelin, T., Rummukainen, A., et al., 2017. Sopeutumisen tila 2017: Ilmastokestävyyden tarkastelut maa-ja metsätalousministeriön hallinnonalalla. Luonnonvara- ja biotalouden tutkimus. 18, p. 2017 (in Finnish).

Pirinen, P., Simola, H., Aalto, J., Kaukoranta, J.-P., Karlsson, P., Ruuhela, R., 2012. Tilastoja Suomen ilmastosta 1981–2010. *Finnish Meteorological Institute Reports* 2012:1. Finnish Meteorological Institute, Helsinki (in Finnish).

Rasmus, S., Kumpula, J., Jylhä, K., 2014. Suomen poronhoitoalueen muuttuvat talviset sääolosuhteet. Terra 126, 169–185 (in Finnish with English summary).

Rasmus, S., Kivinen, S., Bavay, M., Heiskanen, J., 2016. Local and regional variability in snow conditions in northern Finland: a reindeer herding perspective. Ambio 45 (4), 398–414. https://doi.org/10.1007/s13280-015-0762-5.

Rasmus, S., Kivinen, S., Irannezhad, M., 2018. Basal ice formation in Northern Finland snow covers during 1948–2016. Environ. Res. Lett. 13, 114009. https://doi.org/10.1088/1748-9326/aae541.

RHA (Reindeer Herders'' Association), 2014. Opas poronhoidon tarkastelemiseen maankäyttöhankkeissa. Pohjolan Painotuote Oy, Rovaniemi (in Finnish).

RHA (Reindeer Herders" Association), 2018. Reindeer Statistics for Finland.

Riseth, J.Å., Tømmervik, H., Bjerke, J.W., 2016. 175 years of adaptation: North Scandinavian Sámi reindeer herding between government policies and winter climate variability (1835–2010). J. For. Econ. 24, 186–204. https://doi.org/10.1016/j.jfe.2016.05.002.

Ruosteenoja, K., Räisänen, J., Venäläinen, A., Kämäräinen, M., 2015. Projections for the duration and degree days of the thermal growing season in Europe derived from CMIP5 model output. Int. J. Climatol. https://doi.org/10.1002/joc.4535.

Ruosteenoja, K., Jylhä, K., Kämäräinen, M., 2016. Climate projections for Finland under the RCP forcing scenarios. Geophysica 51, 17–50.

Ryd, Y., 2001. Snö – En renskötare Berättar. Ordfront, Stockholm.

Screen, J.A., 2014. Arctic amplification decreases temperature variance in northern mid- to high-latitudes. Nat. Clim. Chang. 4, 577–582. https://doi.org/10.1038/nclimate2268.

Sepp, M., Jaagus, J., 2011. Changes in the activity and tracks of Arctic cyclones. Clim. Chang. 105, 577–595. https://doi.org/10.1007/s10584-010-9893-7.

Sillmann, J., Kharin, V.V., Zhang, X., Zwiers, F.W., Bronaugh, D., 2013. Climate extremes indices in the CMIP5 multimodel ensemble: part 1. Model evaluation in the present climate. Journal of Geophysical Research: Atmosphere 118, 1716–1733. https://doi.org/10.1002/jgrd.50203.

Soppela, P., 2009. The energetic aspects of migration in northern ungulates, the caribou and reindeer (*Rangifer tarandus*). In: Morris, S., Vosloo, A. (Eds.), Molecules to Migration: The Pressures of Life. Medimond Publishing, Bologna, Italy.

Soppela, P., Turunen, M., 2017. Sopeutuuko porotalous kasautuvien muutosten paineessa? In: Tennberg, M., Emelyanova, A., Eriksen, H., Haapala, J., Hannukkala, A., Jaakkola, J.J.K., Jouttijärvi, T., et al. (Eds.), The Barents Area Changes – How Will Finland Adapt?. *Publications of the Govenrment's analysis, assessment and research activities 31*/2017. Prime minister's office, Helsinki

Soppela, P., Nieminen, M., Timisjärvi, J., 1986. Thermoregulation in reindeer. Rangifer 1, 273–278.

Turunen, M., Vuojala-Magga, T., 2014. Past and present winter feeding of reindeer in Finland: herders adaptive learning of the practices. Arctic 67 (2), 173–188. https://doi.org/10.14430/arctic4385.

Turunen, M., Soppela, P., Kinnunen, P., Sutinen, M.-L., Martz, F., 2009. Does climate change influence the availability and quality of reindeer forage plants? Polar Biol. 32, 813–832.
Turunen, M., Oksanen, P., Vuojala-Magga, T., Markkula, I., Sutinen, M.-L., Hyvönen, J., 2013. Impacts of winter feeding of reindeer on vegetation and soil in the sub-Arctic: insights from a feeding experiment. Polar Res. 32, 18610. https://doi.org/10.3402/polar.v32i0.18610.
Turunen, M., Rasmus, S., Bavay, M., Ruosteenoja, K., Heiskanen, J., 2016. Coping with increasingly difficult weather and snow conditions: reindeer herders' views on climate change impacts and coping strategies. Clim. Risk Manag. 11, 15–36. https://doi.org/10.1016/j.crm.2016.01.002.
Turunen, M.T., Rasmus, S., Järvenpää, J., Kivinen, S., 2019. Relations between forestry and reindeer husbandry in northern Finland – perspectives of science and practice. For. Ecol. Manag., 117677 https://doi.org/10.1016/j.foreco.2019.117677.
Tveraa, T., Stien, A., Bårdsen, B.-J., Fauchald, P., 2013. Population densities, vegetation green-up, and plant productivity: impacts on reproductive success and juvenile body mass in reindeer. PLoS One 8 (2), e56450. https://doi.org/10.1371/journal.pone.0056450.
Tyler, N.J.C., Turi, J.M., Sundset, M.A., Bull, K.S., Sara, M.N., Reinert, E., Oskal, N., et al., 2007. Saami reindeer pastoralism under climate change: applying a generalized framework for vulnerability studies to a sub-arctic social-ecological system. Glob. Environ. Chang. 17, 191–206.
Vikhamar-Schuler, D., Hanssen-Bauer, I., Førland, E., 2010. Long-term Climate Trends of Finnmarksvidda, Northern-Norway. *Norwegian Meteorological Institute Reports* 6. Norwegian Meteorological Institute, Oslo.
Vikhamar-Schuler, D., Isaksen, K., Haugen, J.E., Tømmervik, H., Luks, B., Schuler, T.V., Bjerke, J.W., 2016. Changes in winter warming events in the Nordic Arctic Region. J. Clim. 29, 6223–6244.
Virtanen, R., Luoto, M., Rämä, T., Mikkola, K., Hjort, J., Grytnes, J.-A., Birks, H.J.B., 2010. Recent vegetation changes at the high-latitude tree line ecotone are controlled by geomorphological disturbance, productivity and diversity. Glob. Ecol. Biogeogr. 19, 810–821.
Virtanen, R., Oksanen, L., Oksanen, T., Cohen, J., Forbes, B.C., Johansen, B., Käyhkö, J., et al., 2016. Where do the treeless tundra areas of northern highlands fit in the global biome system: toward an ecologically natural subdivision of the tundra biome. Ecology and Evolution https://doi.org/10.1002/ece3.1837.
Vuojala-Magga, T., Turunen, M., Ryyppö, T., Tennberg, M., 2011. Resonance strategies of Sami reindeer herding during climatically extreme years in northernmost Finland in 1970–2007. Arctic 64 (2), 227–241.
Wei, L., Qin, T., Li, C., 2017. Seasonal and inter-annual variations of Arctic cyclones and their linkage with Arctic sea ice and atmospheric teleconnections. Acta Oceanol. Sin. 36, 1. https://doi.org/10.1007/s13131-017-1117-9.
Weladji, R.B., Holand, Ø., Almøy, T., 2003. Use of climatic data to assess the effect of insect harassment on the autumn weight of reindeer (*Rangifer tarandus*) calves. J. Zool. 260 (1), 79–85. https://doi.org/10.1017/S0952836903003510.
Zahn, M., Akperov, M., Rinke, A., Feser, F., Mokhov, I.I., 2018. Trends of cyclone characteristics in the Arctic and their patterns from different re-analysis data. J. Geophys. Res. 123, 2737–2751. https://doi.org/10.1002/2017JD027439.
Zhang, X., Walsh, J.E., Zhang, J., Bhatt, U.S., Ikeda, M., 2004. Climatology and interannual variability of arctic cyclone activity: 1948–2002. J. Clim. 17, 2300–2317. https://doi.org/10.1175/1520-0442(2004) 017<2300:CAIVOA>2.0.CO;2.

Acts

Act on compensating the damages caused to reindeer herding, 655/2016. https://www.finlex.fi/fi/laki/ajantasa/2016/20160655.
Act on compensating the damages caused to reindeer herding, 987/2011. https://www.finlex.fi/fi/laki/alkup/2011/20110987.
Act on Metsähallitus, 234/2016. http://www.finlex.fi/fi/laki/alkup/2016/20160234.
Act on the Saami Parliament, 974/1995. http://www.finlex.fi/fi/laki/kaannokset/1995/en19950974.pdf.
Mining Act. http://www.finlex.fi/fi/laki/kaannokset/2011/en20110621.pdf.
Reindeer Husbandry Act, 848/1990. http://www.finlex.fi/fi/laki/kaannokset/1990/en19900848.pdf.

III

Tellus SERIES A DYNAMIC METEOROLOGY AND OCEANOGRAPHY
PUBLISHED BY THE INTERNATIONAL METEOROLOGICAL INSTITUTE IN STOCKHOLM

Multimodel estimates of the changes in the Baltic Sea ice cover during the present century

By ANNA LUOMARANTA[1], KIMMO RUOSTEENOJA[1], KIRSTI JYLHÄ[1]*, HILPPA GREGOW[1], JARI HAAPALA[1] and ARI LAAKSONEN[1,2], [1]*Finnish Meteorological Institute, FI-00101 Helsinki, Finland*; [2]*Department of Applied Physics, University of Eastern Finland, FI-70211 Kuopio, Finland*

(Manuscript received 15 August 2013; in final form 5 March 2014)

ABSTRACT

We project changes in the annual maximum ice extent and the maximum coastal fast ice thickness in the Baltic Sea during the ongoing century. The influence of future warming on the ice conditions was assessed using the November–March Baltic coastal mean temperature as a predictor for the annual maximum ice extent (MIB), and the local freezing degree-day sum as a predictor for the fast ice thickness. Future winter temperatures were derived by adjusting observational baseline-period temperatures in accordance with temperature projections based on 28 global climate models (GCMs) participating in the Coupled Model Intercomparison Project Phase 5. Under the Representative Concentration Pathway (RCP) 4.5 scenario, the ensemble-mean trend of MIB is -6400 km^2/10 yr, and from the 2060s onwards in a typical winter MIB remains below 80×10^3 km^2. If the RCP8.5 scenario is realised, the corresponding estimates are $-10\,900$ km^2/10 yr for the trend and 60×10^3 km^2 for a typical MIB. For cold rather than typical winters, the projected rate of decrease in MIB is even faster. During the late century under RCP8.5, in 9 out of 10 yr the ice would only cover 5–20% of the total sea area. The projected trends in the mean annual maximum ice thickness are $-7.6 \ldots -3.3$ cm/10 yr, depending on location and applied scenario. In the 2040s under both scenarios, and in the 2080s under RCP4.5, the ice thickness may still exceed 60 cm in the northernmost Bay of Bothnia, while elsewhere in the Gulf of Bothnia and in the Gulf of Finland, it will vary between about 10 and 40 cm. In the 2080s under RCP8.5, virtually no ice occurs outside the Bay of Bothnia. For both the ice extent and thickness, the spread among the responses based on the temperature projections of individual GCMs is considerable. Nonetheless, a robust finding is that the Baltic Sea is unlikely to become totally ice-free during this century.

Keywords: sea ice extent, ice thickness, climate change, CMIP5 models, inter-model differences, inter-annual variability

1. Introduction

The seasonal ice cover of the Baltic Sea exhibits a large inter-annual variability which is mainly driven by variations in the large-scale atmospheric circulation, such as the North-Atlantic Oscillation (Omstedt and Chen, 2001; Vihma and Haapala, 2009). Of all the sea ice parameters, such as thickness, concentration, freezing and break-up dates, the maximum ice extent of the Baltic Sea (MIB) is the mostly widely used parameter to indicate climate variability in the region. Recordings of the MIB date back to 1720 (Seinä and Palosuo, 1996), but the most reliable observations begin in the late 19th century (Vihma and Haapala, 2009). During the most severe winters the Baltic Sea has been entirely ice-covered, equivalent to an ice extent of 420×10^3 km^2. The minimum MIB observed thus far, 49×10^3 km^2, occurred in 2008. The northernmost sub-basin of the Baltic Sea, the Bay of Bothnia, has so far been entirely ice-covered and the eastern Gulf of Finland partially so, even during the mildest winters.

Winters can be sorted into ice severity classes on the basis of MIB observations. According to the present revised standards that correspond to the recent climate (Vainio, 2011), winters with an ice extent smaller than 115×10^3 km^2 (or 27% of the total sea area) are classified as mild, those from 115 to 230×10^3 km^2 (27–55%) as average and those from 230 to 345×10^3 km^2 (55–82%) as severe. If the ice extent exceeds 345×10^3 km^2, the winter is regarded as extremely severe. Since the smallest MIB observed thus far is 49×10^3 km^2 (12%), winters

*Corresponding author.
email: kirsti.jylha@fmi.fi

Citation: Tellus A 2014, **66**, 22617, http://dx.doi.org/10.3402/tellusa.v66.22617

with an even smaller ice extent than this are termed unprecedentedly mild.

The variability of the sea ice cover in the Baltic Sea is a sensitive indicator of climatic fluctuations and changes in northern Europe. Several studies have reported a declining trend in MIB (Jevrejeva et al., 2004; Schmeltzer et al., 2008; Vihma and Haapala, 2009; BACC II Author Team, 2014). Considering the winters of 1901–2013, we did not, however, find any statistically significant linear trend in MIB (Fig. 1a) or in the decadal sums of severe and extremely severe ice winters (Fig. 1b). Instead, there were strong inter-annual and inter-decadal variations. A noteworthy feature is, nonetheless, the scarcity of extremely severe ice winters since the late 1980s.

One of the most robust features of future climate projections is that the surface air temperature will increase within the Baltic Sea catchment area in winter (BACC II Author Team, 2014). A warming trend can be expected to directly impact the duration, thickness, extent and other properties of the sea ice cover, as well as the partitioning between snowfall and rainfall. Such changes in turn will have a major impact on oceanographic and hydrological conditions, the ecosystems, the biogeochemical cycles, coastal erosion, ice roads and winter navigation in the Baltic Sea.

Previous estimates of the sensitivity of the Baltic Sea ice cover to climatic changes have been based on numerical modelling (Omstedt and Nyberg, 1996; Haapala and Leppäranta, 1997; Omstedt et al., 2000; Haapala et al., 2001; Meier et al., 2004; Meier, 2006) or on using statistical methods to correlate sea ice variability to atmospheric conditions (Tinz, 1996; Omstedt and Chen, 2001; Jylhä et al., 2008; Luomaranta et al., 2010). In conjunction with projections of future warming, considerable thinning of the ice and shrinking of the ice cover, as well as a shortening of

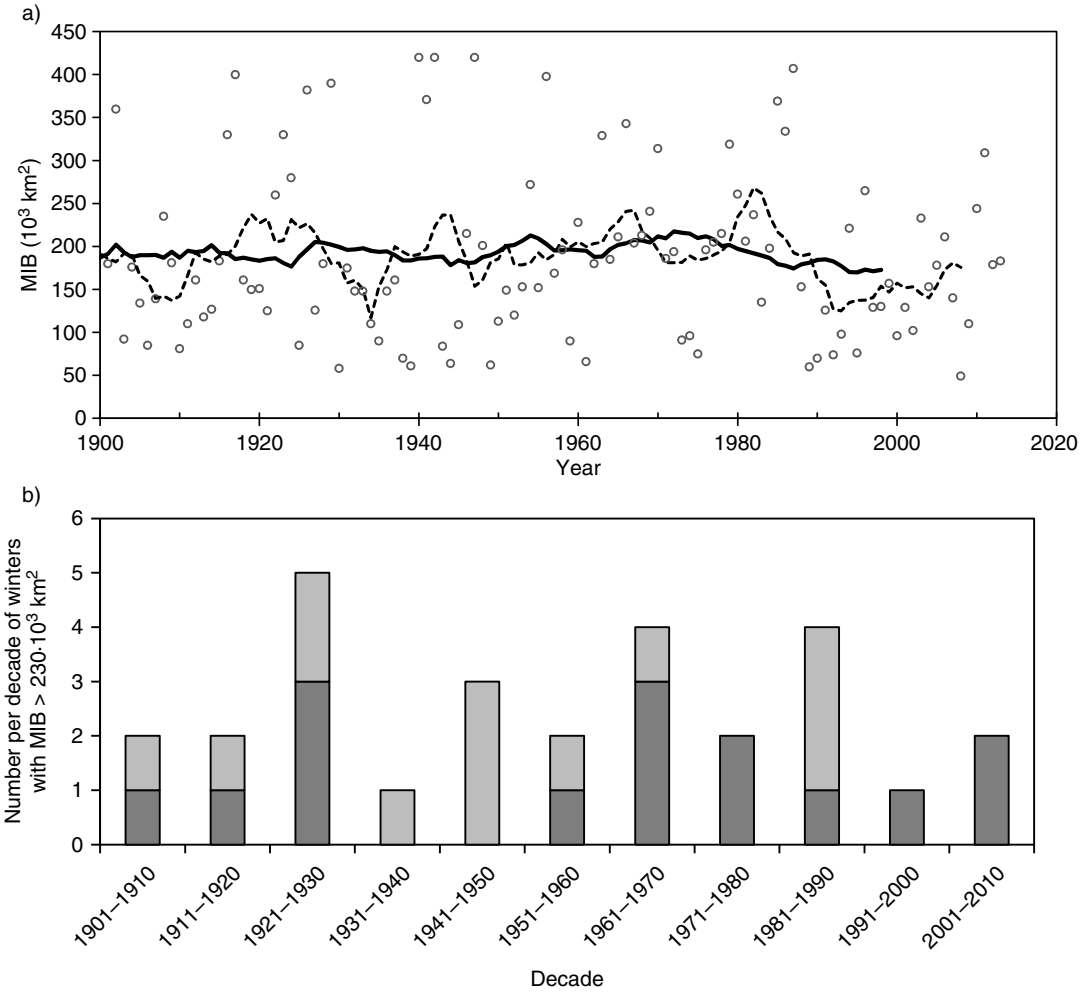

Fig. 1. Past records of the Baltic Sea ice cover. (a) The annual maximum ice extent (MIB) in 1901–2013; (b) the number per decade of severe (dark grey) and extremely severe (light grey) ice winters, that is, winters with MIB exceeding 230×10^3 km^2 or 345×10^3 km^2, respectively, during 1901–2010. The dotted and solid curves in panel (a) show the 10 and 30 yr running means, respectively.

the ice season in the Baltic Sea, are foreseen in these studies, but there are differences in the strength of the responses. For example, Haapala et al. (2001) assessed a reduction of the mean MIB by one-third or a half by the late 21st century, the range corresponding to two regional ice-ocean models that had been run with equal future atmospheric forcing. In the works of Meier et al. (2004) and Meier (2006), two different scenarios for the concentrations of greenhouse gases (GHGs) and altogether four modelling systems were applied, the corresponding projected decreases in mean MIB ranging from a half to four-fifths. Despite these drastic reductions, no totally ice-free winters were simulated to occur during 2071–2100. In contrast, in a model experiment conducted by Omstedt et al. (2000), there was almost no ice in 3 out of 10 winters.

As regards statistical methods, Omstedt and Chen (2001) established a multiple regression equation that linked MIB to the large-scale atmospheric circulation. An exponential regression model between MIB and the mean air temperature from November to March was in turn developed by Tinz (1996) and updated by Jylhä et al. (2008) and Luomaranta et al. (2010). Based on that approach and on temperature projections derived from a set of global and regional climate model experiments, Jylhä et al. (2008) assessed MIB to become smaller than 80×10^3 km^2 in the majority of years during 2071–2100. Using a subsequent (but not the most recent) generation of climate projections, Luomaranta et al. (2010) inferred that winters with an MIB larger than 280×10^3 km^2 would be very improbable in 2041–2050.

In the papers referred to above, the differences in the responses of the Baltic Sea ice conditions arose from the divergent climate projections applied and the differences in numerical models or statistical approaches. Regional Baltic Sea circulation models, including the dynamics of the ice cover, are the most advanced tools to estimate the impacts of changes in the global climate system on a local scale, but due to the heavy computational requirements, their capacity to produce simulations under a wide ensemble of climatic forcing is limited. Conversely, statistical approaches cannot capture the real physical linkages among the various components of the climate system, but require very little computing resources compared to the numerical models. Statistical models are thus feasible tools for producing estimates of ice cover changes based on a large number of climate change scenarios. For example, it is possible to analyse a multitude of alternative temperature change projections produced by a wide ensemble of models forced by several greenhouse gas concentration scenarios.

In the present work, our objectives are to assess the temporal evolution of the Baltic Sea ice cover during the period 2021–2090 and to give an insight into the related uncertainties. We consider two sea ice quantities: the annual MIB and the climatological mean of the maximum fast ice thickness. Statistical methods are employed for both quantities: a non-linear regression model for the former and an analytical solution for the ice growth rate equation for the latter. Both approaches required projections of future changes in air temperature; these were based on data retrieved from the recently published global climate model (GCM) simulations within the Coupled Model Intercomparison Project Phase 5 (CMIP5, see Taylor et al., 2012). The CMIP5 simulations are forced by the new Representative Concentration Pathway (RCP) scenarios for GHGs and aerosol particles (Moss et al., 2010; van Vuuren et al., 2011); the simulations forced by RCP4.5 and RCP8.5 were selected for the present analysis.

In addition to the best estimates for changes in average sea ice conditions, derived from multimodel ensemble means, we explore three aspects not adequately addressed in previous studies: inter-annual variations, scatter across a multitude of climate models and the uncertainty induced by future GHG emissions. In order to consider inter-annual variability, frequency distributions of MIB in the future climate are constructed and three percentiles in them are considered. This allows us to compare the influence of climate change on winters that represent typical ice conditions versus those with very extensive or scant ice cover. Second, to assess the uncertainty associated with modelling differences, we examine the scatter of the responses produced by 28 individual models. Finally, the uncertainty induced by future emissions is considered by analysing the responses to two very divergent GHG scenarios.

2. Data and methods

2.1. Data

2.1.1. Ice and temperature observations. Our observational data consisted of observations of annual maximum ice extent in the Baltic Sea in the years 1952–2012 and air temperature observations in the coastal area of the Baltic Sea during the same period. Furthermore, observations of the annual maximum ice thickness in 1971–2000 were available for Kemi (65.73°N, 24.55°E) and Loviisa (60.42°N, 26.27°E) (Jevrejeva et al., 2002).

Most of the observed MIBs in 1952–2012 can be classified as average ice winters (Fig. 2). The date refers to the year of January in each winter; that is, the first and last winters included in our study were the cold seasons of 1951–1952 and 2011–2012.

For air temperature observations on the coasts of the Baltic Sea, we used the E-OBS gridded dataset (Haylock et al., 2008) within the latitudes of 53–67°N and longitudes

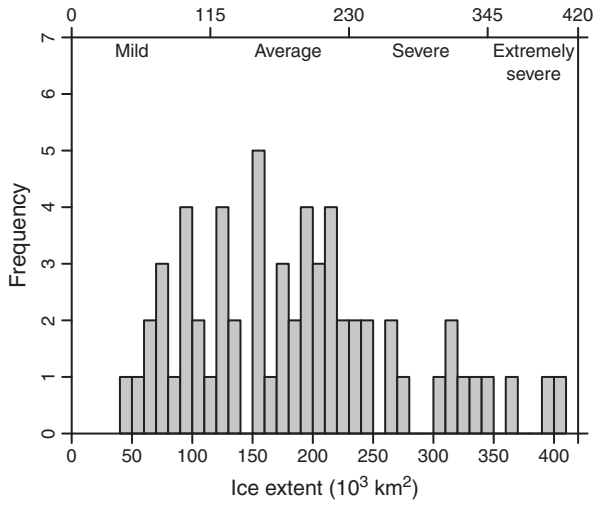

Fig. 2. The frequency distribution of the observed annual maximum ice extent in 1952–2012. The ice winter classification is shown along the upper horizontal axis showing the ice extent limits for mild, average, severe and extremely severe ice winters.

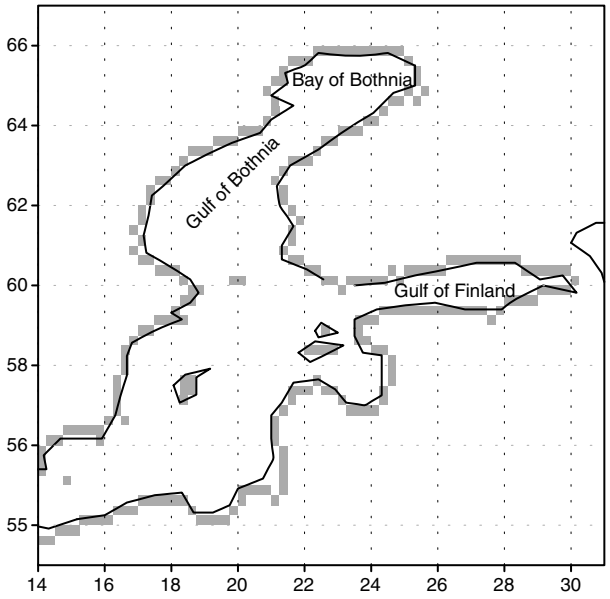

Fig. 3. The coastal grid points in the E-OBS gridded data set for the observational air temperatures. The positions of three of the sub-basins of the Baltic Sea are shown: the Bay of Bothnia, the Gulf of Bothnia and the Gulf of Finland.

of 14–31°E (Fig. 3). The spatial resolution of the dataset was 0.25°, and the number of coastal grid points used here was 245. E-OBS version 7.0 was employed (except for the years 1951–1960 that were covered by version 6.0).

2.1.2. Climate model output. Climate model simulations of air temperature under the RCP4.5 and RCP8.5 scenarios (Moss et al., 2010; van Vuuren et al., 2011), extending until the end of this century, were downloaded from the CMIP5 archive. Of these two greenhouse gas scenarios, the RCP4.5 scenario is mid-range, in which the actions of climate policy are moderately effective. The RCP8.5 scenario, by contrast, represents very high emissions. In RCP4.5, the CO_2 concentration stabilises at around 540 ppm by the end of the century; in RCP8.5 the concentration at that time exceeds 900 ppm. The differences between the scenarios are small at the beginning of the study period, but increase over time.

Monthly mean temperature data for both the RCP4.5 and RCP8.5 scenarios were available for a total of 35 GCMs. However, models failing to meet three fundamental conditions were omitted from the analysis. First, two of the models (BNU-ESM and FGOALS-s2) were severely biased in simulating the sensitivity to recent past forcing, the simulated global mean temperature trend during the past 50 yr exceeding the observation-based estimate by more than 0.4°C. Second, in four models (FGOALS-s2, FIO-ESM, GFDL-ESM2G and HadGEM2-AO) the projected global mean temperature increase under the various RCP scenarios behaved inconsistently. For example, the global mean temperature response to the RCP8.5 forcing simulated by FIO-ESM was 2.7 times as large by 2070–2099 as the corresponding response to RCP4.5, while the multimodel median of that ratio was 1.8. Third, there were five models (BNU-ESM, CSIRO-Mk3-6-0, FGOALS-s2, FIO-ESM and IPSL-CM5B-LR) for which the simulated baseline-period climatological mean temperature and/or precipitation in Europe deviated markedly from their observational counterparts. Note that for some models there were several objections; for example, the FGOALS-s2 model failed to fulfil all three criteria.

Since the above-discussed seven models were disregarded, the present analysis is based on 28 GCMs in total (Table 1). For control purposes, however, we also calculated the multimodel mean temperature response to the RCP8.5 forcing as a mean of all the 35 models. The outcome proved to be nearly indistinguishable from the 28-model mean.

The climate model data were smoothed by applying a 30 yr running mean and interpolated onto the same 0.25° grid that was used for the observational temperatures. The November–March mean temperature change from 1971–2000 to 2031–2060, averaged over the coastal grid points (Fig. 3), differs from model to model (Table 1). In the RCP4.5 scenario, the change varies between 0.8 and 4.9°C, while in the RCP8.5 scenario the range is 1.9–5.2°C. In Table 1, the models are ordered according to their projected temperature response (shown in parentheses).

2.1.3. Evaluation of the model simulations. Although the 28 GCMs selected behave reasonably on the large scale, biases may still exist on regional scales, resulting, for

Table 1. The CMIP5 models used in this study

Model	Country of origin	Mean (i) (°C)	Range (ii) (°C)	Trend (iii) (°C/10 yr)	ΔT (°C): RCP4.5		ΔT (°C): RCP8.5	
MIROC5	Japan	−3.4	26.5	0.41	2.8	(16)	2.9	(14)
MIROC-ESM	Japan	−0.4	22.0	0.28	3.2	(23)	3.9	(24)
MIROC-ESM-CHEM	Japan	−0.6	22.6	0.11	3.5	(25)	4.1	(25)
MRI-CGCM3	Japan	−4.1	20.3	0.21	1.8	(6)	2.8	(11)
BCC-CSM1-1	China	−5.1	20.7	0.72	2.6	(15)	3.7	(20)
INMCM4	Russia	−3.4	21.2	0.14	1.9	(8)	2.0	(2)
NorESM1-M	Norway	−1.4	18.8	0.19	2.4	(11)	2.6	(10)
NorESM1-ME	Norway	−1.2	18.7	0.17	2.0	(9)	2.8	(12)
HadGEM2-ES	UK	−3.4	22.4	0.38	2.8	(18)	3.4	(18)
HadGEM2-CC	UK	−6.1	24.8	0.34	2.8	(17)	3.9	(23)
MPI-ESM-LR	Germany	−2.3	20.1	0.34	1.8	(7)	2.6	(9)
MPI-ESM-MR	Germany	−2.4	19.7	0.34	2.4	(12)	2.4	(5)
CNRM-CM5	France	−3.6	24.8	0.56	2.5	(13)	3.1	(16)
IPSL-CM5A-LR	France	−6.7	27.2	0.42	4.0	(26)	4.6	(27)
IPSL-CM5A-MR	France	−3.5	23.7	0.42	3.2	(24)	3.0	(15)
CMCC-CM	Italy	−7.0	21.4	0.70	4.5	(27)	5.2	(28)
CMCC-CMS	Italy	−6.4	22.4	0.72	4.9	(28)	4.4	(26)
GFDL-CM3	USA	−1.2	17.4	0.46	3.2	(21)	3.8	(22)
GFDL-ESM2M	USA	−4.2	21.6	0.23	2.9	(19)	2.9	(13)
GISS-E2-R	USA	−6.0	25.6	0.39	2.5	(14)	3.8	(21)
GISS-E2-H	USA	−5.1	22.8	0.22	3.2	(22)	3.4	(17)
CCSM4	USA	−0.8	21.0	0.31	1.6	(4)	1.9	(1)
CESM1-CAM5	USA	−0.9	20.5	0.18	1.6	(3)	2.5	(8)
CESM1-BGC	USA	−0.4	20.5	0.59	0.8	(1)	2.5	(7)
CanESM2	Canada	−1.3	22.3	0.48	3.0	(20)	3.6	(19)
ACCESS1-0	Australia	−1.8	18.6	0.22	1.4	(2)	2.1	(3)
ACCESS1-3	Australia	−0.3	17.2	0.09	2.2	(10)	2.5	(6)
EC-EARTH	Several	0.0	16.6	0.27	1.7	(5)	2.4	(4)
28-model mean		−3.0	21.5	0.35	2.6		3.2	
Observations		−2.4	21.3	0.48				

Columns 3–5 show (i) the November–March mean temperature (°C), (ii) the annual temperature range (°C) and (iii) the trend (°C/decade) in November–March mean temperature, all calculated for the period 1961–2010. The November–March mean temperature change ΔT (°C) between the periods 1971–2000 and 2031–2060 is given separately for the RCP4.5 and RCP8.5 scenarios. All quantities are averaged over the coastal grid points. The ordinal numbers of the models, shown in parentheses, are determined by the magnitude of the projected temperature change (in ascending order) under these two scenarios. The countries involved in the development of the EC-EARTH model are Belgium, Denmark, Ireland, Italy, the Netherlands, Norway, Portugal, Spain, Sweden and Switzerland.

example, from a crudely resolved topography and land-sea distribution in the Baltic Sea and its adjacent areas. Hence, this sub-ensemble of the original set of 35 models was further evaluated by comparing the modelled temperature climate on the Baltic Sea coasts with its observational counterpart. The comparison covers the years 1961–2010, that is, the same period that was used as a baseline in deriving the statistical distributions of ice extent for the future time slices (section 2.2). Note that this evaluation was only made with respect to one variable (air temperature) and a limited area; it is not intended to be used for far-reaching inferences on the quality of the models in general.

In the model comparison, three quantities were examined: (1) the climatological long-term (50 yr) mean temperature in November–March, (2) the annual temperature range, that is, the 50 yr mean of July minus February temperature and (3) the 50 yr linear least-squares trend of the November–March mean temperature. All quantities are averages over the coastal grid points of the Baltic Sea (Fig. 3).

In studying the 28-model mean, quantities (1) and (2) proved to be simulated well, even though there was rather a large scatter across the models (Table 1). The observation-based November–March mean coastal temperature in 1961–2010 was −2.4°C. The corresponding multimodel mean is −3.0°C, with individual models simulating mean temperatures ranging from −7.0°C (CMCC-CM) to 0.0°C (EC-EARTH). For the annual temperature range, the corresponding values are 21.3°C (observational), 21.5°C (multimodel mean), 16.6°C (minimum among the GCMs) and 27.2°C (maximum). The modelled biases in quantities (1) and (2) bear a strong inverse correlation (Table 2), reflecting the fact that the simulated temperatures vary more strongly

Table 2. Correlations between various temperature indices derived from the 28 GCMs listed in Table 1

Index	Range (ii)	Trend (iii)	RCP4.5	RCP8.5
November–March mean temperature (i)	−0.62	−0.48	−0.60	−0.61
Annual temperature range (ii)		0.30	0.45	0.47
November–March temperature trend (iii)			0.40	0.53

The indices representing the simulated recent past climate are (i) the November–March mean temperature, (ii) the annual temperature range, and (iii) the trend in November–March mean temperature, all calculated over the period 1961–2010. The index representing the future climate is the projected change in November–March temperature from the period 1971–2000 to 2031–2060; the correlations for this index are given separately for the RCP4.5 and RCP8.5 scenarios. Temperatures are averaged over the Baltic Sea coastal grid points (Fig. 3). Significance limits for the correlations: 0.37 ($p = 0.05$), 0.48 (0.01), 0.59 (0.001).

across the models in winter than in summer. Of these two variables, we therefore concentrate on exploring the November–March mean temperature (quantity (1)).

As far as quantity (3) is concerned, the observation-based Baltic Sea coastal temperatures in 1961–2010 show a warming trend of 0.48°C/decade. The corresponding multimodel mean trend is 0.35°C/decade, while the trends simulated by individual models vary from 0.09 to 0.72°C/decade (Table 1). In total, 22 out of 28 models simulate trends that are weaker than observed. Nevertheless, this does not necessarily indicate that the models do in fact tend to underestimate the actual warming signal; in such a small area as the Baltic Sea the observed trend may be severely affected by noise originating from natural climatic fluctuations. In fact, there was a distinct jump in the time series of winter temperatures around the year 1988, with cold winters occurring much more frequently before than after that year. The discontinuity is apparent in the ice extent observations as well (see Fig. 1a).

Several previous studies (see Bracegirdle and Stephenson (2013) and references therein) have suggested that models simulating a cold bias in baseline climate have a tendency to produce large future temperature responses in high latitudes, particularly close to the sea ice edge. Here, we discuss the relation between the model biases and their projections of future temperatures under the RCP8.5 scenario. The conclusions also hold for RCP4.5, even though the correlations are somewhat weaker (see Table 2). In the model ensemble, there is a significant positive correlation ($r \approx 0.5$) between the modelled past (1961–2010) trends and the changes projected from 1971–2000 to 2031–2060. Moreover, both quantities correlate negatively ($r \approx -0.5$ to -0.6; Table 2) with the modelled bias of the November–March temperature. In part, this may be explained by local feedback phenomena. Models producing too low winter temperatures typically simulate sea ice and snow cover in excess, the resulting large albedo and effective thermal isolation further strengthening the coldness. As climate warms, this cooling effect is mitigated, leading these models to simulate strong increases in temperature. In other models with high baseline temperatures, this feedback works less effectively.

Using all the 28 models included in the analysis, the multimodel mean temperature response to the RCP8.5 forcing for the 2040s was 3.2°C. We next studied the influence of further reducing the ensemble size by excluding models with a lower performance, that is, the three models simulating the largest positive and the three producing the largest negative bias in mean temperature. As a consequence, the multimodel mean temperature response would only be reduced by 5%, but the scatter among the modelled responses would be diminished by 23%. A less drastic elimination, only omitting those three models producing the largest bias in absolute terms (in all of them, the bias was negative), would reduce the multimodel mean temperature response by 6% and the standard deviation by 21%. Accordingly, disregarding the models having the largest difficulties in simulating the recent past climate in the target area would not substantially affect the best-estimate (multimodel mean) temperature response, but the apparent uncertainty interval would be curtailed appreciably.

At first sight, any prospect of narrowing the uncertainty interval sounds beneficial. Nonetheless, as shown by Huybers (2010), the various feedback effects (cloud, albedo and the combined water vapour plus lapse rate) tend to co-vary negatively in the GCM ensemble. This kind of compensation between the feedbacks may spuriously curtail the inter-model spread of climate sensitivity. Therefore, in order to avoid the risk of determining too small error bars for the Baltic Sea ice projections, it was decided in this work to accept for analysis all the 28 models showing reasonable skill in simulating the present past climate.

2.2. Methods

2.2.1. Annual maximum ice extent. Broadly following Tinz (1996) and Jylhä et al. (2008), we fitted a non-linear regression model to the observed November–March mean temperature and annual maximum ice extent data for the years 1952–2012 (Fig. 4). The regression equation is given by:

$$MIB = Ae^{-BT} \quad (1)$$

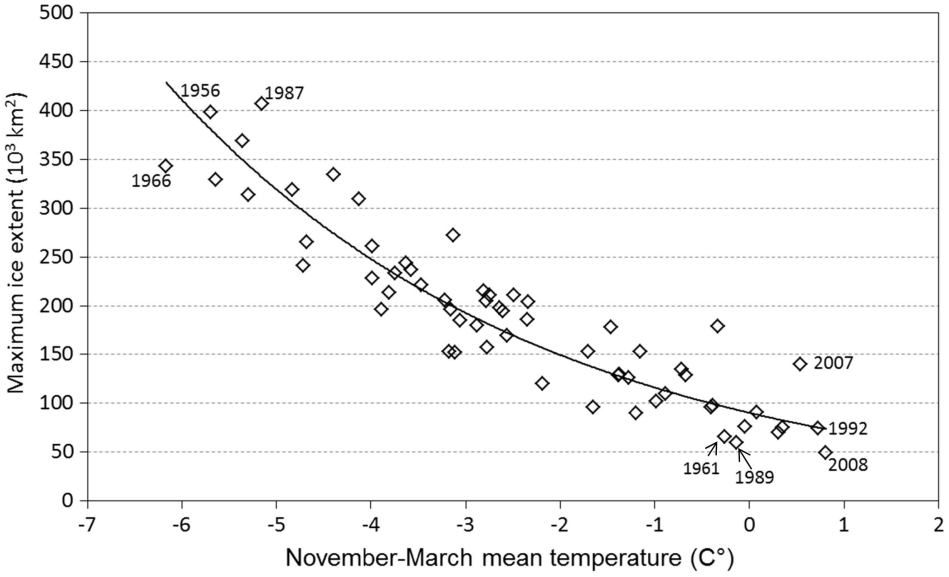

Fig. 4. The regression model for the ice extent. The model was fitted to the observed annual maximum ice extent and the November–March mean temperature at coastal grid points in 1952–2012. Some winters with a very high or low value of air temperature or ice extent are annotated. The date refers to the month of January in each winter.

where MIB is the annual maximum ice extent (km^2) and T is the November–March mean temperature (°C) averaged over the coastal grid points. Based on the data, the following values were derived for the coefficients: $A = (90.2 \pm 4.2) \times 10^3$ km^2 and $B = (0.253 \pm 0.015)$ $(°C)^{-1}$. The coefficient of determination of the model, R^2, is 82.8%. At $T = -3°C$, the error in MIB due to the standard errors of the coefficients A and B is about 10%, and from -1 to $+1°C$ about 5%.

The regression model [eq. (1)] was applied to project the probability distributions of MIB during the coming decades of this century. At first, a sample of size 50 was constructed to represent November–March temperatures T for each decade. This was produced by adding the GCM-based temperature increases ΔT for the decade in question to the observed values of T in the years 1961–2010 (a delta-change method). In order to reduce random effects, ΔT for each decade was calculated as a 30 yr mean, centred on that decade. For example, the mean temperature change for the period 2011–2040 represents the decade 2021–2030. Next, using these samples of T in eq. (1), we produced artificial frequency distributions of MIB for the seven future decades in the period 2021–2090. Finally, we determined three percentiles of the MIB distributions: the 5th (lower tail), 50th (median) and 95th (upper tail), the first and the third roughly corresponding to values that are fallen short of or exceeded, respectively, on average once in 20 yr. In 9 out of 10 yr, MIB can be expected to remain between the 5th and 95th percentiles.

The calculations were performed for each climate model listed in Table 1 and for both RCP scenarios. This enabled us to assess the uncertainty in MIB caused by the differences in the GHG scenarios and by the scatter of the temperature responses in the various GCMs. In order to obtain the best estimates for the long-term trends in the three percentiles of MIB, we also derived their 28-model averages. The model uncertainty assessment focused on the decade 2041–2050. This decade was selected for three reasons. First, it is sufficiently distant to exhibit a clear climate change signal compared to the noise due to internal climate variability. Second, it is sufficiently near not to be disturbed by a simplification made in our calculations, that is, the omission of potential changes in the inter-annual variability of winter temperatures. This omission mainly affects results at the end of the century, an issue to be discussed later. Third, an insight into the reliability of the sea ice projections for the first half of this century is of the highest relevance for many practical applications, such as designing fleets of icebreakers.

2.2.2. Sea ice thickness. The 30 yr mean of the annual maximum fast ice thickness was assessed using an analytical solution for the thermodynamic ice growth equation that is based on the sum of freezing degree-days (Stefan, 1890; Zubov, 1945; Leppäranta, 1993):

$$h = \sqrt{a^2 S + d^2} - d \tag{2}$$

where $a = 3$ cm$(°C \times d)^{-1/2}$, $d = 10$ cm and S is the annual cumulative sum (°C × d) of daily mean air temperatures

below 0°C (freezing degree-day sum). The approach, the so-called FDD model, is suitable for assessing ice thickness during the ice growth phase, up to an annual maximum value of h, but is no longer valid when the ice is melting (Stefan, 1890).

Our method of estimating the freezing degree-day sum S in eq. (2) was based on local monthly mean temperatures. We first multiplied the negative monthly mean temperatures in Celsius by the number of days in the month to get an approximation for the monthly freezing degree-day sums. The sum of the contributions of all months with a sub-zero mean temperature, that is, S in eq. (2), was then used to obtain the maximum ice thickness h.

For the baseline period 1971–2000, we used the observed monthly 30 yr mean temperatures to compute S and thereby h. The climatological monthly mean temperature for a future decade was obtained by adding the GCM-based 30 yr mean temperature response, centred on the target decade, to the observational baseline-period temperatures. The temperature projections were calculated separately for each individual GCM and, in addition, as 28-model means. Our results for the climatological maximum ice thickness h thereby represent responses to a range of individual temperature projections as well as to their average.

The FDD model [eq. (2)] does not take into account the snow layer lying on top of the ice cover. Ice thicknesses are thus systematically overestimated by up to 40 cm, and the value of h resulting from the model can be considered as the upper limit for ice growth in a typical winter (Leppäranta, 1993). The present approach is only valid for the coastal fast ice, since in the drift ice regions, sea ice thickness depends substantially on the dynamical processes like rafting and ridging (Vihma and Haapala, 2009). Furthermore, as the E-OBS gridded dataset does not cover air temperatures over sea areas, the ice thickness could only be assessed in coastal areas.

The 30 yr means of the observed maximum fast sea ice thickness at Kemi and Loviisa in 1971–2000 were 75 and 38 cm, respectively. The corresponding values of h based on eq. (2) are 98 and 66 cm, respectively, implying an overestimation of 24 cm (32%) for Kemi and 28 cm (74%) for Loviisa. The insulating effect of snow-on-ice, ignored here, is presumably the main reason for this overestimation. Additionally, the exact locations of the ice thickness observation sites may have changed in time during the 30 yr period, which may have influenced the quality of the observational time series. At Loviisa, the proximity of a nuclear power plant, with its condensation water having a warming effect, may also be seen in the ice thickness statistics.

3. Results

3.1. Annual maximum ice extent

We first focus on the ensemble-mean changes in the distribution of the annual maximum ice extent. Three percentiles (95th, 50th and 5th) were derived from the artificial 50 yr samples that were produced for each decade of the period 2021–2090. The 95th percentile, representing winters with an uncommonly wide ice cover, is projected to diminish faster than the median or the 5th percentile (Fig. 5). The linear trends under the RCP4.5 scenario for the three quantities are $-12\,700$ km^2/10 yr, -6400 km^2/10 yr and -2900 km^2/10 yr, respectively. The decline is faster under the RCP8.5 than the RCP4.5 scenario, in accordance with the more ample warming in the former scenario. The corresponding linear trends in the percentiles for RCP8.5 are $-21\,600$ km^2/10 yr, $-10\,900$ km^2/10 yr and -5000 km^2/10 yr, respectively. If the RCP8.5 scenario is realised, average ice winters, according to the current standards, would be very exceptional from the 2060s onward, but under the RCP4.5 scenario the 95th percentile of MIB falls to that category even in the 2080s. Under both scenarios, the probability of unprecedentedly mild ice winters will increase during the study period. In the RCP8.5 scenario, even the median MIB would belong in that category from the 2080s onward.

We next address the uncertainty caused by different temperature responses in the various GCMs, first discussing the inter-model scatter of the medians of MIB. The median values decreased in time in all model projections, faster so in the RCP8.5 scenario than in RCP4.5. For RCP8.5, the inter-model range of median MIB became smaller during the study period, with the standard deviation of the medians decreasing from 19 000 km^2 in the 2020s to 14 000 km^2 in the 2080s. The standard deviation under RCP4.5 was larger than under the RCP8.5 scenario, ranging over the whole period between 19 000 and 22 000 km^2 without any clear temporal trend. The smaller scatter among the model projections in the RCP8.5 than in the RCP4.5 scenario is, however, less evident when the normalised standard deviations (or coefficients of variance) of the medians are considered.

The multimodel means and the inter-model scatter for all three percentiles of MIB are exemplified for 2041–2050 in Fig. 6. The mean median value for the RCP4.5 scenario is about 93×10^3 km^2 and for RCP8.5 about 80×10^3 km^2 (see also Fig. 5). For the RCP8.5 scenario, there is a strong consensus among the model projections that the median MIB falls into the class of mild ice winters. For RCP4.5, most of the models likewise agree with that. The scatter is wider for the 95th percentile, representing winters with a more widespread ice cover. For most of the model

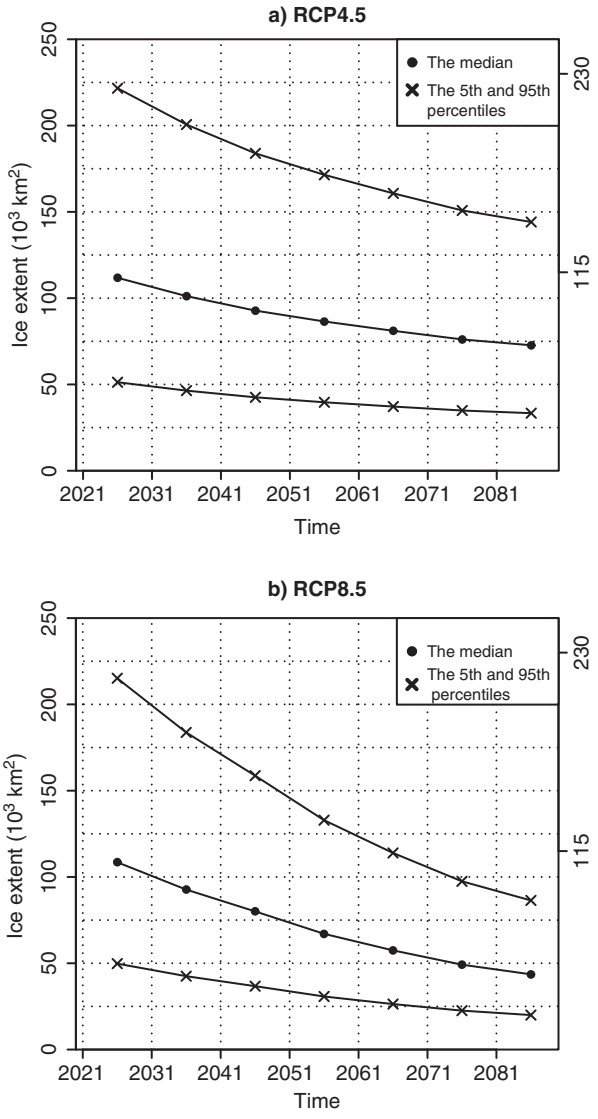

Fig. 5. Temporal evolution of the annual maximum ice extent during the course of this century. The estimates are given separately for the median values, representing a typical winter (line with dots), and for the 5th and 95th percentiles, corresponding to scant and widespread ice cover (lines with crosses). All the results are ensemble means of sea ice projections, derived from temperature responses of 28 individual CMIP5 models (Table 1). The vertical axis on the right shows the upper class limits for mild and average ice winters, according to current standards. The limit for unprecedentedly mild winters is 49×10^3 km^2. (a) The RCP4.5 scenario, (b) the RCP8.5 scenario.

projections, this high percentile belongs to the class of average ice winters. However, according to the model ensemble, there is a small probability for the upper tail of the MIB distribution to be classified as a severe ice winter in RCP4.5, or as a mild ice winter in RCP8.5. The scatter is smallest around the 5th percentile, representing the lower tail

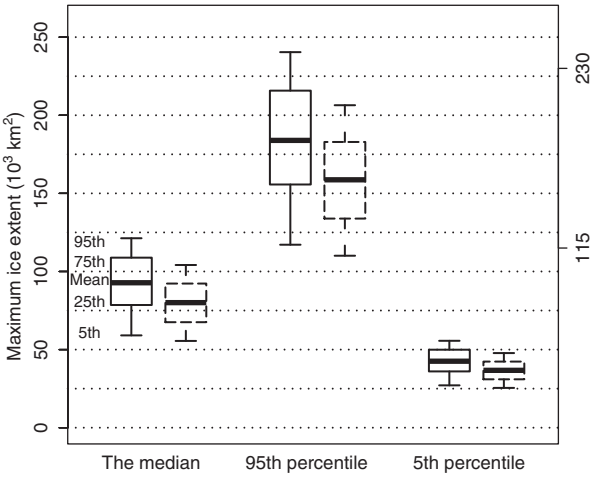

Fig. 6. Inter-model scatter and inter-annual variability of the annual maximum ice extent in 2041–2050. The median and the 5th and 95th percentiles (the horizontal axis) demonstrate inter-annual variability and the box-and-whiskers plots illustrate inter-model scatter. Within each box, the thick solid line refers to the 28-model mean ice extent, also shown in Fig. 5. The box depicts the upper and lower quartiles of the sea ice projections, whiskers the 5th and 95th quantiles. The boxes drawn with solid lines show the RCP4.5 scenario and those with dashed lines RCP8.5. The vertical axis on the right shows the upper class limits for mild and average ice winters. The limit for unprecedentedly mild winters is 49×10^3 km^2.

of the MIB distribution. All the models are strongly unanimous in the 5th percentile belonging to the class of mild or even unprecedentedly mild ice winters. Inferring from the observations performed thus far, in the mild winters of the 2040s, ice only occurs in the Bay of Bothnia and perhaps in the eastern Gulf of Finland.

Finally, we consider MIB in 2041–2050 separately for each ensemble member (Fig. 7). In that decade under the RCP4.5 scenario, the model with the weakest warming (Table 1) and thereby the largest mean MIB is CESM1-BGC; this model produces the widest range between the 5th and 95th percentiles (Fig. 7a). The model projecting the strongest warming (Table 1), CMCC-CMS, is that also producing the smallest mean MIB and the narrowest range. In RCP8.5 (Fig. 7b), the corresponding extreme models are CCSM4 (the largest MIB) and CMCC-CM (the smallest MIB). Under the RCP4.5 scenario, the mean MIBs derived from the temperature responses of seven models (25% out of the total number) can be classified as average, the rest of the model-based estimates belonging to the class of mild ice winters. The 95th percentiles of four models can be classified as severe, and the 5th percentiles of 21 models as unprecedentedly mild. Under the RCP8.5 scenario, the mean values of all models fall into the class of mild (but not unprecedentedly mild) ice winters, and none of the 95th percentiles exceeds the class limit of a severe ice winter.

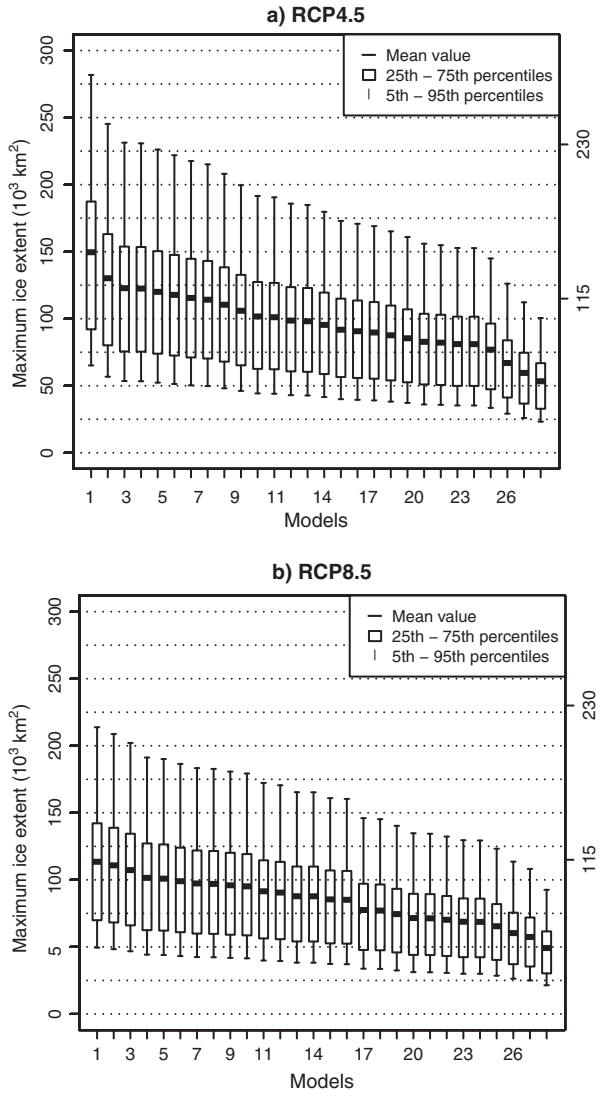

Fig. 7. The annual maximum ice extent (MIB) in 2041–2050 according to each individual GCM. The numbers on the horizontal axis show the GCMs in ascending order of the projected November–March mean temperature response (for identifying the models, see Table 1). The short black line inside a box denotes the mean value of the distribution, the boxes the 25th and 75th percentiles and the whiskers the 5th and 95th percentiles of inter-annual variability for each model. The vertical axis on the right shows the upper class limits for mild and average ice winters. (a) RCP4.5, (b) RCP8.5.

3.2. Ice thickness

The mean annual maximum fast ice thickness for the whole study area was examined as a response to the 28-model mean temperature projection in two future decades, 2041–2050 and 2081–2090. In addition, the results based on the individual model projections were calculated for the whole study period at three locations: Kemi, representing the coast of the Bay of Bothnia; Loviisa, representing the eastern Gulf of Finland; and Vilsandi (58.38°N, 21.82°E), representing the Baltic Sea Proper (for the locations, see Fig. 8a).

When applied to the observed temperatures of the baseline period 1971–2000, the FDD model [eq. (2)] implied that most of the coastal areas become ice-covered in a typical contemporary winter (Fig. 8a). The resulting mean maximum ice thickness varies substantially, being locally more than 90 cm in the Bay of Bothnia and only 0–10 cm in the south-western parts of the Baltic Sea.

The mean maximum ice thickness is projected to decrease in coming decades (Fig. 8b–8e). Based on the 28-model mean temperature projections, for the northern coast of the Bay of Bothnia in 2041–2050, the ice thickness is about 60–80 cm under the RCP4.5 scenario (Fig. 8b) and about 50–70 cm under RCP8.5 (Fig. 8c). The differences between the scenarios increase by the end of the study period. In 2081–2090 under RCP4.5, the ice thickness in the Bay of Bothnia may locally still exceed 60 cm, whereas elsewhere in the Gulf of Bothnia and in the Gulf of Finland it is 10–40 cm (Fig. 8d). According to the RCP8.5 scenario, most of the Baltic Sea is projected to be ice-free in 2081–2090 (Fig. 8e). In the northernmost Bay of Bothnia, however, h is then mainly 20–40 cm. This indicates that even if the high-emission RCP8.5 is realised, in a typical winter the Baltic Sea is unlikely to become totally ice-free during this century.

The linear trends in h, derived from the 28-model mean temperature projection under the RCP4.5 scenario, were −3.4 cm/10 yr, −3.3 cm/10 yr and −1.0 cm/10 yr for Kemi, Loviisa and Vilsandi, respectively (Fig. 9a). The inter-model standard deviation in the projected ice thickness in 2021–2030 was 6 cm at all three sites. At Kemi and Loviisa, the deviation increased to 15 cm and 11 cm, respectively, by the end of the study period. The southernmost location of the three, Vilsandi, already remains ice-free in the first decade, 2021–2030, according to six of the 28 models. In the last decade 2081–2090, the temperature projections of only five models allow the formation of ice there. In contrast to Kemi and Loviisa, the standard deviation at Visandi decreased towards the end of the period, being only 2 cm in 2081–2090.

The thinning of the ice is faster in the RCP8.5 scenario (Fig. 9b) than in RCP4.5. The linear trends of the ice thickness for Kemi, Loviisa and Vilsandi are now −7.6 cm/10 yr, −7.0 cm/10 yr and −0.8 cm/10 yr, respectively. The zero-values at Vilsandi in the last three decades made the trend notably weaker there than at Kemi or Loviisa. At Kemi, the inter-model standard deviation of the mean maximum ice thickness increased from 7 to 19 cm during the study period. At Kemi, two of the 28 modelled temperature projections produced no ice for a typical winter in

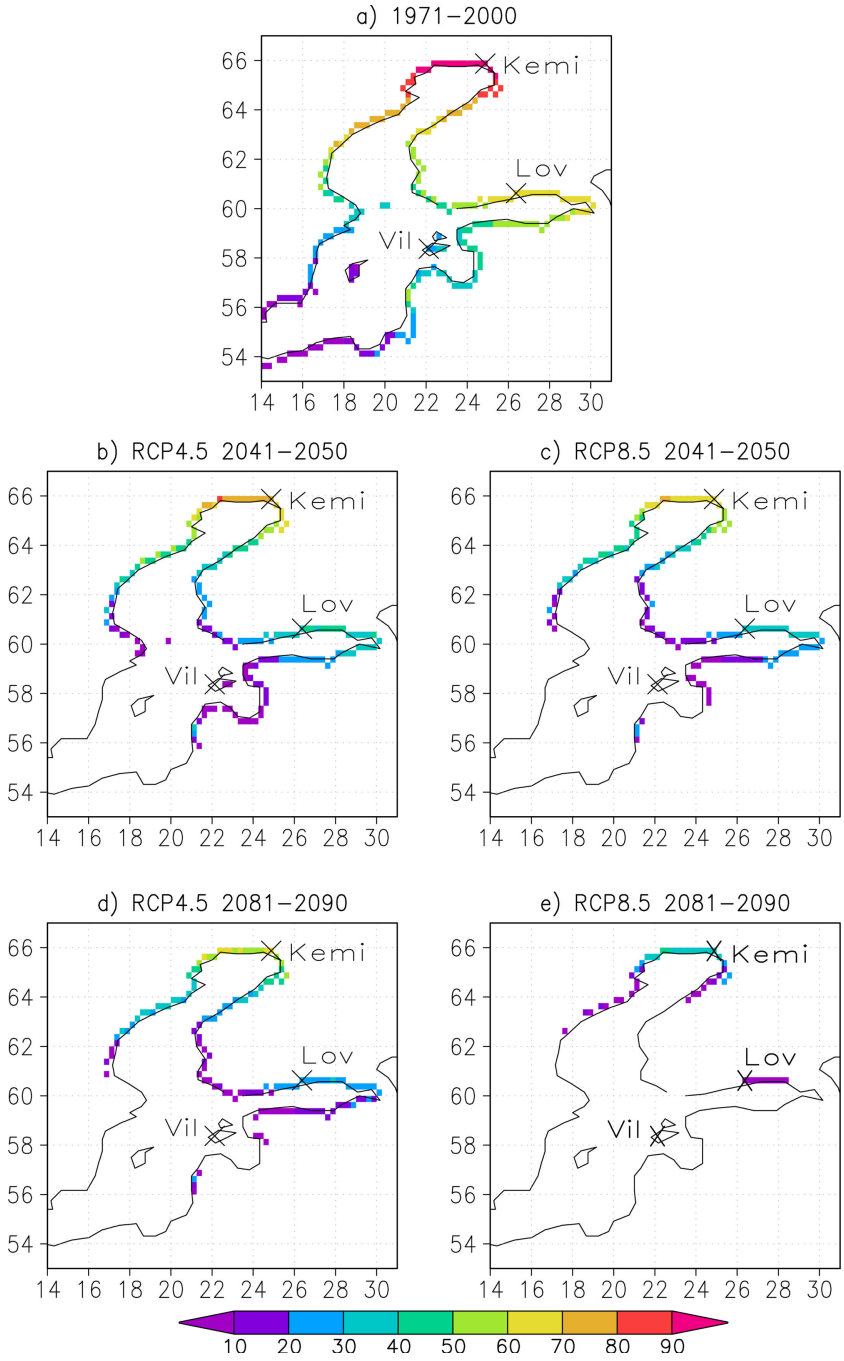

Fig. 8. The annual maximum coastal sea ice thickness (cm) in typical past and future winters. The calculations with the FDD method are based on (a) observed temperatures in 1971–2000 and (b–e) the 28-model mean temperature projections under the two RCP scenarios for two future decades. The crosses denote the locations of Kemi, Loviisa (Lov) and Vilsandi (Vil).

2081–2090. At Loviisa, the corresponding number was 15 of the 28 models. The ice cover for an average winter disappears at Vilsandi in 2061–2070, as it stays ice-free according to the temperature projections of all the models in the last three decades. This does not, however, mean that sea ice cannot occur at Vilsandi at all in the late 21st century. Our results for the ice thickness portray climatological means, but do not provide inter-annual variations.

As mentioned earlier, due to the calculation method these results should be considered as an upper limit for the ice growth in a typical winter (Leppäranta, 1993). Because of this tendency towards an overestimation in the absolute

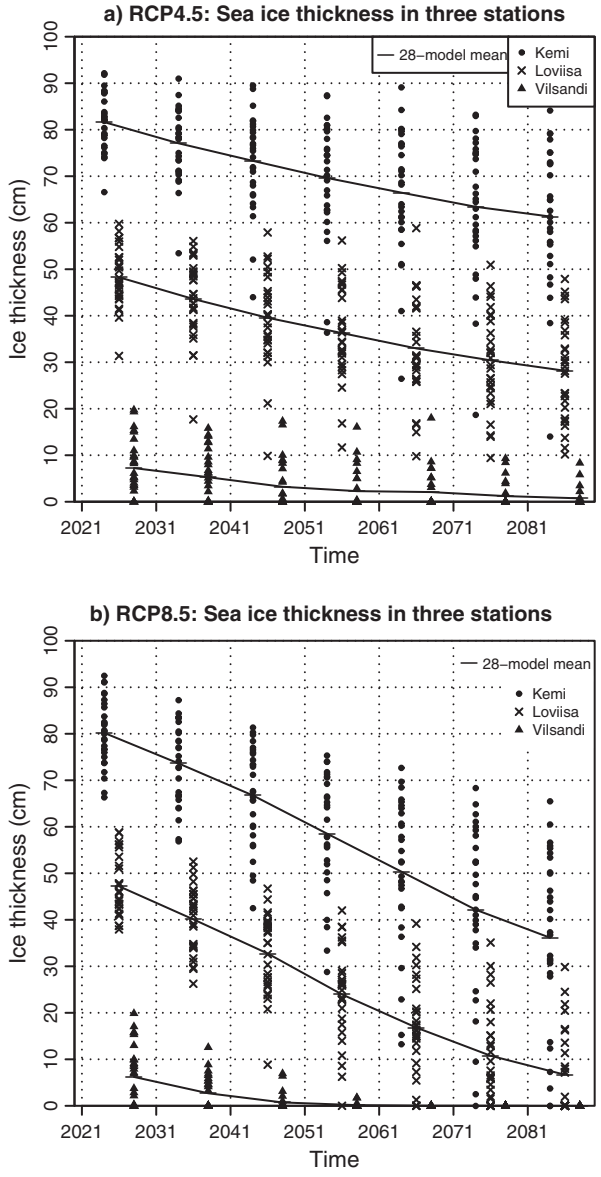

Fig. 9. Temporal evolution of the mean maximum ice thickness at three locations during the course of this century. The ice projections for Kemi (dots), Loviisa (crosses) and Vilsandi (triangles) are based on the temperature responses of the individual GCMs. The short horizontal lines show the mean values of all the model-based projections for each decade. Note that the position of the symbols within each decade is slightly shifted to make the figure more readable. (a) RCP4.5, (b) RCP8.5.

values of h, we also considered the percentage changes relative to the period 1971–2000. When derived from the 28-model mean temperature projections, the decline in 2041–2050 would be about 25–30% at Kemi and 40–50% at Loviisa, only weakly depending on the RCP scenario (Table 3). In 2081–2090, the ensemble-mean change at Kemi is about 40% under RCP4.5 and about 60% under RCP8.5. Further southwards, the projected percentage changes are stronger, that is, 60–90% at Loviisa and up to 100% at Visandi. Apart from Visandi under RCP8.5, however, the ranges of the responses derived from the individual GCMs are considerable. In the 2040s at Loviisa, for example, the uncertainty range is 20–67% when both RCP scenarios are taken into account (Table 3).

4. Discussion

4.1. Causes of uncertainties

The wide uncertainty ranges in our results are caused by differences in the climate models employed to produce the temperature projections, by the two different RCP scenarios and by internal climate variability. Owing to the large number of climate models used, the uncertainty related to model formulation could be estimated rather reliably. It appeared that the inter-model spread of temperature responses would be reduced appreciably if six out of 28 models, that is, those showing the lowest performance in simulating the observed climate, were omitted (Section 2.1.3). However, Huybers (2010) argued that GCMs in general rather underthan over-estimate the uncertainty of climate sensitivity. As previously mentioned, we therefore decided to retain all of the 28 models in order to avoid the risk of estimating too small error bars for the Baltic Sea ice projections.

Besides the issues mentioned above, some additional uncertainties arise from the calculation methods used in this work. For the estimates of the future ice extent, the exponential regression model [eq. (1)] had to be extrapolated outside the temperature range that was used to establish it. The model uses the average November–March temperature over the whole coastal Baltic Sea. Since it is possible to have freezing temperatures and sea ice in some parts of the study area (particularly in the north) and, at the same time, a considerably warmer winter elsewhere, the model produces non-zero ice extent even for spatially averaged temperatures above 0°C, in accordance with the observations (Fig. 4). But, because of its exponential form, the model actually never gives a zero MIB. Even with unrealistically high temperatures, it still would produce a small area of ice. On the other hand, the uncertainty related to the regression equation is relatively small compared to the inter-GCM scatter. For the 2080s, the error in MIB due to the standard errors of the regression coefficients is about 5000 km^2, whereas the inter-model standard deviation of the medians of MIB is 14 000 km^2 for RCP8.5 and even larger for RCP4.5. Even so, with the climate change continuing, higher temperatures will evidently occur, and the regression equation should be revised accordingly.

The delta-change method that we have used in constructing the probability distributions of the average coastal

Table 3. The projected percentage reductions in the mean maximum ice thickness (h)

	Observation	RCP4.5		RCP8.5	
	1971–2000 (cm)	2041–2050 (%)	2081–2090 (%)	2041–2050 (%)	2081–2090 (%)
Kemi	75	25 (16–44)	37 (19–59)	32 (18–50)	63 (40–99)
Loviisa	38	40 (20–63)	57 (32–81)	50 (34–67)	89 (64–100)
Vilsandi		88 (46–100)	97 (81–100)	97 (80–100)	100

The best estimates for the declines from the period 1971–2000 to the decades 2041–2050 and 2081–2090 are based on the 28-model mean temperature projections under the RCP4.5 and RCP8.5 scenarios. The 90% confidence intervals, derived from the inter-model differences in the temperature responses, are given in parentheses. The 30 yr mean values of the observed annual maximum ice thickness in 1971–2000 at Kemi and Loviisa are shown in Column 2.

November–March temperatures for future decades assumes that the shape and width of the distribution remain unchanged. In particular, any possible changes in the inter-annual temperature variability are not taken into account. In near-term temperature projections, this simple constant delta-change method is found to be a reasonable approach (Räisänen and Räty, 2013; Kämäräinen, 2013). However, for projections targeted to the end of the century it would probably be beneficial if a method that includes changes in both the average values and the inter-annual variability were employed.

As mentioned earlier, the FDD model [eq. (2)] does not take into account the snow cover on the top of the ice. This causes an overestimation of up to 40 cm in the ice thickness estimates (Leppäranta, 1993). Despite a general decreasing trend in snow (Räisänen and Eklund, 2012), a similar bias exists to some degree in estimates of h both in the current and the future climate. We can therefore assume that the magnitude of the change is a fair estimate, perhaps more so in percentage terms (Table 3). Another feature related to eq. (2) is that our method of estimating the freezing degree-day sum S on the basis of monthly mean temperatures is somewhat inaccurate. Only months with a negative mean temperature were taken into account. For example, at the beginning of March, the month typically having the thickest ice cover in the Gulf of Finland (SMHI and FIMR, 1982), there may be sub-zero temperatures that still favour ice growth. This increase in the ice thickness is ignored in calculations of h, if a warm period later on during the month causes the monthly mean temperature to rise above zero. The impact of this error source is, however, reduced by the fact that the annual maximum ice thicknesses were examined as 30 yr mean values.

Important factors that could not be taken into account in this study are possible changes in precipitation, wind and ocean salinity. Based on the GCMs in Table 1, we assessed that in our study area the winter mean precipitation would increase by 20–31% under RCP8.5 by the 2080s. Both directly and through river runoff, this may affect salinity, and thereby the growth of ice. Because wind conditions control ice dynamics, potential changes in windiness are also of relevance. Wind speeds, especially in storms, have a large impact on the sea ice thickness distribution in drift ice regions, where ridging and new ice production in the leads may double the mass of thermodynamically produced ice (Vihma and Haapala, 2009). Besides wind speed, wind direction should also be considered. The prevailing wind direction determines in which coastal regions of the Baltic Sea ice ridging and compression predominantly occur. South-westerly to north-westerly winds increase the need for ice-breaking near the harbours of Finland and Russia, whereas easterly to northerly winds are likewise influential in Sweden and Estonia. However, the differences in responses between the current and the previous generation of GCMs make the projections for wind in the Baltic Sea area far more uncertain than those for temperature and precipitation. According to previous estimates for the winter season (November–March), both mean and extreme wind speeds would increase by approximately 2–5% by the end of this century (Gregow et al., 2012). On the other hand, our preliminary CMIP5-based calculations for monthly mean wind speeds, without investigations into extremes, only suggest a large inter-model scatter but no significant multimodel mean response.

4.2. *Comparison to previous studies*

The annual maximum Baltic Sea ice extent and thickness in the future have been a subject of several earlier studies. However, the surveys are not completely comparable, as they were based on different generations of climate models and GHG scenarios, analysed different time ranges or reported diverse aspects of the results. In the following, we compare our findings for the late century to the outcomes of the studies by Haapala et al. (2001), Meier et al. (2004) and Meier (2006); they used numerical sea ice models to estimate future changes in the Baltic Sea. Comparisons for the middle of the century are made between the present work and Luomaranta et al. (2010).

In the study by Haapala et al. (2001), two coupled ice-ocean models were applied to simulate ice conditions during two 10 yr periods, one representing pre-industrial atmospheric conditions and the other a climate generated by a 150% increase in the CO_2 concentration. Meier et al. (2004) employed a regional atmosphere–ocean climate model driven by two GCMs, both forced by the SRES A2 and B2 scenarios. Two 30 yr time slices were considered: 1961–1990 and 2071–2100. Meier (2006) widened the investigation by including four additional experiments that were conducted with a regional ocean climate model. The simulated mean MIB during the late 21st century varied between $(117–190) \times 10^3$ km^2 in Haapala et al. (2001) and between $(48–113) \times 10^3$ km^2 in Meier et al. (2004) and Meier (2006), depending on the modelling system and the GHG scenario. In the present work, for comparison, the multimodel average for the median MIB in the 2080s under the RCP4.5 and RCP8.5 scenarios was 73×10^3 km^2 and 44×10^3 km^2, respectively (Fig. 5).

In order to cursorily view to what degree the deviations in the results for MIB may be explained by divergent GHG scenarios, we now focus on multimodel mean percentage changes (Table 4). By examining percentage changes, the influence of model biases both in numerical and statistical studies can be alleviated. The scenarios were ordered based on the corresponding multimodel mean global temperature changes. For the 2040s, the responses to the RCP4.5 forcing scenario, derived in the current work, were very close to those presented by Luomaranta et al. (2010). For the 2080s, it appeared that the decrease in MIB was clearly weakest in the work by Haapala et al. (2001). Based on the remaining studies, the percentage declines in typical and high values of MIB tended to strengthen with increasing degree of global warming. For low values of MIB, representing winters with only a minor ice cover, the differences across the GHG scenarios were less evident (Table 4). Note, however, that the ensemble sizes diverged a lot between the studies, which hinders us from making robust inferences. Besides, the definitions of the low and high values of MIB given in the studies were not exactly equivalent.

Sensitivity studies performed by Meier et al. (2004) and Meier (2006) showed that severe ice winters are more responsive to the warming climate than are mild ones. This is also seen in our results shown in Fig. 5, where the rate of decrease of the 95th percentile is, in absolute terms, faster than that for the median or, especially, for the 5th percentile. In percentage terms, however, the changes for winters with scant ice cover are comparable (our study) or even larger than for winters with a more widespread ice cover (Table 4).

In the present paper, the mean annual maximum ice thickness (h) was only estimated in the coastal areas of the Baltic Sea. In the work by Meier et al. (2004), an assessment was made of h in the centre of the Bay of Bothnia (65°N 27′, 23°E 33′) for 2071–2100. The mean ice thickness there decreased from 58 cm to 23–39 cm, that is, 50–60%, depending on the scenario (Table 4). According to Haapala et al. (2001), the mean annual maximum ice thickness at the same location at the end of the century would be 27–43 cm, depending on the modelling system used. The two-model mean corresponded to a relatively modest percentage reduction of 42%, consistent with the moderate decline in MIB (Table 4). In our work, the RCP4.5 scenario produced a 28-model mean thickness of 61 cm for Kemi in 2081–2090. According to the RCP8.5 scenario, the corresponding thickness was 36 cm. The percentage declines were 37 and 63%, respectively (Table 4). Despite the differences in the study locations, the coastal area on the one hand, and the

Table 4. The projected percentage changes in the annual maximum ice extent (MIB) and the mean maximum ice thickness (h)

Scenario	Global ΔT (°C)	Ensemble size	Low	MIB (%) typical	High	h (%) Mean	Reference
Mid-century (2040s)							
RCP4.5	1.4	28	−47	−46	−47	−25	This study
SRES A1B	1.4	19	−49	−44	−47		Luomaranta et al., 2010
RCP8.5	1.8	28	−55	−53	−54	−32	This study
Late century (2080s)							
RCP4.5	2.1	28	−58	−58	−59	−37	This study
SRES B2	2.5	4	−81	−58	−51	−50	Meier et al., 2004; Meier, 2006
150%[a]	2.6[b]	2	−74	−44	−42	−42	Haapala et al., 2001
SRES A2	3.3	4	−88	−70	−65	−60	Meier et al., 2004; Meier, 2006
RCP8.5	3.7	28	−76	−74	−75	−63	This study

The multimodel mean responses by the 2040s and 2080s under various GHG scenarios are based on previous studies and the current work. The multimodel global mean temperature change (ΔT) is derived directly from the GCMs used (this work and Luomaranta et al. (2010)) or, for the dynamical downscaling experiments, is obtained from the references for the driving GCMs (the other studies). Low, typical and high MIB refer to the 5th, 50th and 95th percentiles of inter-annual variability, respectively (this work), or to the minimum, mean and maximum values during the simulation period. The results for h refer to Kemi (this work) or the centre of the Bay of Bothnia.
[a]150% increase in the atmospheric CO_2 concentration, compared to pre-industrial conditions. [b]Räisänen et al. (2001).

open sea, considered by Meier et al. (2004), on the other, the results are in good agreement. The differences among the GHG scenarios are clear. It can be inferred from Table 4 that, owing to two very divergent GHG scenarios and a multitude of alternative GCM-based temperature projections for both scenarios, the uncertainty in future ice thickness could be estimated more comprehensively in the current work than in the previous studies.

4.3. *Consequences of a mainly ice-free Baltic Sea*

According to our results for the RCP8.5 scenario, most of the Baltic Sea would be ice-free in the typical winters of the 2080s (Fig. 8e), the ensemble-mean estimate for the annual maximum ice extent ranging between about 20 and 85×10^3 km^2 (or 5–20% of the total sea area) on an average in nine out of 10 yr (Fig. 5b). The decreases in ice cover will affect the ecosystems in the Baltic Sea. For example, the Baltic ringed seal, breeding on the ice, will probably lose many of its southern breeding habitats. In 2071–2100, the breeding of the Baltic ringed seal will be most likely to succeed in the Bay of Bothnia only (Meier et al., 2004). If the Baltic Sea, excluding the Bay of Bothnia, becomes ice-free during early spring by the end of the century the spring bloom of phytoplankton will start and end notably earlier (Eilola et al., 2013). Another consequence of the early ice break-up is that the mean significant wave height in spring will increase by 30 to 50 cm in many areas of the Gulf of Finland and the Gulf of Bothnia (Eilola et al., 2013).

Some consequences of the future loss of ice for the human activities are positive. The shipping in the area will benefit from the longer ice-free period, and the ice-breaking assistance will probably only be needed in the northern and the most eastern parts of the Baltic Sea (Haapala et al., 2001). However, when the sea remains ice-free, wave damage on the coastline may become more severe during winter storms. Wintertime cold outbreaks over an ice-free gulf with warm surface water (for example the Gulf of Finland) may cause intense snow showers in coastal areas (Savijärvi, 2012) presenting challenges to the maintenance of road networks and towns.

5. Conclusions

In this work, we have estimated future changes in the annual maximum sea ice extent and the mean maximum coastal sea ice thickness in the Baltic Sea under the RCP4.5 and RCP8.5 scenarios. The ice cover projections were based on temperature responses produced by 28 CMIP5 GCMs that showed reasonable performance in simulating the recent past climate in the Baltic Sea area. The sea ice projections were examined both as an ensemble-mean and separately for individual GCM-based temperature projections.

The annual maximum ice extent was estimated by a non-linear regression model, which was fitted to the observed values of wintertime temperature and annual maximum ice extent in the years 1952–2012. Applying this regression model to the GCM-based temperature projections, we derived frequency distributions for annual maximum ice extent for seven future decades within the period 2021–2090. According to both RCP scenarios studied, the annual maximum ice extent was found to decrease markedly. According to the RCP8.5 scenario, virtually only mild ice winters (ice extent $< 115 \times 10^3$ km^2) occur from the 2060s onwards. Under RCP4.5, the decline of the ice extent is slower: average ice winters (ice extent between 115×10^3 km^2 and 230×10^3 km^2) may still occur even in the 2080s.

The mean maximum sea ice thickness in coastal areas was assessed based on the sum of freezing degree-days. As expected, the decrease in ice thickness is faster in the RCP8.5 than in the RCP4.5 scenario. According to RCP8.5, in a conventional winter of the 2080s, sea ice would only occur in the Bay of Bothnia, with a maximum ice thickness of 30–40 cm, and in the north-eastern parts of the Gulf of Finland, with an ice thickness of 0–10 cm. According to RCP4.5, the coastal areas of the Gulf of Bothnia and the Gulf of Finland will still be ice-covered in the 2080s. Maximum ice thicknesses, locally exceeding 60 cm, would be found in the Bay of Bothnia.

Uncertainties in the results arise partially from the statistical calculation methods that we used in this work. On the other hand, since the statistical approaches required very little computing resources, we were able to incorporate a large number of different climate change scenarios. The spread among the changes derived from individual climate models appeared to be rather large. This suggests that when regional Baltic Sea circulation models are used to assess the impacts of climate change on ice cover, it would be necessary to employ the wide range of boundary conditions provided by a number of different climate models in order to adequately quantify the uncertainty in the estimates.

Despite the scatter in the rate of the projected changes, no uncertainty prevails about the direction of the long-term trend in sea ice. We conclude that sea ice will significantly decrease during this century. Although the Baltic Sea is unlikely to become totally ice-free in the typical winters of these coming decades, it is evident that the consequences of the ice reduction for ecosystems and communities will be notable.

6. Acknowledgements

This work was partially funded by the Academy of Finland through the ClimNext (no. 127239) and the MARISPLAN/FICCA (No. 140828) projects. Climate model data were downloaded from the Earth System Grid Federation data

archive (http://pcmdi9.llnl.gov). Climate modelling groups (models listed in Table 1 of this paper) are acknowledged for providing the model output, and the World Climate Research Programme's Working Group on Coupled Modelling for maintaining the archive.

References

BACC II Author Team. 2014. *Second BALTEX Assessment of Climate Change for the Baltic Sea Basin*. Series: Regional Climate Studies. Springer, Berlin. (in print).

Bracegirdle, T. J. and Stephenson, D. B. 2013. On the robustness of emergent constraints used in multimodel climate change projections of Arctic warming. *J. Clim.* **26**, 669–678.

Eilola, K., Mårtensson, S. and Meier, H. E. M. 2013. Modeling the impact of reduced sea ice cover in future climate on the Baltic Sea biogeochemistry. *Geophys. Res. Lett.* **40**, 149–154.

Gregow, H., Ruosteenoja, K., Pimenoff, N. and Jylhä, K. 2012. Changes in the mean and extreme geostrophic wind speeds in Northern Europe until 2100 based on nine global climate models. *Int. J. Climatol.* **32**, 1834–1846.

Haapala, J. and Leppäranta, M. 1997. The Baltic Sea ice season in changing climate. *Boreal Environ. Res.* **2**, 93–108.

Haapala, J., Meier, M. and Rinne, J. 2001. Numerical investigations of future ice conditions in the Baltic Sea. *Ambio*. **30**, 237–244.

Haylock, M. R., Hofstra, N., Klein Tank, A. M. G., Klok, E. J., Jones, P. D. and co-authors. 2008. A European daily high-resolution gridded dataset of surface temperature and precipitation. *J. Geophys. Res. Atmos.* **113**, D20119.

Huybers, P. 2010. Compensation between model feedbacks and curtailment of climate sensitivity. *J. Clim.* **23**, 3009–3018.

Jevrejeva, S., Drabkin, V. V., Kostjukov, J., Lebedev, A. A., Leppäranta, M. and co-authors. 2002. *Ice Time Series of the Baltic Sea*. Report series in geophysics, No 44. University of Helsinki, Helsinki.

Jevrejeva, S., Drabkin, V. V., Kostjukov, J., Lebedev, A. A., Leppäranta, M. and co-authors. 2004. Baltic Sea ice seasons in the twentieth century. *Clim. Res.* **25**, 217–227.

Jylhä, K., Fronzek, S., Tuomenvirta, H., Carter, T. R. and Ruosteenoja, K. 2008. Changes in frost, snow and Baltic Sea ice by the end of the twenty-first century based on climate model projections for Europe. *Clim. Change*. **86**, 441–462.

Kämäräinen, M. 2013. *Projections of Future Daily Temperatures in Finland*. Master's Thesis. University of Helsinki, 53 p.

Leppäranta, M. 1993. A review of analytical models of Sea-Ice growth. *Atmos. Ocean*. **31**, 123–138.

Luomaranta, A., Haapala, J., Gregow, H., Ruosteenoja, K., Jylhä, K. and co-authors. 2010. Itämeren jääpeitteen muutokset vuoteen 2050 mennessä [*The Changes in the Baltic Sea Ice Cover by 2050*]. Reports 2010:4, Finnish Meteorological Institute, 23 p. [In Finnish with English abstract]. Online at: https://helda.helsinki.fi/handle/10138/24433.

Meier, H. E. M. 2006. Baltic Sea climate in the late twenty-first century: a dynamical downscaling approach using two global models and two emission scenarios. *Clim. Dyn.* **27**, 39–68.

Meier, H. E. M., Döscher, R. and Halkka, A. 2004. Simulated distributions of Baltic sea-ice in warming climate and consequences for the winter habitat of the Baltic ringed seal. *Ambio*. **33**, 249–256.

Moss, R. H., Edmonds, J. A., Hibbard, K. A., Manning, M. R., Rose, S. K. and co-authors. 2010. The next generation of scenarios for climate change research and assessment. *Nature*. **463**, 747–756.

Omstedt, A. and Chen, D. 2001. Influence of atmospheric circulation on the maximum ice extent in the Baltic Sea. *J. Geophys. Res.* **106**, 4493–4500.

Omstedt, A., Gustafsson, B., Rodhe, J. and Walin, G. 2000. Use of Baltic Sea modelling to investigate the water cycle and the heat balance in GCM and regional climate models. *Clim. Res.* **15**, 95–108.

Omstedt, A. and Nyberg, L. 1996. Response of Baltic sea ice to seasonal, interannual forcing and climate change. *Tellus A*. **48**, 644–662.

Räisänen, J. and Eklund, J. 2012. 21st Century changes in snow climate in Northern Europe: a high-resolution view from ENSEMBLES regional climate models. *Clim. Dyn.* **38**, 2575–2591.

Räisänen, J. and Räty, O. 2013. Projections of daily mean temperature variability in the future: cross-validation tests with ENSEMBLES regional climate simulations. *Clim. Dyn.* **41**, 1553–1568.

Räisänen, J., Rummukainen, M. and Ullerstig, A. 2001. Downscaling of greenhouse gas induced climate change in two GCMs with the Rossby Centre regional climate model for northern Europe. *Tellus A*. **53**, 168–191.

Savijärvi, H. I. 2012. Cold air outbreaks over high-latitude sea gulfs. *Tellus A*. **64**, 12244.

Schmeltzer, N., Seinä, A., Lundqvist, J. E. and Sztobryn, M. 2008. Ice. In: *State and Evolution of the Baltic Sea, 1952–2005* (eds. R. Feistel, G. Nausch, and N. Wasmund). Wiley and Sons, pp. 199–240. Online at: http://eu.wiley.com/WileyCDA/WileyTitle/productCd-0471979686.html.

Seinä, A. and Palosuo, E. 1996. The classification of the maximum annual extent of ice cover in the Baltic Sea 1720–1995. *Meri.* (Report Series of the Finnish Institute of Marine Research, Helsinki) **27**, 79–91.

SMHI and FIMR. 1982. *Climatological Ice Atlas for the Baltic Sea, Kattegat, Skagerrak and Lake Vänern (1963–1979)*. Swedish Meteorological and Hydrological Institute, Norrköping, 220 p.

Stefan, J. 1890. Über die Theorie der Eisbildung, insonderes über die Eisbildung im Polarmeere [On the theory of ice formation, in particular in polar seas]. *Ann. Phys. U. Chem. Neue Folge*. **42**, 269–286.

Taylor, K. E., Stouffer, R. J. and Meehl, G. A. 2012. An overview of CMIP5 and the experiment design. *Bull. Am. Meteorol. Soc.* **93**, 485–498.

Tinz, B. 1996. On the relation between annual maximum extent of ice cover in the Baltic Sea level pressure as well as air temperature field. *Geophysica*. **32**, 319–341.

Vainio, J. 2011. Jäätalvien ankaruuden uusi luokittelu. *Ilmastokatsaus* [Revised severity classification of the maximum annual extent of ice cover in the Baltic Sea] **2011**, 2. Finnish Meteorological Institute. ISSN: 1239-0291. [In Finnish only.]. Online at: http://ilmatieteenlaitos.fi/c/document_library/get_file?uuid=3475052f-c3c7-4016-9e68-a35a70563c05&groupId=30106.

van Vuuren, D. P., Edmonds, J. A., Kainuma, M., Riahi, K., Thomson, A. M. and co-authors. 2011. The representative concentration pathways: an overview. *Clim. Change*. **109**, 5–31.

Vihma, T. and Haapala, J. 2009. Geophysics of sea ice in the Baltic Sea—a review. *Prog. Oceanogr*. **80**, 129–148.

Zubov, N. N. 1945. *L′dy Arktiki [Arctic Ice]. Izdatel′stvo Glavsermorputi, Moscow*. [English translation 1963] US Naval Oceanographic Office and American Meteorological Society, San Diego.

IV

Geosci. Model Dev., 7, 3037–3057, 2014
www.geosci-model-dev.net/7/3037/2014/
doi:10.5194/gmd-7-3037-2014

Geoscientific Model Development
Open Access

Evaluation of North Eurasian snow-off dates in the ECHAM5.4 atmospheric general circulation model

P. Räisänen[1], A. Luomaranta[1], H. Järvinen[2], M. Takala[1], K. Jylhä[1], O. N. Bulygina[3], K. Luojus[1], A. Riihelä[1], A. Laaksonen[1,4], J. Koskinen[5], and J. Pulliainen[1]

[1]Finnish Meteorological Institute, Helsinki, Finland
[2]Department of Physics, University of Helsinki, Helsinki, Finland
[3]All-Russian Research Institute of Hydrometeorological Information, World Data Centre, Obninsk, Russian Federation (RIHMI-WDC), Russia
[4]Department of Physics, University of Eastern Finland, Kuopio, Finland
[5]Finnish Geodetic Institute, Masala, Finland

Correspondence to: P. Räisänen (petri.raisanen@fmi.fi)

Received: 19 March 2014 – Published in Geosci. Model Dev. Discuss.: 5 June 2014
Revised: 7 November 2014 – Accepted: 24 November 2014 – Published: 18 December 2014

Abstract. The timing of springtime end of snowmelt (snow-off date) in northern Eurasia in version 5.4 of the ECHAM5 atmospheric general circulation model (GCM) is evaluated through comparison with a snow-off date data set based on space-borne microwave radiometer measurements and with Russian snow course data. ECHAM5 reproduces well the observed gross geographical pattern of snow-off dates, with earliest snow-off (in March) in the Baltic region and latest snow-off (in June) in the Taymyr Peninsula and in north-eastern parts of the Russian Far East. The primary biases are (1) a delayed snow-off in southeastern Siberia (associated with too low springtime temperature and too high surface albedo, in part due to insufficient shielding by canopy); and (2) an early bias in the western and northern parts of northern Eurasia. Several sensitivity experiments were conducted, where biases in simulated atmospheric circulation were corrected through nudging and/or the treatment of surface albedo was modified. While this alleviated some of the model biases in snow-off dates, 2 m temperature and surface albedo, especially the early bias in snow-off in the western parts of northern Eurasia proved very robust and was actually larger in the nudged runs.

A key issue underlying the snow-off biases in ECHAM5 is that snowmelt occurs at too low temperatures. Very likely, this is related to the treatment of the surface energy budget. On one hand, the surface temperature T_s is not computed separately for the snow-covered and snow-free parts of the grid cells, which prevents T_s from rising above 0 °C before all snow has vanished. Consequently, too much of the surface net radiation is consumed in melting snow and too little in heating the air. On the other hand, ECHAM5 does not include a canopy layer. Thus, while the albedo reduction due to canopy is accounted for, the shielding of snow on ground by the overlying canopy is not considered, which leaves too much solar radiation available for melting snow.

1 Introduction

Snow cover is one of the most important elements in the climate and hydrology of the Northern Hemisphere. Large areas of the Eurasian and North American continents are covered by seasonal snow. The varying snow cover affects directly the surface energy balance by interfering with the energy storage, net radiation and fluxes of sensible and latent heat. A significant positive feedback mechanism of the snow, albedo and solar radiation amplifies the climatic effects related to the snow cover: decreasing snow cover reduces the surface albedo and increases the amount of absorbed solar radiation at the surface, leading to increased melting and further reduction in the snow cover. The snow–albedo feedback (SAF) is largest when changes in snow cover area are linked with substantial changes in regional albedo (Brown, 2000). This coincides with the maximum influence of snow cover

on surface net radiation in spring, typically in April and May, when strong solar radiation and snow cover co-exist (Groisman et al., 1994). Snow cover also serves as a fresh water reservoir, thus regulating run-off in winter and spring, and influencing soil moisture content. Typically, delayed snowmelt can increase spring and summer soil moisture content which can further contribute to cooler and wetter weather conditions even after the snowmelt (Cohen, 1994), and conversely for early snowmelt (Wetherald and Manabe, 1995; Rowell and Jones, 2006; Kendon et al., 2010).

The key climatic role of snow cover has prompted a wide range of observational and modelling studies on the topic. These include several intercomparisons of snow conditions simulated by atmospheric and fully coupled general circulation models (GCMs) with observational data (Foster et al., 1996; Frei and Robinson, 1998; Frei et al., 2003, 2005; Roesch, 2006; Derksen and Brown, 2012; Brutel-Vuilmet et al., 2013). Most recently, Brutel-Vuilmet et al. (2013) evaluated the snow cover simulated by models participating in Phase 5 of the Coupled Model Intercomparison Project (CMIP5). In terms of the multi-model average, the models reproduced the observed snow cover extent very well, with a slight tendency toward too late snowmelt in Eurasia and too early snowmelt in northern North America. However, there was still substantial inter-model dispersion around the multi-model average. Moreover, the results highlighted two issues already found in earlier intercomparison studies. First, the interannual variability in Northern Hemisphere snow cover extent was underestimated by almost all models, which was already noted by Frei and Robinson (1998) in an analysis of Atmospheric Model Intercomparison Project, phase 1 (AMIP1) models. Second, the models underestimated considerably the observed negative trend in snow cover in spring (for years 1979–2005), which is similar to the findings of Roesch (2006) for CMIP3 models. Derksen and Brown (2012) further demonstrated, for a subset of eight CMIP5 models, that the models failed to capture the rapid decline in Northern Hemisphere late spring (May–June) snow cover observed in 2008–2012.

Regarding the reasons for biases in modelled snow conditions, the intercomparison studies have, in general, not been very conclusive. Most attention has been paid to biases in simulated air temperature (Foster et al., 1996; Räisänen, 2008) and total precipitation or snowfall (Foster et al., 1996; Roesch, 2006; Brutel-Vuilmet et al., 2013). Frei et al. (2005) further suggested that the exclusion of subgrid-scale treatments for terrain and land cover contributed to overestimated ablation rate of snow in spring over North America in AMIP2 models.

Multi-model intercomparisons have also demonstrated that the strength of SAF varies substantially among both CMIP3 (Hall and Qu, 2006; Qu and Hall, 2007; Fletcher et al., 2012) and CMIP5 models (Qu and Hall, 2014). There is a strong correspondence between the SAF evaluated based on transient climate change experiments and based on the seasonal cycle. Model results for the seasonal SAF fall on both sides of the corresponding observational estimates (Hall and Qu, 2006; Fletcher et al., 2012; Qu and Hall, 2014). The simulated SAF is strongly influenced by the climatological surface albedo of snow-covered land, which shows a surprisingly large spread even among the CMIP5 models. Presumably, this is related to how vegetation masking of snow-covered land is treated (Qu and Hall, 2007, 2014).

The focus of the current work is narrower than in the multi-model intercomparisons discussed above, which, however, allows for more in-depth analysis. We look in detail at the performance of a single model, the ECHAM5 atmospheric GCM (Roeckner et al., 2003, 2006), in simulating the timing of snowmelt in spring in northern Eurasia, north of latitude 55° N. Specifically, we focus on the average timing of the end of the snowmelt season (i.e. the snow-off date; the day when all snow accumulated during the winter has vanished). Snow-off dates simulated by ECHAM5 are compared with snow-off dates derived from two observational data sets: first, a satellite data set based on data from passive multichannel microwave radiometers (Takala et al., 2009), and second, Russian in situ snow course measurements (Bulygina et al., 2011a). The geographical focus on northern Eurasia is motivated by the vast area of the continent, which makes Eurasian snow conditions important for understanding the planetary climate as a whole.

The performance of a slightly earlier version of ECHAM5 in simulating the Northern Hemisphere snow depth, snow-covered area and surface albedo was assessed by Roesch and Roeckner (2006). By using snow products based on visible and microwave remote-sensing data, they found that ECHAM5 reproduces the amplitude and phase of the annual snow depth cycle quite precisely – however, with a slight overestimation of the snow depth in late winter and spring over Eurasia. The present work builds on Roesch and Roeckner (2006) but goes deeper in analysing the regional details and causes underlying the biases in modelled snow-off dates. Thus, while it is shown that in ECHAM5 simulations, snow-off tends to occur too late in the eastern part of northern Eurasia (especially southeastern Siberia) and too early in the western and northern parts, the most fundamental issue is that snow-off occurs at lower-than-observed air temperatures. The likely main reason for this are simplifications inherent to the model's surface energy budget calculation in the presence of partial snow cover and in the treatment of forest canopy. This highlights the need to consider carefully the treatment of the surface energy budget in the models, in addition to the fidelity of simulated temperature and precipitation fields.

The rest of this paper is organized as follows. First, in Sect. 2 we introduce the ECHAM5 model and the experiments conducted. In Sect. 3, the observational data sets used in this work are described. Section 4 addresses the non-trivial issue of the definition of snow-off dates. Results are reported in Sect. 5, both for the default version of ECHAM5 and for

sensitivity experiments, in which biases in simulated atmospheric circulation were corrected through nudging and/or the treatment of surface albedo was modified. The reasons underlying the biases in modelled snow-off dates are further discussed in Sect. 6, followed by conclusions in Sect. 7.

2 Model and experiments

2.1 Model description

Version 5.4 of the ECHAM5 atmospheric general circulation model (Roeckner et al., 2003, 2006) was used. The dynamical part of ECHAM5 is formulated in spherical harmonics, while physical parameterizations are computed in grid point space. The simulations reported were conducted at horizontal resolution T63 (corresponding to a grid spacing of 1.875°) with 31 layers in the vertical and model top at 10 hPa. A semi-implicit time integration scheme is used for model dynamics with a time step of 12 min. Model physical parameterizations (Roeckner et al., 2003) are invoked at every time step, except for radiation, which is computed once in 2 hours.

The snow scheme in ECHAM5 is relatively simple: the snow water equivalent (SWE; $\mathrm{kg\,m^{-2}}$) is a prognostic quantity, but changes in snow density or grain size are not considered. In the presence of snow, the top of the snow layer is treated as the top of the soil model. For snow-free and snow-covered land alike, the surface temperature is determined through the surface energy balance, while the thermal diffusion equation is used to calculate the soil (or snow) temperature profile. Five layers within the topmost 10 m are considered, with thicknesses of 0.065, 0.254, 0.913, 2.902 and 5.700 m, respectively. For snow-free land, spatially varying volumetric heat capacity and thermal diffusivity are prescribed for five soil types according to the FAO soil map (Gildea and Moore, 1985; Henderson-Sellers et al., 1986). For snow-covered land the procedure is the same except that the thermal properties are modified. For example, if snow fills the top soil layer completely, and the second layer partially, the thermal properties of snow are used for the top layer while a mass-weighted mixture of soil and snow properties is used for the second layer. A constant snow density of $330\,\mathrm{kg\,m^{-3}}$ is assumed in this procedure.

The ECHAM5 snow scheme considers both SWE intercepted by the canopy (Roesch et al., 2001) and SWE on the ground (Roeckner et al., 2003). The budget equation for snow on the ground accounts for snowfall through the canopy, sublimation/deposition, melting, and unloading of snow from the canopy due to wind. The snowmelt rate M is computed from the surface energy budget equation:

$$C_{\mathrm{L}}\frac{\partial T_{\mathrm{s}}}{\partial t} = R_{\mathrm{net}} + H + \mathrm{LE} + G - M, \tag{1}$$

where C_{L} is the heat capacity of the surface layer, T_{s} the surface temperature, R_{net} the surface net radiation, H the sensible heat flux, LE the latent heat flux, and G the ground heat flux (all defined positive when the surface layer gains energy). A preliminary estimate for T_{s} at the next time step (T^*) is obtained by considering everything else but snowmelt ($M = 0$). If T^* exceeds the melting point ($T^* > T_0 = 0\,^{\circ}\mathrm{C}$), the snowmelt rate is inferred from the condition that the heat consumed in melting snow restores T_{s} to T_0:

$$M = \frac{C_{\mathrm{L}}}{L_{\mathrm{f}}}\left(\frac{T^* - T_0}{\Delta t}\right), \tag{2}$$

where L_{f} is the latent heat of fusion and Δt the model time step.

The snow cover fraction on the ground (SCF) is diagnosed following Roesch et al. (2001):

$$\mathrm{SCF} = 0.95\tanh(100h_{\mathrm{sn}})\sqrt{\frac{1000h_{\mathrm{sn}}}{1000h_{\mathrm{sn}} + 0.15\sigma_z + \epsilon}}, \tag{3}$$

where h_{sn} is SWE expressed in metres of liquid water, σ_z (m) is the subgrid-scale standard deviation of surface elevation and ϵ is a small number used to avoid division by zero for totally flat and snow-free grid cells.

The parameterized grid-mean surface albedo depends on the specified background albedo, the fractional forest area of the grid cell, the snow cover on the canopy, the snow cover on the ground, and a specified snow albedo. While a complete description of the parameterization can be found in Roeckner et al. (2003), two details are mentioned here to provide a background for the sensitivity tests in Sect. 2.2.3. First, the albedo of snow on land (α_{sn}) depends on the surface temperature T_{s} according to

$$\alpha_{\mathrm{sn}} = \alpha_{\mathrm{sn,\,min}} + \left(\alpha_{\mathrm{sn,\,max}} - \alpha_{\mathrm{sn,\,min}}\right) f(T_{\mathrm{s}}), \tag{4}$$

where

$$f(T_{\mathrm{s}}) = \min\left[\max\left(\frac{T_0 - T_{\mathrm{s}}}{T_0 - T_{\mathrm{d}}}, 0\right), 1\right] \tag{5}$$

and $\alpha_{\mathrm{sn,\,min}} = 0.3$, $\alpha_{\mathrm{sn,\,max}} = 0.8$, $T_0 = 0\,^{\circ}\mathrm{C}$ and $T_{\mathrm{d}} = -5\,^{\circ}\mathrm{C}$. Second, the albedo of snow-covered forests is parameterized according to

$$\alpha_{\mathrm{for}} = \mathrm{SVF}\alpha_{\mathrm{g}} + (1 - \mathrm{SVF})\alpha_{\mathrm{can}}, \tag{6}$$

where α_{g} is the ground albedo ($\alpha_{\mathrm{g}} = \alpha_{\mathrm{sn}}$ if the ground is completely snow covered), α_{can} is the albedo of the canopy (0.2 for completely snow-covered canopy) and the sky view factor (SVF) depends on the leaf-area index (LAI):

$$\mathrm{SVF} = e^{-\mathrm{LAI}}. \tag{7}$$

2.2 Experiments

A total of six ECHAM5 experiments were conducted. All experiments were run for years 1978–2006, and years 1979–2006 were used for analysis of the results. Note that the

years 2008–2012 during which a rapid reduction in Northern Hemisphere May–June snow cover has been observed (Derksen and Brown, 2012) fall outside this period. All simulations used observed sea surface temperatures (SSTs) and sea ice (AMIP Project Office, 1996), and some of them used nudging fields and/or observed albedo fields that likewise included "real" year-to-year variations (see below). The concentrations of well-mixed greenhouse gases were held constant following AMIP II guidelines (AMIP Project Office, 1996), at 348 ppmv for CO_2, 1650 ppbv for CH_4, 306 ppbv for N_2O, 280 pptv for CFC-11, and 484 pptv for CFC-12. For aerosols, a climatological distribution was assumed (Tanré et al., 1984). The distribution of ozone, vegetation area and LAI followed a prescribed climatological seasonal cycle.

Three of the experiments (REF, ALB1 and ALB2) were run in an ordinary climate simulation mode. In the remaining three experiments (REF_NDG, ALB1_NDG and ALB2_NDG), four model fields were nudged towards ERA-Interim reanalysis data (Dee et al., 2011): vorticity (relaxation timescale 6 h), divergence (48 h), atmospheric temperature (24 h) and logarithm of surface pressure (24 h). Nudging acts to minimize the errors in simulated atmospheric circulation, which is one of the possible causes for differences between simulated and observed snow-off dates.

2.2.1 REF and REF_NDG

The reference experiment (REF) and the corresponding nudged experiment (REF_NDG) used the default version of ECHAM5.4. To evaluate the impact of model internal variability on the results, three runs were conducted for the REF experiment. The runs were started from different initial dates (1, 2 and 3 January 1978, respectively), which is sufficient for ensuring that within a few weeks, the weather conditions in the three runs become essentially independent of each other. Where not otherwise stated, the mean value of these three runs is reported. REF_NDG, as well as ALB1, ALB1_NDG, ALB2 and ALB2_NDG consist of a single run for years 1978–2006.

2.2.2 ALB1 and ALB1_NDG

Surface albedo influences strongly the energy available for melting snow in spring. In an attempt to eliminate errors in surface albedo, in the experiments ALB1 and ALB1_NDG the model's albedo field over continents was replaced by prescribed surface albedos based on observations. Monthly mean albedos in the CLARA-SAL data set derived from AVHRR satellite data (Riihelä et al., 2013) were applied. Since this data set starts from year 1982, for years 1978–1981 the average annual cycle of CLARA-SAL albedo for years 1982–2006 was employed. While this approach is instructive for diagnostic purposes, it has the major weakness that the albedo is independent of simulated land-surface properties, including snow cover.

2.2.3 ALB2 and ALB2_NDG

In an attempt to reduce biases in ECHAM5's surface albedo field while keeping it interactive, experiments ALB2 and ALB2_NDG were conducted. Two modifications were implemented in ECHAM5's surface albedo parameterization. First, for snow-covered forests, the sky-view factor in Eq. (7) was replaced by

$$\mathrm{SVF} = e^{-(\mathrm{LAI}+\mathrm{SAI})}. \quad (8)$$

Here, the stem area index (SAI) assumes a constant value of 2 for all forest types, following the Biosphere–Atmosphere Transfer Scheme (Dickinson et al., 1993). This modification was motivated by Roesch and Roeckner (2006), who noted that ECHAM5 overestimates the total surface albedo in eastern Siberia in the dormancy season of deciduous needleleaf trees, and ascribed this problem to the fact that the shadowing of the ground below the canopy by stems and branches is neglected. Second, the value of $\alpha_{\mathrm{sn,\,min}}$ in Eq. (4) was increased from 0.3 to 0.6. This was motivated by the findings of Pedersen and Winther (2005) and Mölders et al. (2008), who note that for ECHAM5's snow albedo parameterization, and also for ECHAM4 for which $\alpha_{\mathrm{sn,\,min}} = 0.4$, snow albedo decreases too early and too fast during snowmelt.

3 Observational data

Seven observational data sets were used in the present work. First, a snow-off date data set based on remote sensing of snow with space-borne microwave radiometer measurements (Takala et al., 2009) was used for evaluating snow-off dates in the ECHAM5 simulations. The Eurasian region is well suited for remote sensing of snowmelt for two reasons. First, temperatures in much of the Eurasian region are very low in winter-time, which leads to the formation of a dry snow pack. Second, as tundra is the predominant surface type, the snow conditions are relatively homogeneous over extended areas in the absence of e.g. mountain regions with a complicated topography. These properties are profitable for microwave instruments that measure highly contrasting surface brightness temperatures for dry vs. melting snow related to the progression of spring.

The remote-sensing data set utilized measurements by the Scanning Multichannel Microwave Radiometer (SMMR; Knowles et al., 2002) onboard Nimbus 7 for years 1978–1987 and measurements by the Special Sensor Microwave/Imager (SSM/I) (Armstrong et al., 1994) onboard the Defence Meteorological Satellite Program (DMSP) satellites D-11 and D-13 for years 1988–2007. A time series thresholding algorithm based on the brightness temperature difference between vertically polarized radiances around 37 and 19 GHz was used to determine the snow-off date for each year (see Takala et al., 2009 for details). The snow-off dates

(given as day-of-year from 1 to 180) are provided at a nominal resolution of 25 km × 25 km.

The snow-off date estimates in the microwave data set were calibrated against the INTAS-SCCONE observations (Kitaev et al., 2002; Heino and Kitaev, 2003) of snow depth and snowmelt flag at Eurasian, mostly Russian, weather stations. Specifically, for the calibration data, the snow-off date was defined as the last event during spring when the station snow status flag changed from "snow depth is correct" to "temporary melting" or "continuous melting", both of which refer to a situation in which there is no snow left at the station. Thus, in principle, the microwave data set is targeted at presenting the final snow-off date at each station. This is discussed further in Sect. 4.

Second, snow course measurements made in Russia (or the former Soviet Union) were used for evaluating both the simulated snow-off dates and the seasonal cycle of SWE. These data were acquired from the Russian Hydrometeorological Centre; http://meteo.ru/english/climate/snow1.php (Bulygina et al., 2011a). The "routine snow surveys" data set contains data from 517 meteorological stations (288 within the region considered here), for which either open-terrain[1] or forest snow course measurements (or both) have been performed. These are a subset of the 958 stations considered in Bulygina et al. (2011b).

The SWE was measured at 100 m intervals along the forest snow courses, which had a total length of 1 km, and at 200 m intervals along the open-terrain snow courses with a total length of 2 km. Typically, measurements are provided at 10-day intervals in winter and 5-day intervals in spring (starting from March or April). The data availability varies, however, and not all stations provide data throughout the period 1979–2006 considered here. To compare with ECHAM5, the SWE values were regridded to the T63 grid, by averaging the SWE values over the stations if several stations existed in a grid cell. The procedure for estimating the snow-off date from the snow course data is described in the Appendix. We include in our analysis those grid cells for which the snow-off date could be determined for at least 5 years during 1979–2006.

Third, for surface albedo, we employ the monthly mean version of the CLARA-SAL data set (Riihelä et al., 2013), which is based on a homogenized AVHRR radiance time series. These data provide black-sky albedo values from January 1982 onwards. The data, originally given at a 0.25° × 0.25° resolution, were averaged to the T63 grid for comparison with modelled values, and for use as input for the ALB1 and ALB1_NDG experiments (Sect. 2.2.2).

Fourth, for snow cover fraction, we use version 2.0 of the snow extent (SE) data set created in the European Space Agency's (ESA) Data User Element project GlobSnow (Metsämäki et al., 2015). The GlobSnow SE is based on data acquired by the ERS-2/ATRS-2 and Envisat/AATSR satellite instruments, and is provided on a 0.01° × 0.01° grid. Here, monthly mean data averaged to the T63 grid are used. The years for which there is springtime snow cover data both for GlobSnow and the current ECHAM5 experiments are 1997–2006, but 2002 was discarded due to issues with data quantity and quality. While longer-term snow cover data sets exist (Zhao and Fernandes, 2009; Brown and Robinson, 2011), GlobSnow was selected for the present study because its retrieval algorithm was specifically designed to enable accurate snow mapping also in forests, which cover a large part of northern Eurasia.

Fifth, information on forest cover from the GlobCover 2009 data set (Bontemps et al., 2011; Arino et al., 2012) is used, along with the GlobSnow snow cover data, to aid the interpretation of the differences between modelled and observed albedo fields.

Sixth, for 2 m air temperature, Climate Research Unit (CRU) land surface air temperature data, version 3 (CRUTEM3; Brohan et al., 2006) is employed.

Seventh, daily measurements of snow depth and diurnal-mean temperature conducted at the Finnish Meteorological Institute Arctic Research Centre at Sodankylä (67.37° N, 26.63° E, 179 m a.s.l.) in January–June 1979–2006 are employed for a detailed comparison with ECHAM5 experiments in Sect. 6. The Sodankylä site belongs to the northern boreal forest zone with the snow type of taiga, which is typical of most of northern Eurasia.

4 Definition of snow-off date

Snow-off date is evaluated in ECHAM5 based on daily mean SWE values. There are several possible methods for defining the snow-off date, the most obvious ones being (1) the first snow-off date (i.e. the first day with zero SWE after a winter's SWE maximum) and (2) the final snow-off date (i.e. the day following the last day with SWE > 0 in spring). In some cases, the first and final snow-off dates differ substantially. As an example, Fig. 1 shows the time series of SWE for spring 1988 for a grid point in western Russia (60.6° N, 39.4° E) in one of the REF runs. The first snow-off date is day 99 (8 April), but three separate short periods with snow occur after it, the final snow-off date being day 129 (8 May).

In this paper, we use the first snow-off date for ECHAM5 because it is a more robust indicator of model behaviour than the final snow-off date. The first snow-off date represents an integral measure of how much snow accumulates during the winter and how fast it melts in the spring. In contrast, when the final snow-off date differs from the first snow-off date, it is, in essence, determined by the last occurrence of solid or mixed-phase precipitation in spring. This makes the final snow-off date much more sensitive to day-to-day weather patterns in spring than the first snow-off date.

[1] The term "open-terrain snow courses" is used here instead of the term "field snow courses" used in Bulygina et al. (2011a, b). These refer to non-forested snow courses in general, some of which are above (or north of) the treeline.

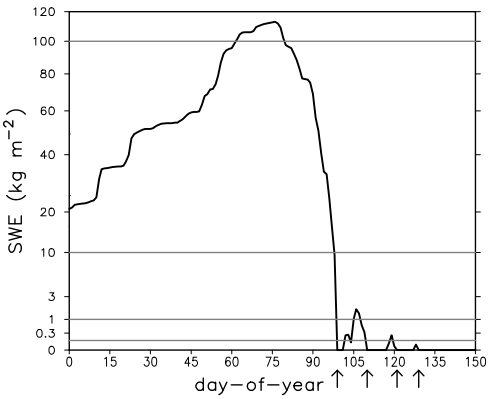

Figure 1. Time series of snow water equivalent (kg m^{-2}) in days 0–150 of year 1988 for a grid cell in western Russia (60.6° N, 39.4° E) for one of the ECHAM5 runs included in the REF experiment (SWE plotted in a square root scale for a better viewing of small values). The grey horizontal lines correspond to SWE values of 100, 10, 1 and 0.1 kg m^{-2}. The four arrows at days 99 (8 April), 110 (19 April), 121 (30 April) and 129 (8 May) indicate possible snow-off days (first day with SWE = 0 after a period with SWE > 0). The first snow-off day is employed in this paper for comparison with observational data.

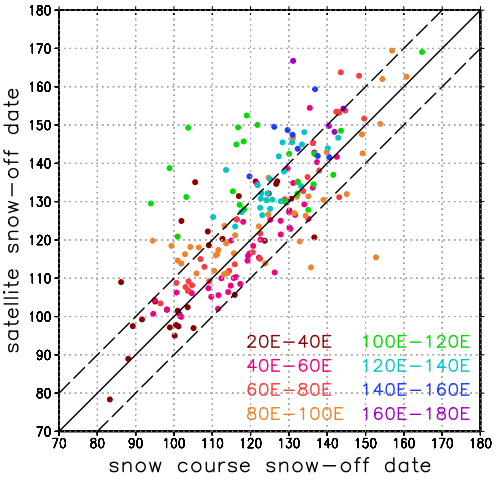

Figure 2. The relationship between time-mean snow-off dates based on the snow course data and the satellite retrievals. The satellite snow-off dates were averaged to the T63 horizontal resolution and screened according to the availability of snow course data. Only those grid cells for which the snow-off date in the snow course data could be determined for at least 5 years during 1979–2006 are included. The data points are colour-coded according to longitude. The solid diagonal line indicates equal snow-off dates for the two data sets, while the dashed diagonals correspond to a difference of ±10 days.

Even when setting aside potential issues related to spatial and temporal resolution, the definition of snow-off date in ECHAM5 results is not fully compatible with how the snow-off date is derived from the microwave satellite data. As noted in Sect. 3, the satellite snow-off date represents, in principle, the final snow-off date rather than the first snow-off date; that is, it can be affected by secondary periods of snow after the first snow-off date. Nevertheless, the use of final snow-off date in ECHAM5 for comparison with the satellite data would be problematic. The secondary periods of snow after the first snow-off date in ECHAM5 are often short and the values of SWE very low (e.g. SWE ∼ 0.1 kg m^{-2} for the last two periods of snow in Fig. 1) so it is unclear whether they would really be detected by the satellite algorithm. Thus, we opt to use the first snow-off date for ECHAM5, but acknowledge that this may contribute towards an early bias in snow-off dates when compared with the satellite data.

In the comparisons with the snow course data, the snow-off date in ECHAM5 is evaluated as the first snow-off date, but using SWE for only those days for which snow course measurements are available (i.e. every 5th or 10th day). This is fully consistent with how the snow-off date is derived from the snow course data (see the Appendix).

Figure 2 compares time-average snow-off dates derived from the snow course data and the satellite data, for each ECHAM5 grid cell separately. While these estimates are, of course, strongly correlated ($r = 0.775$), there is an appreciable scatter among them. For some grid cells, the difference between satellite and snow-survey snow-off dates is more negative than −10 days, and for many more grid cells (especially in Siberia, in particular between 100 and 120° E) more positive than 10 days. The mean difference between the satellite and snow survey snow-off dates is 5.1 days, while the rms difference is 12.2 days. The positive mean difference is, in principle, consistent with the notion that the satellite snow-off date may be in some cases influenced by secondary periods of snow after the first snow-off date; however, the substantial scatter indicates that there must be other factors at play. Unravelling the causes of these differences falls beyond the scope of this paper. Rather, we focus on what can be concluded from the model behaviour, given the observational uncertainty.

5 Results

5.1 Reference experiment REF

5.1.1 Snow-off timing

The geographical distribution of the mean snow-off date during the period 1979–2006 in the satellite retrievals is shown in Fig. 3a. In general, springtime snow-off progresses gradually from the southwestern parts of the domain towards the northern and eastern parts. Earliest snow-off occurs in the Baltic Sea area (around 20° E), before day 90 (end of March). An area of rather early snow-off dates can also be found in eastern Siberia where around the latitude 60° N snow melts right after day 120 (beginning of May). Snow melts latest

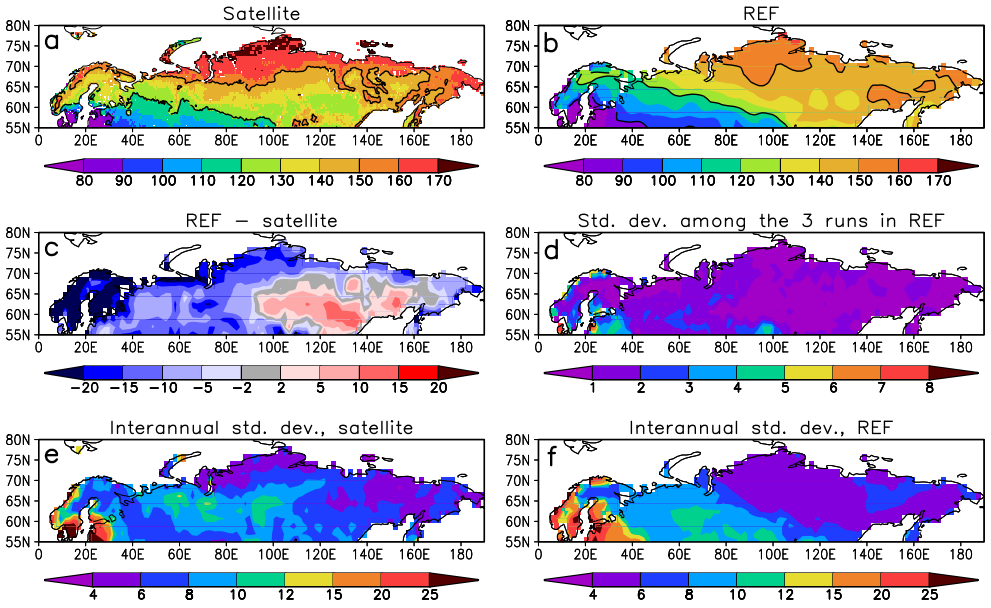

Figure 3. Mean snow-off date in years 1979–2006 based on **(a)** the satellite retrievals and **(b)** the REF experiment. Unit: day of year (Julian day). Snow-off dates of 90, 120 and 150 corresponding approximately to the beginning of April, May and June are indicated with black lines. **(c)** The difference in the average snow-off date between the REF experiment and the satellite retrievals. For computing the difference, the satellite snow-off dates were averaged to the model grid. **(d)** The standard deviation (σ_{n-1}) in 28-year mean snow-off date among the $n = 3$ differently initialized runs included in the REF experiment. **(e)** The standard deviation of yearly snow-off dates in the satellite retrievals (for snow-off dates averaged to the model grid), and **(f)** in the REF experiment (computed first separately for the three runs in REF and then averaged).

in the Taymyr Peninsula (around 75° N, 100° E), after day 170 (about 20 June). Snow also persists until June in parts of Russian Far East (east of 160° E). In addition to the general southwest-to-northeast gradient, some orographic effects can be detected. In the Ural Mountains (60° E) and in the Scandinavian (about 20° E) and Verkhoyansk (130° E) mountain ranges, snow melts later than in the surrounding regions, by up to 30 days in the Ural region. Although mountainous areas are problematic to handle in algorithms based on microwave radiometer data (Mialon et al., 2008; Pulvirenti et al., 2008), these features are expected on physical grounds: colder temperatures and orographically enhanced precipitation favour later snowmelt.

The REF experiment (Fig. 3b) reproduces well the general pattern of snow-off dates seen in the satellite data, the snow-off being latest in the Taymyr Peninsula (between days 150 and 160) and earliest in the Baltic Sea region (around day 80). However, in most of northern Eurasia, snow melts earlier in the model results than in the satellite retrievals (Fig. 3c). The difference to the satellite retrievals is mainly 5–20 days but locally exceeds 20 days in northern Europe. In contrast, in eastern Siberia and in some far eastern parts of Russia, snow melts locally over 10 days later in REF than in the satellite data. The orographic effects seen in Fig. 3a are absent in the model results, presumably because the model resolution (T63) is too coarse for describing them.

Figure 3d displays the standard deviation in the 28-year mean (1979–2006) snow-off date among the three runs included in the REF experiment. For most of northern Eurasia, the standard deviation is less than 2 days, with larger values mainly confined to the southwestern part of the domain and the Scandinavian coastline. In general, the standard deviation is much smaller than the respective differences between REF and the satellite data. This provides a justification for including only a single model run in the sensitivity experiments. Finally, Fig. 3e and f show the interannual standard deviation of snow-off dates for the satellite retrievals averaged to the model grid and for the REF simulation, respectively. Overall, the magnitude and the geographic pattern of the standard deviation are similar for the model results and for the observations, typical values ranging from 5–6 days in central and eastern Siberia to $\sim$ 20 days in the Baltic Sea region. Naturally, there are some differences in the details, such as, for example, a smaller standard deviation of snow-off dates in REF than in the satellite data set in western Siberia.

Figure 4a compares the snow-off dates in the REF experiment with those derived from the snow course data. The general tendency towards too early snow-off dates in the west (about 30–90° E) and too late snow-off dates in the east in REF as compared with the snow course data is in qualitative agreement with the corresponding comparison with satellite data (Fig. 3c). However, the positive differences in

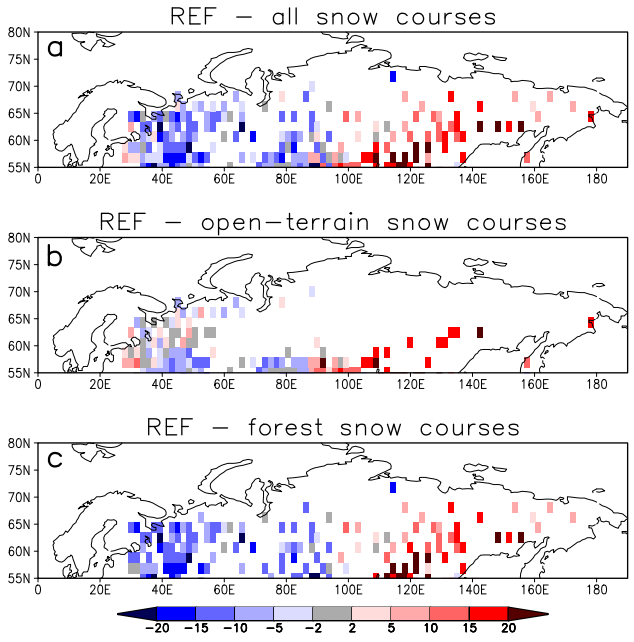

Figure 4. The difference in the average snow-off date for years 1979–2006 between the REF experiment and Russian snow course data for **(a)** all snow courses, **(b)** open-terrain snow courses, and **(c)** forest snow courses. Only those grid cells with snow-off data for at least 5 years are included.

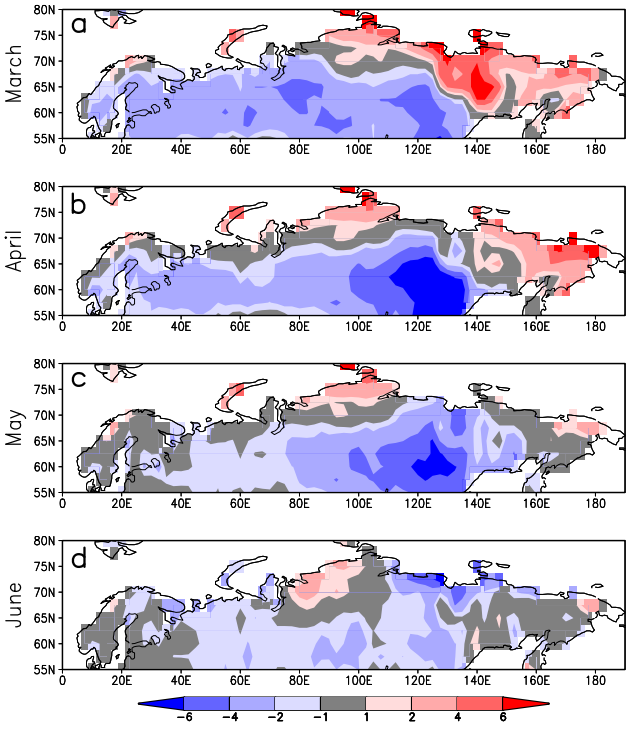

Figure 5. Differences in 2 m air temperature [K] for years 1979–2006 between the REF experiment and the CRUTEM3 data set for the months of March, April, May and June.

the east, indicating delayed snow-off in ECHAM5, are more widespread and more pronounced than those in Fig. 3c, exceeding 20 days at some locations. Figure 4b and c show a similar comparison as Fig. 4a, but separately for open-terrain and forest snow courses. It is seen that particularly in the west, the model snow-off dates are rather close to those derived from the open-terrain snow courses, the differences being only slightly negative, and in some cases slightly positive. In contrast, a comparison with the forest snow courses west of 90° E shows a persistent negative bias, indicating too early snowmelt in the model. The more negative differences for the forest snow courses than for the open-terrain courses indicate that snow tends to persist longer in forests than on open ground. For those grid cells (located mainly in western Russia) that have both forest and open-terrain courses, the snow clearance occurs on average 10.5 days later for the forest courses. In ECHAM5, however, neither snow-off dates nor SWE values are defined separately for the forested and non-forested parts of a grid cell.

The later snow-off for forests is consistent with the findings of Lundquist et al. (2013) for locations with cold winters (December–January–February (DJF) mean temperatures colder than −6 °C, which applies to most of northern Eurasia). However, the opposite behaviour (earlier snow-off in forests than on open ground) was observed in climates with warm winters (DJF mean temperature > −1 °C). In general, several factors influence the relative timing of snow-off in forests and on open ground (e.g. Essery et al., 2009; Strasser et al., 2011). During the accumulation season, the interception and subsequent sublimation of canopy snow reduces accumulation of snow in forests, while wind-blown snow from open areas may be deposited around forest edges, thus increasing the snow depth. In spring, less solar radiation is available for melting the snow under a forest canopy than on open ground, but increased downwelling long-wave radiation may partly compensate for this.

5.1.2 Other snow-related quantities

To set the stage for further discussion, 2 m air temperature (T_2), surface albedo, SCF and SWE are considered. Figure 5 shows a comparison of T_2 in REF and in the CRU data for the extended spring season (March through June). A cold bias prevails through most of the spring and peaks at −7 K in southeastern Siberia in April. Positive temperature biases occur in the Taymyr region (throughout the spring) and in the Russian Far East (mainly in March and April).

The left half of Fig. 6 displays a comparison of surface albedo in the REF experiment with the CLARA-SAL data set. Two pronounced biases appear. First, in agreement with Roesch and Roeckner (2006), a positive bias prevails in the central and eastern parts of Siberia for much of the spring, especially in March and April. Second, a negative albedo bias occurs in the northernmost parts of northern Eurasia (espe-

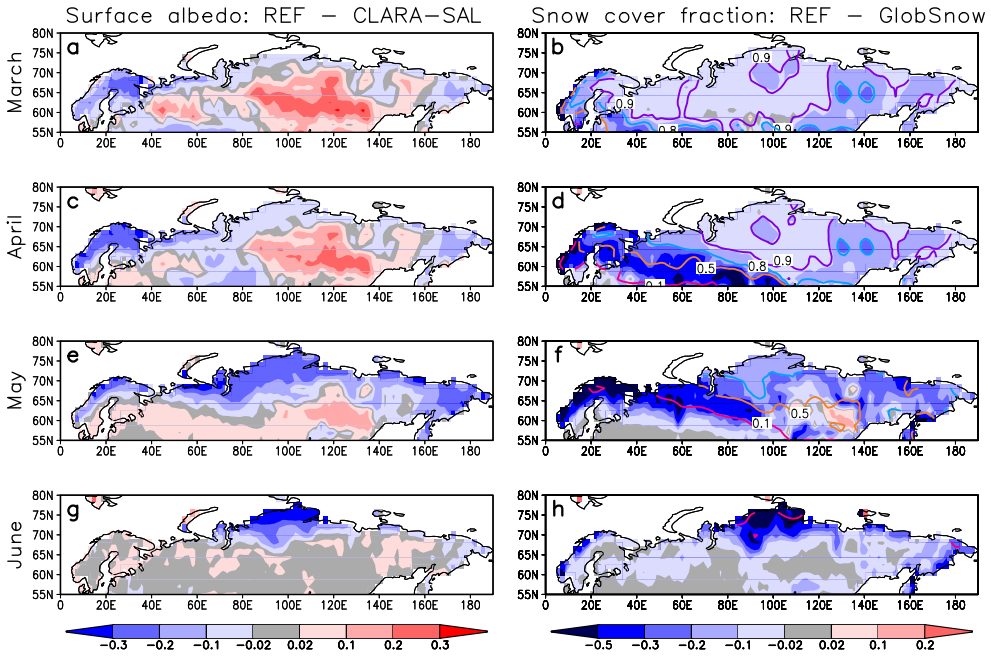

Figure 6. (a, c, e, g) Differences in surface albedo for years 1982–2006 between the REF experiment and the CLARA-SAL data set for the months of March, April, May, and June. **(b, d, f, h)** Corresponding differences in snow cover fraction for years 1997–2006 (excluding 2002) between the REF experiment and the GlobSnow data set. The coloured contours (magenta = 0.1; orange = 0.5; blue = 0.8; and violet = 0.9) indicate the snow cover fraction in REF.

cially in the Taymyr region) in May and June, and in northern Fennoscandia especially in April. Some understanding of the albedo biases can be gained by considering the snow cover fraction along with forest fraction and LAI.

The right half of Fig. 6 shows monthly mean SCF differences between the REF simulation and the GlobSnow data set for the years 1997–2006, excluding 2002. Although this period is shorter than the period 1982–2006 used for the albedo comparison, the REF vs. CLARA-SAL albedo differences for these two periods are very similar, with monthly spatial correlations of 0.98–0.99. Interestingly, ECHAM5 underestimates SCF compared to GlobSnow almost throughout northern Eurasia, with the exception of parts of southeast Siberia in May, where snow-off is delayed in the REF simulation. During March and April, the GlobSnow SCF is very high (0.99–1) through much of the central and northern parts of northern Eurasia. For ECHAM5, SCF is typically 0.90–0.95 in non-mountainous regions, but locally only $\approx$0.75–0.8 in the Verkhoyansk range in eastern Siberia, where SWE is relatively low (60–80 kg m^{-2}) and subgrid orographic variability is fairly large, $\sigma_z \approx 250$ m (see Eq. 3). The largest negative SCF differences to GlobSnow occur, however, in the snowmelt season, in April and May in the western parts of northern Eurasia and in June in the Taymyr peninsula, consistent with the too early snow-off in these regions. The small negative SCF biases that appear in June in southern and western parts of northern Eurasia in Fig. 6h are, however, artifacts related to clouds misinterpreted as snow in the GlobSnow data set.

The impact of SCF biases on surface albedo is best discernible in tundra (i.e. forest-free) regions (see Fig. 7a, b for the distribution of forests). In particular, the strong negative albedo bias in June in the Taymyr peninsula in Fig. 6g is related to insufficient snow cover in the REF simulation. The negative albedo bias in the northernmost parts of Fennoscandia and Russia in May can also be partly ascribed to underestimated SCF. However, especially in the Taymyr peninsula, the albedo bias (≈ -0.24, averaged over land grid points north of 72.5° N) is larger than the SCF bias (≈ -0.12). Very likely, this is related to the unrealistically low value (0.3) assumed for the albedo of "warm" snow ($T_s \geq 0$ °C).

The positive albedo bias that prevails in central and eastern Siberia (and to a lesser extent, in parts of western Russia) in March and April is related to the treatment of forests. Indeed, the regions with most pronounced positive albedo bias are associated with a high forest fraction (locally higher than 0.9) in the GlobCover 2009 data set (Fig. 7a). In ECHAM5, the forest fraction is somewhat smaller, typically $\approx$0.5–0.6. This difference should be interpreted with caution, however, as the dominant GlobCover land cover class in forested parts of Siberia is "open needle-leaved deciduous or evergreen forest", which has a canopy coverage of 15–40 % when viewed from directly above. The reason why the albedo bias is especially large in central and eastern Siberia is related to the LAI. There, the LAI in ECHAM5 is very low in the dor-

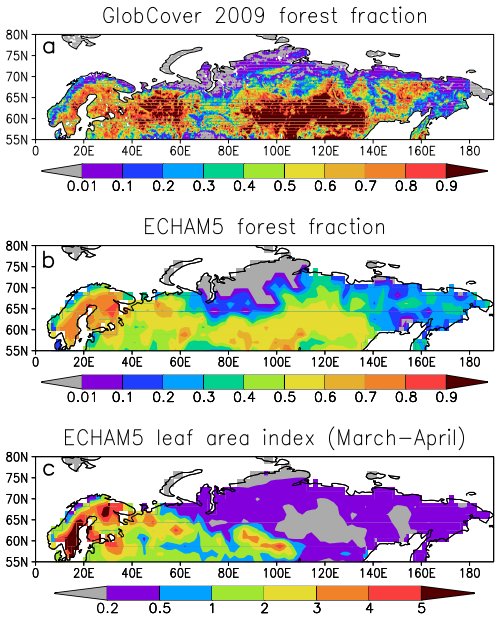

Figure 7. **(a)** Forest fraction in the GlobCover 2009 land cover map (computed as the sum of land cover classes 40, 50, 60, 70, 90 and 100). **(b)** Forest fraction assumed in the ECHAM5 simulations. **(c)** Leaf area index assumed in the ECHAM5 simulations, averaged over March and April.

mancy season of deciduous needleleaf trees, including March and April (Fig. 7c). When only the leaves (and not the stems and branches) are considered in the computation of the sky-view factor (Eq. 7), this results in very little shading of the snow surface by the forest. Therefore, as previously discussed by Roesch and Roeckner (2006), the albedo is overestimated substantially.

Figure 8 shows the average annual cycle of SWE in the REF experiment and in the snow course measurements, for the entire northern Eurasia and for two subregions denoted as western Russia (55–70° N, 30–70° E) and eastern Siberia (55–70° N, 100–140° E). Note that grid cells without snow course data are not included in the averages, and therefore, for example, the average over the entire northern Eurasia gives more weight to the western and southern parts of the region than its eastern and northern parts, especially when considering open-terrain snow courses. With this caveat in mind, we note that the domain-mean annual cycle of SWE over the entire northern Eurasia in REF agrees well with the snow course data, although the maximum is slightly higher and occurs 5–10 days earlier than observed (Fig. 8a). There are, however, regional differences. For western Russia (Fig. 8b), the simulated maximum SWE is very close to that observed, but SWE starts to decrease earlier than observed in the spring, in agreement with the too early snow-off days in Figs. 3c and 4a. In contrast, for eastern Siberia, the REF experiment overestimates substantially the accumulation of snow during winter (Fig. 8c), and the timing of maximum SWE and snowmelt is delayed, which is again consistent with Fig. 4a.

When considering the open-terrain snow courses only, the simulated SWE maximum is higher than observed for all three regions (Fig. 8d–f), and the overestimate is especially pronounced for eastern Siberia. In contrast, when compared with the forest snow courses, the simulated maximum SWE is slightly too low for the entire northern Eurasia (Fig. 8g) and for western Russia (Fig. 8h) and only moderately overestimated for eastern Siberia (Fig. 8i). The more positive ECHAM5 vs. observation differences for open-terrain than forest snow courses suggest that in reality (but not in ECHAM5), more snow accumulates in forests than on open ground. We verified that this also holds true when the comparison is restricted to grid cells and years with both forest and open-terrain observations. It is worth noting that often the opposite has been reported (though mainly for sites at lower latitudes): less accumulation in forests due to sublimation of intercepted snow or due to midwinter melt induced by the larger downwelling long-wave flux in forests (Essery et al., 2009; Strasser et al., 2011; Lundquist et al., 2013).

The delayed snow-off in the REF experiment in central and eastern Siberia is physically consistent with the low-temperature bias and high-albedo bias in spring. On one hand, overestimated surface albedo keeps the absorbed solar radiation low, which favours cold temperatures and delays the onset of snowmelt. On the other hand, delayed snowmelt provides a positive feedback by keeping the albedo high. Furthermore, too large accumulation of snow in winter contributes to the delayed snow-off in eastern Siberia (Fig. 8c). Similarly, underestimated albedo and overestimated T_2 in spring in the Taymyr region are consistent with the snow vanishing too early. For western Russia, however, the main reason for the earlier than observed snow-off dates (Figs. 3c and 4a) seems to be that at least in a domain-average sense, snowmelt starts somewhat too early (Fig. 8b). Intriguingly, this occurs in spite of a slightly negative temperature bias in spring (Fig. 5).

5.2 Sensitivity experiments

The sensitivity experiments show that both nudging and changes in the treatment of surface albedo have substantial impacts on the snow-off date simulated by ECHAM5 (Fig. 9). Nudging makes snow-off occur earlier in most of northern Eurasia, with largest effect (over 15 days) in southeastern Siberia and locally in Fennoscandia. The earlier snow-off in REF_NDG is both due to higher temperatures (as discussed below) and due to slightly reduced snowfall in eastern Siberia, as reflected in the seasonal cycle of SWE in Fig. 8c, f and i. However, in the Taymyr region, snow-off is delayed by more than 5 days in REF_NDG as compared with REF (Fig. 9a). Use of observed (CLARA-SAL) albedo in ALB1 likewise makes the snowmelt earlier in southeastern Siberia and later in the Taymyr region, with larger im-

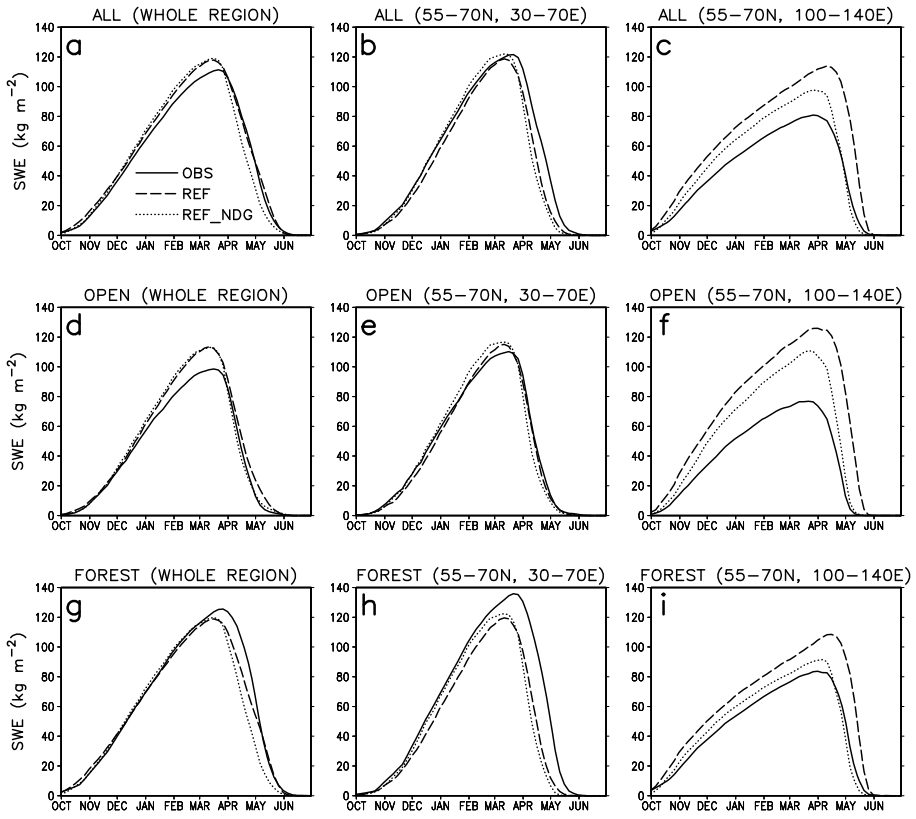

Figure 8. Mean annual cycle of SWE according to the snow course measurements (solid line), in the REF experiment (dashed line) and in the REF_NDG experiment (dotted line) for **(a)** all snow courses for the whole northern Eurasian domain, **(b)** for western Russia (55–70° N, 30–70° E) and **(c)** for eastern Siberia (55–70° N, 100–140° E). **(d–f)** as **(a–c)** but including only open-terrain snow courses. **(g–i)** as **(a–c)** but including only forest snow courses. Only those ECHAM5 grid cells with snow course data are included in the domain-mean values. For clarity, results for the ALB1, ALB2, ALB1_NDG and ALB2_NDG experiments are not shown. In general, albedo changes had little effect on SWE, except for the snowmelt season.

pact in the latter (ALB1–REF differences of ≈ -5 days and ≈ 15 days, respectively; Fig. 9b). In general, snow-off is delayed somewhat in the northern parts of northern Eurasia, and also in central Russia. For the ALB2 experiment with changed albedo parameterization, snow-off occurs up to 5 days earlier in southeastern Siberia than in REF (Fig. 9c). This is very similar to the ALB1 experiment, and results from the modification of the sky-view factor in the calculation of surface albedo in forested regions. However, due to the increase of the albedo of "warm" snow ($T_s \geq 0\,^{\circ}\mathrm{C}$) from 0.3 to 0.6, snow-off is delayed in the northeastern parts of the Russian Far East and particularly in the Taymyr region, locally by 5–10 days. This response is qualitatively similar but somewhat weaker than that in ALB1. Finally, when nudging is combined with changed treatment of albedo (ALB1_NDG and ALB2_NDG; Fig. 9c and e), the earlier snow-off in southeastern Siberia and delayed snow-off in the Taymyr region become even more pronounced. In southeastern Siberia, the difference to REF reaches locally -20 days.

Figures 10 and 11 compare the snow-off dates in all ECHAM5 experiments with the snow-off dates derived from microwave satellite data and Russian snow course data, respectively. In spite of the inter-experiment differences noted above, all free-running (i.e. non-nudged) simulations show the same basic pattern of differences compared to the satellite data (Fig. 10): too early snow-off dates in the west, along with regions of delayed snow-off in eastern parts of northern Eurasia. The ALB1 and ALB2 experiments show some improvement in southeastern Siberia, where the positive bias in snow-off date is reduced but not eliminated. Furthermore, the negative bias in the Taymyr region is reduced in the ALB2 experiment with changed snow albedo parameterization, and turned into a slight positive bias in ALB1, which uses observation-based CLARA-SAL albedo data.

Nudging eliminates entirely the positive bias in snow-off date in southeastern Siberia as compared with the satellite data. As a consequence, the REF_NDG experiment features an early bias throughout northern Eurasia (Fig. 10b), with largest biases in the west. Likewise, for the nudged simulations with albedo changes (ALB1_NDG and ALB2_NDG), snow-off generally occurs earlier than in the satellite data, the most notable exception being that for ALB1_NDG, near-zero

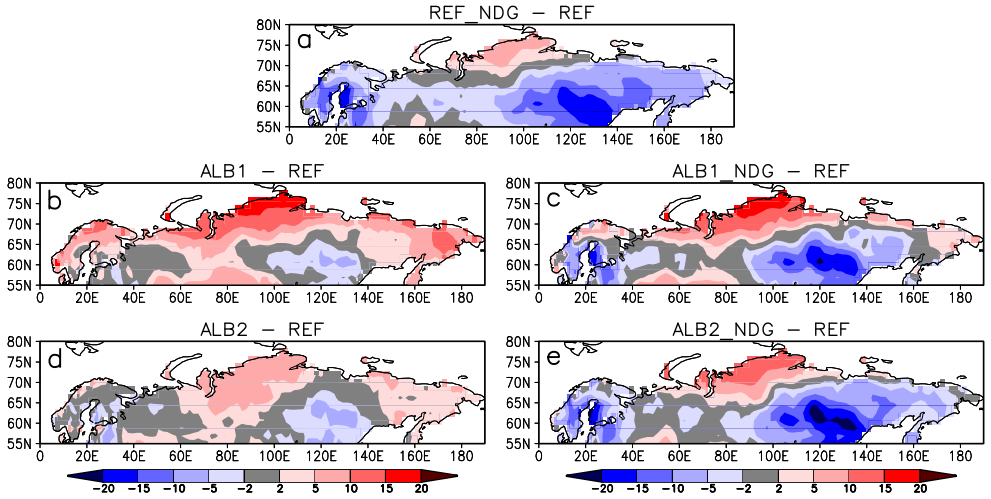

Figure 9. Differences in average snow-off date between the five sensitivity experiments (REF_NDG, ALB1, ALB1_NDG, ALB2 and ALB2_NDG) and the REF experiment.

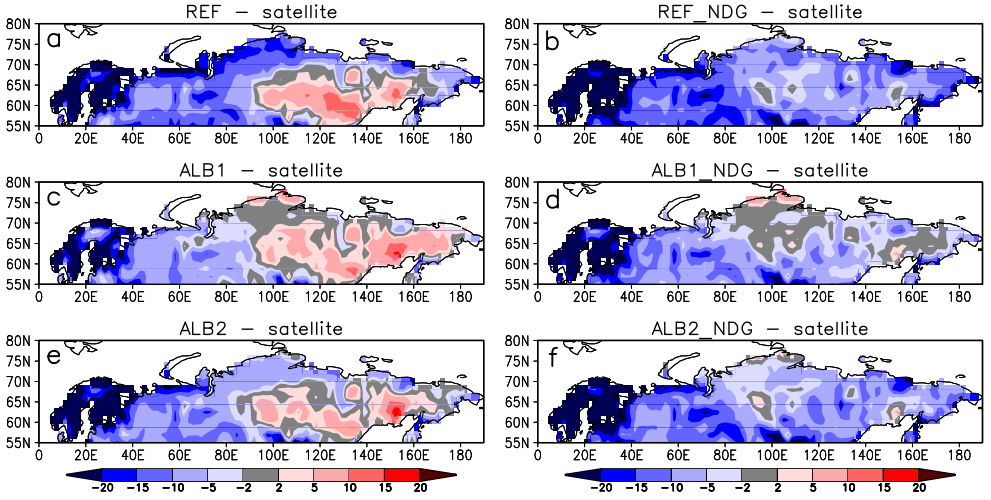

Figure 10. Differences in average snow-off date between the six ECHAM5 experiments and the satellite retrievals.

or even positive differences (i.e. delayed snow-off) appear in the Taymyr region.

It should be recalled that the early bias in snow-off dates compared with the satellite data may be, in part, an artifact related to differences in the definition of snow-off time between the ECHAM5 simulations and the satellite data (Sect. 4). Indeed, when compared with the snow course data (Fig. 11), all free-running simulations feature delayed snow-off in eastern Siberia and in the Russian Far East. The differences between REF, ALB1 and ALB2 are rather small in comparison with their biases with respect to the snow course data. Even for the nudged simulations (REF_NDG, ALB1_NDG, and ALB2_NDG), positive differences indicating delayed snow-off prevail for many measurement stations in eastern Siberia and in the Russian Far East, although slightly negative differences occur for some stations. In the western parts of northern Eurasia, however, all simulations feature negative biases, snow-off occurring 10–20 days earlier than in the snow course data for many stations in western Russia. The negative biases are, in general, slightly larger for the nudged simulations, especially in the westernmost parts of Russia. Furthermore, as noted in Sect. 5.1 for the REF experiment, the negative biases are especially pronounced when compared with forest snow courses.

The changes in snow-off timing are influenced by, and they feed back on, simulated 2 m air temperature (Fig. 12) and surface albedo (Fig. 13) in the sensitivity experiments. For brevity, only mean values over the months of April and May are shown. All experiments feature a cold bias in southeastern Siberia, which amounts down to −7 K in REF (Fig. 12a). Consistent with the earlier snowmelt (Fig. 9), this bias is reduced in ALB1 (Fig. 12c) and ALB2 (Fig. 12e), and espe-

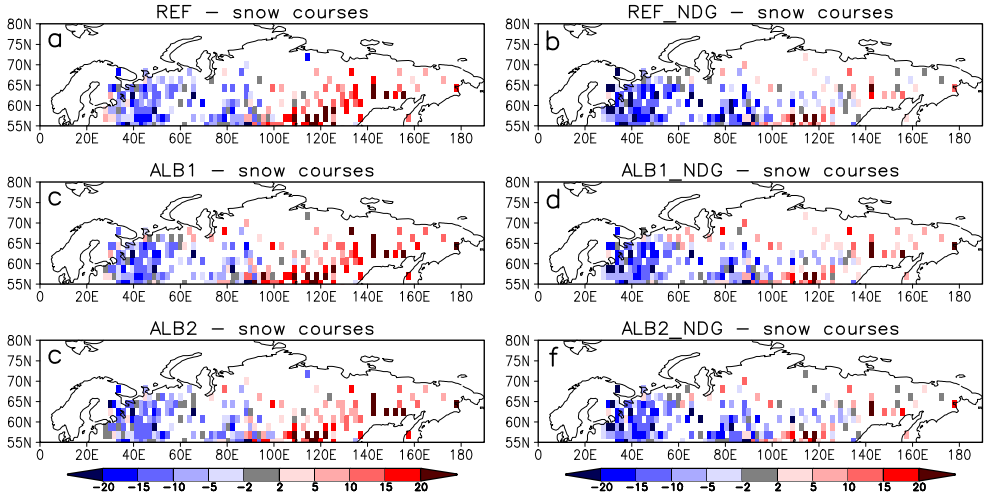

Figure 11. Differences in average snow-off date between the six ECHAM5 experiments and the Russian snow course data. Both open-terrain and forest snow courses are included in the comparison.

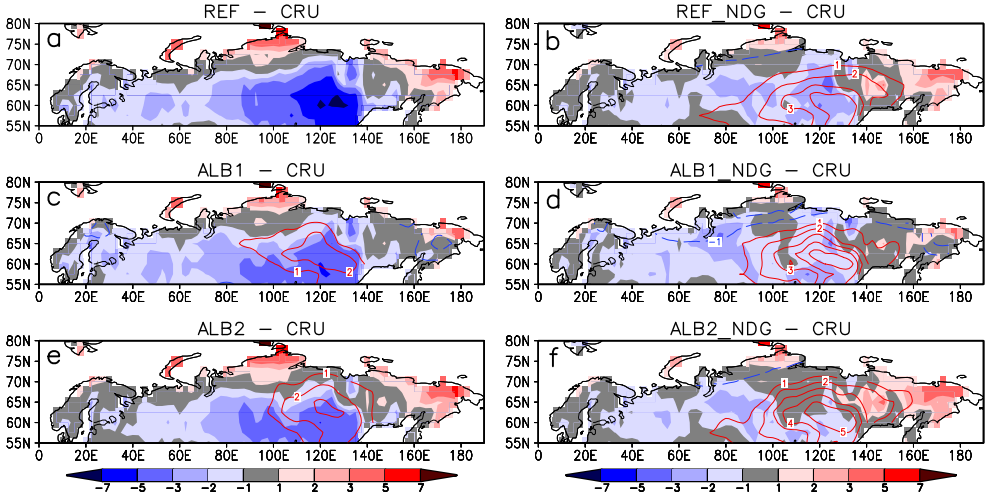

Figure 12. Differences in April–May mean 2 m air temperature between ECHAM5 and the CRUTEM3 data set for the **(a)** REF, **(b)** REF_NDG, **(c)** ALB1, **(d)** ALB1_NDG, **(e)** ALB2 and **(f)** ALB2_NDG experiments. The contours in **(b–f)** indicate the difference from the REF experiment (contour interval 1 K; zero contour omitted).

cially in the nudged experiments (Fig. 12b, d and f). A slight negative temperature bias (≈ -2 to -1 K) prevails in large parts of western and central Russia, and this feature varies only slightly between the experiments. Positive temperature biases are seen in all experiments in the Taymyr region and in parts of the Russian Far East.

Figure 13 displays surface albedo differences from the CLARA-SAL data for the REF, REF_NDG, ALB2 and ALB2_NDG experiments (for ALB1 and ALB1_NDG, the differences are zero by construction). It is seen that the high-albedo bias in southeastern Siberia is reduced substantially in both REF_NDG and ALB2, and it is eliminated completely in ALB2_NDG. In the case of ALB2 and ALB2_NDG, the modified computation of the sky-view factor in the albedo parameterization for forested regions contributes to this. For REF_NDG, however, the change in surface albedo stems entirely from changes in meteorological conditions, the reduced negative temperature bias (Fig. 12b) leading to both lower snow albedo and reduced snow cover. However, all four experiments show some common biases, most distinctly an underestimation of albedo compared to the CLARA-SAL data in the northern parts of northern Eurasia and in the Russian Far East. Interestingly, the use of a higher value for the albedo of "warm" snow (0.6 instead of 0.3 when $T_s \geq 0\,^{\circ}$C) in the ALB2 and ALB2_NDG experiments reduces somewhat the negative bias in the Taymyr region but does not eliminate it. A negative SCF bias likely contributes to the remaining albedo bias, the average difference to GlobSnow

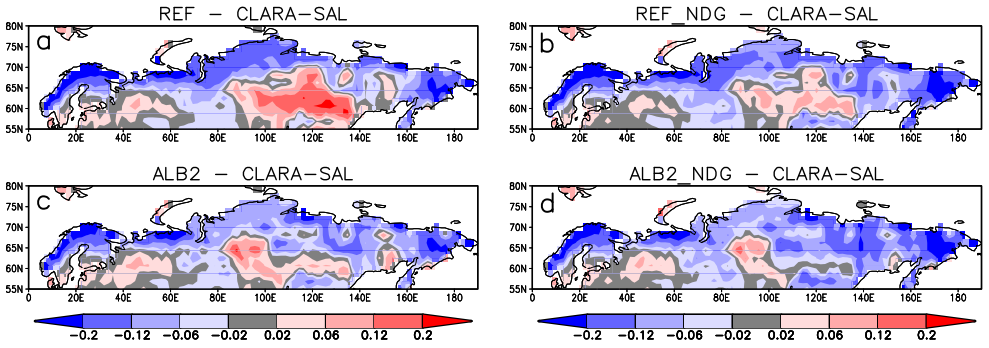

Figure 13. Differences in April–May mean albedo between ECHAM5 and the CLARA-SAL data set for the **(a)** REF, **(b)** REF_NDG, **(c)** ALB2 and **(d)** ALB2_NDG experiments. In ALB1 and ALB1_NDG (not shown) the albedo values are, by construction, identical to the CLARA-SAL data.

data in the Taymyr peninsula being $\Delta\mathrm{SCF} \approx -0.08$ both in April and May. However, it still appears that snow albedo is underestimated in May, which suggests that even the value of 0.6 is too low at least in this region.

6 Discussion

The analysis of the sensitivity experiments in Sect. 5.2 showed that nudging and changes in the treatment of surface albedo in the presence of snow alleviated some of the model biases in snow-off dates, 2 m temperature and surface albedo. Nevertheless, many of the biases seen in Figs. 10–13 are quite similar for all experiments. Regarding the timing of springtime snow-off, the results are somewhat ambiguous for the eastern parts of northern Eurasia, due to large differences between observational snow-off date estimates from satellite and snow course data, and hence in the resulting model biases. For western Russia, however, comparisons with the satellite data and the snow course data indicate unanimously that snow-off occurs too early in ECHAM5 for all experiments, with only moderate variations due to nudging or changes in the treatment of surface albedo (Figs. 10 and 11). Moreover, surprisingly, the too early snow-off co-occurs with a slight negative temperature bias in the snow-melt season (Fig. 12).

To shed more light on the seemingly contradictory biases in temperature and snow-off dates, a detailed comparison of ECHAM5 results with observations at Sodankylä in Finnish Lapland is presented. The black line in Fig. 14a displays the mean seasonal cycle of snow depth measured at Sodankylä in 1979–2006, for days of year 1–165 (i.e. from 1 January until 14 June). The other curves show the corresponding seasonal cycle of SWE for four ECHAM5 experiments (REF, REF_NDG, ALB1 and ALB2). While there is no one-to-one correspondence between snow depth and SWE, due to variations in snow density, it is clear from Fig. 14a that in three of the four ECHAM5 experiments (REF, REF_NDG and ALB2), snowmelt occurs earlier than in the observations, by roughly 10–15 days. This is consistent with Fig. 3c, which indicates that in the Finnish Lapland, snow-off in the REF experiment occurs ∼ 15 days earlier than in the satellite data. The exception is that in the experiment ALB1, which prescribes surface albedo from the AVHRR-based CLARA-SAL data set, the timing of snowmelt coincides well with the observations.

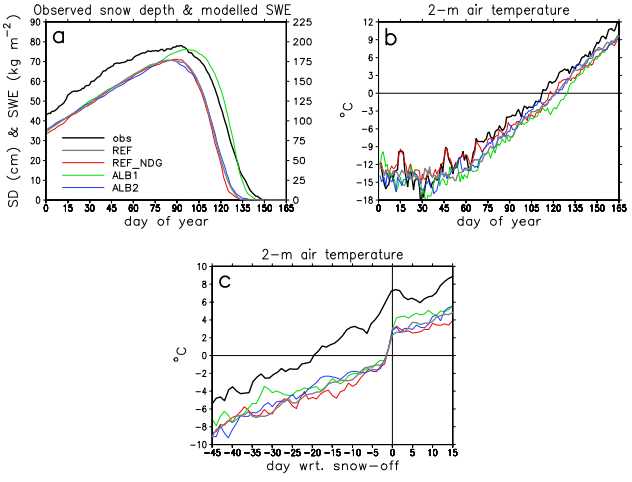

Figure 14. Comparison of ECHAM5 simulations with observations at Sodankylä (67.37° N, 26.63° E). **(a)** Mean seasonal cycle of observed snow depth (black line, scale on the left) and modelled SWE (four curves for different ECHAM5 experiments, scale on the right) in 1979–2006. **(b)** Mean seasonal cycle of 2 m air temperature. **(c)** Mean 2 m air temperature composited with respect to the snow-off date, "day 0" representing the first completely snow-free day. The ECHAM5 results are taken from the grid point nearest to the Sodankylä site (68.08° N, 26.25° E).

Figure 14b shows a comparison for the seasonal cycle of 2 m air temperature. From mid-March (day 75) onwards, all ECHAM5 simulations underestimate the average T_2 systematically. The average underestimate in the primary snowmelt season (mid-April to mid-May; days 105–135), is ≈ 1.8 K

for REF, REF_NDG and ALB2, and ≈ 3.5 K for ALB1. Thus the Sodankylä site represents a case where snowmelt (and snow-off) occurs earlier in ECHAM5 than in the observations, in spite of a negative temperature bias in the snowmelt season.

The problems with representing correctly the relationship between snowmelt timing and temperature become even more obvious, when the temperature data are composited with respect to the snow-off date. Thus, for each year in 1979–2006, the snow-off date ("day 0") was defined as the first day after the winter's snow maximum completely without snow (in ECHAM5) or with snow depth equal to zero in the morning (in the observations), and the average T_2 was computed for each day in the range from 45 days before snow-off to 15 days after snow-off (Fig. 14c). Note specifically that as "day 0" represents the first completely snow-free day, snow actually vanishes sometimes during "day −1", and "day −2" is (generally) the last day with snow persisting throughout the day.

It is clear from Fig. 14c that ECHAM5 substantially underestimates T_2 in the snowmelt season. Strikingly, this depends quite little on the experimental details such as nudging or changed treatment of surface albedo. The negative bias in T_2 culminates just before snow-off, being ≈ −7 K on "day −2". Furthermore, it is noted that in ECHAM5, the average T_2 reaches 0 °C as late as "day −1", during which the snow vanishes in the model. In the observations, the average T_2 reaches 0 °C already on "day −20", and climbs to 7 °C by "day −1". It is further seen that in ECHAM5, there is a substantial jump in temperature from "day −2" (the last day with snow throughout the day) to "day 0" (the first completely snow-free day), 2.9–3.9 °C depending on the experiment, whereas the observed change is only 1.0 °C. A similar composite analysis of temperature with respect to snow-off date was repeated for ECHAM5 for the entire northern Eurasia, and it confirmed that the behaviour seen in Fig. 14 is quite universal. In particular, throughout the region, the average T_2 stayed below 0 °C until and including "day −2" (not shown).

The likely main reason for the fact that T_2 simulated by ECHAM5 stays close to 0 °C in the snowmelt season is that the surface energy budget (and hence surface temperature) is not computed separately for the snow-free and snow-covered parts of the grid cell. Rather, while snow cover fraction is taken into account in defining grid-mean properties like surface albedo and roughness length, a single snow-covered energy balance computation is performed (Eq. 1).

As explained in Sect. 2.1, the amount of snowmelt is determined from the condition that, when the surface temperature T_s would rise above 0 °C without considering snowmelt, the heat consumed in melting snow restores T_s to 0 °C (Eq. 2). Here, T_s refers to the grid-mean surface temperature, not the temperature of melting snow. Therefore, as long as there is any snow left in the grid cell, T_s is not allowed to rise above 0 °C, irrespective of the snow cover fraction. Naturally, this acts to suppress the sensible heat flux (or even makes it negative), so 2 m air temperature cannot rise much above 0 °C either. In reality, in a region with partial (patchy) snow cover, surface temperature is kept to zero only in the patches of melting snow. In the snow-free patches, T_s, and consequently, T_2, can rise substantially above 0 °C. Furthermore, local temperature advection from snow-free to snow-covered patches and subsidence associated with a "snow breeze" circulation can increase T_2 over the latter (e.g. Yamazaki, 1995; Liston, 1995).

In summary, the use of a single surface energy budget computation leads to a misrepresentation of grid-mean surface fluxes in the presence of fractional snow cover (Liston, 2004): too much energy is spent in melting snow, and too little in warming the air and the ground. Consequently, T_2 stays too low in the snowmelt season (Fig. 14c). This likely explains why ECHAM5 features a persistent cold bias in springtime T_2 even in regions where snow-off occurs earlier than observed (Figs. 10–12).

In addition, there is another factor related to the treatment of surface energy budget that may contribute to the too early snow-off: ECHAM5 does not include a canopy layer. In ECHAM5, forests influence the energy budget through changing the surface albedo and roughness length, but, for example, the shading of the surface by the canopy is not considered. Since forests reduce the surface albedo in the presence of snow (or more precisely, the combined albedo of the surface and the canopy) in ECHAM5, this implies that the amount of solar radiation available for snowmelt at ground is increased in forests. In reality, the opposite happens, which acts to delay springtime snowmelt in forests relative to non-forested areas (Strasser et al., 2011). This may explain why, in comparison with the snow course data, ECHAM5's tendency toward too early snow-off is more pronounced for forest than open-terrain measurements (Fig. 4b–c).

Recently, Brutel-Vuilmet et al. (2013) found that, while there is still substantial intermodel dispersion among the CMIP5 models, on average the springtime snowmelt is slightly delayed in northern Eurasia. Taken at face value, the default version of ECHAM5 agrees with this result for the eastern parts of northern Eurasia, while in the west, snow vanishes too early (Figs. 3 and 4). However, such regional features are not discussed in Brutel-Vuilmet et al. (2013), and moreover, a rigorous comparison with their results is difficult due to the different data sets and analysis methods used (e.g. Brutel-Vuilmet et al., 2013, used only monthly data). An interesting question for further research is how well the CMIP5 models are able to represent the relationship between springtime temperature and snow-off timing. In particular, is the problem of snowmelt occurring at too cold grid-mean temperatures, as demonstrated in the current study, an exception or the rule for the CMIP5 models? A priori, we would expect some of the models to behave better (or at least differently) than ECHAM5. A prime example is the CLM4 land-surface model (Oleson et al., 2010) employed in the Com-

munity Earth System Model (CESM) (Hurrell et al., 2013), which addresses all the main limitations of ECHAM5 identified in this work: the energy budget computation is separated for the snow-covered and snow-free parts of a grid cell, the computation of radiative fluxes at the snow surface accounts for the shading by the overlying forest canopy, and the snow albedo computation is more rigorous, based on radiative transfer modelling and a prognostic effective radius of snow grains. The CLASS land surface scheme (Verseghy, 2000) used in the CanCM4 climate model (von Salzen et al., 2013) also separates the energy budgets for snow-covered and snow-free land.

7 Conclusions

In the present work, we have evaluated the timing of springtime snow-off in northern Eurasia in the ECHAM5 (version 5.4) atmospheric GCM. Simulated snow-off dates were compared with a snow-off date data set based on space-borne microwave radiometer measurements and with Russian snow course data. The primary conclusions are as follows:

- In general, the default version of ECHAM5 reproduces well the observed geographic pattern of snow-off dates, with earliest snowmelt (snow disappearing in March) in the Baltic region, and latest snowmelt (in June) in the Taymyr region and parts of the Russian Far East. However, compared to the satellite data, snow-off occurs too early in the western parts of northern Eurasia, and also in the northernmost regions like the Taymyr peninsula, with largest differences (locally over 20 days) in northern Europe. In contrast, in southeastern Siberia and in some far eastern parts of Russia, snow melts locally over 10 days later than in the satellite data. Comparison with the Russian snow course data confirms the pattern of too early snow-off in the west and too late snow-off in the east, although the former is slightly less pronounced, and the latter more pronounced, than in the corresponding comparison with the satellite data set.

- The later than observed snow-off in southeastern Siberia is associated both with overestimated snow accumulation during winter and a springtime cold bias, which exceeds -6 K in April. The latter is, in part, related to an overestimation of surface albedo, which arises from insufficient shadowing of the snow surface by the canopy in ECHAM5 in the dormancy season of deciduous needleleaf trees. In contrast, surface albedo is underestimated in late spring especially in the Taymyr region, both due to underestimated snow cover and because an unrealistically low albedo (0.3) is assumed for "warm" snow ($T_s \geq 0\,^\circ$C). This promotes too early snow-off in this region.

- Several sensitivity experiments were conducted, where biases in simulated atmospheric circulation were corrected through nudging and/or the treatment of surface albedo was modified. Both nudging and surface albedo modifications alleviated some of the model biases in snow-off dates, 2 m temperature (T_2) and surface albedo. In particular, it proved possible to reduce substantially the biases in snow-off date in southeastern Siberia and in the Taymyr region. In contrast, the early bias in snow-off in the western parts of northern Eurasia was not reduced appreciably in any of the experiments; rather it was slightly increased by nudging. Furthermore, surprisingly, this early bias in snow-off was accompanied by a slight negative bias (≈ -2 to -1 K) in springtime T_2, both for the default version of ECHAM5 and for the sensitivity experiments.

- The combination of a too early snow-off with a cold springtime temperature bias implies that temperature stays too low in the snowmelt season. In fact, as long as there is any snow left on the ground, the daily mean T_2 simulated by ECHAM5 rarely rises above 0 °C. In contrast, as demonstrated for the Sodankylä site in Finnish Lapland, the observed daily mean T_2 typically climbs several degrees above 0 °C before all snow has vanished.

- The likely main reason for the fact that T_2 in ECHAM5 stays close to 0 °C in the snowmelt season is that the surface energy budget (and hence the surface temperature T_s) is not computed separately for the snow-free and snow-covered parts of the grid cell. Thus, even if the diagnosed snow cover fraction is well below 1, the grid-mean T_s is not allowed to rise above 0 °C. This acts to suppress the sensible heat flux (or even makes it negative), so T_2 cannot rise much above 0 °C either, and leaves too large a fraction of the grid-mean surface net radiation to be consumed in melting snow.

- There is another factor related to the treatment of surface energy budget, which also likely contributes to the too early snow-off: ECHAM5 does not include a canopy layer. Thus, in particular, the shielding of snow on ground by the overlying canopy is not accounted for, which leaves too much solar radiation available for melting snow. This may explain why the early bias of snow-off in ECHAM5 in western Russia is especially pronounced when compared with snow course measurements made in forests.

Overall, the present study highlights the fact that snow-off timing in an atmospheric GCM depends on the simulation of a number of processes: large-scale circulation and temperature (which mainly determine the snowfall during winter), computation of snow properties on ground, treatment of surface albedo, and in general, the surface energy budget (which

plays a key role for snowmelt). In such a situation, as often in climate modelling, compensating errors are likely, so that improving any single process in the model may either improve or deteriorate the agreement with observations. An example of this is that for ECHAM5, the general tendency towards too early snow-off becomes clearer when biases in atmospheric circulation and temperature are corrected by nudging. This exposes more clearly the problems related to the treatment of surface energy budget, especially in the presence of partial snow cover and forests. Beyond that, an obvious area for further development would be the snow scheme itself, which is rather simplistic in ECHAM5. Only the SWE and snow temperature are computed, with no consideration of snow density and snow grain size. Furthermore, the temperature dependent snow albedo scheme in ECHAM5 is very simple and, as demonstrated in this and previous work, to some extent unrealistic.

Finally, according to our preliminary tests, snowmelt also occurs at too low (grid-mean) temperatures in the Max Planck Institute's newest atmospheric GCM, ECHAM6 (Stevens et al., 2013). Like ECHAM5, ECHAM6 does not define separately the surface temperature for the snow-free and snow-covered parts of a grid cell. It is an intriguing question to which extent this issue pertains to other global and regional climate models.

Appendix A: Determination of snow-off dates based on Russian snow course data

In the Russian snow course data (Bulygina et al., 2011a), SWE measurements are typically provided at 10-day intervals in winter and 5-day intervals in spring (starting from March or April). A major issue in defining the snow-off date based on these data is, however, that in the absence of snow, SWE measurements are generally not reported. Thus one cannot always be sure whether missing data indicate that there is no snow left to be measured, or that the measurement was not performed for some other reason. To define the snowmelt date, we adopted the following procedure.

1. The observation date with maximum SWE ($d_{\max}$) for the winter was located.

2. The part of the SWE time series after $d_{\max}$ was studied, and cases were sought in which a valid measurement of SWE was followed by missing data, with the corresponding dates denoted by $d_{\text{miss-1}}$ and d_{miss}.

3. In such cases, it was assessed whether the missing data could plausibly indicate the absence of snow. For this end, we evaluated the statistics of SWE changes between two observation times (either 5 or 10 days apart from each other) within 1 month of the date in question, considering all years for which the station reported data. If the change in SWE from $d_{\text{miss-1}}$ to d_{miss} required for all snow to melt by the time d_{miss} (i.e. $\Delta\text{SWE\_required} = -\text{SWE}_{\text{miss-1}}$) was within two standard deviations ($\sigma_{\Delta\text{SWE}}$) of the mean value ($\overline{\Delta\text{SWE}}$) of SWE changes for the time of the year, that is

$$\Delta\text{SWE\_required} \geq \overline{\Delta\text{SWE}} - 2\sigma_{\Delta\text{SWE}}, \qquad \text{(A1)}$$

   it was assumed that the missing SWE value at day d_{miss} indicates the absence of snow ($\text{SWE}_{\text{miss}} = 0$).

4. If the missing value was deemed to be zero, all subsequent missing values were also interpreted as zero, until (possibly) a positive SWE value was found.

5. After the SWE time series was corrected as outlined above, the snow-off date was determined. Data for three observation days were used: the first observation day (d_{zero}) with corrected SWE = 0 after the winter's SWE maximum ($d_{\max}$), and the 2 observation days preceding it with SWE > 0 (denoted as d_{m2} and d_{m1}, with SWEs of SWE_{m2} and SWE_{m1}, respectively). If linear extrapolation based on the values SWE_{m2} and SWE_{m1} suggested all snow to have melted before d_{zero}, the snow-off date was computed as

$$d_{\text{snow-off}} = d_{m1} + (d_{m1} - d_{m2})\frac{\text{SWE}_{m1}}{\text{SWE}_{m2} - \text{SWE}_{m1}}, \qquad \text{(A2)}$$

   otherwise, it was assumed that $d_{\text{snow-off}} = d_{\text{zero}}$.

6. Finally, if the SWE reached values higher than $20\,\text{kg}\,\text{m}^{-2}$ after the determined snow-off date, the case was considered suspicious; thus this winter's data for this snow course were ignored in further analysis. Cases in which the above algorithm failed to find a snow-off date were likewise ignored in the subsequent analysis.

Clearly, the above algorithm involves some arbitrary choices (especially the criterion of two standard deviations in Eq. (A1) and the limit of $20\,\text{kg}\,\text{m}^{-2}$ in step 6 of the algorithm). However, a number of sensitivity tests were conducted regarding the choice of these parameters, and it was found that the statistics of model vs. observation differences were largely insensitive to them. For example, changing the criterion of two standard deviations in Eq. (A1) to either one or three standard deviations changed the average model vs. observation difference in snow-off dates by less than 1 day.

Lastly but importantly, to compare ECHAM5's snow-off dates with the snow course data as consistently as possible, the simulated SWE time series were first subsampled according to the availability of the snow course data (i.e. including only the days with measurements), and the snow-off dates for ECHAM5 were then determined according to the algorithm outlined above. For comparison with satellite data, however, the simulated snow-off dates were derived from the complete time series of daily mean SWE.

Acknowledgements. This research was supported by the Academy of Finland (project numbers 116109, 140915 and 254195). The Russian Hydrometeorological Centre and the Climatic Research Unit, University of East Anglia, respectively, are acknowledged for making available the snow course data and the 2 m temperature data used in this study. Sebastian Rast (Max Planck Institute for Meteorology, Hamburg, Germany) is thanked for producing the ERA-Interim files for nudged ECHAM5 runs. Jaakko Ikonen (FMI) is thanked for help with the GlobCover data. Finally, thanks are due to Richard Essery and an anonymous reviewer for their helpful comments on the paper.

Edited by: D. Roche

References

AMIP Project Office: AMIP II Guidelines, AMIP Newsletter, 8, available at: http://www-pcmdi.llnl.gov/projects/amip/NEWS/amipnl8.php (last access: 6 November 2014), 1996.

Arino, O., Ramos Perez, J. J., Kalogirou, V., Bontemps, S., Defourny, P., and Van Bogaert, E.: Global land cover map for 2009 (GlobCover 2009), European Space Agency (ESA) and Université Catholique de Louvain (UCL), doi:10.1594/PANGAEA.787668, 2012.

Armstrong, R. L., Knowles, K. W., Brodzik, M. J., and Hardman, M. A.: DMSP SSM/I Pathfinder Daily EASE-Grid Brightness Temperatures, January 1987–July 2008, National Snow and Ice Data Center, Boulder, Colorado, USA, digital media, 1994.

Bontemps, S., Defourny, P., Van Bogaert, E., Arino, O., Kalogirou, V., and Ramos Perez, J. J.: GLOBCOVER 2009 Products description and validation report. Université Catholique de Louvain (UCL) and European Space Agency (ESA), Vers. 2.2, 53 pp., available at: http://epic.awi.de/31014/16/GLOBCOVER2009_Validation_Report_2-2.pdf (last access: 6 November 2014), 2011.

Brohan, P., Kennedy, J. J., Harris, I., Tett, S. F. B., and Jones, P. D.: Uncertainty estimates in regional and global observed temperature changes: a new data set from 1850, J. Geophys. Res., 111, D12106, doi:10.1029/2005JD006548, 2006.

Brown, R. D.: Northern Hemisphere snow cover variability and change, 1915–97, J. Climate, 13, 2339–2355, 2000.

Brown, R. D. and Robinson, D. A.: Northern Hemisphere spring snow cover variability and change over 1922–2010 including an assessment of uncertainty, The Cryosphere, 5, 219–229, doi:10.5194/tc-5-219-2011, 2011.

Brutel-Vuilmet, C., Ménégoz, M., and Krinner, G.: An analysis of present and future seasonal Northern Hemisphere land snow cover simulated by CMIP5 coupled climate models, The Cryosphere, 7, 67–80, doi:10.5194/tc-7-67-2013, 2013.

Bulygina, O. N., Razuvaev, V. N., and Aleksandrova, T. M.: Description of data set "Routine snow surveys", available at: http://meteo.ru/english/climate/snow1.php (last access: 6 November 2014), 2011a.

Bulygina, O. N., Groisman, P. Ya., Razuvaev, V. N., and Korshunova, N. N.: Changes in snow cover characteristics over Northern Eurasia since 1966, Environ. Res. Lett., 6, 045204, doi:10.1088/1748-9326/6/4/045204, 2011b.

Cohen, J.: Snow cover and climate, Weather, 49, 150–156, 1994.

Dee, D. P., Uppala, S. M., Simmons, A. J., Berrisford, P., Poli, P., Kobayashi, S., Andrae, U., Balmaseda, M. A., Balsamo, G., Bauer, P., Bechtold, P., Beljaars, A. C. M., van de Berg, L., Bidlot, J., Bormann, N., Delsol, C., Dragani, R., Fuentes, M., Geer, A. J., Haimberger, L., Healy, S. B., Hersbach, H., Hólm, E. V., Isaksen, L., Kållberg, P., Köhler, M., Matricardi, M., McNally, A. P., Monge-Sanz, B. M., Morcrette, J.-J., Park, B.-K., Peubey, C., de Rosnay, P., Tavolato, C., Thépaut, J.-N. and Vitart, F.: The ERA-Interim reanalysis: configuration and performance of the data assimilation system, Q. J. Roy. Meteor. Soc., 137, 553–597, 2011.

Derksen, C. and Brown, R.: Spring snow cover extent reductions in the 2008–2012 period exceeding climate model projections. Geophys. Res. Lett., 39, L19504, doi:10.1029/2012GL053387, 2012.

Dickinson, R. E., Henderson-Sellers, A., and Kennedy, P. J.: Biosphere-atmosphere Transfer Scheme (BATS) Version 1e as Coupled to the NCAR Community Climate Model, NCAR Technical Note NCAR/TN-387+STR, doi:10.5065/D67W6959, 1993.

Essery, R., Rutter, N., Pomeroy, J., Baxter, R., Stähli, M., Gustafsson, D., Barr, A., Bartlett, P., and Elder, K.: SNOWMIP2: An evaluation of forest snow process simulations, B. Am. Meteorol. Soc., 90, 1120–1135, doi:10.1175/2009BAMS2629.1, 2009.

Fletcher, C. G., Zhao, H., Kushner, P. J., and Fernandes, R.: Using models and satellite observations to evaluate the strength of snow albedo feedback, J. Geophys. Res., 117, D11117, doi:10.1029/2012JD017724, 2012.

Foster, J., Liston, G., Koster, R., Essery, R., Behr, H., Dumenil, L., Verseghy, D., Thompson, S., Pollard, D., and Cohen, J.: Snow cover and snow mass intercomparisons of general circulation models and remotely sensed datasets, J. Climate, 9, 409–426, 1996.

Frei, A. and Robinson, D. A.: Evaluation of snow extent and its variability in the Atmospheric Model Intercomparison Project, J. Geophys. Res., 103, 8859–8871, 1998.

Frei, A., Miller, J., and Robinson, D. A.: Improved simulations of snow extent in the second phase of the Atmospheric Model Intercomparison Project (AMIP-2), J. Geophys. Res., 108, 4369, doi:10.1029/2002JD003030, 2003.

Frei, A., Brown, R., Miller, J. A., and Robinson, D. A.: Snow mass over North America: observations and results from the second phase of the Atmospheric Model Intercomparison Project, J. Hydrometeorol., 6, 681–695, 2005.

Gildea, M. P. and Moore, B.: FAOSOL – A global soil archive, Complex systems research center, University of New Hampshire, Durham, New Hampshire (unpublished data tape and documentation), 1985.

Groisman, P. Y., Karl, T. R., and Knight, R. W.: Changes of snow cover, temperature and radiative heat balance over the Northern Hemisphere, J. Climate, 7, 1633–1656, 1994.

Hall, A. and Qu, X.: Using the current seasonal cycle to constrain snow albedo feedback in future climate change, Geophys. Res. Lett., 33, L03502, doi:10.1029/2005GL025127, 2006.

Heino, R. and Kitaev, L.: INTAS project (2002–2005): snow cover changes over Northern Eurasia during the last century: circulation consideration and hydrological consequences (SCCONE), BALTEX Newsletter, 5, 8–9, available at: www.

baltex-research.eu/publications/Newsletter/Newsletter5.pdf (last access: 6 November 2014), 2003.

Henderson-Sellers, A., Wilson, M. F., Thomas, G., and Dickinson, R. E.: Current global land-surface data sets for use in climate-related studies, NCAR Tech. Note NCAR/TN-272+STR, doi:10.5065/D6FQ9TK5, available at: http://opensky.library.ucar.edu/collections/TECH-NOTE-000-000-000-525 (last access: 6 November 2014), 1986.

Hurrell, J. W., Holland, M. M., Gent, P. R., Ghan, S., Kay, J. E., Kushner, P. J., Lamarque, J.-F., Large, W. G., Lawrence, D., Lindsay, K., Lipscomb, W. H., Long, M. C., Mahowald, N., Marsh, D. R., Neale, R. B., Rasch, P., Vavrus, S., Vertenstein, M., Bader, D., Collins, W. D., Hack, J. J., Kiehl, J., and Marshall, S.: The Community Earth System Model: a framework for collaborative research, B. Am. Meteorol. Soc., 94, 1339–1360, doi:10.1175/BAMS-D-12-00121.1, 2013.

Kendon, E. J., Rowell, D. P, and Jones, R. G.: Mechanisms and reliability of future projected changes in daily precipitation, Clim. Dynam., 35, 489–509, doi:10.1007/s00382-009-0639-z, 2010.

Kitaev, L., Kislov, A., Krenke, A., Razuvaev, V., Martuganov, R., and Konstantinov, I.: The snow cover characteristics of northern Eurasia and their relationship to climatic parameters, Boreal Environ. Res., 7, 437–445, 2002.

Knowles, K., Njoku, E., Armstrong, R., and Brodzik, M. J.: Nimbus-7 SMMR Pathfinder Daily EASE-Grid Brightness Temperatures, National Snow and Ice Data Center, Boulder, CO, USA, digital media and CD-ROM, 2002.

Liston, G. E.: Local advection of momentum, heat, and moisture during the melt of patchy snow covers, J. Appl. Meteorol., 34, 1705–1715, 1995.

Liston, G. E.: Representing subgrid snow cover heterogeneities in regional and global models, J. Climate, 17, 1381–1397, 2004.

Lundquist, J. D., Dickerson-Lange, S. E., Lutz, J. A., and Cristea, N. C.: Lower forest density enhances snow retention in regions with warmer winters: A global framework developed from plot-scale observations and modeling, Water. Resour. Res., 49, 6356–6370, doi:10.1002/wrcr.20504, 2013.

Metsämäki, S., Pulliainen, J., Salminen, M., Luojus, K., Wiesmann, A., Solberg, R., Böttcher, K., Hiltunen, M., and Ripper, E.: Introduction to GlobSnow Snow Extent products with considerations for accuracy assessment, Remote Sens. Environ., 156, 96–108, doi:10.1016/j.rse.2014.09.018, 2015.

Mialon, A., Coret, L., Kerr, Y. H., Sécherre, and Wigneron, J.-P.: Flagging the topographic impact on the SMOS signal, IEEE T. Geosci. Remote, 46, 689–694, 2008.

Mölders N., Luijting, H., and Sassen, K.: Use of atmospheric radiation measurement program data from Barrow, Alaska, for evaluation and development of snow-albedo parameterizations, Meteorol. Atmos. Phys., 99, 199–219, 2008.

Oleson, K. W., Lawrence, D. M., Bonan, G. B., Flanner, M. G., Kluzek, E., Lawrence, P. J., Levis, S., Swenson, S. C., Thornton, P. E., Dai, A., Decker, M., Dickinson R., Feddema, J., Heald, C. L., Hoffman, F., Lamarque, J.-F., Mahowald, N., Niu, G.-Y., Qian, T., Randerson, J., Running S., Sakaguchi, K., Slater, A., Stöckli, R, Wang, A., Yang, Z.-L., Zeng, Xi., and Zeng, Xu.: Technical Description of version 4.0 of the Community Land Model (CLM), NCAR Technical Note NCAR/TN-478+STR, National Center for Atmospheric Research, Boulder, CO, 257 pp., available at: http://www.cesm.ucar.edu/models/cesm1.0/clm/CLM4_Tech_Note.pdf, (last access: 6 November 2014), 2010.

Pedersen, C. A. and Winther, J.-G.: Intercomparison and validation of snow albedo parameterization schemes in climate models, Clim. Dynam., 25, 351–362, 2005.

Pulvirenti, L., Pierdicca, N., and Marzano, S.: Topographic effects on the surface emissivity of a mountainous area observed by a spaceborne microwave radiometer, Sensors, 8, 1459–1474, 2008.

Qu, X. and Hall, A.: What controls the strength of snow-albedo feedback?, J. Climate, 20, 3971–3981, 2007.

Qu, X. and Hall, A.: On the persistent spread in snow-albedo feedback, Clim. Dynam., 42, 69–81, doi:10.1007/s00382-013-1774-0, 2014.

Räisänen, J.: Warmer climate: less or more snow?, Clim. Dynam., 30, 307–319, 2008.

Riihelä, A., Manninen, T., Laine, V., Andersson, K., and Kaspar, F.: CLARA-SAL: a global 28 yr timeseries of Earth's black-sky surface albedo, Atmos. Chem. Phys., 13, 3743–3762, doi:10.5194/acp-13-3743-2013, 2013.

Roeckner, E., Bäuml, G., Bonaventura, L., Brokopf, R., Esch, M., Giorgetta, M., Hagemann, S., Kirchner, I., Kornblueh, L., Manzini, E., Rhodin, A., Schlese, U., Schulzweida, U., and Tompkins, A.: The atmospheric general circulation model ECHAM5, Part I, Model description, Max Planck Institute for Meteorology Rep. 349, 127 pp., available at: www.mpimet.mpg.de/fileadmin/publikationen/Reports/max_scirep_349.pdf (last access: 6 November 2014), 2003.

Roeckner, E., Brokopf, R., Esch, M., Giorgetta, M., Hagemann, S., Kornblueh, L., Manzini, E., Schlese, U., and Schulzweida, U.: Sensitivity of simulated climate to horizontal and vertical resolution in the ECHAM5 atmosphere model, J. Climate, 19, 3771–3791, 2006.

Roesch, A.: Evaluation of surface albedo and snow cover in AR4 coupled climate models, J. Geophys. Res., 111, D15111, doi:10.1029/2005JD006473, 2006.

Roesch, A. and Roeckner, E.: Assessment of snow cover and surface albedo in the ECHAM5 general circulation model, J. Climate, 19, 3828–3843, 2006.

Roesch, A., Wild, M., Gilgen, H., and Ohmura, A.: A new snow cover fraction parametrization for the ECHAM4 GCM, Clim. Dynam., 17, 933–946, 2001.

Rowell, D. P. and Jones, R. G.: Causes and uncertainty of future summer drying over Europe, Clim. Dynam., 27, 281–299, 2006.

Stevens, B., Giorgetta, M., Esch, M., Mauritsen, T., Crueger, T., Rast, S., Salzmann, M., Schmidt, H., Bader, J., Block, K., Brokopf, R., Fast, I., Kinne, S., Kornblueh, L., Lohmann, U., Pincus, R., Reichler, T., and Roeckner, E.: Atmospheric component of the MPI-M Earth System Model: ECHAM6, J. Adv. Model. Earth Syst., 5, 146–172, doi:10.1002/jame.20015, 2013.

Strasser, U., Warscher, M., and Liston, G. E.: Modeling snow-canopy processes on an idealized mountain, J. Hydrometeorol., 12, 663–677, 2011.

Takala, M., Pulliainen, J., Metsämäki, S., and Koskinen, J.: Detection of snow melt using spaceborne microwave radiometer data in Eurasia from 1979 to 2007, IEEE T. Geosci. Remote, 47, 2996–3007, 2009.

Tanré, D., Geleyn, J. F., and Slingo, J. M.: First results of the introduction of an advanced aerosol-radiation interaction in the

ECMWF low resolution global model, in: Aerosols and Their Climatic Effects, A. Deepak Publishing, Hampton, Virginia, USA, 133–177, 1984.

Verseghy, D. L.: The Canadian Land Surface Scheme (CLASS): Its history and future, Atmos. Ocean, 38, 1–13, doi:10.1080/07055900.2000.9649637, 2000.

von Salzen, K., Scinocca, J. F., McFarlane, N. A., Li, J., Cole, J. N. S., Plummer, D., Verseghy, D., Reader, M. C., Ma X., Lazare, M., and Solheim, L.: The Canadian Fourth Generation Atmospheric Global Climate Model (CanAM4), Part I: Representation of physical processes, Atmos. Ocean, 51, 104–125, doi:10.1080/07055900.2012.755610, 2013.

Wetherald, R. T. and Manabe, S.: The mechanisms of summer dryness induced by greenhouse warming, J. Climate, 8, 3096–3108, 1995.

Yamazaki, T.: The influence of forests on atmospheric heating during the snowmelt season, J. Appl. Meteorol., 34, 511–519, 1995.

Zhao, H. and Fernandes, R.: Daily snow cover estimation from Advanced Very High Resolution Radiometer Polar Pathfinder data over Northern Hemisphere land surfaces during 1982–2004, J. Geophys. Res., 114, D05113, doi:10.1029/2008JD011272, 2009.

Geophysica (2018), 53(1), 65–91

Sea-Effect Snowfall Case in the Baltic Sea Region Analysed by Reanalysis, Remote Sensing Data and Convection-Permitting Mesoscale Modelling

Taru Olsson[1], Piia Post[2], Kalev Rannat[3], Hannes Keernik[3,4], Tuuli Perttula[1], Anna Luomaranta[1], Kirsti Jylhä[1], Rigel Kivi[1] and Tanel Voormansik[2]

[1]Finnish Meteorological Institute, Finland
[2]University of Tartu, Institute of Physics, Estonia
[3]Tallinn University of Technology, Estonia
[4]Estonian Environmental Research Centre, Estonia

(Submitted: August 30, 2018; Accepted: December 3, 2018)

Abstract

A sea-effect snowfall accumulated a national record-breaking snowdrift of 73 cm in Merikarvia, on the west coast of Finland, in less than one day on 8 January 2016. A good understanding of such heavy sea-effect snowfalls in the present climate is essential if we want to assess the probability of their occurrence and intensity in the future. Since very few in situ observations were made of the Merikarvia snowfall event in the sea area where the convection cells developed, we investigated the case with an ERA5 reanalysis, the Global Navigation Satellite System (GNSS), and the numerical weather prediction model HARMONIE, using weather radar information as a reference. We aimed to study the feasibility of the reanalysis and GNSS methods for investigating the basic characteristics of the snowband. In addition, we examined whether the assimilation of observed radar reflectivities could improve the HARMONIE simulations. In addition to snowfall patterns, the vertical structure of the atmosphere during the sea-effect snowfall case was analysed. HARMONIE was able to simulate the intensity of the sea-effect snowfall situation well, but the spatial spread of the snowfall remained too narrow, and the snowband was located slightly too far north compared to the radar observations. Assimilation of radar reflectivities increased the simulated moisture content in the vertical direction and spread the precipitation area horizontally, especially in the north-south direction, but shifted the most intense precipitation even more to the north. The location of the snowfall area was captured by ERA5, but the intensity was estimated to be considerably weaker, and the site of the most intense snowfall was more offshore compared to the radar observations and HARMONIE simulations. The vertical structure of specific humidity was similar and of the same order of magnitude in HARMONIE and ERA5. The GNSS, ERA5 and HARMONIE showed reasonably good agreement on the precipitable water content. The case study demonstrated that the three methods, and combinations of them, can be useful in order to obtain the best possible view of local severe weather events as possible.

Keywords:

1 Introduction

Weather can change rapidly during the cold Nordic winter. Even small changes in the moisture content of the air and slight variations in temperature near zero degrees Celsius may determine whether precipitation will fall as snow, sleet, rain, freezing rain, or ice pellets. Extreme weather events, such as sea-effect snowfall, can have severe im-

pacts on infrastructure and human safety. Prediction and forewarning of intense snowfall events is highly important, especially for road traffic, because rapidly decreasing road surface friction and reduced visibility increase the probability of severe accidents (*Juga et al*., 2012).

In Finland, an essential source of energy for sea-effect snowfall is the Baltic Sea. When cold air outbreaks originating from the north or east pour over the still unfrozen, relatively warm Baltic Sea, the moisture flux and instability from the temperature contrast between the air mass and the sea surface build snowbands, which are then deposited downwind from the sea. These kinds of cold outbreaks are quite common over the Baltic Sea in the autumn and winter and have been investigated by several authors. Most of the studies have aimed to understand the associated dynamical processes and thermodynamic aspects by modelling the cases numerically, e.g., *Andersson and Gustafsson* (1994), *Gustafsson et al. (*1998), *Vihma and Brümmer* (2002), *Savijärvi* (2012), *Mazon et al. (*2015) and *Olsson et al. (*2017).

Based on previous studies, it is possible to sum up a set of local preconditions that favour sea/lake-effect snowfalls (*Jeworrek et al*., 2017 and the references therein). The large air-water temperature difference is the most important precondition for forming snowbands, but there are other factors that support their formation. Relatively strong wind, higher than 10 m s^{-1}, is often found to be an important factor (*Andersson and Nilsson*, 1990, *Savijärvi*, 2015). The ratio between the wind speed and the fetch (distance over ice-free water) is found to be between 0.02 and 0.09 m s^{-1} km^{-1}, which means lower wind speeds in the case of shorter fetches (*Laird et al*., 2003). The directional wind shear from the surface up to 700 hPa is expected to be small, less than 60° (*Niziol*, 1987). The shape and the topography of the coasts surrounding the water body and their exposure to the prevailing wind is also crucial for the mesoscale structures to be formed.

However, in addition to the local preconditions, it has also been noted that the real evolution of processes depends strongly on large-scale atmospheric patterns (*Savijärvi*, 2012, *Mazon et al*., 2015, *Savijärvi*, 2015). An interesting point, not covered in detail earlier, is the role of water vapor transport from longer distances in causing very severe snowfalls in a relatively cold atmosphere (see section 3.1). The sea-effect snowfall cases typically have temporal and spatial scales smaller than what can be covered by the conventional weather station network and resolved by climate models. Therefore, to analyse them and their impacts, additional high-resolution information is needed. Examples of such observations are precipitation fields from weather radar and integrated precipitable water (IPW) from the Global Navigation Satellite System (GNSS).

This paper is an extension of a former study of a record-breaking snowfall of 73 cm (31 mm as liquid water) that fell in less than a day in Merikarvia, Finland, on 8 January 2016 (*Olsson et al*., 2017). In the previous study, it was found that the HARMONIE/AROME numerical weather prediction system captured the overall sea-effect snowfall quite well, but the simulated weaker snowfall did not spread as broadly along the coastline as was observed by weather radar. Numerically simulated atmospheric vertical profiles of equivalent potential temperatures indicated that the atmosphere was unstable to vertical motions, with decreasing equivalent potential temperature

with height. Together with colliding winds over the relatively warm and ice-free sea, a very localised extreme snowfall was produced. In the current study, we used a newer version of HARMONIE/AROME, and unlike the previous study, where the observations of radar reflectivities were applied only for qualitative evaluation of the model results, here, the radar reflectivities were assimilated into the modelling system. Because very few in situ observations were made in the sea area where the convection cells developed, we examined whether assimilation of observed radar reflectivities could improve the results of the simulations. Since earlier studies suggest that assimilation of the radar reflectivity observations have a beneficial effect on numerical weather prediction, and especially on humidity forecasts (*Ridal and Dahlbom*, 2017, and references therein), we might expect some improvement in the forecast accuracy.

The Merikarvia snow event evolved relatively quickly and, as shown later, with an extremely low background level of IPW in the atmosphere. Therefore, we have chosen the GNSS as a method that is possibly suitable for detecting small changes in IPW with a high enough temporal resolution to analyse this kind of extreme event (*Guerova et al*., 2016).

Reanalyses are dynamically consistent methods to reprocess observational data and are therefore widely used in weather and climate research. Improvements in modelling and data assimilation are accommodated into the new generations of reanalysis. With increasing spatial and temporal resolutions, as well as advancing assimilation capabilities, the chance to detect small-scale extreme weather events with reanalysis products increases. In this work, we put the latest reanalysis, ERA5, to the test. The authors of this work are not aware of any published research using reanalyses to reconstruct a severe small-scale snowfall event. ERA5 moisture profiles and maps are investigated here in detail in the snowfall case, and its 2-metre temperature and pressure data are used as an input for the GNSS analysis.

In general, the ultimate purpose of the simulations is to obtain an upper estimate of how reliable model-based assessments can be with regard to the occurrence and characteristics of sea-effect snowfall events. Case studies of intense snowfall events also increase the scientific understanding of favourable atmospheric conditions for severe wintertime convective weather. This is useful from the viewpoint of developing sea-effect snowfall detection algorithms (e.g., *Jeworrek et al*., 2017, *Kämäräinen and Jokinen*, 2014), which could be applied to output from high-resolution climate models. In the future, a warmer climate due to climate change might favour the occurrence of snowbands over the Baltic Sea, because the length of the ice season is expected to decrease (*Vihma and Haapala*, 2009, *Mazon et al*., 2015). This could increase the probability of cold-air outbreaks occurring over the relatively warm open sea in late autumn and early winter.

In this study, we first give a description of the reanalysis data, remote sensing data, and the HARMONIE/AROME model in section 2, as well as the simulations that were run. Then, the results of the simulations are presented and discussed in sections 3 and 4, respectively.

2 Data

2.1 Reanalysis

The European Centre for Medium-Range Weather Forecasts (ECMWF) has developed atmospheric reanalyses of the global climate since the 1980s, starting with FGGE reanalyses (*Bengtsson et al*., 1982) and followed by ERA-15 (*Gibson et al*., 1999), ERA-40 (*Uppala et al*., 2005), ERA-Interim (*Dee et al*., 2011) and most recently ERA5 (*Hersbach and Dee*, 2016). The latter has been used in this work. It provides gridded estimates of a large number of atmospheric, land and oceanic climate variables. Although the whole ERA5 dataset is not available yet, a first segment covering the period from 2008 to the present day is available for public use. Compared to ERA-Interim, ERA5 has a better spatial resolution as well as higher output frequency (31 km horizontal, 137-layer vertical and 1-h temporal resolution). Moreover, ERA5 takes into account various newly reprocessed datasets and recent instruments (*Hersbach and Dee*, 2016).

In this work, ERA5 products with a 1-h temporal resolution were used, except for precipitation and convective snowfall, which were accumulated over 3 hours. In addition to investigating ERA5 moisture profiles and maps in detail for the snowfall case, its 2-m temperature and pressure data were used as an input for the GNSS analysis. Both were linearly interpolated to the GNSS stations in the horizontal and vertical.

2.2 Global Navigation Satellite System tropospheric products

Meteorological applications of geodetic satellite observations have existed since the early 1990s, after the publication of *Bevis et al. (*1992 and 1994). Zenith total delay (ZTD) can be computed from the Global Navigation Satellite System (GNSS) observations and turned into an amount of water vapour using surface measurements of pressure and temperature.

Observational data acquired from GNSS receivers are processed by GNSS data processing software to obtain the corresponding tropospheric products, i.e., ZTD and their uncertainties (σ). These values, accompanied by additional meteorological data and different physical constants with their uncertainties are used in a second phase of data processing, the conversion of ZTD and σ_{ZTD} to values of IPW and σ_{IPW}.

Approximately 60 GNSS sites between 50–70° N, 10–37° E were chosen to analyse the Merikarvia snow event (Fig. 1). GNSS data (from national and international networks) was processed with the GAMIT/GLOBK software (*Herring et al*., 2015), with the main attention paid to the evolution of GNSS-IPW in the sub-area of 56–66° N, 16–32° E in 1-h steps.

Surface meteorological data were initially obtained from in situ measurements at co-located meteorological sites, with a co-location radius <30 km, and interpolated to GNSS antenna heights. Additionally, the 2-m air pressure (Ps) and temperature (Ts) were derived from ERA5 and interpolated to the GNSS antenna heights. These data were used to generate meteorological Receiver Independent Exchange Format (RINEX) files for GNSS data processing. ERA5 data has been compared with in situ meteorolog-

ical measurements, and the differences were found to be ca. 1 hPa for pressure and 1 K for temperature.

Due to non-continuous data streams from several meteorological sites and very small differences compared to in situ measurements, it was considered reasonable to base the IPW analysis on ERA5 data.

From a practical point of view, it is necessary to obtain not only values for GNSS-IPW but also the uncertainty (σ_{IPW}) of these values, especially if we want to compare the results with independent techniques and observations. An extensive overview of the methods and relevant error sources of GNSS measurements can be found in *Ning et al*. (2016). For the Merikarvia case, we selected the theoretical method by *Ning et al*. (2016). The choice was based on the fact that we did not have three or more co-located IPW time series from independent techniques, as would have been required for a statistical analysis. Three somewhat different approaches were adopted (Appendix A).

Usually, the realistic GNSS-IPW uncertainty values stay below 1 mm, which makes the conversion process challenging for a winter-season atmosphere with extremely low background IPW values (usually ~1–3 mm) in the northern areas.

2.3 Model description

HARMONIE in the ALADIN-HIRLAM NWP system is a non-hydrostatic convection-permitting mesoscale model (*Bénard et al*., 2010, *Brousseau et al*., 2011, *Bengtsson et al*., 2017). In this work, the HARMONIE-AROME model configuration of the HARMONIE model was used. It is run operationally at the Finnish Meteorological Institute (FMI) at 2.5-km resolution. The model has 65 levels in the vertical, and the top is at 10 hPa. In our model setup, the simulation domain covers Finland, Scandinavia and the Baltic countries (Appendix B). Because the HARMONIE model simulates weather conditions in a limited area, information from the lateral boundaries of this area is needed. The boundary conditions for HARMONIE runs are obtained from the IFS (Integrated Forecast System), which is an operational global forecasting system at the ECMWF. These boundary conditions are updated every hour.

High-resolution models, such as HARMONIE, no longer rely on a convection parameterization scheme since the small-scale convective phenomena can now be resolved. This is advantageous, since parameterization of convection is a large source of error and uncertainty in lower-resolution mesoscale models (*Prein et al*., 2015, *Weusthoff et al*., 2010).

In our research, the HARMONIE model version 40h1.1 was used. In the model setup, the forecast model and analysis system were those of the AROME model from Météo-France (*Seity et al*., 2011, *Brousseau et al*., 2011). Version 7.3 of surface scheme SURFEX was used to calculate atmospheric processes near the underlying surface. SURFEX consists of a set of models for the description of the different types of surfaces: urban environments, soil, and sea and inland water bodies (*SURFEX Scientific Documentation*, *Masson et al*., 2013).

Data assimilation is used in HARMONIE, meaning that a running model simulation is corrected at regular time intervals with observations. In data assimilation, we

compared model predictions and observations and adjusted the model state so that it was closer to the observations. The purpose was to determine the initial state of the atmosphere as accurately as possible to improve the quality of the forecasts. The data assimilation method used in HARMONIE for upper air observations was the 3D-Var data assimilation system. The analysis cycle with data assimilation was performed every three hours. Surface data assimilation was conducted using the optimal interpolation (OI) method. Operationally assimilated in situ observations included surface synoptic observations (SYNOP), sea-based stations (SHIP), aircraft reports (AMDAR, AIREP, ACARS), buoy observations (BUOY), radiosondes (TEMP) and wind profiler (PILOT) observations.

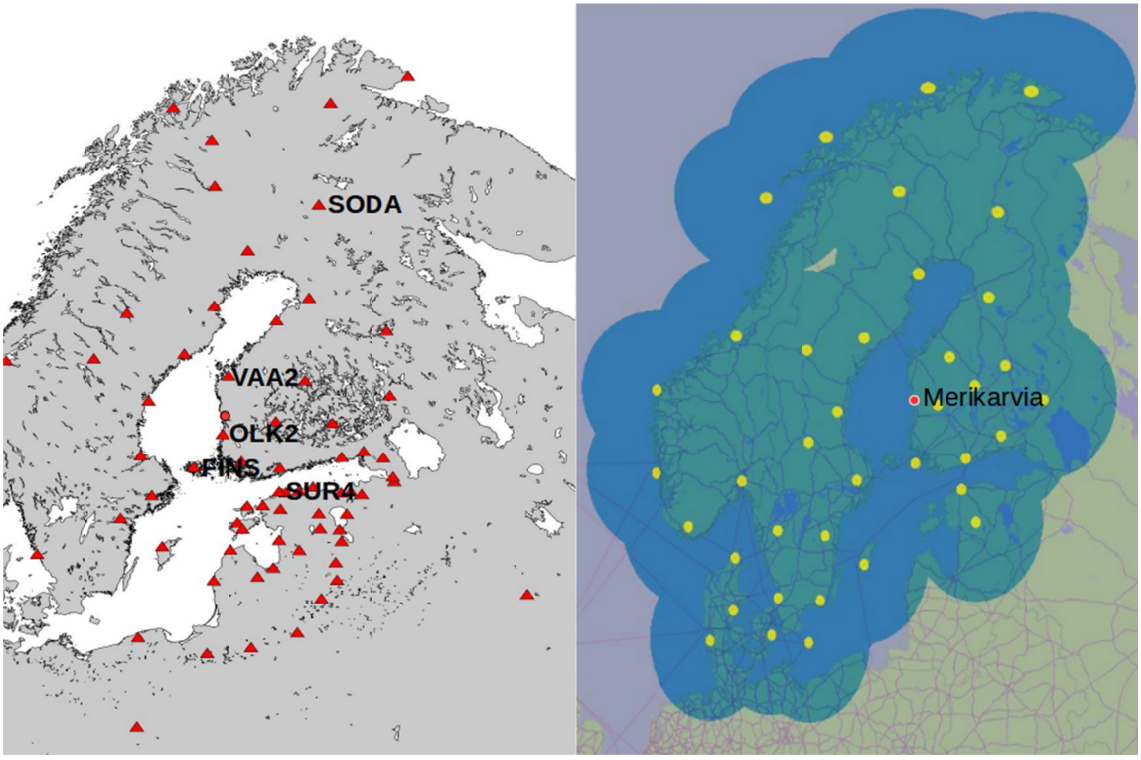

Fig. 1. GNSS sites (left, red triangles, VAA2 - Vaasa, OLK2 - Olkiluoto, FINS - Finstrom, SUR4 - Suurupi, SODA - Sodankylä) used in this study and OPERA radar data (right, yellow spots) from Finland, Sweden, Norway, Denmark and Estonia (radar in use in 2016). Merikarvia is marked with a red spot.

2.4 Pre-processing and assimilation of radar reflectivities

Weather radar observations provide three-dimensional information about precipitation and wind with good temporal and spatial resolution. Observations are made up to 250 km around a single radar location, with sub-kilometre resolution and an interval of 5 to 10 minutes. This makes radar an advantageous tool in detecting sea-effect snowfalls, because they are typically localized and form offshore.

The location and intensity of the precipitation is analysed from radar reflectivities. Radar reflectivities were assimilated using the 1D+3D-Var assimilation method first introduced by *Caumont et al*. (2010) and later operationally implemented by *Wattrelot et al*. (2014). In this method, a one-dimensional Bayesian scheme is first used to retrieve

vertical humidity profiles from radar reflectivities, and these humidity retrievals are then assimilated into the 3D-Var assimilation system. Additionally, dry profiles with no reflectivity were assimilated, since an important part of radar assimilation is also to assimilate areas where the model indicates precipitation but the radar does not. Hence, an observation of reflectivity will either moisten the model in areas where the model indicates no precipitation or adjust the intensity in precipitation areas (*Ridal and Dahlbom*, 2017).

Before assimilation, some quality control steps were performed on the radar data. These included checking for errors and format differences in the data from different countries, horizontal thinning, and blacklisting of the lowest elevation angle scans of each volume to avoid clutter. The quality control steps inside the HARMONIE/AROME radar data assimilation system are described in more detail by *Ridal and Dahlbom* (2017) and *Gustafsson et al*. (2017).

In this work, we used OPERA (The Operational Weather Radar in Europe) data, including radar from Finland, Sweden, Norway, Denmark, and Estonia. The radar in use in 2016 can be seen in Figure 1. Near the edges of the visibility area, radar can detect precipitation only if the precipitation falls from a cloud higher than 6 km. For liquid precipitation, this is a good assumption, but not for snowfall. Precipitation from a cloud higher than 2 km can be detected inside a 120-km radius from the radar. During the winter, the visibility area is somewhere between the 120-km radius and the whole visibility area.

2.5 Simulations

The Merikarvia sea-effect snowfall case was simulated by two experiments with the HARMONIE model: a simulation without assimilation of radar reflectivities (NR hereafter) and a simulation where radar reflectivities were assimilated (R hereafter). The results from the simulations were compared to each other and to radar observations to determine whether the assimilation of the radar reflectivities improves the model performance in simulating the sea-effect snowfall case. Three hours on 8 January 2016 were selected for closer examination: 05 UTC, 13 UTC and 21 UTC. These were the same hours as previously studied by *Olsson et al*. (2017). Due to assimilation, both of our simulations consist of several forecast cycles, starting from 00 UTC with 3-hour intervals, each of which lasts 48 hours. Within both simulations, we qualitatively evaluate which cycle gives the best results compared to radar observations.

3 Results

3.1 The overall meteorological situation

In late December 2015, a very large amount of warm and humid air was transported to the Arctic region by storm “Frank”, one of the strongest North Atlantic storms on record (*Kim et al*., 2017). *Binder et al*. (2017) have shown that the 2015/2016 record-breaking warm winter was the result of a very unusual configuration of large-scale atmospheric flow that came along with other regional extremes. One of these was the

Merikarvia heavy snow event (Fig. 2d). A very important role was played by a blocking anticyclone over Scandinavia and NW Russia, which lasted for more than two weeks and enabled cold and dry air masses over the Northern Baltic Sea region. The favourable conditions for sea-effect convective precipitation were lasting for approximately ten days. Since 2 January 2016, the snowbands were mostly over the Gulf of Finland and the Northern Baltic Proper and Åland Sea, then starting on 6 January, they also extended to the Bothnian Bay and the Bothnian Sea. These snowfall events lasted a few days after the Merikarvia event. The mesoscale structures of precipitation were very variable depending on the larger scale air flow direction and the characteristics of the prevailing air masses. The structure of the cloudfield from MODIS Terra on the morning of 8 January 2016 is given by Figure 2a. All favourable conditions for cold-season convection (*Jeworrek et al*., 2017) were fulfilled on 8 January: the 10-m wind was stronger than 10 m/s, the 2-m temperature was lower than 278 K, the temperature difference between the

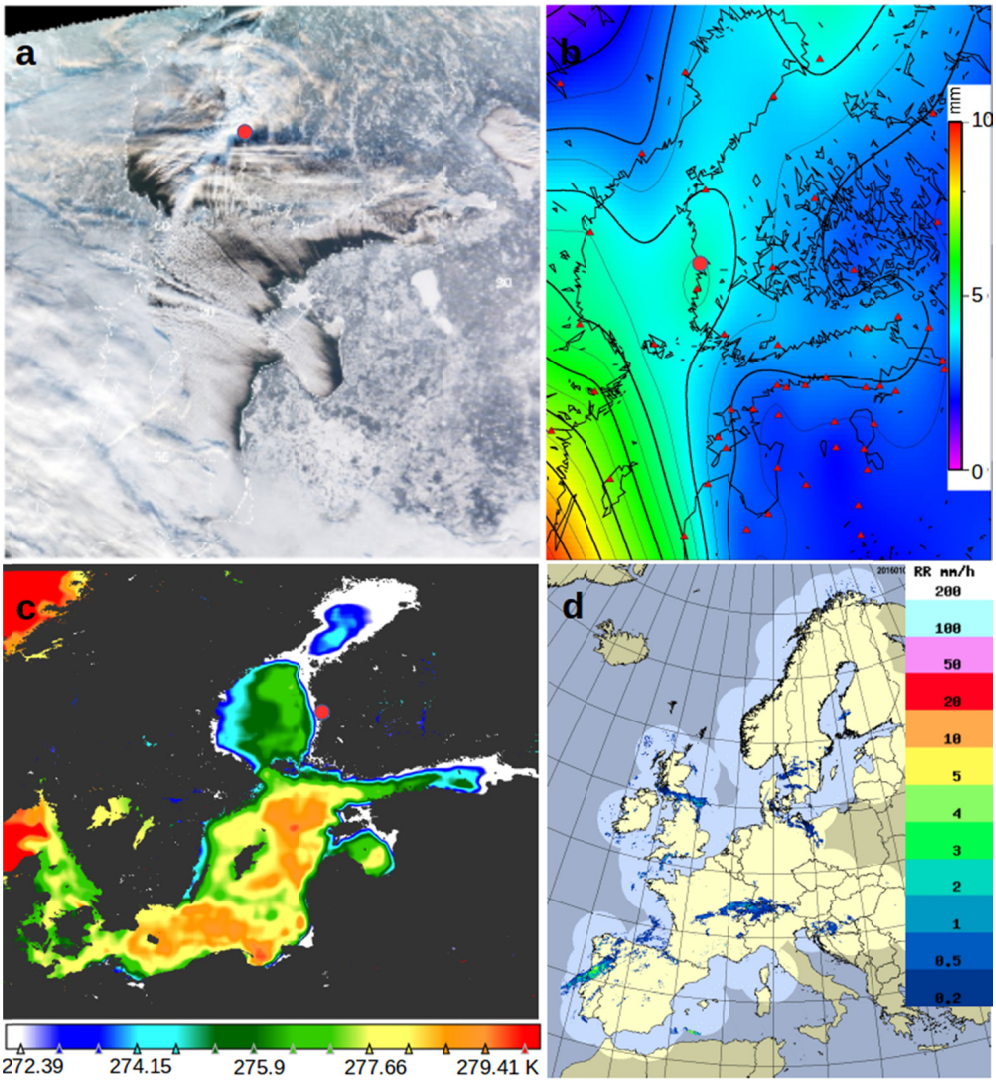

Fig. 2. (a) MODIS Terra RGB showing various types of convective snowbands over the Northern Baltic Sea on 8 January 2016 at 10:20 UTC. (b) GNSS-IPW fields (mm) at 13 UTC. (c) Copernicus CMEMS sea surface temperature (K) at 00 UTC. (d) One-hour accumulated precipitation (mm/h) observed by weather radar at 13 UTC. Merikarvia is marked with a red spot.

surface and 850 hPa was more than 15 K, the boundary layer height exceeded 1000 m and there was a wind shear in the layer between 10 m and 700 hPa. Due to the warm autumn, the Baltic Sea was still open, enabling a long fetch over relatively warm water (Fig. 2c) when cold arctic air masses reached the area.

3.2 Atmospheric moisture fields

As seen from Figure 3, the most intense snowfall (as measured by the weather radar network) is well captured by ERA5. Regarding the timing and location, there is a good agreement between ERA5 and the HARMONIE output and radar observations. However, ERA5 estimates precipitation to be considerably weaker (more than 7 times), showing the highest values above the sea (approximately 3 mm from 12 to 15 UTC on

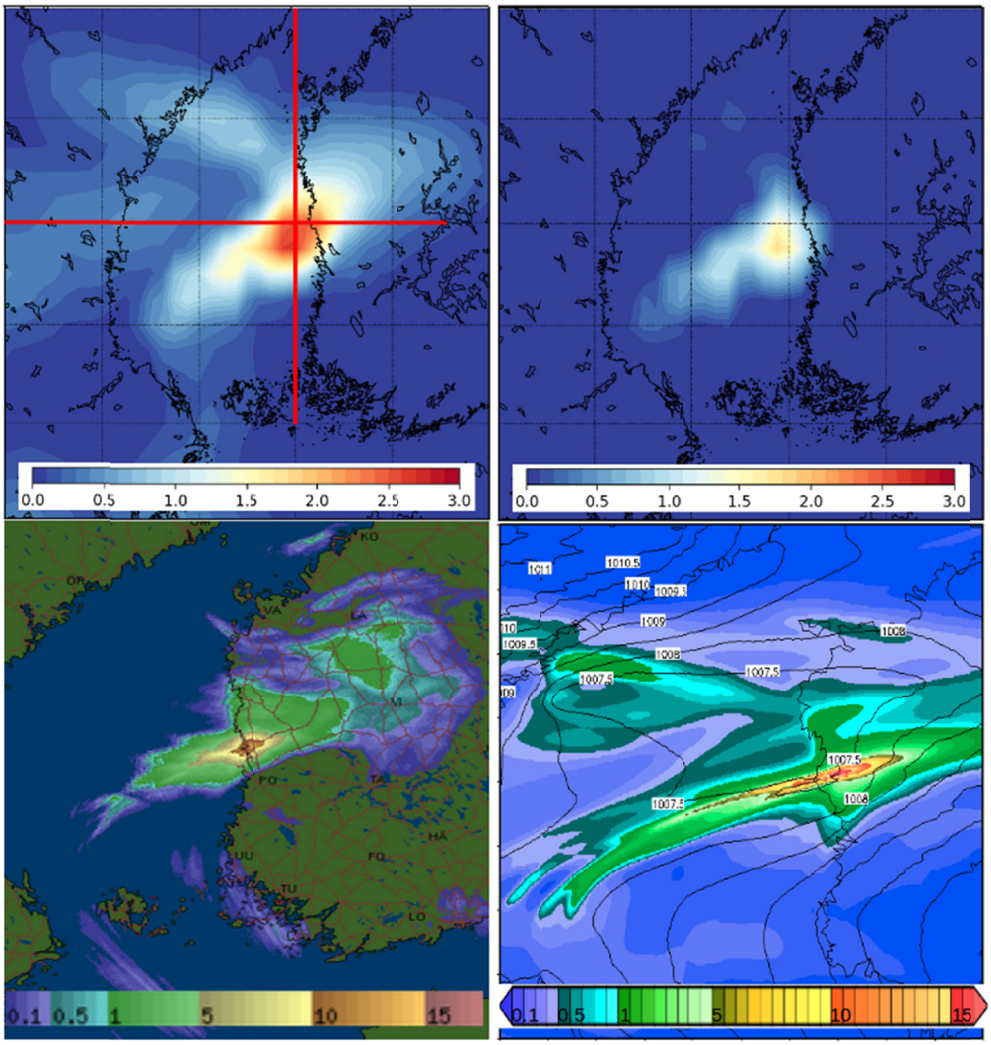

Fig. 3. Three-hour accumulated precipitation (mm, top left) and convective snowfall (mm of water equivalent, top right) estimated by ERA5 on 8 January 2016 at 15 UTC. For comparison, three-hour accumulated precipitation from radar images (bottom left) and the HARMONIE simulation with assimilated radar reflectivities (bottom right) are shown. The sea level pressure (hPa) is also shown for HARMONIE (bottom right). The vertical sections along 21° E and 62° N used in Figures 4 and 7 are marked in the top left figure.

8 January), where most of the precipitation occurs due to the convective snowfall. The latter contributes up to 65% of the total precipitation. According to ERA5, precipitation above land was less pronounced, reaching its maximum intensity three hours later (approximately 1.8 mm from 15 to 18 UTC at 62.2° N 21.5° E, not shown).

Vertical cross-sections of specific humidity along 62° N and 21° E up to the 700 hPa level reveal that the maximum values appeared at approximately 12 UTC near the surface (approximately 2.2 g/kg, Fig. 4). The humidity decreased linearly with height. Such layering was present roughly two degrees in the northward/southward and westward/eastward directions from 62° N, 20.5° E. A very similar situation was detected in the temperature fields. The 2-m temperature at this point is just below 273 K, while the temperature 200 km farther is 5–10 K lower (not shown).

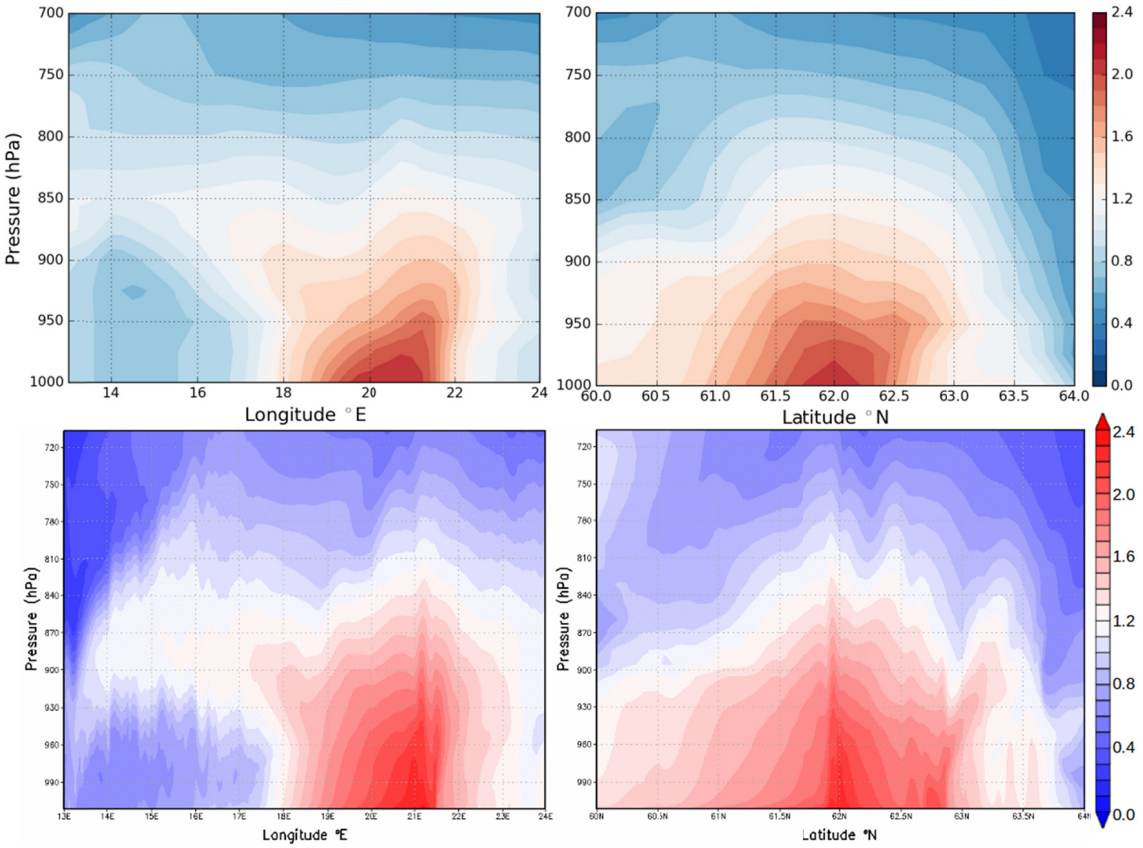

Fig. 4. Vertical cross-sections of specific humidity (g/kg) up to 700 hPa along 62° N (left) and along 21° E (right) based on ERA5 data (top row) and the HARMONIE simulation with assimilated radar reflectivities from forecast cycle 2016010812 on 8 January 2016 13 UTC.

The time evolution of IPW, as generated using the GNSS method in 1-hour time steps, is presented in Figure 5 for a selection of GNSS stations over Finland. A rapid increase in IPW during a 16-hour time period can be seen. An interesting feature is the more humid air that approached from the south (Fig. 2b). We note an advection of moisture from Sweden over the Turku archipelago at 05 UTC. The well-developed IPW peak over Olkiluoto (the closest GNSS site to Merikarvia) developed within a few hours,

reaching the peak value at 13 UTC and completely disappearing at 21 UTC. No similar peaks that are clearly distinguishable from the background can be noticed in adjacent GNSS sites (Finstrom and Vaasa, Fig. 5) or the eastern GNSS sites inland. This coincides well with the information obtained from the radar and from the HARMONIE model. Unfortunately, we do not have GNSS data from the open sea.

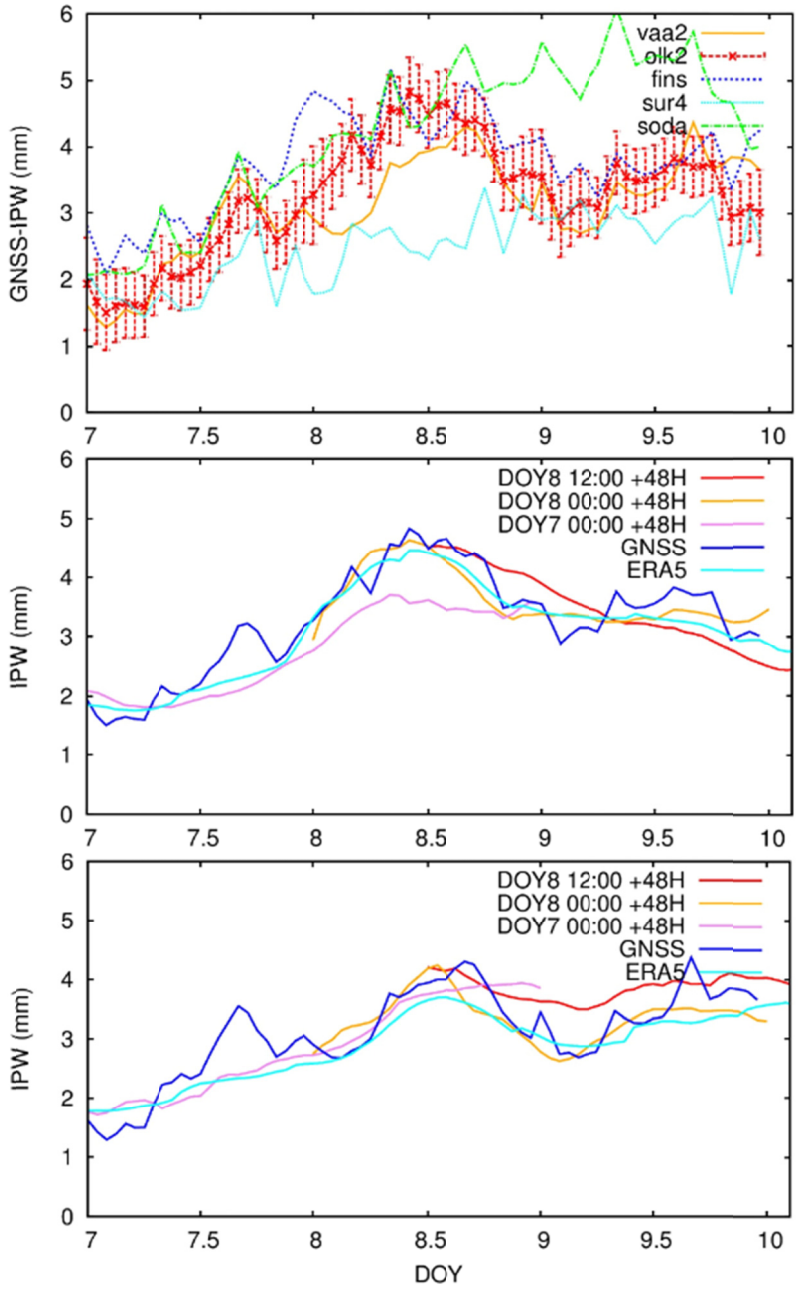

Fig. 5. Top panel: Integrated precipitable water (IPW) time series for 7–10 January 2016 are shown for five GNSS sites (VAA2 - Vaasa, OLK2 - Olkiluoto, FINS - Finstrom, SUR4 - Suurupi, SODA - Sodankylä) with error bars for the nearest site, Olkiluoto (red). Comparison of GNSS-IPW with IPW extracted from ERA5 and HARMONIE for the Olkiluoto (middle panel) and Vaasa (bottom panel) GNSS sites. Three different forecast cycles (red, yellow and pink, 2016010812, 2016010800 and 2016010700, respectively) are shown for HARMONIE with assimilated radar reflectivities. DOY stands for day of the year.

An analysis of the uncertainty σ_{IPW} in the IPW values obtained from GNSS measurements was performed using three methods (Appendix A). The results for temporal averages of σ_{IPW} at seven GNSS stations during 7–9 January 2016, given in Table A1, show slight differences between the methods. In the top panel of Figure 5, the GNSS-IPW uncertainty ranges are depicted for Olkiluoto, the nearest GNSS site to Merikarvia.

To gain better confidence in the GNSS results, we compared the GNSS-IPW at two sites (Olkiluoto and Vaasa) with the IPW extracted from ERA5 and HARMONIE simulations (middle and bottom panels in Figure 5). The comparison of IPWs from GNSS, ERA5 and HARMONIE shows relatively small differences (~1 mm), while the uncertainty σ_{IPW} in the GNSS values at Olkiluoto stay within ± 0.5 mm during the peak of the snow event (top panel Fig. 5). Similar tendencies, such as that described in Figure 5, were noticed for all sites – the ERA5 results were smoother, but the differences stayed within ~1 mm. It can be concluded that the GNSS-IPW values used in this analysis are reliable.

3.3 Outcomes from the HARMONIE simulations

Radar observations of the Merikarvia snowfall case at 05, 13, and 21 UTC on 8 January (Fig. 6) were chosen for closer analysis. At 05 UTC, the snowfall band was directed from the south to the north and was still located in the sea area in front of Merikarvia. At 13 UTC, the snowfall had intensified and was partly located over land areas. At 21 UTC, the snowfall area had grown smaller and slightly weaker.

Throughout 8 January, according to the HARMONIE simulations, the sensible heat flux over the sea was directed upwards to the atmosphere (i.e., heat loss from the sea) due to the cold south-westerly flow over the relatively warm Baltic Sea, supporting convection. The sensible heat flux was strongest during the night, 00–06 UTC, over the sea area from Åland to the west coast of Finland (not shown). The highest values, up to 350 W/m^2, were found near the west coast, decreasing there towards the end of the day to 60–140 W/m^2. The upward latent heat flux from the sea had a temporal and spatial variability similar to that of the sensible heat flux. The highest values, up to 160 W/m^2, occurred during the night and decreased to 50–80 W/m^2 over the course of the day. The correspondence between HARMONIE and ERA5 was good for temporal and spatial patterns of the heat fluxes, but in ERA5, the values were distinctly smaller, 80 W/m^2 at the highest for the sensible heat flux and 50 W/m^2 at the highest for the latent heat flux.

There is a good agreement of the HARMONIE output with ERA5 and the GNSS method. Although ERA5 estimates precipitation to be relatively weaker in contrast to HARMONIE simulations (Fig. 3), the vertical profiles of specific humidity (Fig. 4) are very similar in ERA5 and the HARMONIE simulation according to shape and maximum values. The greatest difference comes from the resolution, as HARMONIE is able to simulate more distinct variations in the specific humidity fields.

Additionally, the IPW time series show good agreement between ERA5, the GNSS method and HARMONIE simulations, with GNSS showing the largest variations. Thus, the greatest differences can be found between different forecast cycles and simulation with (R) and without (NR) radar assimilation (Fig. 5). The R simulation ini-

tiated at 7 January at 00 UTC (2016010700) was not able to forecast the highest peak of IPW in Olkiluoto at approximately noon on 8 January, as the simulated values were 0.8–0.9 mm lower compared to ERA5, the GNSS method and forecast cycles initiated later. Nevertheless, in Vaasa, the forecast cycle 2016010700 performed as well as the other methods. In both locations, the forecast cycle initiated on 8 January 00 UTC (2016010800) simulated the cycle and variation of IPW closest to ERA5 and the GNSS method. The cycle initiated closest to the most intense precipitation (2016010812) simulated the peak values close to ERA5 and the GNSS method, but the forecast for the following hours was too moist in both locations.

Adding radar assimilation to HARMONIE increased the moisture content, especially in the lower model levels and within the precipitating cloud. HARMONIE NR simulations had IPW values that were too low (0.5–1 mm lower), especially between 12–24 UTC on 8 January, compared to ERA5, GNSS and HARMONIE with R.

Figure 6 shows the hourly accumulated total precipitation for a simulation with assimilation of radar reflectivities (R) and the difference between the R and NR simulations for the cycle initiated at 03 UTC on 8 January 2016. When the results from the simulations are compared with the radar observations at the same hour (the left panel in Fig. 6), we note that the location of the strongest snowband offshore of Merikarvia is well captured by HARMONIE in both simulations. The assimilation of radar reflectivities spread the total area of simulated precipitation, produced a clearer hook to the coastline, and the area of maximum precipitation grew slightly stronger. In particular, the HARMONIE with an R simulation intensified the precipitation north of the NR simulation.

In Figure 6, convergence zones are also shown. In these zones, near-surface winds converged, which led to vertical air movement that further enhanced the convective snowfall. In both simulations, NR and R, the offshore convergence zones were located very close to the snowband. When the snowfall reached the coast at approximately 10 UTC, two convergence zones formed, one along the coastline on both sides of the strongest snowfall and another along the strongest snowband, perpendicular to the coastline.

Figure 7 illustrates the vertical cross-section of the simulated sum of cloud ice and water, as well as the meridional wind speed. The convergence zones near the coastline can be seen distinctly as the meridional winds show a sharp gradient in wind speed and direction. Data assimilation intensified the near-coastline cloud water and ice (Fig. 7, columns A and B) and spread them in a south-north direction (Fig. 7, columns C and D) compared to the simulation without assimilation of radar reflectivities. In addition, the assimilation of radar reflectivities removed an upper-level tail from cloud water and ice content above the sea (Fig. 7, columns A and B). The cloud water and ice content was higher in the lower model levels with assimilated radar reflectivities, and the cloud water and ice were preserved longer during the day (Fig. 7). Assimilation of radar reflectivities increased the southerly wind speeds in all forecast cycles compared to HARMONIE with NR.

When the results from other forecast cycles (not shown) were compared with radar images, it was found that the location of the snowband differed from the radar observations the most in the first four forecast cycles, initiated 23–41 hours before the time of analysis. The simulated location of the snowband was far too north in both the simulations, and the precipitation area was smaller than in forecast cycles initiated later. The last three forecast cycles were more accurate with the location of the snow band, but the extent of the strongest snowfall area was still narrower than observed and located slightly too far north (not shown).

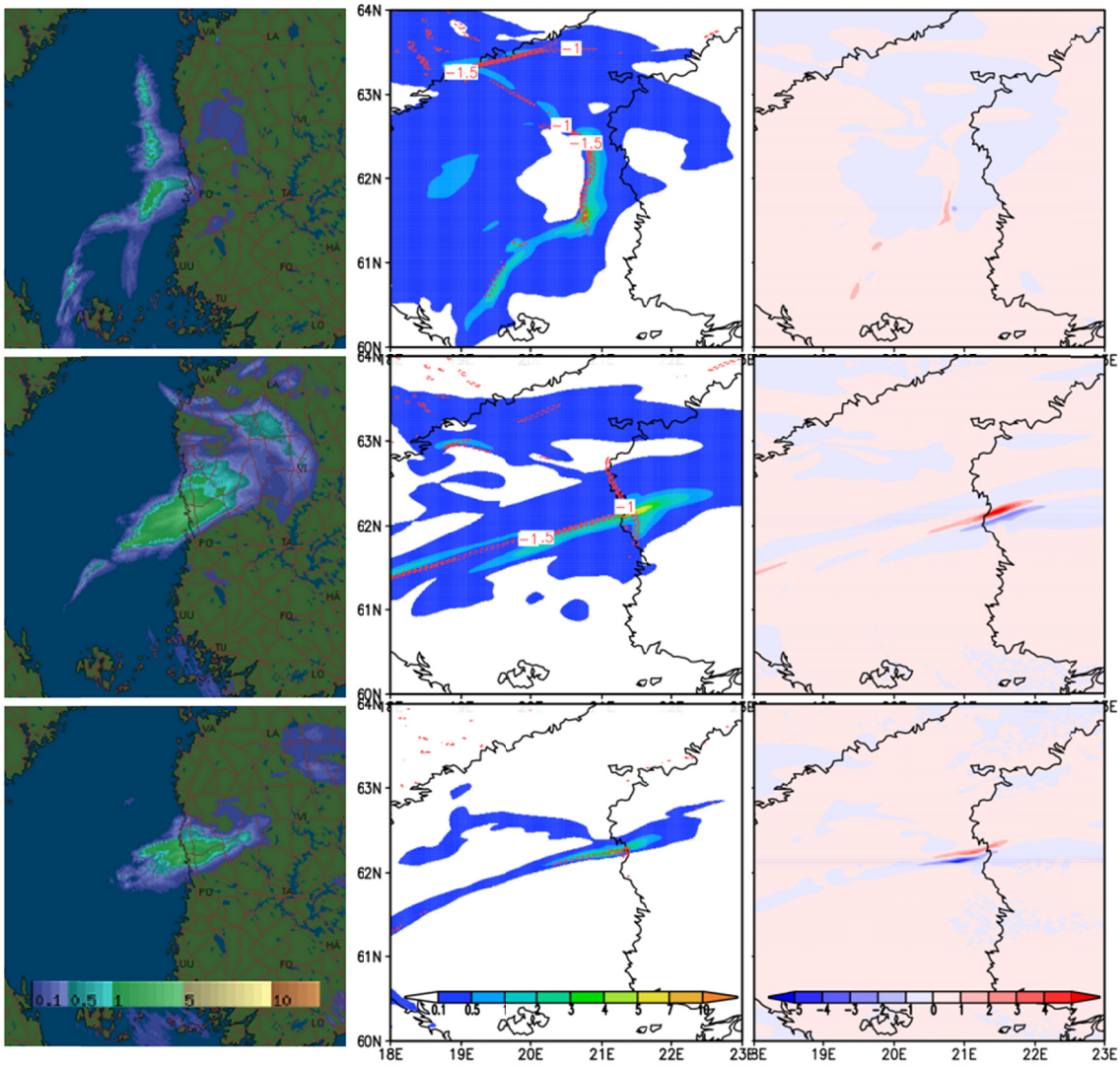

Fig. 6. One-hour cumulative precipitation (mm/h) in the radar images (left panel) and forecast cycle 2016010803 at 05 (top), 13 (middle), and 21 (bottom) UTC on 8 Jan 2016 simulated with HARMONIE with assimilated radar reflectivities (middle panel). Simulated convergence zones are shown with red contours. The difference between HARMONIE with (R) and without (NR) radar assimilation is in the right column (mm/h).

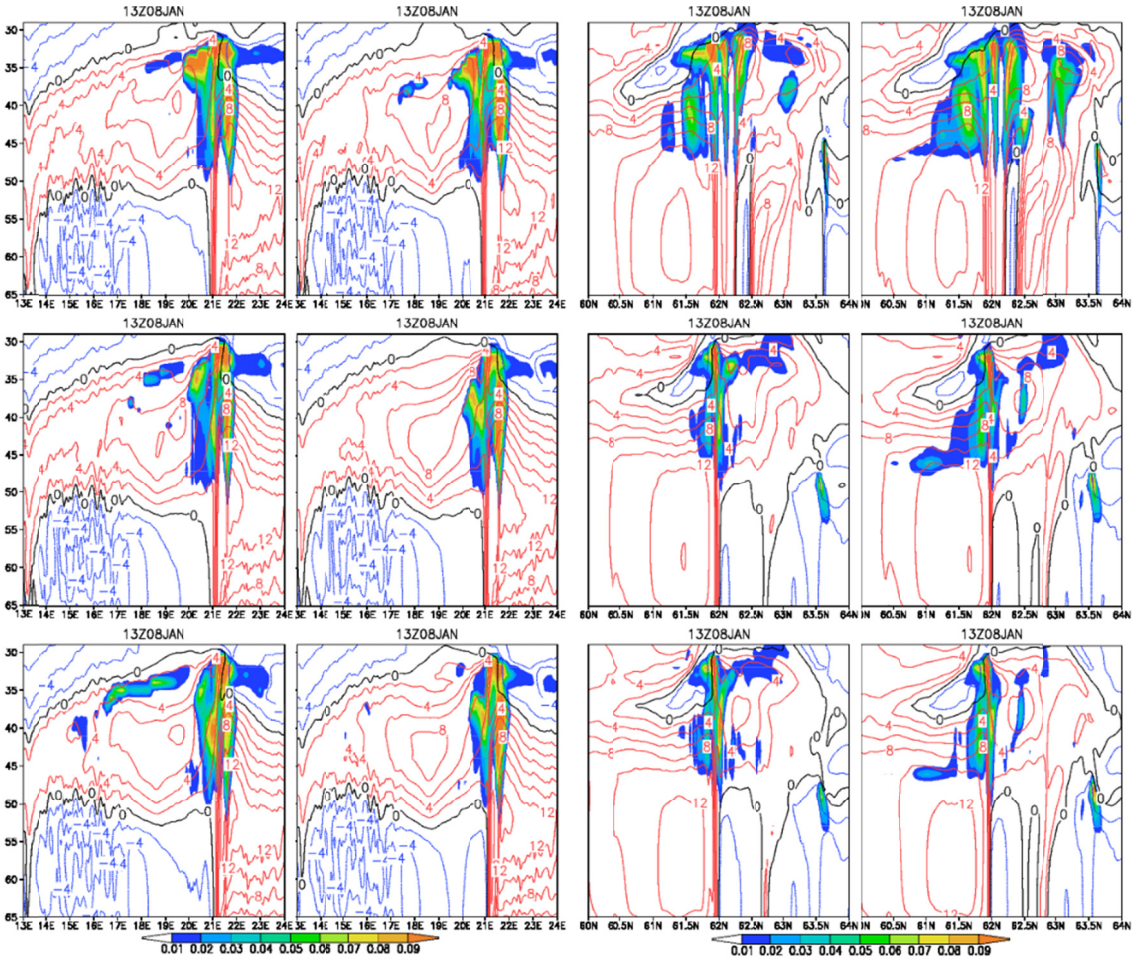

Fig. 7. Vertical cross-section from model levels 29–65 (up to ~700 hPa) of cloud water and ice (g/m2) and meridional wind speed (m/s, southerly in red, northerly in blue) along 62° N (13°–24° E, columns A and B) and along 21° E (60°–64° N, columns C and D), as simulated by HARMONIE for NR (columns A and C) and R (columns B and D). The forecast cycles are 2016010806 (top row), 2016010809 (middle row), and 2016010812 (bottom row) at 13 UTC on 8 Jan 2016.

4 Discussion

The source of the moisture for precipitation above the sea cannot be distinguished in the detection process of past sea-effect cases. The moisture can drift long distances instead of originating from the non-frozen Baltic Sea, and remote sources of moisture hamper the detection. Since very few in situ observations were made in the sea area where the convection cells developed, we investigated this case with an ERA5 reanalysis, the Global Navigation Satellite System (GNSS), weather radar, and the numerical weather prediction model HARMONIE to the best possible view of the snowband.

We treated radar measurements as a reference method because they provide the needed temporal and spatial coverage to monitor precipitation on a regional scale. The typical measurement resolution and coverage over sea areas of an operational weather radar (~500 metres, ~5 minutes) is superior in comparison, e.g., to a network of precipitation gauges. Nevertheless, quantitative snowfall estimates with weather radar are still a challenge because of the variability in the properties of snow crystals and snowflakes

that evolve inside a snowstorm (*von Lerber*, 2018). The challenge stems from the large uncertainty in the microphysical properties of snowfall, i.e., the effect of the density and size of snow particles on the measured back-scattered power. In addition, since radar observes precipitating clouds above the ground and the measurement height increases with distance from the radar, the actual accumulated snowfall on the ground might be some kilometres off depending on the wind speed and direction.

From radar snowfall images, it can be seen that the area of the actual snow event was extremely narrow, not exceeding ca. 35 km. Taking into account the temporal and spatial scale of such a sea-effect case, ERA5 as a global reanalysis with a 30-km horizontal resolution showed good agreement with the other methods used. The timing and location of the snowfall were accurately estimated. This suggests that reanalyses are able to detect not only regional long-term trends but also local short-term extreme weather events. This benefit is clearly overlooked, and more is yet to be discovered in the future as reanalyses keep improving. On the other hand, the magnitude of the snowfall intensity was underestimated, and correctly capturing it still appeared to be beyond the capabilities of ERA5.

The GNSS-IPW maps generated for 7–9 January 2016 show the evolution of IPW fields during this time period. Local peak values of IPW can be observed on 8 January at Olkiluoto. The density of GNSS sites situated in and around the Merikarvia area is not sufficient for a more detailed analysis of the precipitation process at this scale. It is also impossible to obtain GNSS-data from the sea area. However, the GNSS results can be used to calibrate NWP models at GNSS sites at the areas of interest (OLKI, VAA2, FINS, etc.). Additional benefit from GNSS observations can come for operational weather services if the GNSS data could be assimilated in near real time.

According to the WMO Rolling Review of Requirements for IPW (http://www.wmo-sat.info/oscar/variables/view/162), the goal for nowcasting, NWP and climate research is to reach uncertainty values below 1 mm. A theoretical analysis (*Ning et al*., 2016) of GNSS-IPW uncertainty for Merikarvia case demonstrates that these requirements are fulfilled, but it is not the final truth, because statistical analyses (with three or more independent methods) may give higher uncertainty values. A statistical analysis of the results could be possible only for the Sodankylä site (has at least three independent techniques for obtaining the IPW time series), but it would be too far to make decisions about the extremely local Merikarvia snow event.

However, there is great improvement to be gained for data availability and quality. One issue is the density of the GNSS sites in the network, but it is equally important operatively to have high-quality meteorological data for these GNSS sites. Ideally an automatic weather station (AWS) should be installed together with the GNSS receivers (which is true for the majority of Estonian sites used in this analysis) to avoid interpolation errors from co-located meteorological sensors in a radius of ca. 10–30 km. High-quality meteorological data will ensure more accurate ZTDs thanks to realistic *a priori* meteorological constraints for the GNSS data processing software.

Models are a powerful tool in estimating the state of the atmosphere and investigating possible changes in it, as well as in making physical sense of observational data.

This is especially true for areas where the scarcity of observing systems restricts investigation (e.g., seas, large lakes, polar regions). We performed two HARMONIE simulations: one with the assimilation of radar reflectivities and the other without. The assimilation of radar reflectivities did not significantly improve the skill of the forecast in this particular case, as HARMONIE performed well even without radar reflectivities. Nevertheless, the assimilation of radar reflectivities lowered the top of the cloud water and ice and added moisture to lower model levels. It also spread the precipitation area in the south-north direction on the coastline and intensified the strongest snowband over the land, which improved the results compared to ERA5, the GNSS method and radar images.

The forecast cycles that were initiated more than 24 hours before the event gave the weakest results, especially concerning the location of the snowband when compared to radar observations. The results in the forecast cycles that were initiated closer to the event corresponded best with the radar observations in both simulations. In these cycles, the location and the pattern of the precipitation area was well simulated but still slightly too far north.

When radar reflectivities were assimilated to HARMONIE the most intense precipitation area was shifted even more to the north. The reason for this behaviour is beyond the scope of this study. One possibility is that increased southerly winds drive the precipitation towards the north. Some of the difference in the location originates from the analysis of the precipitation, because radar sees the precipitating cloud and HARMONIE simulates the accumulated snow cover over land. In addition, because the radar reflectivities are assimilated into HARMONIE at the time of analysis, the effect of added/reduced moisture fields might not be long-lasting in model simulations as added moisture is precipitated out. Due to this fact, the impact of the assimilation of radar reflectivities might not be visible many hours after the analysis time. However, the forecast cycle with radar reflectivities initiated as close to the maximum intensity of the snowband as possible did not improve the accuracy of the simulation, because the maximum intensity of the precipitation added to the HARMONIE increased the moisture content too much, preserving IPW values that were too high for too long compared to ERA5 and the GNSS method. The snowband was still visible, although distinctly weaker, in radar images on 9 January, but because the radar reflectivities were assimilated to HARMONIE only at the analysis time, the information of the evolution of the snowband observed with radar was not added to the simulation.

Advanced methods are required in order to be able to produce a comprehensive view of the probability of occurrence of sea-effect snowfall in the past and to assess the influence of climate change in the future. In the future, we plan to perform a similar analysis of simulations of known past sea-effect cases in Finland. It would be of great relevance to see whether and how the assimilation of radar reflectivities affects simulated precipitation and air flow patterns in several recent past sea-effect snowfall cases. The findings would increase the scientific understanding of favourable atmospheric conditions for the occurrence of severe wintertime convective weather. They would also be useful from the viewpoint of developing sea-effect snowfall detection algorithms (as

in *Jeworrek et al*., 2017), analogous to the freezing rain algorithm developed and utilized by *Kämäräinen et al*. (2017a, 2017b).

5 Conclusions

We analysed a strong small-scale sea-effect snowfall case in Merikarvia, Finland. In this work, we had three main questions: 1) Is ERA5 reanalysis capable of reconstructing a severe snowfall event? 2) Is the density of the GNSS sites in and around Merikarvia sufficient for a detailed analysis of IPW within such a small area? 3) And finally, could assimilation of observed radar reflectivities improve HARMONIE simulations? The last question was motivated by the fact that no assimilation of radar reflectivity data in HARMONIE has been previously performed in Finland for the purpose of studying sea-effect snowfall.

We treated radar as the reference method in this study. Regarding intensity and location, radar may give the most accurate precipitation estimate, but it does not provide much information about the origin of the event. Hence, it is useful to pair radar observations with models and the GNSS output.

Reanalysis involves significant time latency – it cannot give any improvement for severe weather forecasting, but it can be used afterwards to check whether the forecasts and measurements (including possible measurement errors) were realistic. The state-of-the-art ERA5 reanalysis should presently be the most reliable reference, at least on a larger scale. However, it is a result from a model. In this case study, ERA5 showed good agreement with other methods, but the magnitude of the small-scale snowfall intensity was distinctly underestimated.

The GNSS method for IPW is based on in situ measurements, and the results can be obtained in near real time. An uncertainty analysis shows that the IPW values obtained from GNSS measurements can be trusted over land and satisfy the requirements set for NWP and climate research. However, in our Merikarvia example, it is observed that the GNSS data is problematic for processes evolving over the sea. As an example, we could detect a clear increase in IPW at only one coastal site (Olkiluoto), without any idea about the true horizontal scale of the anomaly. The results with given uncertainties could be compared with different independent techniques (including calibration of numerical models). It may help in forecasting severe weather events if the GNSS products could be assimilated into the forecast model. They can also serve as a near real-time reference and in early warning systems for severe weather events.

Finally, adding data assimilation of radar reflectivities did improve the HARMONIE simulations by increasing the moisture content of the boundary layer and spreading the most intense precipitation area. We found, however, that the cycle that initiated the closest (12 UTC) to the most intense precipitation did increase the precipitable water content of the forecast too much and preserved it for too long compared to ERA5 and GNSS data. The forecast cycle initiated 12 hours prior to the most intense precipitation simulated the snowfall case well and outperformed the HARMONIE simulation without data assimilation of radar reflectivities.

Acknowledgements

We acknowledge Harri Hohti (FMI) for the support given with radar images and data, Annakaisa von Lerber (FMI) for the valuable comments on radar detecting snowfall, and Tiina Nygård (FMI) and Laura Rontu (FMI) for the guidance concerning heat fluxes. The work by the authors at the FMI was partially supported by the State Nuclear Waste Management Fund in Finland through the Finnish Nuclear Power Plant Safety Research Programme 2015–2018. The research at TU and FMI was partially supported by the EU Project GAIA-CLIM. The RINEX-files for the GNSS data processing were provided by Maanmittauslaitos, Estonian Land Board, Latvian Geospatial Information Agency and EUREF. The GNSS-IPW maps were generated with the GMT software (Wessel and Smith 1998).

References

Andersson, T. and N. Gustafsson, 1994. Coast of departure and coast of arrival: two important concepts for the formation and structure of convective snowbands over seas and lakes. *Mon. Weather Rev*. **122**, 1036–1049.

Andersson, T. and S. Nilsson, 1990. Topographically induced convective snowbands over the Baltic Sea and their precipitation distribution. *Weather Forecast.*, **5**, 299–312.

Bénard, P., J. Vivoda, J. Masek, P. Smolíková, K. Yessad, C. Smith, R. Brozková , and J.-F. Geleyn, 2010. Dynamical kernel of the Aladin-NH spectral limited-area model: Revised formulation and sensitivity experiments. *Quart. J. Roy. Meteor. Soc*., **136**, 155–169.

Bengtsson, L., M. Kanamitsu, P. Kållberg, and S. Uppala, 1982. FGGE research activities at ECMWF. *Bull. Amer. Meteor. Soc*., **63**, 277–303. doi:10.1175/1520-0477-63.3.277.

Bengtsson, L., U. Andrae, T. Aspelien, Y. Batrak, J. Calvo, W. de Rooy, E. Gleeson, B. Hansen-Sass, M. Homleid, M. Hortal, K.-I. Ivarsson, G. Lenderink, S. Niemelä, K.P. Nielsen, J. Onvlee, L. Rontu, P. Samuelsson, D.S. Muñoz, A. Subias, S. Tijm, V. Toll, X. Yang, and M. Ødegaard Køltzow, 2017. The HARMONIE–AROME Model Configuration in the ALADIN–HIRLAM NWP System. *Mon. Wea. Rev*., **145**, 119–1935. doi:10.1175/MWR-D-16-0417.1.

Bevis, M., S. Businger, T. Herring, C. Rocken, R. Anthes and R. Wave, 1992. GPS meteorology: remote sensing of atmospheric water vapor using the global positioning system. *J. Geophys. Res*., **97**, 15787–15801, doi:10.1029/92JD01517.

Bevis, M. S. Businger, S. Chiswell, T.A. Herring, R.A. Anthes, C. Rocken and R.H. Ware, 1994. GPS meteorology–Mapping zenith wet delays onto precipitable water. *J. Appl. Meteorol*., **33**, 379–386.

Binder, H., M. Boettcher, C.M. Grams, H. Joos, S. Pfahl and H. Wernli, 2017. Exceptional Air Mass Transport and Dynamical Drivers of an Extreme Wintertime Arctic Warm Event. *Geophysical Research Letters,* **44**, 12028–12036.

Brousseau, P., L. Berre, F. Bouttier and G. Desroziers, 2011. Background-error covariances for a convective-scale data-assimilation system: AROME–France 3D-Var. *Q.J.R. Meteorol. Soc*., **137**: 409–422. doi:10.1002/qj.750.

Caumont, O., V. Ducrocq, É. Wattrelot, G. Jaubert and S. Pradier-Vabre, 2010. 1D+3DVar assimilation of radar reflectivity data: a proof of concept. *Tellus A*, **62**(2). doi:10.3402/tellusa.v62i2.15678.

Dee, D.P., S.M. Uppala, A.J. Simmons, P. Berrisford, P. Poli, S. Kobayashi, U. Andrae, M.A. Balmaseda, G. Balsamo, P. Bauer, P. Bechtold, A.C.M. Beljaars, L. van de Berg, J. Bidlot, N. Bormann, C. Delsol, R. Dragani, M. Fuentes, A.J. Geer, L. Haimberger, S.B. Healy, H. Hersbach, E.V. Hólm, L. Isaksen, P. Kållberg, M. Köhler, M. Matricardi, A.P. McNally, B.M. Monge-Sanz, J.-J. Morcrette, B.-K. Park, C. Peubey, P. de Rosnay, C. Tavolato, J.-N. Thépaut, F. Vitart, 2011. The ERA-Interim reanalysis: configuration and performance of the data assimilation system. *Quart. J. R. Meteorol. Soc*., **137**(656), 553–597. doi:10.1002/qj.828.

Gibson, J.K., P.W. Kållberg, S. Uppala, A. Hernandez, A. Nomura and E. Serrano, 1999. ERA 15 description. *ECMWF Reanalysis Project Report Series* **1**, 86 pp. https://www.ecmwf.int/sites/default/files/elibrary/1997/9584-era-description.pdf.

Guerova, G., J. Jones, J. Douša, G. Dick, S. de Haan, E. Pottiaux, O. Bock, R. Pacione, G. Elgered, H. Vedel and M. Bender, 2016. Review of the state of the art and future prospects of the ground-based GNSS meteorology in Europe. *Atmos. Meas. Tech*., 9, 5385–5406. doi:10.5194/amt-9-5385-2016.

Gustafsson, N., L. Nyberg and A. Omstedt, 1998. Coupling of a high-resolution atmospheric model and an ocean model for the Baltic Sea. *Mon. Weather Rev*. **126**, 2822–2846.

Gustafsson, N., T. Janjić, C. Schraff, D. Leuenberger, M. Weissman, H. Reich, P. Brousseau, T. Montmerle, E. Wattrelot, A. Bučánek, M. Mile, R. Hamdi, M. Lindskog, J. Barkmeijer, M. Dahlbom, B. Macpherson, S. Ballard, G. Inverarity, J. Carley, C. Alexander, D. Dowell, S. Liu, Y. Ikuta and T. Fujita, 2017. Survey of data assimilation methods for convective-scale numerical weather prediction at operational centres. *Q.J.R. Meteorol. Soc*. Accepted Author Manuscript. doi:10.1002/qj.3179.

Herring, T.A., R.W. King, M.A. Floyd and S.C. McClusky, 2015. GAMIT Reference Guide, Rel. 10.6, Department of Earth, Atmospheric, and Planetary Sciences, Massachusetts Institute of Technology.

Hersbach, H. and D. Dee, 2016. ERA5 reanalysis is in production. *ECMWF Newsletter* No. **147**, 7.

Høyer, J.L. and J.She, 2007. Optimal interpolation of sea surface temperature for the North Sea and Baltic Sea. *J. Mar. Sys*., Vol **65**, 1–4, pp. 176–189.

Jeworrek, J., L. Wu, C. Dieterich A. and Rutgersson, 2017. Characteristics of convective snow bands along the Swedish east coast. *Earth Syst. Dynam*., **8**, 163–175. doi:10.5194/esd-8-163-2017.

Juga, I., M. Hippi, V. Karsisto and P. Nurmi, 2014. Weather factors triggering the massive car crashes on 3 February 2012 in the Helsinki metropolitan area, in: Proceedings Of the 17th SIRWEC conference, 30 January-1 February 2014, La Massana, Andorra.

Kim, B.-M., J.-Y. Hong, S.-Y. Jun, X. Zhang, H. Kwon, S.-J. Kim, J.-H. Kim, S.-W. Kim and H.-K. Kim, 2017. Major cause of unprecedented Arctic warming in January 2016: Critical role of an Atlantic windstorm. *Sci. Rep*., **7**, 40,051. doi:10.1038/srep40051.

Kämäräinen, M. and P. Jokinen, 2014. Severe winter weather in Finland. PART II: Freezing rain and lake-effect snowfall. EXWE/SAFIR2014 project report 2014, Finnish Meteorological Institute.

Kämäräinen, M., O. Hyvärinen, K. Jylhä, A. Vajda, S. Neiglick, J. Nuottokari and H. Gregow, 2017a. A method to estimate freezing rain climatology from ERA-Interim reanalysis over Europe. *Nat. Hazards Earth Syst. Sci*., **17**, 243–259. doi:10.5194/nhess-17-243-2017.

Kämäräinen, M., K. Jylhä, O. Hyvärinen and A. Vajda, 2017b. Present-day and future probabilities of severe freezing rain at the nuclear power plant sites in Finland. EXWE/SAFIR2018 project report 2017, Finnish Meteorological Institute.

Laird, N.F., D.A.R. Kristovich and J.E. Walsh, 2003. Idealized model simulations examining the mesoscale structure of winter lake-effect circulations. *Mon. Weather Rev*. **131**, 206–221.

von Lerber, A., 2018. Challenges in measuring winter precipitation: Advances in combining microwave remote sensing and surface observations, Finnish Meteorological Institute Contributions 143. http://hdl.handle.net/10138/231104.

Masson, V., P. Le Moigne, E. Martin, S. Faroux, A. Alias, et al., 2013. The SURFEXv7.2 land and ocean surface platform for coupled or offline simulation of earth surface variables and fluxes. *Geosci. Model Dev*., **6**, 929–960. doi:10.5194/gmd-6-929-2013

Mazon, J., S. Niemela, D. Pino, H. Savijarvi and T. Vihma, 2015. Snow bands over the Gulf of Finland in wintertime. *Tellus A*, **67**, 25102. doi:10.3402/tellusa.v67.25102

Ning, T., J. Wang, G. Elgered, G. Dick, J. Wickert, M. Bradke, M. Sommer, R. Querel and D. Smale, 2016. The uncertainty of the atmospheric integrated water vapour estimated from GNSS observations. *Atmos. Meas. Tech*., **9**, 79–92. doi:10.5194/amt-9-79-2016.

Niziol, T.A., W.R. Snyder and J.S. Waldstreicher, 1995. Winter weather forecasting throughout the eastern United States. Part IV: lake-effect snow. *Weather Forecast.* **10**, 61–77.

Olsson, T., T. Perttula, K. Jylhä and A. Luomaranta, 2017. Intense sea-effect snowfall case on the western coast of Finland. *Adv. Sci. Res*., **14**, 231–239. doi:10.5194/asr-14-231-2017.

Prein, A.F., W. Langhans, G. Fosser, A. Ferrone, N. Ban, K. Goergen, M. Keller, M. Tölle, O. Gutjahr, F. Feser and et al., 2015. A review on regional convection-permitting climate modeling: Demonstrations, prospects, and challenges. *Rev. Geophys*., **53**, 323–361. doi:10.1002/2014RG000475.

Ridal, M. and M. Dahlbom, 2017. Assimilation of Multinational Radar Reflectivity Data in a Mesoscale Model: A Proof of Concept. Journal of Applied Meteorology and Climatology. doi:10.1175/JAMC-D-16-0247.1.

Savijärvi, H.I., 2012. Cold air outbreaks over high-latitude sea gulfs, *Tellus A: Dynamic Meteorology and Oceanography*, **64**:1, 12244. doi:10.3402/tellusa.v64i0.12244

Savijärvi, H., 2015. Cold air outbreaks along a non-frozen sea channel: effects of wind on snow bands. *Meteorol. Atmos. Phys*. **127**, 383–391. doi:10.1007/ s00703-015-0370-8.

Seity, Y., P. Brousseau., S. Malardel, G. Hello, P. Bénard, F. Bouttier, C. Lac and V. Masson, 2011. The AROME-France Convective-Scale Operational Model. *Mon. Wea. Rev*., **139**, 976–991. doi:10.1175/2010MWR3425.1.

SURFEX Scientific Documentation: http://www.cnrm.meteo.fr/surfex/spip.php?rubrique11

Uppala, S.M., P.W. Kållberg, A.J. Simmons, U. Andrae, V. da Costa Bechtold, M. Fiorino, J.K. Gibson, J. Haseler, A. Hernandez, G.A. Kelly, X. Li, K. Onogi, S. Saarinen, N. Sokka, R.P. Allan, E. Andersson, K. Arpe, M.A. Balmaseda, A.C.M. Beljaars, L. van de Berg, J. Bidlot, N. Bormann, S. Caires, F. Chevallier, A. Dethof, M. Dragosavac, M. Fisher, M. Fuentes, S. Hagemann, E. Hólm, B.J. Hoskins, L. Isaksen, P.A.E.M. Janssen, R. Jenne, A.P. McNally, J.-F. Mahfouf, J.-J. Morcrette, N.A. Rayner, R.W. Saunders, P. Simon, A. Sterl, K.E. Trenberth, A. Untch, D. Vasiljevic, P. Viterbo and J. Woollen, 2005. The ERA-40 re-analysis. *Quart. J. R. Meteorol. Soc*., **131**, 2961–3012. doi:10.1256/qj.04.176.

Vihma, T., and Brummer, B., 2002. Observations and modelling of on-ice and off-ice flows in the northern Baltic Sea. *Bound. Layer Meteorol*. **103**, 1–27.

Vihma, T. and J. Haapala, 2009. Geophysics of sea ice in the Baltic Sea – a review. *Prog. Oceanogr*. **80**, 129–148.

Wattrelot, E., O. Caumont and J.-F. Mahfouf, 2014. Operational Implementation of the 1D+3D-Var Assimilation Method of Radar Reflectivity in the AROME Model. *Monthly Weather Review*. Vol. **142**. 1852–1873.

Wessel, P. and W.H.F. Smith, 1998. New, improved version of Generic Mapping Tools released, *EOS Trans. Amer. Geophys. U.*, vol. **79** (47), pp. 579.

Weusthoff, T., F. Ament, M. Arpagaus and M.W. Rotach, 2010. Assessing the Benefits of Convection- Permitting Models by Neighborhood Verification: Examples from MAP D-PHASE. *Mon. Wea. Rev*., **138**, 3418–3433. doi:10.1175/2010MWR3380.1.

Appendix A. *Uncertainty analysis of integrated precipitable water from GNSS*

The temporal mean uncertainties σ_{IPW} in the IPW values obtained from GNSS measurements were calculated by three methods: A) obtained directly from GAMIT *metutil*, B) derived from calculated ZTD and σ_{ZTD} by a method described by Ning et al. (2016) and C) by method B, but with a constant σ_{ZTD} = 4 mm, as claimed by the International GNSS Service (IGS) for their tropospheric product.

In this work, the method developed by Ning et al. (2016) for the GRUAN GNSS product is currently used without information on additional uncertainties from orbital errors (adding ca. 3 mm to the σ_{ZTD} values calculated by EPOS8 software for GRUAN). Not using these additional uncertainties is compensated for by the use of different methods by GAMIT for deriving realistic uncertainties and optionally by the use of the IGS-supported σ_{ZTD} = 4 mm (method C).

Table A1. GNSS-IPW mean uncertainties (in mm), as calculated by methods A, B and C and averaged over the 7th to 9th of January 2016.

Site	σ_{IPW} (method A)	σ_{IPW} (method B)	σ_{IPW} (method C)
OLKILUOTO	0.45	0.51	0.63
TUORLA	0.45	0.5	0.62
VAASA	0.44	0.49	0.62
FINSTROM	0.43	0.5	0.64
SUURUPI	0.39	0.45	0.63
SODANKYLÄ	0.56	0.6	0.62

Appendix B. *Model domain in the HARMONIE-AROME simulations*

The model domain in the simulations is shown in Figure B1.

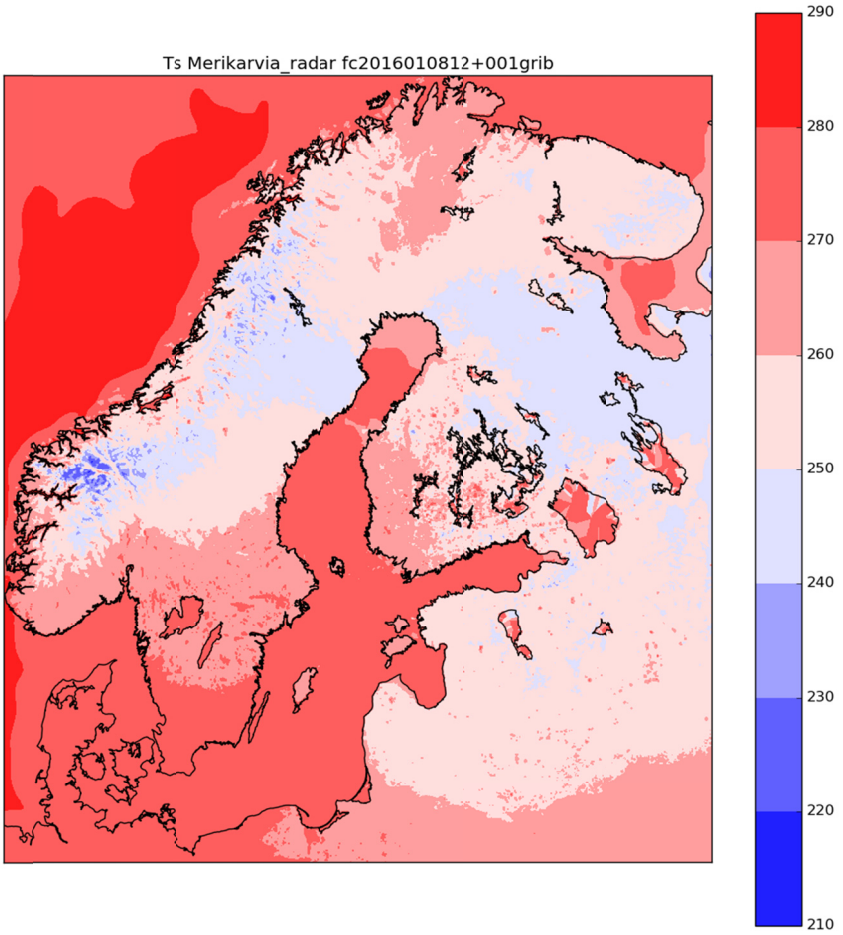

Fig. B1. Example of a surface air temperature (K) in HARMONIE showing the size of the model domain.

***Appendix C**. Abbreviations*

ECMWF	European Centre for Medium-Range Weather Forecasts
EPOS8	Earth Parameter and Orbit System Software, developed by GFZ
FMI	Finnish Meteorological Institute
GAMIT/GLOBK	a comprehensive suite of programs for analyzing GNSS measurements, developed by MIT, Scripps Institution of Oceanography and Harvard University with support from the National Science Foundation
GNSS	Global Navigation Satellite System
GRUAN	Global Climate Observing System (GCOS) Reference Upper-Air Network
IFS	Integrated Forecast System
IGS	International GNSS Service
IPW	integrated precipitable water
OI	Optimal Interpolation method
OPERA	The Operational Weather Radars in Europe
RINEX	Receiver Independent Exchange Format - a data interchange format for raw satellite navigation system data
WMO	World Meteorological Organization
ZTD	Zenith total delay

ILMATIETEEN LAITOS
METEOROLOGISKA INSTITUTET
FINNISH METEOROLOGICAL INSTITUTE

FINNISH METEOROLOGICAL INSTITUTE
Erik Palménin aukio 1
P.O. Box 503
FI-00560 HELSINKI
tel. +358 29 539 1000
WWW.FMI.FI

FINNISH METEOROLOGICAL INSTITUTE
CONTRIBUTIONS No. 169
ISSN 0782-6117
ISBN 978-952-336-115-7 (paperback)
ISBN 978-952-336-116-4 (pdf)
https://doi.org/10.35614/isbn.9789523361164

Helsinki, 2020
Edita Prima Oy